Terms and Conditions of Use of Digitised Theses from Trinity College Library Dublin

Copyright statement

All material supplied by Trinity College Library is protected by copyright (under the Copyright and Related Rights Act, 2000 as amended) and other relevant Intellectual Property Rights. By accessing and using a Digitised Thesis from Trinity College Library you acknowledge that all Intellectual Property Rights in any Works supplied are the sole and exclusive property of the copyright and/or other IPR holder. Specific copyright holders may not be explicitly identified. Use of materials from other sources within a thesis should not be construed as a claim over them.

A non-exclusive, non-transferable licence is hereby granted to those using or reproducing, in whole or in part, the material for valid purposes, providing the copyright owners are acknowledged using the normal conventions. Where specific permission to use material is required, this is identified and such permission must be sought from the copyright holder or agency cited.

Liability statement

By using a Digitised Thesis, I accept that Trinity College Dublin bears no legal responsibility for the accuracy, legality or comprehensiveness of materials contained within the thesis, and that Trinity College Dublin accepts no liability for indirect, consequential, or incidental, damages or losses arising from use of the thesis for whatever reason. Information located in a thesis may be subject to specific use constraints, details of which may not be explicitly described. It is the responsibility of potential and actual users to be aware of such constraints and to abide by them. By making use of material from a digitised thesis, you accept these copyright and disclaimer provisions. Where it is brought to the attention of Trinity College Library that there may be a breach of copyright or other restraint, it is the policy to withdraw or take down access to a thesis while the issue is being resolved.

Access Agreement

By using a Digitised Thesis from Trinity College Library you are bound by the following Terms & Conditions. Please read them carefully.

I have read and I understand the following statement: All material supplied via a Digitised Thesis from Trinity College Library is protected by copyright and other intellectual property rights, and duplication or sale of all or part of any of a thesis is not permitted, except that material may be duplicated by you for your research use or for educational purposes in electronic or print form providing the copyright owners are acknowledged using the normal conventions. You must obtain permission for any other use. Electronic or print copies may not be offered, whether for sale or otherwise to anyone. This copy has been supplied on the understanding that it is copyright material and that no quotation from the thesis may be published without proper acknowledgement.

Studies on Human Biliverdin-IXα Reductase and Linear Tetrapyrrole Signaling.

A dissertation submitted to Trinity College, Dublin
for the degree of Doctor of Philosophy

by

Aisling Dunne

Department of Biochemistry
Trinity College
Dublin 2.

October 2000

TABLE OF CONTENTS

CHAPTER 2 Materials and Methods

CHAPTER 3 Cloning, Overexpression and Purification of Human Biliverdin-IXα reductase

CHAPTER 4 Kinetic Studies on Recombinant Human Biliverdin-IXα Reductase

DECLARATION

I give permission for the Library to lend or copy this thesis upon request.

Signed: Aisling Dunne

Declaration

I declare that the results presented in this thesis are entirely my own work. None of the work described in this thesis has been submitted for any other degree or diploma at this or any other university.

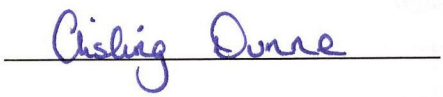

Aisling Dunne

October 2000

Acknowledgements

I would like to thank my supervisor Dr. Tim Mantle for his support, advise and enthusiasm over the last three years, long may it continue. I meant it when I said that I didn't want to have anything to do with enzyme kinetics but you managed to convert me what - don't you just love those "vile bile pigments". I would also like to thank the members of lab 6 or is it lab 2.5 or is it lab 00..... To Orla and Gav, I don't think I could have managed in the early days without your help. A special thanks to Seamus for supplying me with greasy chips on those late nights in the lab and to Ed for all the lifts when I was laden down with books. (I'll finally be able to accompany you on one of your infamous 'Slim Shady Tours'!!) Thanks also to Heberto for assisting with my computer difficulties - I would have thrown it out the window! Thanks also to Sinead for making sure we had our caffeine fix every morning and also for your assistance with the preparation of our paper.

A big thank you to all the prep room staff, technical staff, BRU, stores, academic staff and the secretaries in the Biochemistry department. A special thankyou to the members of the O'Neill lab for assisting me with my cell-culture work and to Yana whom I have tormented over the years. I would also like to acknowledge the financial assistance of BRI, Enterprise Ireland and the Trinity Trust.

I would also like to extend my gratitude to members of the Biochemistry Department in the University of Southampton. A big thankyou to Dr. Mike Gore for your hospitality during my visits and also for your assistance with our stopped-flow experiments. Thanks to Dr. Darren Thompson for volunteering your expert crystallography experience, we won't give up. Thanks also to Dr. Ian Campuzanu for carrying out mass spectroscopic experiments and finally a big thank you to Professor Peter Shoolingin-Jordon.

To all my friends, thanks for distracting me and encouraging me throughout the years. I would especially like to thank Caroline (my partner in crime), Catriona, Babs, Sorcha, Louise, Gordon, Caroline 2 and Ciaran (I hope I haven't forgotten anybody). Thanks to my brother, Elton, for the late night lifts when I was stuck in the lab. And finally, a big thankyou to 'Jamela' - this ones for you.

ABSTRACT

Human Biliverdin-IXα reductase (BVR-A) has been cloned and overexpressed in *E.coli* as a GST- and Hexahistidine fusion protein. The full length cDNA encoding the enzyme has been amplified *via* PCR and ligated into the pGEX-KG and pTrcHis B expression vectors in order to produce the respective fusions. Induction of TG1 cells transformed with the pGEX-BVR-A and pTrc-BVR-A constructs has culminated in the expression of a recombinant protein of the correct size and antigenicity in both cases. Purification of the GST-fusion protein on a glutathione affinity resin yields approximately 40 mg of fusion protein per litre of culture. The fusion protein has a molecular weight of 66 kDa, however, it is possible to remove the GST tag using the proteolytic enzyme, thrombin. The purified hBVR-A protein migrates on SDS-PAGE with a mobility corresponding to 40 kDa, however, mass spectroscopic analysis has confirmed the true relative molecular mass to be 34 kDa. A selenomethionine derivative of the recombinant hBVR-A protein has been prepared for use in Multiwavelength Anomalous Diffraction experiments and crystals diffracting at 3Å have recently been obtained.

A steady-state kinetic study of recombinant hBVR-A has revealed that the enzyme is subject to potent substrate inhibition with biliverdin as the variable substrate. This effect is alleviated to some extent in presence of BSA which serves to reduce the free concentration of biliverdin. A number of curve fitting routines have been performed in order to test the reliability of using such methods to determine kinetic constants for hBVR-A. The recombinant enzyme exhibits two distinct pH optima depending on whether NADH or NADPH is used as cofactor in the reductive process. The nature of this dual pH/cofactor specificity has been defined and is clearly dependant on the experimental conditions used to assess the relationship between pH and activity. Stopped-flow studies indicated that the human BVR-A enzyme exhibits a burst of bilirubin production, which reflects a pre-steady state rate of product formation that is greater than that observed in the steady state, consistent with the findings for the ox kidney and rat kidney enzyme. NADPH binding to the free enzyme was also characterised using the stopped-flow technique, and a K_d of 8.4 μM was calculated. Equilibrium fluorescence quenching experiments indicated a K_d of 1 μM, suggesting that an enzyme-NADPH encounter complex isomerizes to a more stable "nucleotide-induced' conformation.

The stereospecificity of the oxidation of NADH was determined by reducing NAD (labelled in the 4-position with ^3H) using bovine glutamate dehydrogenase and yeast alcohol dehydrogenase to obtain A and B-face labelled NADH, respectively. These two stereoisomers were then used as substrates in the BVR-A catalysed reduction of biliverdin. Incorportation of [^3H] into bilirubin was seen only in the case of the reaction

in which [4-^{3}H]NADH-B was used as co-factor, indicating that BVR-A has B-face stereospecificity.

Protein folding studies have revealed that hBVR-A can reversibly unfold to a kinetically distinct intermediate. Denaturation curves were generated in both urea and guanidine hydrochloride and the change in free energy for the folding/unfolding reaction was calculated based on these results. In the presence of 3 M urea the substrate inhibition exhibited by BVR-A is alleviated such that the apparent K_m and substrate inhibitory K_i for NADH and NAD^+, respectively, are increased. Similar results were obtained with NADPH as cofactor. In the presence of 6 M urea, the activity of hBVR-A is reduced by approximately 60 %. Upon dilution in sodium phosphate buffer, enzyme activity returns to normal.

A comparison of the initial rates for human BVR-A and BVR-B with a series of synthetic biliverdins with propionate side chains 'moving' from a bridging position across the central methene bridge to a 'γ - configuration' reveals quite distinct models for the two active sites. For human BVR-A, it appears that at least one bridging propionate is required for binding and catalytic activity, while two are preferred. All other configurations studies were substrates albeit poor ones, suggesting that a pair of side chains with positive charge play a key role in optimally binding the IXα isomer. In the case of BVR-B, the enzyme cannot tolerate even one propionate in the bridging position due to the presence of a hindrance domain within the enzyme active site.

Activation of the AhR signalling pathway by biliverdin has been demonstrated in murine Hepa1c1c7 cells. While the concentrations of biliverdin used did not induce XRE-luciferase expression to the levels previously reported, the fold increase was sufficiently high to permit inhibition studies to be carried out. Overexpression of p65 effectively suppressed both BNF and biliverdin-induced XRE-driven luciferase activity, consistent with the finding that NF-kB suppresses AhR-mediated transcriptional activation. Treatment of Hepa1c1c7 cells with pro-inflammatory cytokines failed to drive the kB-dependent promoter sufficiently over control vehicle treated cells due to the high level of basal NF-kB activity, therefore it was not possible to test the hypothesis that linear tetrapyrroles inhibit NF-kB-mediated transcriptional activation.

Publications

Cunningham, O., Dunne, A., Sabido, P., Lightner, D. & Mantle, T.J. (2000) J. Biol. Chem. **275**, 19009-19017. Studies on the Specificity of the Tetrapyrrole Substrate for Human Biliverdin-IXα Reductase and Biliverdin-IXβ Reductase: Structure-Activity Relationships Define Models for Both Active Sites.

Abbreviations

ALA	5-aminolaevulinic acid
Abs	absorbance
bp	basepairs
BSA	bovine serum albumin
BVR-A	biliverdin-IXα reductase
BVR-B	biliverdin-IXβ reductase
°C	degrees celcius
CYP	cytochrome p450
Da	daltons
DNA	deoxyribonucleic acid
DNase	deoxyribonuclease
dNTP	deoxyribonucleotide triphosphate
DTT	dithiothreitol
EDTA	ethylenediaminetetra-acetic acid
EtBr	ethidium bromide
Fig.	figure
GSH	glutathione
GST	glutathione-S-transferase
HO	haem oxygenase
g	gram
h	hour
Ig	immunoglobulin
IPTG	isopropylthio-β-D-galactoside
kb	kilobase pairs
kDa	kilodalton
l	litre
LB	Luria bertani broth
m	milli
M	Molar
mg	milligram
µg	microgram
min	minute
ml	millilitre
M_r	relative molecular mass
ng	nanogram
nM	nanomolar

$NAD(P)^+$	nicotinamide adenine dinucleotide (phosphate) [oxidised]
NAD(P)H	nicotinamide adenine dinucleotide (phosphate) [reduced]
PBS	phosphate buffered saline
PEG	polyethylene glycol
PCR	polymerase chain reaction
RNA	ribonucleic acid
RNase	ribonuclease
rpm	revolutions per minute
SDS	sodium dodecyl sulphate
SDS-PAGE	SDS-polyacrylamide gel electrophoresis
SeMet	Selenomethionine
TAE	Tris-acetate/EDTA electrophoresis buffer
TBE	Tris-borate/EDTA electrophoresis buffer
TCA	trichloroacetic acid
TE	Tris/EDTA buffer
TEMED	N, N, N', N'-tetramethylenediamide
Tris	2-amino-2-(hydroxymethyl)-propane-1, 3, -diol
TBS	tris-buffered saline
TTBS	tris-buffered saline/tween 20
Tween 20	polyoxyethylene (20) sorbitan monolaurate
UDPGT	uridine-5'-diphosphate glucuronyl transferase
UV	ultraviolet
v/v	volume per volume
w/v	weight per volume
XRE	xenobiotic response element

Chapter 1

Introduction

1.1 Haem and Tetrapyrroles.

Cyclic tetrapyrrole structures are found in many biochemical compounds and naturally occurring pigments such as chlorophyll and haem. The latter represents one of the most important and versatile tetrapyrroles existing in nature. Functioning as the prosthetic moiety of many proteins, haem plays a key role in many biological processes. The cytochromes, for example, constitute a family of coloured proteins that are related by the presence of a bound haem moiety. The ability of the iron atom in haem to exist in two possible oxidation states i.e. Fe (II) and Fe (III), allows these proteins to function in electron transport. Haem is also associated with haemoglobin and myoglobin for oxygen transport and storage, respectively, and is pivotal in the decomposition of hydrogen peroxide, as catalysed by catalase, the activation of peroxide, as catalysed by peroxidase and the oxygenation reactions catalysed by cytochrome P450 and tryptophan pyrrolase.

The basic unit of all tetrapyrroles is the N-heterocyclic compound pyrrole (see Fig. 1.1). The most important natural tetrapyrroles are composed of a macrocycle in which four pyrrole residues are linked by single bridging carbon atoms. The basic porphin structure is a planar, highly conjugated system and is shown in Fig. 1.2 with the commonly used Fisher numbering system (Fischer & Orth, 1937; cited in Lemberg & Legge, 1949). The four pyrrole rings are designated I, II, III and IV and the linking methene bridges are termed α, β, γ and δ, respectively. The peripheral pyrrole carbon atoms of the macrocycle are numbered 1 to 8 and bear additional side chains, differing between pigments. In haem an iron atom is chelated at the centre of the macrocycle and its methyl, vinyl and propionate side-chains are arranged to give the ferrous protoporphyrin IX isomer (see Fig. 1.3) found at the active site of many proteins.

Linear tetrapyrroles or bilins with the basic structure shown in Fig. 1.4 are also of biological significance and include animal bile pigments, the phycobilin accessory photosynthetic pigments of some algae and the chromophore of the plant photoregulatory pigment, phytochrome. In animals, linear tetrapyrroles occur either as precursors in the formation of haem or as the catabolic products of haem degradation. The carbon bridges linking linear pyrroles exist as saturated ($-CH_2$) or unsaturated (-CH=) forms. Bilenes, bilidienes and bilitrienes are structures having one, two and three unsaturated bridges, respectively. The porphyrin ring of haem is cleaved enzymatically at the α-methene bridge by haem oxygenase to form biliverdin IX-α, a green bilitriene (other isomers of biliverdin arise if cleavage occurs at a methene bridge other than the α-meso bridge). In most mammals, the central -CH= group is subsequently reduced by biliverdin reductase (BVR) to $-CH_2-$, giving rise to the yellow bilidiene, bilirubin-IXα. Bilirubin-IXα is

Figure 1.1.

(a) Pyrrole

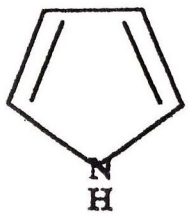

(b) Basic Porphyin Structure

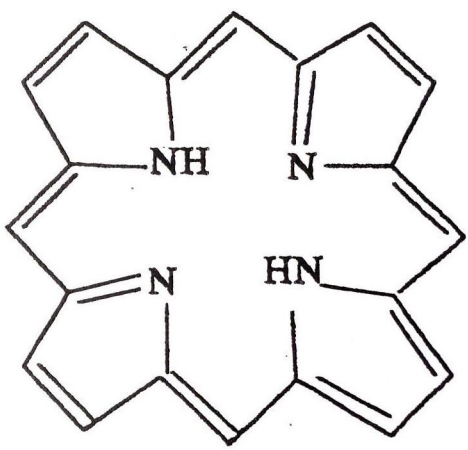

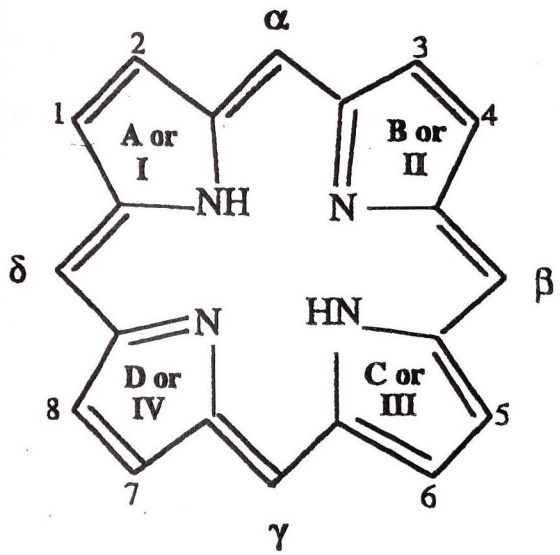

Figure 1.2. The Fischer Labelling System for the Porphyrin Structure.

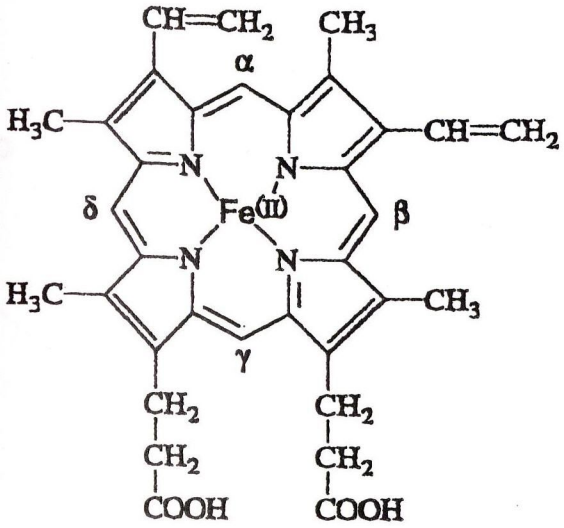

Figure 1.3. The Structure of Haem b (Protoporphyrin IX or Ferrous Protoporphyrin IX.

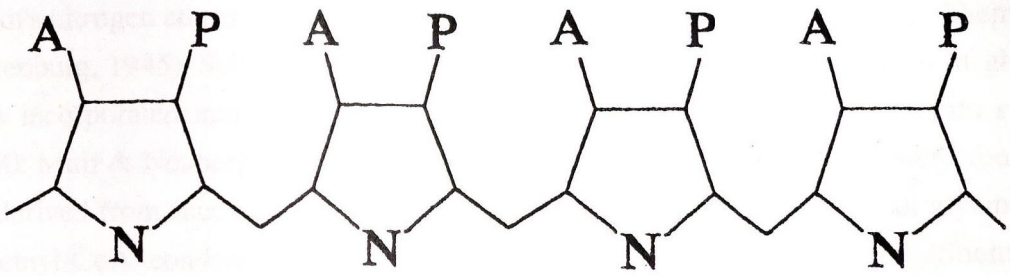

Figure 1.4. The Basic Structure of the Bilin Skeleton.
(Substituents derived from aetic acid are denoted by A; propionic acid side chains are denoted by P)

conjugated with two molecules of glucuronic acid, exported to the bile and passed through the intestine where intestinal flora bring about further reductions, producing colourless products such as the bilane urobilinogen. Reduction of the vinyl side chains of these linear tetrapyrroles to ethyls also occurs to give "meso" structures and these products are subsequently oxidised to the yellow-brown bilenes stercobilin and urobilin, which are largely responsible for the colour of urine.

1.2 Haem Biosynthesis.

The early use of isotopic tracers to elucidate metabolic pathways demonstrated that all of haem's nitrogen atoms and eight of the carbon atoms are derived from glycine (Shemin & Rittenburg, 1945). Subsequent experiments revealed that the C-2 carbon atom of glycine was incorporated into 8 of the positions in the haem macrocycle ring (Shemin *et al.*, 1950: Muir & Neuberger, 1950). The remaining 26 carbon atoms of haem were found to be derived from succinyl CoA (Gibson *et al.*, 1958) and it was proposed that glycine and succinyl-CoA condense together to form 5-aminolevulinic acid (5-ALA) (Shemin & Russell, 1953). The enzyme responsible for catalysing this condensation reaction, 5-aminolevulinic acid synthase (5-ALA synthase) was simultaneously described by Shemin and co-workers (Kikuchi *et al.*, 1958) in bacterial extracts and by Neuberger and his group in avian preparations (Gibson *et al.*, 1958). The enzyme has since been purified from a wide variety of sources. As the first enzyme of the pathway, 5-ALA synthase has been a major focus for attention in the study of the regulation of tetrapyrrole biosynthesis. It is now known that haem is an important regulator, acting as both a feedback inhibitor and also as a regulator at the transcriptional and translational level. In many anaerobic bacteria and in plants, 5-ALA is derived from the carbon skeleton of glutamate in what has been termed the C-5 pathway, discovered by Beale and Castelfranco (1974). Experiments with [^{14}C] glutamate in greening barley showed that it was incorporated into 5-ALA with the carbon skeleton intact, and with the C-1 of glutamate giving rise to the C-5 of 5-ALA (Kannangara & Gough, 1977).

The earlier stages of tetrapyrrole biosynthesis as far as the formation of uroporphyrinogen III are believed to be similar in all living systems and are summarized in Fig. 1.5. In the first stage, two molecules of 5-ALA condense to form the basic tetrapyrrole building block, porphobilinogen, in a reaction catalysed by 5-ALA dehydratase. Four molecules of porphobilinogen subsequently polymerise to form the highly unstable intermediate, preuroporphyrinogen. This tetrapolymerisation reaction is catalysed by porphobilinogen deaminase. Uroporphyrinogen synthase catalyses the cyclisation of preuro-porphyrinogen, with rearrangement of one of the pyrrole rings, the

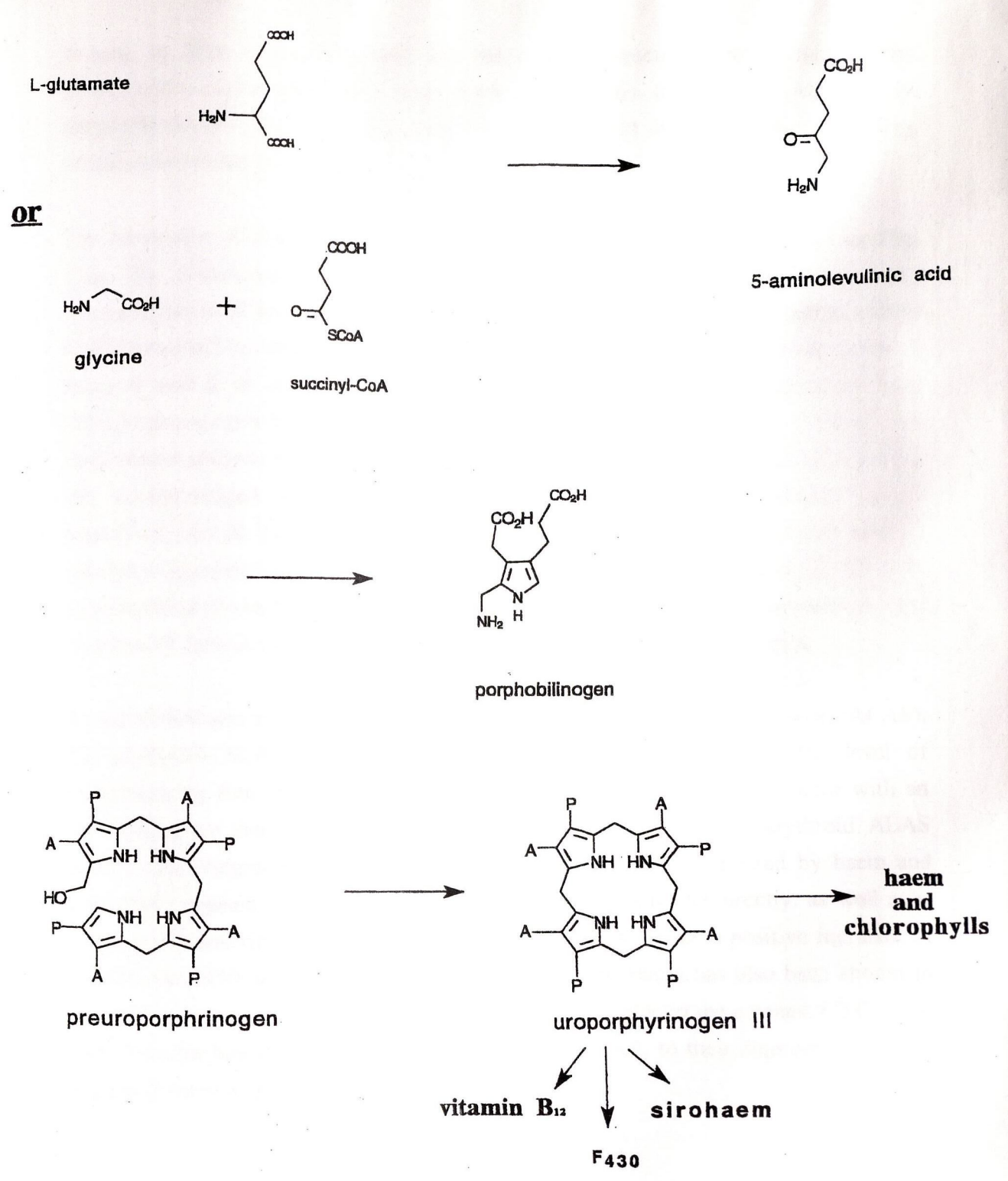

Figure 1.5. The Early Stages in the Tetrapyrrole Biosynthetic Pathway.

D ring, to form uroporphyrinogen III, the common precursor from which haems, chlorophylls, bacteriophylls and other cyclic tetrapyrroles are derived. Alternatively, uroporphyrinogen III may be methylated for transformation into sirohaem, vitamin B_{12}, or the nickel cofactor, F_{430}.

The conversion of uroporphyrinogen III to haem involves four enzymatic steps (see Fig. 1.6). The conversion of uroporphyrinogen III to coproporphyrinogen III occurs by decarboxylation of the acetate side-chains at positions 2, 7, 12 and 18 to methyl groups and is catalysed by uroporphyrinogen decarboxylase. The two propionate side chains in rings A and B of coproporphyrinogen III are subsequently decarboxylated to form protoporphyrinogen IX in a reaction catalysed by coproporphyrinogen III oxidase. The third and penultimate step of the pathway, involves the formation of the porphyrin from the porphyrinogen nucleus i.e. the conversion of protoporphyrinogen IX to protoporphyrin IX. The enzyme that catalyses this reaction, protoporphyrinogen oxidase, has been described in rat liver mitochondria (Sano & Granick, 1961) and bovine liver mitochondria (Porra & Falk, 1961). The final step in the haem biosynthetic pathway, the insertion of ferrous iron into protoporphyrin IX, is catalysed by ferrochelatase.

As mentioned above, haem negatively regulates the synthesis of ALA synthase (ALAS). The erythroid ALAS gene in developing erythrocytes is regulated at the level of translation, by iron levels, through the interaction of the iron-regulatory factor with an iron responsive element located in the 5'-untranslated region of the erythroid ALAS mRNA (Shoolingin-Jordon, 1994). Human liver ALAS is downregulated by haem and this control appears to occur by feedback inhibition of the enzyme directly, as well as at the level of transcription. In addition, haem has been shown to be a positive regulator of cytochrome P450 and haem oxygenase gene expression. Haem has also been shown to be involved in the transcriptional regulation of two yeast cytochrome *c* genes, CYC 1 and CYC 7 *via* the binding of the haem-activating protein, HAP, to their respective promoter regions (Lowry & Zitomer, 1988).

1.3 Haem Metabolism and Degradation.

1.3.1 Sources of Haem for Conversion to Bilirubin

The most useful method for quantifying haem turnover in mammals involves the administration of a radiolabelled precursor of haem, for example 5-[^{14}C]-aminolevulinic acid or 2-[^{14}C]glycine, and measurement of the label in excreted bilirubin or carbon monoxide. In the rat, the time course of haem breakdown indicates a sharp peak in

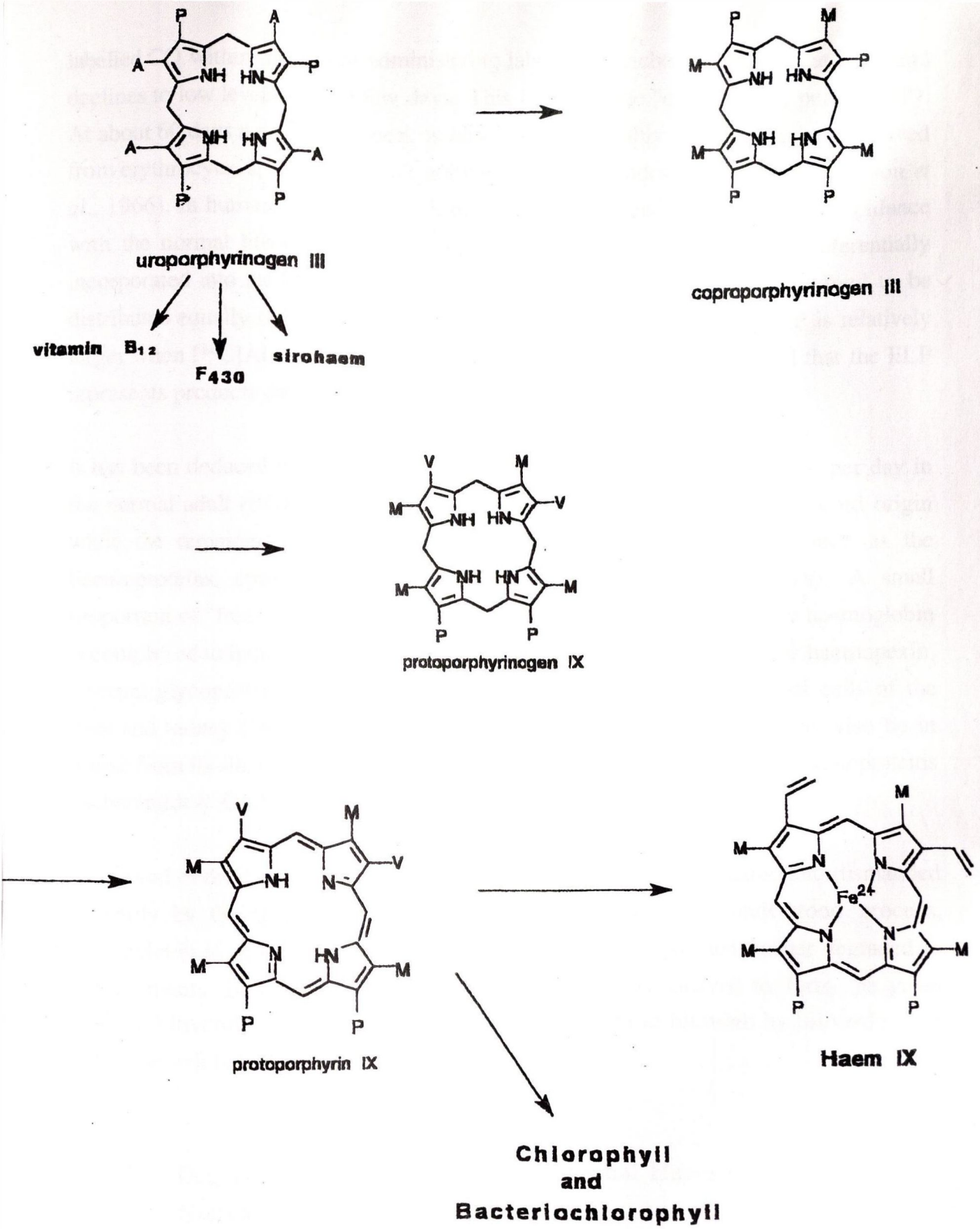

Figure 1.6. Conversion of Uroporphyrinogen III to Haem.

labelled CO within minutes of administering label, that reaches a maximum at 2 hrs and declines to low levels within a few days. This is termed the "early labelled peak" (ELP). At about 60 days a much larger peak is observed, presumably representing haem derived from erythrocytes at the end of their normal life-span (London *et al.*, 1950; Robinson *et al.*, 1966). In humans the second peak occurs at approximately 120 days, in accordance with the normal life-span of human erythrocyte (Lathe, 1972). ALA is preferentially incorporated into the haem of liver cells whereas administered glycine is assumed to be distributed equally into all haem pools (Robinson *et al.*, 1966). As the ELP is relatively larger when [^{14}C]ALA is used, rather than [^{14}C]glycine it can be concluded that the ELP represents products derived mainly from hepatic haem and haemoproteins.

It has been deduced that approximately 3.8 $mg.kg^{-1}$ of bilirubin is produced per day in the normal adult (Berk *et al.*, 1969). It is estimated that 70-80% is of erythroid origin while the remaining haem pool originates from non-erythroid sources such as the haemoproteins, cytochrome P450 and catalase (Granick & Beale, 1978). A small proportion of "free" haem and haemoglobin can be found in the serum. Free haemoglobin is complexed to hapatoglobin and free haem is carried by serum albumin or haemopexin, a serum glycoprotein. These complexes are processed by the parenchymal cells of the liver and kidney (Muller-Eberhardt, 1970). A small proportion of haem may also be in transit from its site of synthesis in the mitochondria to be incorporated into haemoproteins (Scharsmidt & Gollan, 1979).

At the end of their lifespan, erythrocytes are removed from the circulation and dismantled primarily by the spleen and liver sinusoidal cells. In a poorly understood process, haemoglobin is subject to proteolysis, releasing haem which is then further degraded to bile pigments. Both erythroid and non-erythroid haem are cleaved to form the green pigment biliverdin, the subsequent reduction of biliverdin to bilirubin by biliverdin-IXα reductase will be the focus of this study.

1.3.2 Degradation of Haem by the Microsomal Haem Oxygenase System.

The mechanism of haem degradation was originally believed to be a non-enzymatic event involving coupled oxidation of haem with ascorbate or possibly other endogenous reductants (Lemberg, 1956). It was proposed that as the reductant is oxidised, a methene bridge of the haem molecule is also oxidised and carbon monoxide is simultaneously released. As mentioned in Section 1.1., the bulk of naturally occurring haem is the form of protoporphyrin IX. Due to the asymmetric nature of the side chains, cleavage at the

different methene bridges (α, β, δ and γ) will give rise to four isomers of the linear tetrapyrrole biliverdin, denoted IXα, IXβ, IXδ and IXγ as shown in Fig. 5.1 (Chapter 5). Ascorbate served as a very effective electron donor for *in vitro* coupled oxidation experiments, however, non-enzymatic coupled oxidation of different haemoproteins resulted in a mixture of isomers, exclusively the -IXα isomer in the case of myoglobin and a mixture of both -IXα and -IXβ isomers in the case of haemoglobin (the results of these experiments are summarized in Table 1.1). In contrast, the bulk of naturally occurring biliverdin *in vivo* is predominantly the IXα isomer (O'Carra and Colleran, 1970a), therefore, suggesting the existence of a highly specific enzyme system capable of directing cleavage towards the α–methene bridge exclusively.

In 1968, Tenhunen *et al.*. reported a haem oxygenase (HO) activity in the microsomal fraction from liver, spleen and kidney. The enzyme catalysed the production of equimolar amounts of biliverdin IXα and CO from haem IX and is now known to be the rate-limiting enzyme in the catabolic pathway. In 1986, Maines *et al.* described the discovery of two forms of haem oxygenase designated HO-1 and HO-2 and recently this group has reported a third form (HO-3) (McCoubrey *et al.*, 1997). The stereospecificity of the biliverdin isomer produced by HO-3 is not known. The haem oxygenases are membrane bound proteins, but water-soluble catalytically active versions of rat and human HO-1 lacking the 23 carboxyl-terminal amino acid membrane anchor have been expressed in *E.coli* (Wilks, A. & Ortiz de Montellano, P.R., 1993). The HO-1 catalysed oxidation of haem involves sequential α-meso-hydroxylation, oxygen-dependent fragmentation of the α-meso-hydroxyhaem to verdoheme, and oxidative cleavage of verdohaem to biliverdin (Ortiz de Montellano, 1998; cited in Liu & Ortiz de Montellano, 1999) as summarised in Fig. 1.7. α-meso-hydroxylation proceeds *via* a P450 reductase-dependent reduction of the iron to the ferrous state, binding of oxygen to the reduced iron and a second one-electron reduction to the ferrous-dioxy complex. The resulting ferric peroxide complex undergoes electrophilic addition of the distal oxygen to the porphyrin ring to yield α-meso-hydroxyhaem. Verdohaem is subsequently produced *via* a series of as yet undetected intermediates. Fe^{3+}-verdohaem is reduced to Fe^{2+}-verdohaem, which upon binding of oxygen and transfer of a second electron is converted to the Fe^{3+}-biliverdin complex. One-electron reduction of the Fe^{3+}-biliverdin complex by P450 reductase is followed by release of the ferrous iron atom. Finally, the metal-free biliverdin dissociates from the enzyme.

Enzymatic oxidation by HO is selective for the α-methene bridge as demonstrated by Frydman *et al.* (1981) who reported that a large number of synthetic iron porphyrins with two vicinal propionic acid residues at C_6 and C_7 were enzymatically oxidised by a

SOURCE OF HAEM	BILIVERDIN ISOMER COMPOSITION			
	IXα	IXβ	IXγ	IXδ
Haem	31	24	24	21
Pyridine Haemochrome	32	25	23	20
haem-Albumin (Human)	28	21	31	20
Myoglobin	100	0	0	0
Microsomal Haemoprotein *	100	0	0	0
Haemoglobin (Human)	60	40	0	0
Catalase	48	52	0	0

Table 1.1 Methene Bridge Selectivity in the Coupled Oxidation of Various Haem Derivatives and Haemoproteins.

Adapted from O'Carra & Colleran, 1970b, who suggest that the identity of the microsomal haemoprotein (*) is cytochrome P450, or a derivative of it. The coupled oxidations of the various haems were carried out with ascorbate, except in the case of the microsomal preparations where NADPH (with or without ascorbate) was the most effective reductant. The isomer compositions are expressed as percentages.

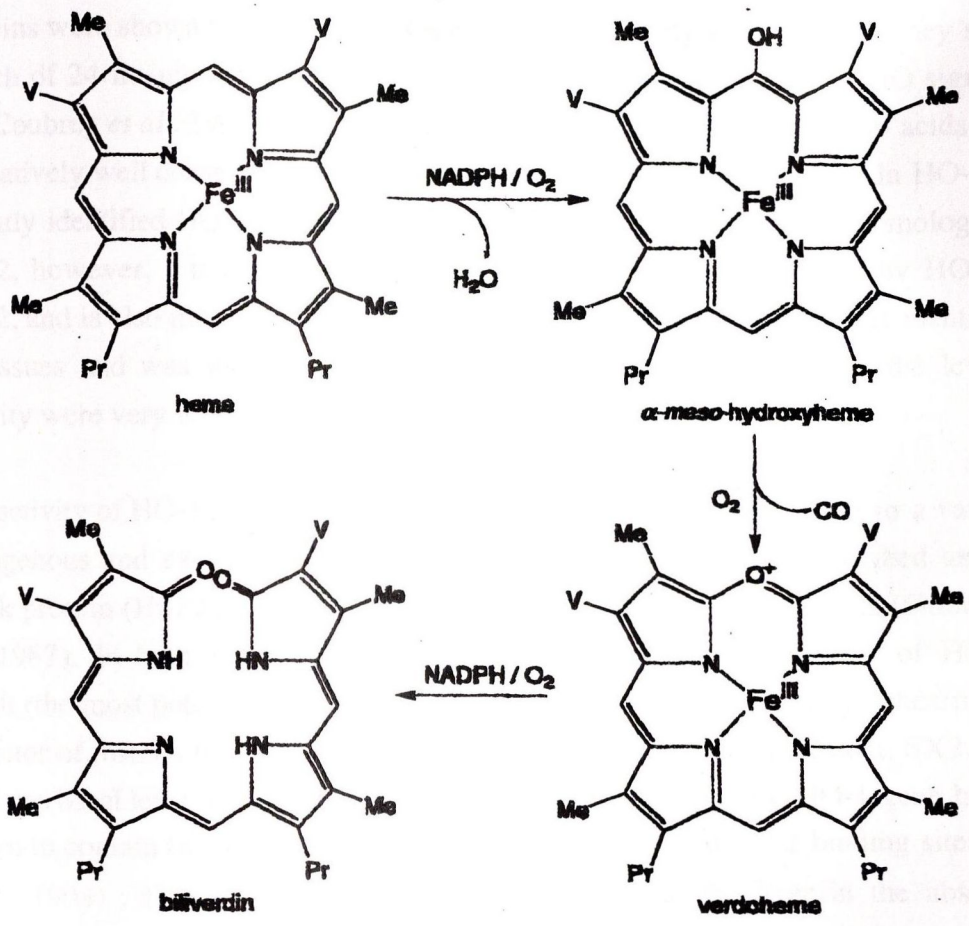

Figure 1.7. Reaction Intermediates in the Haem Oxygenase-Catalysed Oxidation of Haem to Biliverdin-IXα.

microsomal haem oxygenase preparation from the liver. Tomoro *et al.* (1984) studied structural requirements for the enzyme substrate and similarly found that the presence of two vicinal propionic acid side chains were necessary for substrate oxidation.

HO-1 and HO-2 do not share a high degree of amino acid sequence homology and both proteins were shown to be products of separate genes (Kutty *et al.*, 1994). They share a stretch of 24 mainly hydrophobic amino acid residues referred to as the "HO signature" (McCoubrey *et al.*, 1997). They also share a stretch of 21 N-terminal amino acids which is relatively well conserved, amino acids 67 to 88 in HO-1 and 86 to 107 in HO-2. The recently identified HO-3 (McCoubrey *et al.*, 1997) enzyme shares 90% homology with HO-2, however, it is missing the 21 amino acid region which is shared by HO-1 and HO-2, and is also missing the HO signature motif. The HO-3 transcript was identified in all tissues and was shown to possess haem degrading activity although the levels of activity were very low when compared with HO-1 and HO-2.

The activity of HO-1 can be upregulated as much as 100-fold in response to a variety of endogenous and exogenous factors and the enzyme has also been described as a heat shock protein (HSP32) since it's discovery in thermally stressed glial cells (Shibahara *et al.*, 1987). In both rat liver and avian hepatocyte cultures, the induction of HO-1 by cobalt (the most potent inducer of HO-1) was shown to be inhibited by cycloheximide, an inhibitor of mRNA translation (Maines, 1988). A 268 bp 5' distal fragment, SX2, which mediates basal level and inducer-dependent activation of the mouse HO-1 gene has been shown to contain two AP-1 binding sites aswell as NF-κB and AP-2 binding sites (Alam *et al.*, 1994) . HO-2 is the major form of HO found in the liver in the absence of inducers, whereas, HO-1 is the predominant form in the spleen.

1.3.3 Reduction of Biliverdin IXα to Bilirubin IXα.

In 1936, Lemberg and Wyndham observed that minced guinea-pig liver, to which biliverdin had been added, turned yellow. These workers proposed that the reaction was due to the action of non-specific dehydrogenases, however, Singleton and Laster (1965) later confirmed that the reduction of biliverdin to bilirubin was catalysed by a specific enzyme and that this activity was pyridine-nucleotide dependent. Some confusion arose with regards to cofactor requirement when they reported the activity to be mainly NADH-dependent whereas Tenhunen *et al.* (1970) later reported it to be NADPH-dependent. It is now known that biliverdin-IXα reductase is capable of utilising either NADH or NADPH as co-factor in the reduction process. The enzyme was purified from pig spleen (Noguchi *et al.*, 1979), ox kidney (Phillips & Mantle, 1981) and rat liver (Kutty and Maines, 1981)

and found to be a 34 kDa cytosolic monomer. When assayed with the four isomeric biliverdins that can be derived by cleavage of haem IX, biliverdin-IXα reductase showed a very clear cut, but not absolute, specificity for the α-isomer (Colleran & O'Carra, 1977), which is the most abundant isomer, physiologically. In 1994, Yamaguchi *et al.* reported the discovery of a biliverdin-IXβ reductase activity in human liver. Just as biliverdin-IXα reductase does not have an absolute specificity for the IXα isomer of biliverdin, biliverdin-IXβ reductase does not have an absolute specificity for the β-isomer. In this study, biliverdin-IXα reductase will be referred to as BVR-A and biliverdin-IXβ reductase will be referred to as BVR-B. The substrate specificity of both enzymes is discussed in more detail in Chapter 5.

BVR-A has been identified in most mammals and also some fish (Fang & Lai, 1987), however, the enzyme appears to be absent from birds, reptiles and amphibia. The tissues with highest BVR-A activity in most mammals are liver, spleen and kidney (Colleran & O'Carra, 1977), however, it has been observed that the relative distribution of BVR-A between these tissues varies greatly from species to species (Rigney *et al.*, 1988). Interestingly, BVR-A activity has been detected in tissues other than those obviously associated with haem degradation such as the lungs, brain, intestine and muscle (Tenhunen *et al.*, 1970a). BVR-A has also been reported in some micro-organisms and has recently been discovered in the cyanobacterium *Synechocystis* sp. PCC 6803 (Schluchter & Glazer, 1997).

BVR-A occurs as a cytosolic monomer of molecular weight 34 kDa in rat, pig and ox kidney (Kutty & Maines, 1981; Noguchi *et al.*, 1979; Phillips & Mantle, 1981). In 1992, Fakhrai *et al.* expressed and characterised the cDNA for rat kidney BVR-A and presented the nucleotide and deduced amino acid sequence. The open reading frame was found to encode a 295 amino acid protein. Maines and Trakshel (1993) went on to purify and characterise the human enzyme. The cDNA was subsequently cloned and found to encode a 296-amino acid protein. Both enzymes share common catalytic properties and although sequence divergence for short regions, such as the 11 carboxyl terminal amino acids can be as low as 45%, overall the predicted peptide and nucleotide sequences share 83% identity (Maines *et al.*, 1996). The human enzyme exhibits a slower mobility on SDS-PAGE, migrating as a 40 kDa protein. This difference in molecular weight has been attributed to differential post-translational modification (Maines *et al.*, 1996).

Maines *et al.*, (1996) have demonstrated that human BVR-A is a Zn-metalloprotein that contains one atom of zinc per enzyme molecule, and based on the primary structure of the enzyme, likely domains for zinc binding have been proposed. The structural basis of Zn binding is postulated to involve a cluster of Cys and His residues near the carboxy

terminus, as illustrated in Fig. 1.8. Atomic absorption spectroscopy demonstrated that the enzyme contained Zn at an approximate 1:1 molar ratio. Co-ordination with Zn was further substantiated by ^{65}Zn-exchange analysis of both the tissue purified enzyme and the recombinant enzyme expressed in *E.coli*. This association appears to be purely a structural feature and is not required for catalysis. Preliminary crystallisation of rat BVR-A has failed to detect any zinc (personal communication, Kikuchi) in the enzyme structure suggesting that this feature is species specific.

The gene encoding the human enzyme was found to be 12,270 bp in length, consisting of 5 exons and 4 introns (McCoubrey *et al.*, 1995). The gene lacked a conventional TATA box, however, an overlapping pair of TATA-like sequences were identified 80 nucleotides upstream from the start site. The promoter region was also found to contain binding sites for the well known regulatory factors AP-1, HNF-5 and INF-1. Meera-Khan *et al.*, (1983) reported the localisation of the gene for human BVR-A to chromosome 7.

The kinetics of BVR-A are complicated by profound substrate inhibition and the insolubility of the reaction product, bilirubin-IXα, in aqueous conditions. In 1942, Fischer and Plieninger succeeded in synthesizing bilirubin-IXα and presented the structure as shown in Fig. 1.9. The limited solubility of bilirubin-IXα in aqueous media is not predicted from the linear tetrapyrrole structure illustrated in Fig. 1.9 because of the presence of the propionate side chains. X-ray diffraction studies by Bonnett *et al.*, (1976) demonstrated that the tetrapyrrole exists as an involuted hydrogen-bonded structure in which the carboxyl groups of the propionic acid side chains are hydrogen bonded to the terminal pyrrole ring lactams. As a result, the ionisation of the two carboxyl groups is suppressed, accounting for the high pKa (7.95) and the water insolubility of bilirubin. Exposure to light produces forms of bilirubin that are more soluble and, as will be discussed shortly, this forms the basis of the therapy used to treat hyperbilirubineamia. Albumin binds to bilirubin, increasing it's aqueous solubility and has traditionally been included in the assay for BVR-A activity. Alternatively, a high pH may be used, however, both of these approaches complicate the analysis of results obtained. A more detailed introduction to the kinetic properties of BVR-A is provided in Chapter 4.

1.3.4 Biliverdin-IXβ Reductase (BVR-B).

The approximate ratio of biliverdin IX isomers in adult human bile is 95-97% IXα and 3-5% IXβ, however, at 20 weeks gestation the approximate ratio of isomers obtained from foetal bile is 6% IXα, 87% IXβ, 0.5% IXγ and 6% IXδ (Nakajima *et al.*, 1963). A 15-

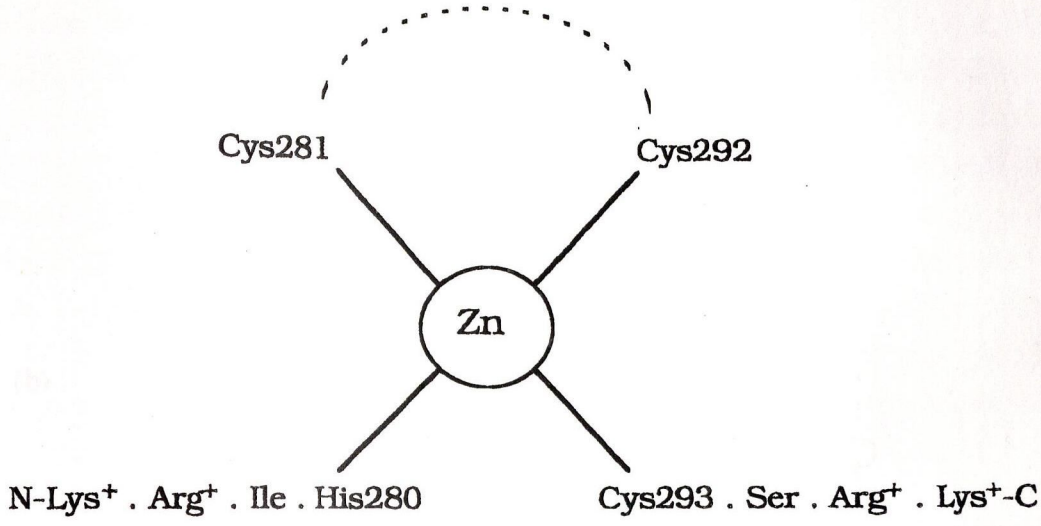

Figure 1.8. Possible Coordination Motif of Zn in the Carboxy-terminus of Human Liver BVR-A (adapted from Maines *et al.*, 1996).

(a)

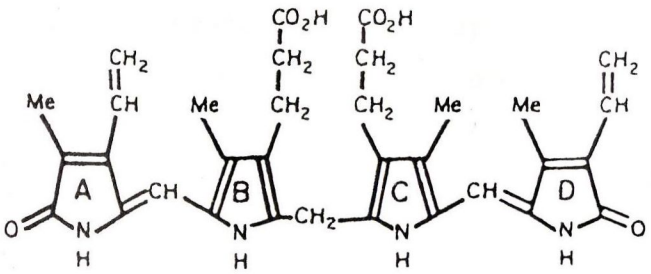

(b)

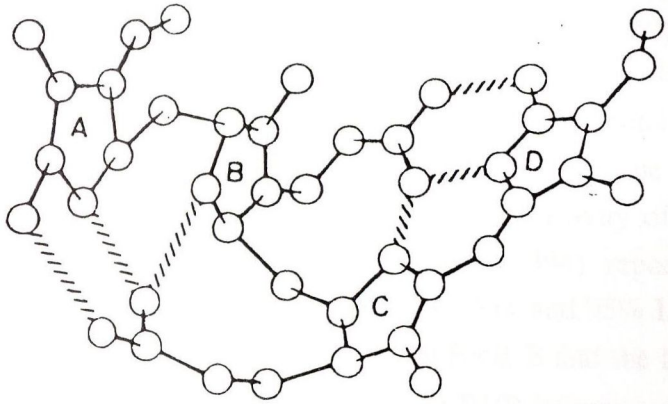

Figure 1.9.

(a) The unfolded or linear tetrapyrrole structure of bilirubin-IXα.

(b) The folded conformation of bilirubin-IXα showing extensive internal hydrogen bonding.

17 weeks, some bilirubin-IXα is present in the bile, but up to 22 weeks, the IXβ isomer predominates. In late foetal gestation, contrary to the decreased ratio of the IXβ isomer, the IXα isomer increases. Blumenthal *et al.* (1979) observed that the meconium of newborn babies contained significant amounts of bilirubin-IXβ. These facts suggested the presence of a biliverdin-IXβ reductase with specificity for biliverdin-IXβ and are consistent with the discovery of such an enzyme (Yamaguchi *et al.*, 1993). Two isozymes of BVR-B with a relative molecular mass of 21kDa were subsequently purified from human liver cytosolic fractions (Yamaguchi *et al*, 1994). BVR-B activity was considerably lower than BVR-A in the adult liver, however, in the foetal liver at 26 weeks gestation, the total activity of both BVR-A and BVR-B was approximately equal. BVR-B shares no sequence similarity with BVR-A, however, sequence data have revealed that human BVR-B and flavin reductase (FR) are identical enzymes (Shalloe *et al.*, 1996). Shalloe and coworkers demonstrated that purified bovine FR activity co-eluted with BVR-B activity. This purified bovine enzyme was a monomer with a molecular weight of approximately 23 kDa and a pI of 6.8 in 8 M urea. It exhibited FR activity of 240 nmol/min/mg, which is comparable to the value reported for the human enzyme (Yubisui *et al.*, 1979), and BVR-B activity of 160 nmol/min/mg compared with the value of 331 nmol/min/mg reported for human liver BVR-B (Yamaguchi *et al*,. 1994). The bovine enzyme was also shown to be incapable of reducing biliverdin-IXα. Once it became clear that BVR-B was in fact identical to FR a purely foetal role for this enzyme had to be ruled out. It was speculated that the BVR-B activity of the enzyme was utilized only in the foetus to any great extent, and that the FR activity of the enzyme became important after birth. However, Yamaguchi *et al.* (1994) reported that the approximate ratio of bilirubin isomers in erythrocytes is 5% IXα, and 95% IXβ, and that BVR-B is predominant in these cells. The exact function of BVR-B and the bilirubin-IXβ it produces, in erythrocytes is unknown. It is possible that BVR enzymes are present in erythrocytes to take part in the haem degradation that occurs when the erythrocytes are ingested by macrophages.

The function of mammalian flavin reductase is still not understood. The enzyme has been variously referred to as erthyrocyte NADPH dehydrogenase, diaphorase and methaemoglobin reductase. Under physiologiacal conditions FR does not act as a methaemoglobin reductase, however, supplementation with riboflavin during reoxygenation after ischaemia or hypoxia has been shown to have cardioprotective effects and this effect is thought to be mediated by flavin reductase (Mack *et al.*, 1995). It has also been demonstrated that pyrroloquinone quinone (PQQ) can act as a substrate for FR with a K_m of 2 μM and provides the same protection against reoxygenation injury *in vitro* as that seen with riboflavin administration (Xu *et al.*, 1993). Whether or nor PQQ is a

physiologically significant substrate has yet to be proven. FR from many bacterial species have been identified with functions relating to bacterial bioluminescence, chorismate synthesis and iron metabolism. Flavin reductases isolated from other species are associated with various proteins and appear to simply provide these proteins with reduced flavins.

1.3.5 Conjugation of Bilirubin by UDP-Glucuronyl Transferase.

After production in peripheral tissues, bilirubin is transported in the blood complexed with serum albumin (K_d approximately 10^{-8} M). In the liver, dissociation from albumin occurs, followed by transfer into hepatic parenchymal cells by what is believed to be a carrier-mediated active transport across the sinusoidal membrane. Once inside the liver, bilirubin is tightly (although reversibly) bound to soluble proteins such as ligandin (now known to be alpha class members of the glutathione-S-transferase supergene family, Hayes *et al.*, 1981) and Z protein. Inside the hepatocytes, the microsomal enzyme bilirubin UDP-glucuronyl transferase (bilirubin UGT-GT) catalyses the formation of bilirubin monoglucuronide. A second glucuronide is then added to form bilirubin diglucuronide at a plasma membrane site (Jansen *et al.*, 1977). Approximately 90% of the glucuronides produced are the diglucuronide form while the monoglucuronides account for the remaining 10%. Once secreted into the upper small intestine, bilirubin glucuronides are hydrolysed by the action of β-glucuronidase and the resulting bilirubin is then reduced by the anaerobic intestinal flora to form a group of three colourless tetrapyrroles, collectively called urobilinogens. The three bilirubin reaction products, stercobilinogen, mesobilinogen and urobilinogen, contain saturated methene bridge carbons. In the lower intestinal tract, the three urobilinogens spontaneously oxidase at the central methene bridge to produce the corresponding bile pigments, stercobilin, mesobilin and urobilin, which are orange-brown in colour. A summary of the haem catabolon is provided in Fig. 1.10.

1.4 Disorders Related to Haem Degradation.

A delay in the expression of UDP-glucuronyl transferase occurs in many newborns particularly premature infants and can lead to an increase in the level of unconjugated bilirubin in the plasma such that it exceeds the binding capacity of serum albumin. The condition referred to as hyperbilirubinaemia or yellow jaundice occurs in 30% - 50% of term neonates and it is estimated that approximately 10% will require treatment (Kivlahan & James, 1984). Bilirubin accumulates in the circulation and extravascular tissues until

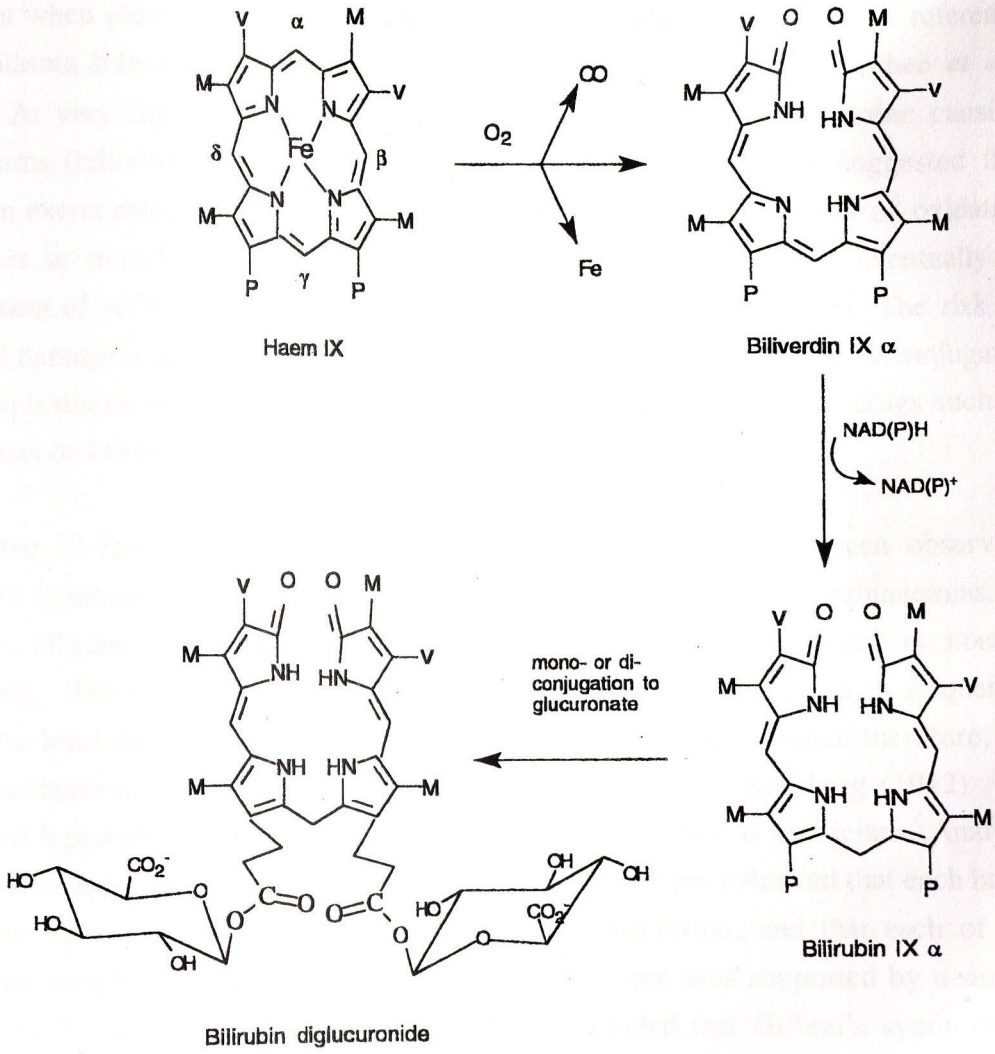

Figure 1.10. The Fate of Haem in Mammals.
Methyl, vinyl and propionate groups are denoted by M, V and P, respectively.

the hepatic system for conjugating and excreting bilirubin becomes fully functional, which usually occurs during the first week after birth. In most cases phototherapy is sufficient to maintain acceptable levels of bilirubin (bathing the infant under a lamp converts bilirubin to a more soluble isomer that can be readily excreted), however, in more severe cases an exchange transfusion may be required. The condition becomes apparent when plasma bilirubin concentrations exceed 35μM, twice the upper reference limit (plasma bilirubin concentrations of 250μM are not uncommon (McPhee *et al.*, 1996). At very high levels, bilirubin may traverse the blood-brain barrier causing kernicturus (bilirubin staining of the basal ganglia of the brain). It is suggested that bilirubin exerts cytotoxic effects in the kernicteric brain through inhibition of oxidative processes in mitochondria thereby diminishing ATP levels and leading eventually to impairment of ATP-dependent cerebral metabolism (Menken *et al.*, 1996). The risk of cerebral damage is increased if plasma albumin concentrations are low or if unconjugated bilirubin is displaced from binding sites by high levels of free fatty acids or drugs such as salicylates or sulphonamides.

A number of hereditary disorders of bilirubin metabolism have also been observed. Gilbert's Syndrome is the most common of the unconjugated hyperbilirubinaemias. In general, bilirubin levels are only slightly elevated and life expectancy is normal (Sherlock, 1968). Because the concentration of bilirubin in the plasma is frequently below the level that causes clinical jaundice, many cases go unrecognised, therefore, the exact incidence in the general population is unknown, although Kornberg (1942) has observed 8 probable cases in a group of 100 medical students and physicians. Analysis of the genes for bilirubin-UGT in six Gilbert's Syndrome patients showed that each had a missense mutation, caused by a single nucleotide substitution, and that each of the mutations were heterozygous (Aono *et al.*, 1995). This work was supported by a similar finding by Koiwai *et al.*(1995) and both groups concluded that Gilbert's syndrome is inherited as a dominant trait. Bosma *et al.*, 1995 found that reduced expression of bilirubin UDP-glucuronyltransferase 1, due to an abnormality in the promoter region of the gene, appears to be necessary for Gilbert's Syndrome but not sufficient for complete manifestation of this disease.

Crigler-Najjar Syndrome(CNS) is a rare genetic disorder involving severe unconjugated hyperbilirubinaemia (Crigler & Najjar, 1952). The disease is classified into two subtypes: Type I CNS is caused by a complete lack of UDP-GT activity whereas Type II CNS arises as a result of reduced but measurable UDP-GT activity in the liver (Seppen *et al.*, 1994). The latter usually has a benign prognosis, however, patients with Type I CNS usually die in infancy due to the development of kernicteris. Goresky *et al.* (1978) found that in the bile-containing duodenal aspirates of patients with Gilbert's Syndrome, the

average proportion of bilirubin found as bilirubin diglucuronide was 68% (normal 88%) and that of bilirubin monoglucuronide was 23% (normal 7%). The deviation of the bilirubin conjugates from the normal pattern was even greater in patients with Type II CNS. Only 10% of the glucuronide was found in the diglucuronide form, while 90% was in the form of bilirubin monoglucuronide (Gordon *et al.*, 1976).

The human UGT 1 gene complex (UGT 1A - UGT 1M) encodes two bilirubin-like and eight phenol transferase enzymes, however, only bilirubin UDP glucuronyltransferase 1 (HUG Br 1) is physiologically relevant in bilirubin glucuronidation in man (Bosma *et al.*, 1994). A deletion in the exon 1 for the UGT 1A gene in a Type I CNS patient has been identified (Aono *et al.*, 1994). The disease is closely mimicked in a strain of jaundiced, genetically inbred rats, known as Gunn rats (Gunn, 1938). The Gunn rat is a mutant strain of the Wistar rat that exhibits unconjugated hyperbilirubinaemia as a result of a defect in hepatic bilirubin UDP-GT (Weatherill *et al.*, 1980). Askari *et al.* (1995) have succeeded in carrying out retrovirus-mediated expression of HUG Br 1 in Type I CNS human fibroblasts, and correction of the genetic defect in Gunn rat hepatocytes.

Dubin-Johnson and Rotor syndromes occur as a result of elevated levels of conjugated bilirubin. In this case, biliary excretion mechanisms are effected. The syndromes are rare and usually benign and both involve excretory defects for several organic anions (Schmid, 1972). In Dubin-Johnson syndrome, the liver is pigmented and may appear black on biopsy. The Rotor syndrome is a similar condition, but the liver pigmentation is absent. Both MRP1 and MRP2 are involved in the transport of bilirubin diglucuronides as a well as a number of other organic anions, therefore, differential expression of the two isoforms may explain the differences observed between the two syndromes.

Acquired abnormalities of bilirubin excretion occur as a result of excessive haemolysis or hepatocellular damage due, for example, to hepatitis or cirrhosis. In the majority of cases both conjugated and unconjugated fractions of bilirubin are elevated.

1.5 Physiological Significance of Haem Degradation.

The precise mechanism of cellular bilirubin toxicity in still uncertain, but may include selective interference with energy metabolism, protein synthesis and carbohydrate metabolism with the target cell. It has puzzled researchers for many years as to why the potentially cytotoxic bilirubin metabolite is produced from the non-toxic precursor biliverdin. Indeed, the end product of haem metabolism in birds, amphibians and reptiles is biliverdin which is excreted directly into the bile. An earlier suggestion was that the

reduction of biliverdin to bilirubin may be necessary for placental transfer of haem catabolites from the foetus, however, the discovery of BVR-A in non-placental animals such as fish and marsupials suggested some other function for bilirubin. It was suggested during the 1950s (Bernhard *et al.*, 1954; Beer & Bernhard, 1959) that biliverdin and bilirubin may protect vitamin A and linoleic acid from oxidative destruction in the intestinal tract. This suggestion was plausible given the extended system of conjugated double bonds within the tetrapyrrole structure. Stocker *et al.*, (1987b) proposed that one beneficial role of bilirubin may be to act as a physiological antioxidant and demonstrated that, at micromolar concentrations, bilirubin could efficiently scavenge peroxyl radicals generated chemically *in vitro*.

Indeed, reactions of bilirubin involving free radicals or toxic oxygen reduction products have been well documented. Unconjugated bilirubin scavenges singlet oxygen with high efficiency (Stevens & Small, 1976), reacts with superoxide anion (Kaul *et al.*, 1979) and peroxyl radicals (Stocker *et al.*, 1987a) and serves as a reducing substrate for peroxidases in the presence of hydrogen peroxide or organic hydroperoxide (Broderson & Bartels, 1969; Jacobson & Fedders, 1970). Investigations have also been carried out on conjugated forms of bilirubin. Stocker *et al.* (1987c) showed that bilirubin ditaurine (BR-DT; a commercially available model compound of conjugated bilirubin), even at concentrations well below those of conjugated bilirubin in human bile, efficiently scavenges peroxyl radicals, thereby preventing lipid peroxidation. Stocker *et al.* (1987a) have also investigated the antioxidant properties of albumin-bound bilirubin (Alb-BR) towards chemically generated peroxyl radicals and have found that Alb-BR efficiently inhibits the peroxyl radical-induced oxidation of albumin-bound fatty acids.

These observations have been supported by the more recent finding that bilirubin inhibits the oxidation of low density lipoprotein more efficiently than Trolox. Neuzil and Stocker (1994) have suggested that this antioxidant activity is likely to be due to an interaction of bilirubin with α-tocopherol (TOH), the biologically most active form of Vitamin E. In order to be an efficient antioxidant, TOH requires a suitable co-antioxidant which prevents the adverse effects of the tocopherol radical ($TO^{\bullet}$) by scavenging it and exporting it from the LDL particle. Given that oxidised lipids and lipoproteins are known to be atherogenic, low serum bilirubin concentrations may be associated with increased risk of coronary heart disease. Schwertner *et al.*, (1994) have noted a statistically significant inverse association between serum total bilirubin and CHD. The strength of this association was similar to that of smoking or high blood pressure. Heyman *et al.*, (1989) reported that hyperbilirubinaemic pre-term infants developed retinopathy of prematurity (ROP) less frequently than pre-term infants with normal levels of plasma bilirubin, and suggested that bilirubin has a protective effect on the development of ROP,

serving as a physiologic chain breaking antioxidant.

It is worth noting that haem oxygenase, the rate limiting enzyme of haem catabolism, is known to be induced by a variety of agents capable of causing oxidative stress. Yamaguchi *et al.* (1995) have published findings suggesting that bilirubin is oxidised in rats treated with endotoxin and that this acts as a physiological antioxidant, synergistically with ascorbic acid *in vivo*.

A Chinese report on traditional oriental medicine revealing that animal biles can be used in the treatment of bronchitis, asthma and other hypersensitivities prompted an investigation into the anti-inflammatory activities of biliverdin, the major bile pigment in chicken bile. Nakagami and co-workers (1993) subsequently demonstrated that biliverdin inhibited complement cascade reactions *in vitro* at the C1 step in the classical pathway. Conjugated bilirubin was also shown to have an inhibitory effect on complement dependant reactions, therefore, it has been proposed that bile pigments serve as endogenous tissue protectors not only in their antioxidant properties but also *via* their anti-complement activities.

The formation of biliverdin by haem oxygenase is the only known biological source of carbon monoxide (CO) which has recently been proposed to act as a neurotransmitter in a manner analogous to nitric oxide (NO). The mRNA encoding HO-2 was found to co-localize in the brain with the mRNA for soluble guanylyl cyclase and zinc protoporphyrin-IX, a potent inhibitor of HO, was shown to deplete endogenous guanosine 3', 5'-monophosphate (cGMP) (Verma *et al.*, 1993). In addition, carbon monoxide, like nitric oxide, was shown to modulate the secretion of corticotrophin-releasing factor (CRF) from rat hypothalamic cell cultures (Parkes *et al.*, 1994). Treatment of these cultures with either gaseous CO or 100 μM hematin (a precursor of CO) resulted in a two-fold increase in CRF levels. In addition, zinc-protoporphyrin-IX decreased CRF secretion in a dose-dependent manner. Hematin (100 μM) was also shown to stimulate the release of gonadotrophin-releasing hormone up to four times above control levels and this effect was again inhibited by zinc-protoporphyrin-IX (Lamar *et al.*, 1996).

Phelan *et al.* (1998) have recently presented evidence indicating that both bilirubin and biliverdin act as endogenous ligands for the aryl hydrocarbon receptor (AhR). This ligand dependent transcription factor mediates many of the biological and toxicological actions of 2,3,7,8-tetrachlorodibenzo-*p*-dioxin (TCDD) and related chemicals. Persistent expression of hepatic CYP1a1/2 (an AhR-dependent response) in congenitally jaundiced Gunn rats prompted investigators to evaluate whether biliverdin and bilirubin are endogenous AhR agonists. Biliverdin and bilirubin not only stimulated AhR

transformation and dioxin-response-element (DRE) binding *in vitro* and in cells in culture, they also exhibited competitive inhibition of [^{3}H]TCDD-specific binding to the Ah receptor. Only a slight elevation in Cyp1a1 gene expression was seen with 10 μM bilirubin, whereas, a 15-fold increase was observed in the presence of 100 μM bilirubin. They concluded from their results that jaundiced Gunn rats lacking the ability to conjugate bilirubin could excrete it in a different form produced by the action of Cyp1a1 and Cyp1a2. It had previously been shown that injection of the dimethyl ester of bilirubin into Gunn rats resulted in the prompt excretion of polar conjugates of this dimethyl ester. These conjugates were identified as epoxide-derived glutathione conjugates and it was predicted that the initial epoxide formation was catalysed by cytochrome P450. It was subsequently observed that pre-treatment with TCDD resulted in a six-fold increase of the biliary excretion of these glutathione conjugates. It could be envisaged that this alternative bilirubin disposal pathway only becomes active in conditions of hyperbilirubinaemia where serum rubin concentrations can reach as high as 500 μM.

In an animal model of inflammation (induced by injection of carageenin), upregulation of HO-1 resulted in a striking suppression of the inflammatory response (Willis *et al.*, 1996) whereas inhibition of HO-1 led to a potentiation of the inflammatory response. The factor responsible for mediating this effect has not been identified, however, AhR ligands are known to exert immunosuppressive effects, therefore, it may be possible that the haem catabolites are modulating the immune response through direct interaction with the AhR. This aspect of haem catabolism is discussed further in Chapter 6.

The majority of iron for essential mammalian processes is provided through reutilization from existing body stores, of which about 70% is maintained within haemoglobin. The dissociation of iron from haem moieties and subsequent cellular release is therefore a major component of iron homeostasis. Poss & Tonegawa (1997) have generated mice lacking functional HO-1 (*Hmox1*$^{-/-}$) in order to assess it's participation in iron reutilization. *Hmox1*$^{-/-}$ mice developed both serum iron deficiency and pathological iron-loading, indicating that HO-1 is crucial for the normal recycling of iron during haem degradation. A second HO-1-independent pathway of haem catabolism which shuttles liberated iron to intracellular stores such as ferritin was proposed, an obvious candidate being HO-2, however, the same group showed that HO-2-deficient mice showed no iron metabolism disorders. The recently described HO-3 (McCoubrey *et al.*, 1997) may be a possible candidate, however, appointment of such a role awaits full characterisation of this enzyme.

1.6 Proposed Study.

There are a number of crystal structures available for tetrapyrrole binding sites on proteins including haemoglobin, myoglobin, cytochrome c and catalase. To date no information has been documented regarding the three-dimensional structure of BVR-A. To this end, it is proposed to develop an expression system for human BVR-A in order to facilitate detailed kinetic and structural studies. The purified hBVR-A will be made available to Dr. Darren Thompson, University of Southampton, for use in a subsequent crystallography study. With this in mind, it is also proposed to determine the stereospecificity of NADH oxidation, as this should provide useful predictive information when examined in the context of the crystallographic data. An attempt will also be made to crystallize BVR-A from the cyanobacteria *Synechocystis* sp. PCC 6803. Information regarding the structure of both proteins should contribute to knowledge of the evolutionary biology of biliverdin reduction.

The discovery of a second biliverdin reducing enzyme (BVR-B) and its identity with flavin reductase suggests that a broader approach is required in future studies on haem cleavage and in the subsequent reduction of the biliverdin isomers produced. A study on the specificity of the tetrapyrrole substrate for human BVR-A and human BVR-B using a series of synthetic biliverdin substrates that have been prepared by Dr. David Lightner, University of Nevada, should define structure-activity relationships that will allow the development of models for the active sites of the two enzymes.

It is now accepted that upregulation of haem oxygenase affords protection through several mechanisms, including production of the antioxidants biliverdin and bilirubin, depletion of the oxidant haem and regulation of vascular tension through carbon monoxide generation. It has also been suggested that both biliverdin and bilirubin are modulators of the immune system. The discovery that the IXα isomers of biliverdin and bilirubin are ligands for the aryl hydrocarbon receptor lends support to this hypothesis as AhR ligands are known to have immunosupressive effects. An attempt will be made to further investigate the physiological significance of the AhR activation by these haem catabolites.

Chapter 2

Materials & Methods

2.1. MATERIALS

Biochemical reagents and chemicals used were of analytical grade, where possible, and were obtained from BDH, Riedel-de Haen and Sigma. The names and addresses of all suppliers can be found in the Appendix.

Materials	Source
Agarose (Mol. Biol. Grade)	Promega
Agarose Gel DNA Extraction Kit	Boehringer
Alcohol Dehydrogenase (from yeast)	Sigma
Ampicillin, sodium salt	Sigma
ATTO Crosspower 500 Power Pack	ATTO Corporation
ATTO mini-gel apparatus, models AE-6100 and AE-6450	ATTO Corporation
Benchtop Microfuge E	Beckman Instruments
Bilirubin-IXα	Sigma
Bovine Serum Albumin (fraction V, 96-99% albumin)	Sigma
4-Chloronapthol	Sigma
Culture Media	Difco Laboratories
DEAE-Cellulose 52	Whatman
Dimethylsulphoxide	BDH

DNA Molecular Weight Marker VII (*SPP1* DNA cut with *Eco R1*)	Boehringer Mannheim
DNase I	Boehringer Mannheim
dNTPs; 40μmoles each	Promega
Folin and Ciocalteau's phenol reagent	BDH
Frac-100 Fraction Collector	Pharmacia
Freund's Adjuvant, complete	Sigma
Freund's Adjuvant, incomplete	Sigma
Geneclean II Kit	BIO 101
Kodak X-omat film	Kodak
Lysozyme	Sigma
MiniCycler PTC-100	MJ Research, Bio-Sciences
3-[N-Morpholino]propane sulphonic acid (MOPS, free acid)	Sigma
β-Nicotinamide adenine dinucleotide, reduced form (β-NADH, Grade III, disodium salt)	Boehringer Mannheim
NAD^+	Boehringer Mannheim
NADP	Boehringer Mannheim
NADPH, tetrasodium salt	Boehringer Mannheim
Nalgene Syringe Filters	Nalgene Company
Nitrocellulose, "Bioblot-NC"	Costar

Oligonucleotide primers	MWG Biotech, U.K.
Pharmacia LKB.REC101 Chart Recorder	Pharmacia
Phenol (AnalaR Grade)	BDH
Phenol:Chloroform:Isoamyl Alcohol [25:24:1 (v/v/v/)]	Sigma
Prestained Molecular Markers, SDS-7B	Sigma
Prestained Protein Markers, 7707S	New England Biolabs
RC-5B Refrigerated Superspeed Centrifuge	Du Pont Instruments
Restriction enzymes	Promega, New England Biolabs
RNase A	Boehringer Mannheim
SDS Molecular Weight Markers, MW-SDS-70L	Sigma
Semi-Phor (semi-dry blotting unit) Model no. TE70	Hoefer Scientific Instruments
Soniprobe Type 7532A	Dawe Instruments Ltd.
T4 DNA Ligase	Promega
Taq Dna Polymerase	Promega
Techne Dri-Block BD-3	Techne
Talon Metal Affinity Resin	Clontech
Thrombin, from human plasma, (lypophilized powder)	Sigma
Unicam 8625 UV/Vis Spectrophotometer	Unicam

2.2. METHODS.

2.2.1. Bacterial Strains, Plasmid Vectors and Culture Media.

The pGEX-KG expression vector (Fig. 2.1) used for the high level expression of cDNAs as fusion proteins was designed by modification of the commercially available vector pGEX-2T (Pharmacia). The cDNA encoding *Schistosoma japonicum* glutathione-S-transferase was engineered into the vector immediately preceeding the multiple cloning site. Proteins of interest are expressed fused to the carboxyl-terminus of the GST moiety and can therefore be affinity purified using glutathione Sepharose 4B. The affinity tag is subsequently removed following cleavage with the proteolytic enzyme thrombin. The vector contains the *tac* promoter for inducible expression and also the laqI^q gene for host independence (Guan & Dixon, 1991).

The vector series pTrcHis A, B and C is derived from pSE420 (Fig. 2.2) and is designed for the expression of proteins as hexahistidine fusions. The N-terminal leader peptide, consisting of six histidine residues in tandem, is derived from the bacteriophage T7 gene 10. Expression in this case is driven by the *trc* promoter which is also controlled by the laqI^q region on the plasmid. Purification is based on the interaction between electropositive transition metals, including Co^{2+},Ni^{2+}, Cu^{2+} and Zn^{2+} and the electron rich histidine residues. Both plasmids confer resistance to 100 μg/ml ampicillin.

Culture media (Luria-Bertani broth and Luria Bertani medium) was made up according to the methods described in Sambrook *et al.* (1989) and selective components were added as required. Stock solutions of ampicillin, lysozyme and isopropyl-β-thiogalactoside were filter sterilised and stored at -20°C. Bacteria were re-plated from single colonies every 4 to 5 weeks and stocks were maintained at -70°C in 15% glycerol. The genotypes of the *E.coli* storage and expression strains are listed in Table 2.1.

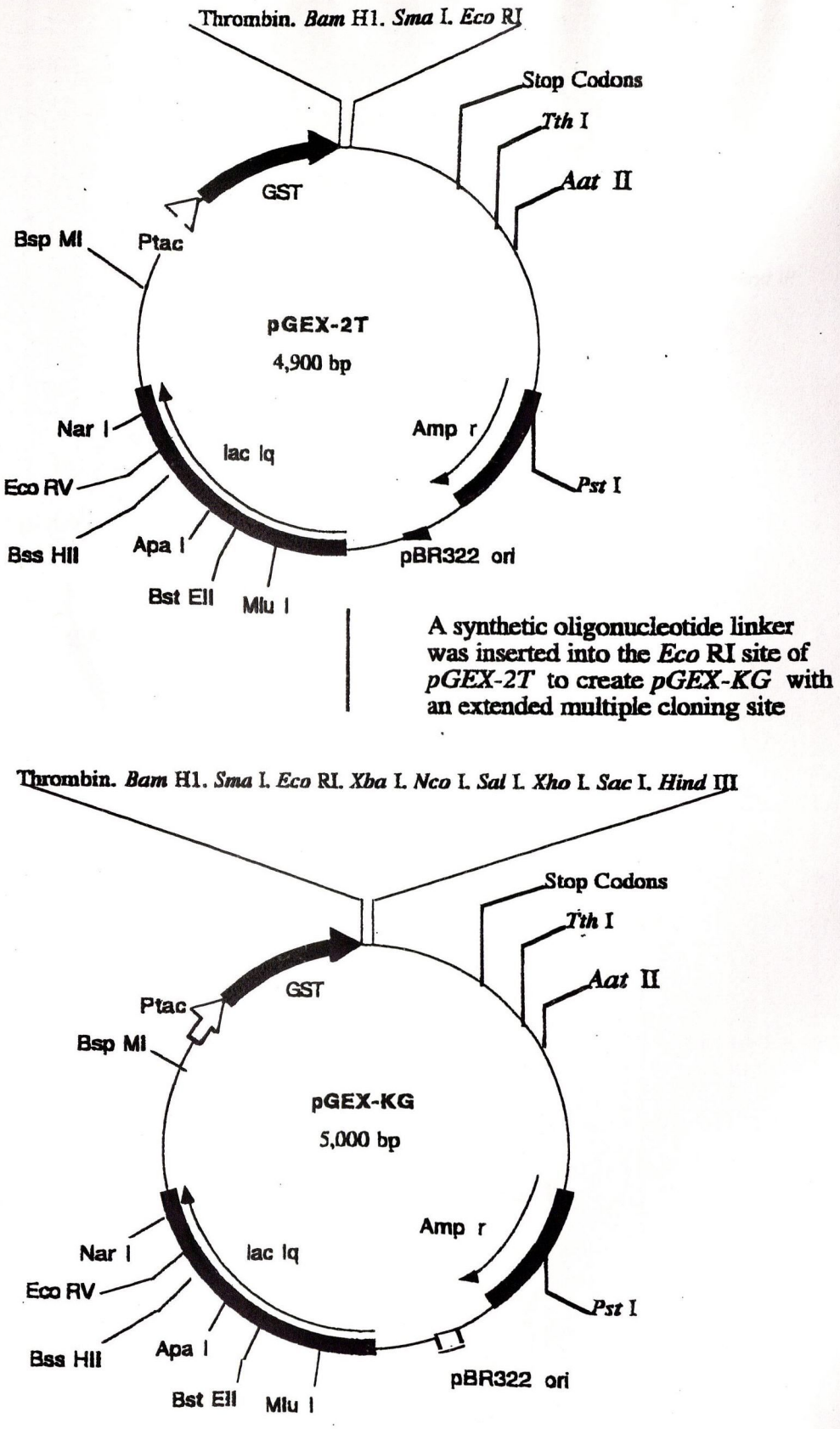

Figure 2.1. **Construction of the pGEX-KG Expression Vector.**
(from Guan & Dixon, 1991)

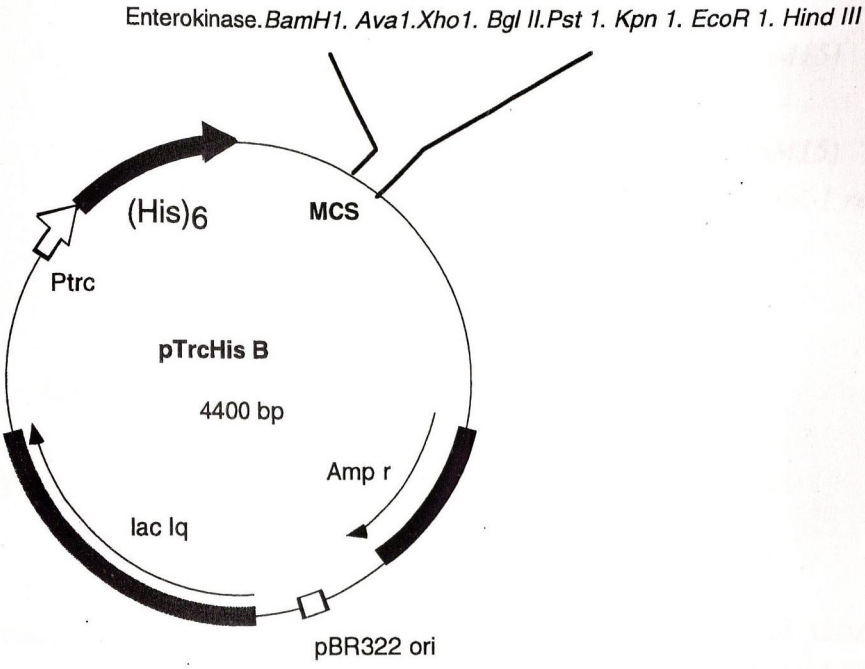

Figure 2.2 Expression Vector pTrcHis B.

Table 2.1. Genotypes of *E.coli* Strains used for the Storage and Propagation of Expression Vectors.

Strain	Genotype
TG1	*supE hsdΔ5 thi Δ(lac-proAB) F'[traD36 proAB+ lacIq lacZΔM15]*
DH5α	*supE44 ΔlacU169 (Ø80 lacZΔM15) hsd R17 recA1 endA1 gyrΔ96 thi-1 relA1*

2.2.2. Genetic Manipulation Techniques.

2.2.2 (a) Extraction and Purification of DNA fragments from agarose gels.

Restriction endonuclease digested DNA fragments were electrophoresed through 1% agarose gels in Tris-acetate electrophoresis buffer. The DNA was visualised under ultraviolet light following staining with ethidium bromide for approximately ten minutes. Digested fragments were purified using an agarose gel DNA extraction kit (Boehringer Mainheim). The bands of interest were excised using a sterile razor blade and transferred to preweighed reaction tubes. Solubilisation buffer was added at 300 µl for every 100 mg of agarose. Approximately 40 µl of resuspended silica solution was added to the tube and the mixture was incubated for 10 minutes at 56°C with intermittent vortexing. The silica beads and bound DNA were pelleted by centrifugation at maximum speed for 30 seconds. The supernatant was discarded and the DNA containing matrix was resuspended with 500 µl of nucleic acid binding buffer and centrifuged as before. The supernatant was again discarded and the matrix was resuspended with 500 µl of wash buffer. Having repeated this step once any remaining liquid was removed from the tube which was then left to dry at room temperature for 15-30 minutes. The bound DNA was eluted from the matrix with 50 µl of TE (10 mM Tris-HCl; 1 mM EDTA, pH 8). The mixture was vortexed and incubated at 56°C for 10 minutes. Following centrifugation for 30 seconds, the DNA containing solution was transferred to a new reaction tube for further manipulation.

2.2.2 (b) Purification of DNA Fragments using the High Pure PCR Product Purification Kit.

The High Pure PCR Product Purification Kit (Promega) is designed for the direct isolation and concentration of PCR products from amplification reactions. In this case a filter-tube unit incorporating a glass fiber fleece is used as a means of binding the DNA fragments and the electrophoresis step is omitted. This kit was also used for the purification of restriction endonuclease digested plasmid DNA with high recovery yields.

DNA binding buffer was added directly to PCR or restriction digest reactions at 500 µl for every 100 µl of reaction mixture. The *High Pure* filter tube was attached to the collection tube and the solution was transferred to the upper resevoir. The mixture was centrifuged at maximum speed for 30 seconds and the flow through discarded. An equal volume of wash buffer was added to the filter tube and centrifuged for 30 seconds. Wash buffer was added for a second time at a reduced volume to ensure optimal purity and the flow through was again discarded following centrifugation. The filter tube was then attached to a clean 1.5 ml reaction tube and 50 µl of distilled water was added in order to elute the DNA from the glass fiber fleece.

2.2.3. Purification of Plasmid DNA.

2.2.3 (a) Large Scale Purification from *E.coli.*

Cells were incubated overnight in 125 ml (x2) of LB broth (containing 100 µg/ml ampicillin), at 37°C and 280 rpm in an orbital shaker. The cells were harvested by centrifugation at 5000 x g for 15 minutes and the pellet was resuspended in 6 ml of freshly prepared TES-sucrose solution [20% (w/v) sucrose in 40 mM Tris-HCl, pH 8; 6 mM EDTA] to which lysozyme had been added at a final concentration of 2 mg/ml. Following a ten minute incubation on ice the pH was raised with the addition of 200 mM NaOH and 1% SDS. The lysate containing the denatured plasmid and chromosomal DNA was incubated on ice for a further 10 minutes after which time 7.5 ml of 3 M sodium acetate was added in order to neutralise the solution resulting in precipitation of cellular debri, renaturation of the plasmid DNA and chromosomal DNA aggregation (due to intrastrand hybridisation). The solution was centrifuged at 33,000 x g for 15 minutes and the pellet discarded. RNase A was added to a final concentration of 20 µg/ml and digestion carried out at 37°C for 40 minutes. The RNase treated lysate was extracted twice with an equal volume of phenol:chloroform. Two volumes of ethanol were added to facilitate DNA precipitation and the solution was left overnight at -20°C. Following

centrifugation at 9,500 x g the resulting DNA containing pellet was dissolved in 1M NaCl and 2 ml of 13% PEG. The mixture was incubated on ice water for 1 hour and centrifuged at 10,000 x g for 15 minutes. The precipitated DNA was washed twice with 70% ethanol and left to dry for approximately 15 minutes at room temperature. The purified plasmid DNA was then resuspended in 50-100 µl of sterile distilled water or TE and analysed on a 1% agarose gel.

2.2.3. (b) Small Scale Boiling Preparation from *E.coli.*

Plasmid DNA from putative expression clones was purified according to the method of Holmes and Quigley (1981). Cells were grown overnight in 1.5 ml of LB broth containing 100 µg/ml ampicillin. The cells were collected by centrifugation in a minifuge for 5 minutes and the pellets resuspended in 500 µl of STET buffer [8% (w/v) sucrose; 5% (v/v) Triton; 50 mM EDTA; 50 mM Tris-HCL, pH 8.0]. Lysozyme was added to a final concentration of 2 mg/ml and the mixture was left on ice for 10 minutes. The lysate was placed in boiling water for two minutes followed by centrifugation at top speed for 20 minutes in order to remove any cell debri. RNase A was added to a final concentration of 20 µg/ml and the lysate was incubated at 37°C for 30 minutes. An equal volume of isopropan-2-ol was added and the mixture was placed at -20°C for 30 minutes. The precipitated DNA was recovered by centrifugation at top speed for 15 minutes. Finally, the pellet was washed with 70% ethanol and resuspended in 50 µls of TE when sufficiently dry.

2.2.4. Preparation and Transformation of Competent Cells.

2.2.4 (a) Preparation of Fresh Competent Cells.

A single colony of *E.coli* TG1 was inoculated into 4 ml of LB broth and incubated overnight at 37°C with shaking at 270 rpm. A 1 ml sample of this overnight culture was transferred to 40 ml of LB broth and incubated for approximately 2.5 hours until an A_{600} of 0.4-0.5 was reached. The cells were then centrifuged at 7000 x g for 10 minutes. The pellet was resuspended in 20 ml of ice-cold 0.3 M $CaCl_2$ and left on ice for a further 40 minutes. Following centrifugation at 4000 rpm for 10 minutes the cells were resuspended in 1 ml of $CaCl_2$. DNA samples were added to 200 µl aliquots of the competent cells and the suspension was subjected to heat-shock treatment involving incubation for 30 minutes on ice followed by 2 minutes at 42°C and finally a further 2 minutes on ice. In order to ensure cell recovery and expression of the gene confering ampicillin resistance 1 ml of LB broth was added and the cells were incubated at 37°C for 1 hour. The cells were then

centrifuged briefly and resuspended in 100-200 µl of LB broth. This suspension was plated onto LB plates containing 100 µg/ml ampicillin and incubated overnight at 37°C.

2.2.4 (b) Preparation of Competent TG1 Cells for Storage.

A single colony of *E.coli* TG1 was inoculated into 25 ml of LB broth and incubated overnight at 37°C. A 2 ml sample of overnight culture was transferred to 500 ml of LB medium and the growth of cells was monitored at 600 nm. When an absorbance value of 0.45 was reached the cells were chilled on ice and recovered by centrifugation at 2500 x g for 20 minutes at 4°C. The resulting cell pellet was resuspended in 20 ml ice-cold trituration buffer (100 mM $CaCl_2$; 70 mM $MgCl_2$; 40 mM sodium acetate, pH 7.5) and diluted to a final volume of 500 ml (250 x 2) with the same solution. Following a 45 minute incubation on ice the suspension was centrifuged at 2000 x g for 15 minutes and the pellet gently resuspended in 10-50 ml of trituration buffer. The cells were pooled and sterile glycerol was added to a concentration of 15% (v/v). Aliqouts were snap frozen in liquid nitrogen and stored at -70°C for later use.

2.2.5. Polymerase Chain Reaction.

PCR primers were designed based on the published cDNA sequence data for BVR-A (Maines *et al.*, 1996). Restriction enzyme recognition sites were introduced into the 5' and 3' ends of DNA fragments during the amplification process in order to facilitate insertion into the pGEX-KG and pTrcHis B vectors. A human cDNA library derived from the monocyte cell line, U937, was used as 'target' and thermal cycling was performed in an MJ Reasearch Minicycler, model number PTC-100. The final mixture in each PCR tube contained template DNA of the appropriate concentration; 1X Taq polymerase buffer, magnesium chloride at a final concentration of 2.0 mM and 3.0 mM for the hexahis- and GST-fusion, respectively; dNTPs at a final concentration of 0.2 mM; forward and reverse primers at 0.4 µM and 0.2 µM, respectively and 2.5 units of *Taq* polymerase in a final volume of 50 µl. The thermal cycles used are listed in Table 2.2.

Table 2.2. Thermal Cycles used for the amplification of BVR-A cDNA.

Fusion	GST BVR-A	HexaHis BVR-A
Hot Start	95°C 5min	----------
Addition of Taq	80°C 5min	----------
Denaturation	95°C 1min	95°C 40 s
Annealing	58°C 1min	58°C 40 s
Extension	72°C 1min	72°C 1 min
No. of Cycles	28	30
Hold	72°C 10min	72°C 10 min
END		

2.2.6. Ligation Reactions.

Amplified DNA fragments and expression plasmids were digested at 37°C for two hours with the appropriate restriction enzymes and purified as outlined in Section 2.2.2. Initial ligation reactions were carried out according to the methods described in Sambrook *et al.*, (1989). The reactions were set up with 50 ng of vector DNA, 150 ng of insert DNA; 0.1 unit of T4 DNA ligase and 1X ligation buffer. Ligation was allowed to proceed at 16°C overnight after which time competent TG1 cells were transformed as outlined in Section 2.2.4 and plated on LB plates containing 100 µg/ml ampicillin. A more successful method employed the Rapid DNA Ligation Kit (Boehringer Mannheim). In this case, vector and insert DNA were first dissolved in 1X DNA dilution buffer. DNA ligation buffer was then added to give a final 1X concentration. After thorough mixing, 0.5 units of T4 DNA ligase was added and the solution was left at room temperature for 30 minutes. Competent TG1 cells were transformed as outlined above and incubated at 37°C overnight.

2.2.7. Preliminary Assay for BVR-A Activity in Putative Expression Clones.

Putative expression clones were replated onto a masterplate and screened for BVR-A activity: Small cultures (3 ml) were grown overnight in LB medium and transferred to

fresh LB (200 µl to 10 ml) the following day. When the A_{600} of the cultures approached 0.45, IPTG was added to a final concentration of 0.2 mM. After a 4 hr induction period the cells were harvested by centrifugation at 7000 x g for 5 minutes. The cell pellet was resuspended in 500 µl of PBS and sonicated for 20 seconds on ice. The suspension was centrifuged in a minifuge at top speed for 3 minutes and the resulting cell supernatant was assayed for BVR activity. The method of assaying for BVR-A activity was based on that of Fahkrai *et al.* (1992) and is outlined in Section 2.2.15 (b). The assay was carried out in a 96 well microtitre plate, each well containing 200 µl of assay mixture and 20 µl of cell supernatant. A colour change from green to yellow signified bilirubin production and the presence of active BVR-A. Positive clones were single colony purified and grown on a larger scale for further analysis.

2.2.8. Sodium Dodecyl Sulphate-Polyacrylamide Gel Electrophoresis (SDS-PAGE).

2.2.8 (a) Gel Preparation and Electrophoresis.

Discontinuous SDS-PAGE was carried out according to the method of Laemmli (1970) in an ATTO AE-6400 mini-gel system. The composition of the polymerising mixtures is outlined in Table 2.3. The components were mixed and poured into a gel mould and overlaid with distilled water. After approximately 15 minutes, the stacking gel was poured on top of the resolving gel and a 1 mm thick Teflon comb was inserted. The electrophoresis buffer consisted of 40 mM Tris; 400 mM glycine; 0.1% (w/v) SDS. Electrophoresis was carried out at 10 mA for 1 hour. Gels were stained in a solution of 10% (v/v) acetic acid; 50% (v/v) methanol and 1.25% (w/v) Coomassie Blue R for 10 minutes. Destaining was carried out overnight in 10% (v/v) acetic acid and 30% methanol.

2.2.8. (b) Preparation of Samples for SDS-PAGE Electrophoresis.

Purified protein samples were diluted such that the final protein content in each well was 5-10 µg. Non-purified protein samples such as cell cytosols were run at 100 µg. A stock solution of 5X sample buffer was stored at -20°C and contained the following components: 2% (w/v) SDS; 10% glycerol; 0.001% (w/v) bromophenol blue and 5% 2-mercaptoethanol in 25 mM Tris-HCL, pH 6.8. Prior to loading, samples were denatured by boiling at 100°C for 2-3 minutes.

Table 2.3.

Components of SDS-PAGE Solutions.

Stocks	15% Resolving Gel (ml)	5% Stacking Gel (ml)
Acrylamide (30%)	3.75	0.835
Bis-Acrylamide (1%)	0.65	0.65
Tris (1.5 M, pH 5.7)	1.875	0
Tris (1M. pH 6.8)	0	0.625
Distilled Water	1.1	2.2
SDS (20%)	0.0375	0.025
TEMED	0.01	0.01
Ammonium persulphate (10% w/v)	0.025	0.025

2.2.8. (c) Preparation of *E.coli* Cells for SDS-PAGE.

Putative expression clones were screened for the presence of recombinant BVR-A as outlined in Section 2.2.7 and also by means of SDS-PAGE and western immunoblotting. Small cultures were grown overnight in LB medium containing 100 µg/ml ampicillin. Expression of the recombinant protein was induced with 0.2 mM IPTG for 1, 4 and 16 hours. At each time point samples were taken and the volume of cells required to give an A_{600} value of 0.2 was determined. The appropriate number of cells were centrifuged at top speed for five minutes and resuspended in 20 µl of 5X SDS-PAGE sample buffer. The samples were boiled for approximately 5 minutes immediately before loading on the gel. The gels were run at 30 mA for 1 hour and protein bands were visualised with Coomassie Blue R staining solution.

2.2.9. Western Blotting.

Directly after SDS-PAGE, protein bands were transferred onto nitrocellulose using a Semi-Dry transfer unit (Hoefer Scientific Instruments). The gel and nitrocellulose were sandwiched in the cassette according to the manufacturer's instructions. Filter paper was soaked in transfer buffer (0.192 M glycine; 0.025 M Tris-HCl, pH 8.3; 0.013 M SDS; 15% (v/v) methanol) before use and transfer was achieved by applying a constant current of 110 mA for 1 h. The nitrocellulose membrane was incubated overnight in TTBS (20 mM Tris-HCL, pH 7.5; 500 mM NaCl; 0.05% (v/v) Tween-20) containing 5% skimmed milk powder (Marvel) in order to block any free binding sites. The following day the membrane was rinsed with several changes of TTBS. A 1:200 dilution of anti-rat BVR-A (prepared by Dr Orla Ennis, 1996) was prepared in TTBS containing 5% Marvel and the blot was incubated for 1 hour with mixing. The membrane was again washed with several changes of TTBS and incubated in a 1:1000 dilution of secondary antibody (goat-anti-rabbit horseradish peroxidase conjugate), diluted in TTBS for 40-60 minutes. The nitocellulose was washed thoroughly in TTBS before being developed.

The chromagen used to develop the blot consisted of 4-chloronaphthol (30 mg) in 10 ml of methanol and 100 ml of 20 mM Tris-HCL, pH 7.2 containing 60 µl of H_2O_2. Both solutions were added to the blot simultaneously which was then washed in water once the bands became visible.

2.2.10. DNA Sequencing.

DNA sequencing was preformed by MWG-Biotech U.K. Ltd. (Waterside House, Peartree Bridge, Milton Keynes MK63BY). A pair of M13-tailed nested primers were designed in this case and used to reamplify the PCR product for DNA sequencing.

2.2.11. Protein Purification Techniques.

2.2.11 (a) Preparation of *E.coli* Cells for Large Scale Column Purification.

E.coli cells for large-scale purification of the recombinant GST- and hexaHis fusion were cultured as follows: TG1 cells transformed with the recombinant pGEX-BVR-A plasmid were grown at 30°C in the presence of 2% glucose while those cells incorporating the recombinant pTrc-BVR-A plasmid were cultured in the absence of glucose at 37°C. Small 10 ml cultures were grown overnight at the given temperatures and transferred to 500 ml of LB the following morning. The cultures were induced overnight with 0.2 mM IPTG, having previously established that this was the optimal concentration for expression. The cells were harvested by centrifugation at 7,700 x g for 10 minutes in a Sorvall GSA rotor and the cell pellets were resuspended in 30 ml of phosphate buffered saline, pH 7.2 containing DTT (Dithiothreitol) at a final concentration of 0.1 mM and lysozyme at a final concentration of 2 mg/ml. Lysis was achieved using a sonicator with a microprobe (Braun). The cell suspension was kept on ice during the sonication process to prevent warming due to the heat of the sonicator probe. The probe was lowered into the cell suspension and sonication was carried using 5 s bursts over a period of five minutes. Each 5 s burst was followed by a 5 s pause to allow cooling. The sonicated suspension was centifuged in an SS-34 rotor at 12,000 x g for 45 minutes and the cleared lysate was transferred to clean tube for further processing.

2.2.11 (b) Ni-Agarose Affinity Chromatography.

A trial purification of the hexaHis fusion was carried out using the Talon Metal Affinity Resin (Clontech). A 5 ml suspension of resin was centrifuged at 700 x g for 2 minutes. The upper layer of ethanol was decanted off and the resin was equilibrated with 5 volumes of sonication buffer (20 mM Tris-HCl, pH 8.0; 100 mM NaCl). The suspension was again centrifuged and the supernatant discarded. A small sample (10 ml) of cell lysate was added to the resin which was then agitated at room temperature for 20

minutes. The resin was pelleted by centrifugation at 700 x g for 5 minutes and the supernatant was transferred to a clean tube. The resin was washed with 10 volumes of sonication buffer and gently mixed at room temperature for 10 minutes.The buffer was removed following centrifugation for 5 minutes. This step was repeated in order to ensure the complete removal of any unbound protein. The resin was then resuspended in 1 bed volume of sonication buffer and transferred to a gravity flow column. Once the resin had settled, the end-cap was removed and the buffer was allowed to drain until it had reached the top of the resin bed. The buffer used for the elution step was the same as that used to equilibrate the resin, however, it was prepared with increasing concentrations of imidazole (15 - 250 mM). Fractions were collected continuously and monitored for BVR-A activity (as was the supernatant that had been collected in the straight through fraction).

2.2.11 (c) Glutathione-Sepharose Affinity Chromatography.

The GST-fusion protein was purified by affinity chromatography on immobilized glutathione. The resin was prepared according to the procedure of Simons and Vander Jagt (1977).

Prior to use, the column (bed volume 30 ml) was washed with 200 ml of PBS, pH 7.2 containing 0.1 mM DTT. Lysate from a 2l culture was loaded onto the column which was subsequently washed until an A_{280} value of < 0.03 had been reached. Elution was carried out by passing 10 mM reduced glutathione in 50 mM Tris, pH 8.0, down the column. Fractions were assayed for BVR-A activity on a 96-well microtitre plate. The A_{280} values of the 'active' fractions were recorded and those fractions around the peak were pooled for further processing.

2.2.11 (d) G-25 Gel Filtration Chromatography.

A Sephadex G-25 gel filtration column was used to remove glutathione from the pooled fractions. The column was equilibrated in PBS and calibrated with Blue Dextran (5 mg) and dinitrophenol (5 mg) in order to determine the void and included volumes. The pooled BVR-A containing fractions were loaded onto the column and 2 ml fractions were collected. The peak A_{280} absorbing fractions were pooled for further processing. The GSH peak was detected by reacting the fractions after the protein peak with 100 µl of 2 mM DTNB.

2.2.12. Thrombin Cleavage of the GST-fusion Protein.

As mentioned in Section 2.2.1., a thrombin cleavage site has been incorporated into the pGEX-KG vector such that the desired polypeptide can be removed from the 26 kDa GST moiety following glutathione-Sepharose affinity chromatography.

Lyophilised human thrombin (1,000 units) was prepared by dissolving the supplied powder in 1ml of PBS, therefore, giving a concentration of 1 unit/µl. The stock solution was stored in small aliqouts at -70°C. Several thrombin cleavage experiments were set up in order to determine the optimal conditions for removal of the GST tag. Cleavage was carried out overnight at 4°C and at room temperature for 10 minutes with increasing concentrations of thrombin. The protein samples were dissolved in 5X sample buffer and analysed by SDS-PAGE to determine the extent of thrombin digestion. The results of these experiments are detailed in Section 3.7.

Following thrombin cleavage, the protein preparation was once again passed down the gluathione affinity column. The GST moiety was bound by the resin while the cleaved BVR-A was eluted in the straight through fraction. The protein was concentrated by ultrafiltration using a centriplus concentrator (Amicon) with a 10 kDa cut off. Concentration is achieved by driving the sample through an ultrafiltration membrane, solutes larger than the membrane cut-off are retained in the sample resevoir. The centriplus sample resevoir containing 15 ml of the protein solution was inserted into the filtrate vial and centrifuged for 1 hour at 5,000 rpm. The filtrate was discarded and the remainder of the protein solution was added to the sample resevoir. The solution was centrifuged as before and the filtrate again discarded. The sample resevoir was attached to a retentate vial, inverted and centrifuged at 4000 rpm for 1 min to transfer the concentrated protein solution to the retentate vial.

2.2.13. Production of Antisera.

2.2.13 (a) Preparation of Protein for Immunisation and the Immunisation Schedule

Antisera were raised against recombinant human BVR-A in New Zealand White rabbits according to the immunisation schedule outlined below.

On the day before commencing the schedule, a sample of blood (approximately 10 ml) was taken from the rabbit and was used to prepare a sample of pre-immune serum. The

blood sample was left to clot at room temperature for 1 hr in a glass vial. The clot was allowed to retract overnight at 4°C and the serum was decanted and centrifuged at 1,000g for 10 min in order to remove any remaining blood cells. The resulting supernatant was stored in aliquots at -70°C.

Between 250 and 400 µg of purified BVR-A was mixed with an equal volume of Freund's complete adjuvant (final volume, 3 ml). The solution was placed in a 20 ml glass bottle and mixed vigourously at room temperature on a "Vortex Whirlmixer" set at full speed for 2 h. The resulting emulsion was injected into multiple sites on the back of a New Zealand White rabbit on day 1 of the immunisation schedule. On day 14 of the schedule, a booster was prepared in the same way and this emulsion was injected intramuscularly into the leg. A second booster was injected in the same way on day 28 of the schedule. A test-bleed was carried out two weeks after this second booster injection. Approximately 10 ml of blood was taken from the rabbit and serum was prepared as described for the pre-immune serum. A "dot-blot" assay was used to determine the antibody titre of this serum (see below). The titre was found to be sufficiently high and exsanguination was carried out one week later. The blood collected upon exsanguination was treated in the same manner as the blood sample from which pre-immune serum was obtained. The final antibody titre was determined using a "dot-blot" assay.

2.2.13 (b) Determination of Antibody Titre using a "Dot-Blot" Assay

Nitrocellulose paper was cut into five strips (7 x 4 cm). Nine dots were marked, with a lead pencil, on each strip, leaving at least 1 cm distance between the dots. Samples (2 µl) containing varying amounts of BVR-A (1 ng to 2 µg) in 10 mM sodium phosphate, pH 7.2, were applied directly onto the marked dots on each strip. As a control, 2 µl of sodium phosphate buffer containing no enzyme was applied onto the first dot on each strip. The strips were allowed to dry at room temperature and were then placed in blocking buffer [5% (w/v) Marvel in TTBS] overnight at 4°C. One dilution of pre-immune serum (1:20) was made up in 1% (w/v) marvel in TTBS. Four dilutions of antibody solution were prepared (1:20, 1:200, 1:500 and 1:1000) in 1% (w/v) Marvel in TTBS. The first nitrocellulose strip was soaked in pre-immune serum, and each of the remaining four strips were placed in antibody solution. The nitrocellulose strips were incubated in these primary antibody solutions for 1.5 hr and then rinsed briefly in TTBS. This was followed by one 15 min wash in TTBS and three 5 min washes in TTBS. The strips were then incubated for 1.5 h in a 1:1000 dilution of secondary antiibody (goat anti-rabbit antiserum) solution in 1% (w/v) Marvel in TTBS. The strips were washed as above, however, the last TTBS wash was replaced by a wash in 20 mM Tris-HCL, pH 7.2. Staining with 4-chloronaphthol was carried out as described in Section 2.2.9.

2.2.14. Mass Spectroscopic Analysis of Recombinant Human Biliverdin-IXα Reductase

A stock solution of biliverdin-IXα reductase (6 mg/ml) was diluted in 200 µl of distilled water to give a final concentration of 0.6 mg/ml and the buffer (10 mM sodium phosphate) was replaced with 50 mM ammonium acetate, pH 6.0, by passage through a PD-10 column, pre-equilibrated in 50 mM ammonium acetate, pH 6.0. Samples containing BVR-A were pooled and the protein concentration was adjusted to 0.4 mg/ml. The buffer composition was finally adjusted to 50% (v/v) acetonitrile and 1% (v/v) formic acid. Mass analysis was carried out using a Micromass triple quadrupole electrospray mass spectrometer. A 10 µl sample was introduced into the electrospray mass spectrometer via a Rheodyne injector valve fitted with a 10 µl injection loop. Analysis was carried out in positive ion mode. Raw data were collected between a mass-to-charge ratio of 600-1700 *m/z*, at a cone voltage of 30 V, HV lens of 0.22 kV, and a capillary voltage of 3.60 kV. The raw data were subjected to maximum entropy analysis according to the Micromass schedule.

2.2.15. Kinetic Studies on Human Hiliverdin-IXα reductase.

2.2.15 (a) Preparation of Biliverdin-IXα.

Biliverdin-IXα was prepared from bilirubin-IXα according to an adaptation of the method of McDonagh (1979). Bilirubin (450 mg) was dissolved in 100 ml of oxygen-free DMSO and oxidised by the addition of 377 mg of 2,3-dichloro-5,6-dicyano-*p* - benzoquinone (DDQ) to the solution. After approximately 2 minutes, the reaction was terminated by the addition of 1.5 l of ice-cold water. The resulting suspension was centrifuged at 13,500 x g for 20 minutes at 4C. The biliverdin containing pellets were washed four times with 100 ml of ice-cold water. This crude biliverdin-IXα was dried overnight in a glass dessicating vessel, under vacuum and further purified as follows: Equal volumes of acetone and methanol were mixed and added to 15 g of Silica gel 60G which was subsequently packed into a sintered glass funnel. The crude biliverdin preparation was dissolved in the same solvent mixture and applied to the silica gel bed. The column was washed with methanol/acetone until the eluate became clear. A mixture of chloroform-methanol-acetic acid (70:30:0.3) was applied to the column in order to elute the biliverdin which was then dried using a rotary evaporator apparatus. Thin layer chromatography was carried out in order to assess the purity of the resulting preparation. The mobile phase consisted of a chloroform-methanol-acetic acid (90:10:1) mixture.

2.2.15 (b) Biliverdin-IXα Reductase Assay.

BVR-A activity was measured by monitoring either the production of bilirubin at 460 nm or the consumption of biliverdin at 660 nm. A concentrated stock solution of biliverdin was prepared by adding an excess of dried powder to 1 ml of 100 mM sodium phosphate, pH 7.2. This suspension was vortexed vigorously and centrifuged at 12,000 rpm in order to remove any undissolved material. The resulting supernatant was removed to a fresh tube and the pellet was again dissolved in buffer and centrifuged at top speed. This procedure was repeated up to three times until most of the biliverdin was in solution. The concentration of the final stock solution was determined using an extinction coefficient value of 12.4 $mM^{-1}.cm^{-1}$ for biliverdin at 660 nm, as reported by Phillips (1981). All assays were conducted at 30°C in the presence and absence of 37 μM BSA, 705 μM NADH or 100 μM NADPH and biliverdin at a concentration of 20 μM (except were stated otherwise).

2.2.15 (c) Pre-steady State Kinetic Studies.

Pre-steady state kinetic studies on human BVR-A were carried out using a Stopped-Flow Multi Mixing Spectrometer (Model SX17) from Applied Photophysics. An initial "burst" of bilirubin production was measured by placing assay mixture containing biliverdin (40 μM) and NADPH (200 μM) in one syringe of the apparatus, and the enzyme solution at a concentration of 5 μM in the second syringe. Prior to recording, three "shots" of assay mix were passed through the mixing chamber in order to negate the possibility of diluting, or contaminating the assay mix of interest with solutions from the previous experiment. For each experiment, a sufficient volume of assay mix was prepared to enable three sets of data to be recorded. Equal volumes from each syringe were injected simultaneously into the recording chamber. The deadtime was approximately 1 msec. All burst rates were recorded in triplicate.

2.2.15 (d) Fluorescence Binding Studies.

The binding of nicotinamide cofactors to human BVR-A was studied by monitoring the quenching of protein fluorescence using a Perkin-Elmer luminescence spectrophotometer (LS 50B). The excitation wavelength was set at 295 nm (half band width, 5 nm) while the emission wavelength scanned 300 to 400 nm (half band width, 5 nm). Prior to scanning, all solutions were filtered through a 0.45 μm filter in order to reduce backround noise interference. A stock solution of BVR-A (2 mg/ml) was diluted in 100 mM sodium phosphate, pH 7.2 to give a final concentration of 1.5 μM. The peak of

BVR-A fluorescence was established prior to each experiment and all measurements thereafter were taken at this wavelength i.e. 340 nm.

Quenching of protein fluorescence was achieved by the sequential addition of NADPH and $NADP^+$ from a 5 mM stock solution. The fluorescence intensity (F_{meas}) was determined after each addition of nucleotide and subsequently corrected for the 'inner filter effect' as described by Levine (1977), using the correction factor:

$$\mathbf{F_{corr} = F_{meas} \times antilog \{(\varepsilon_{excit} + \varepsilon_{emiss})[NAD(P)H](pathlength/2)\}}$$

where, ε_{excit} and ε_{emiss} are the molar extinction coefficients of NAD(P)H at the excitation and emission wavelengths, respectively, and the pathlength is 1 cm.

The extinction coefficients for NADPH and $NADP^+$ were calculated by measuring the absorbance of each cofactor at 295 nm and 340 nm over a series of concentrations where Beer's Law is obeyed. The dissociation constants (K_D) were then calculated from a titration plot of ΔF (the change in fluorescence upon each addition of nucleotide) against nucleotide concentration. Data were processed using the Perkin-Elmer FLWinLab scan application.

2.2.15 (e) Stopped-flow Fluorescence Spectroscopy.

Nucleotide quenching of protein fluorescence was also examined by the stopped-flow technique. hBVR-A (1.25 μM) was mixed with varying concentrations of NADPH (5 to 50 μM) prepared from a 1mM stock solution. The reaction was allowed to go to completion and the dissociation constant was calculated from a plot of k_{app} (apparent burst rate constant) versus nucleotide concentration.

2.2.16. A Comparison of the Substrate Specificity of Human BVR-A and BVR-B.

2.2.16 (a) Preparation of Partially Pure Native BVR-A and BVR-B.

A human blood sample (50 ml) was added directly to a tube containing citrate as an anticoagulant, before being centrifuged at 4,000 x g for 10 min. The supernatant was discarded and the packed erythrocyte pellet was gently resuspended in three volumes of ice-cold 0.9% (w/v) sodium chloride. Centrifugation was carried out as before and the supernatant was again discarded. The erythrocytes were washed twice more after which

time they were lysed in three volumes of ice-cold distilled water. The pH was adjusted to 6.4 using 5M HCl and the suspension was centrifuged at 10,000 x g for 1 hr at 4°C. The pH was finally adjusted to 7.2 with 5M KOH. The lysate was dialyzed against 20 l of 10 mM sodium phosphate , pH 7.2, overnight before being loaded onto a DEAE-cellulose column (5 x 30 cm) equilibrated in 10 mM sodium phosphate, pH 7.2. The column was washed extensively until the A_{280} was below 0.1, and the two forms of biliverdin reductase were then eluted with a 10-350 mM gradient (2 x 250 ml) of sodium phosphate, pH 7.2. All fractions were collected and monitored for absorbance at 280 nm before being assayed for BVR-A activity as described in Section 2.2.15 (b) and flavin reductase activity as described below.

2.2.16 (b) Flavin Reductase Assay.

The flavin reductase activity of BVR-B was measured using the method described by Yubisui *et al.* (1979). Initial rate studies were carried out under saturating concentrations of FMN (150 μM) and NADPH (50 μM) in 10 mM potassium phosphate, pH 7.5. Activity was monitored by following the decrease in absorbance of NADPH at 340 nm. The reaction was carried out at 25°C and initiated by the addition of FMN to the cuvette.

2.2.16 (c) Initial Rate Kinetics.

A colorimetric assay was initially performed on a 96-well microtitre plate in order to compare the native and recombinant enzymes. Each well contained the standard reaction components and the respective biliverdin isomers at a concentration of 20 μM. It was established that the native and recombinant enzymes were behaving in an identical manner, therefore, the kinetic data were generated using the purified recombinant enzymes. Initial rate studies with biliverdin as the variable substrate were made by monitoring biliverdin consumption at 660 nm in the presence and absence of BSA (1 mg/ml) using the extinction coefficients given in Table 5.2.

2.2.17. Protein Folding Studies.

The effect of denaturants such as guanidine hydrochloride and urea on the fluorescence and activity of hBVR-A was studied using conventional spectroscopic and fluorometric techniques. In initial experiments, the activity and fluorescence intensity of the enzyme was measured as a function of denaturant concentration. Binding studies and initial rate kinetics were subsequently performed at various concentrations of denaturant. The details of these experiments are described in Chapter 4.

2.2.18. Stereochemical Studies of NADH Oxidation.

2.2.18 (a) Enzyme-Catalysed Synthesis of Stereoisomers of [4-^{3}H] NADH.

The A and B stereoisomers of [4-^{3}H]NADH were prepared from commercially available [4-^{3}H]NAD$^+$ using two enzymes that have opposite stereospecificity for NAD$^+$. Alcohol dehydrogenase (ADH) transfers hydrogen from ethanol to position A of carbon 4 on the nicotinamide ring of NAD$^+$, hence the reduced coenzyme formed in the reaction will have tritium at position B, i.e. B-[4-^{3}H]NADH. Glutamate dehydrogenase (GDH) transfers hydrogen from glutamate to position B of NAD$^+$, therefore, forming A-[4-^{3}H]NADH.

ADH [Sigma; A3263] was made up to a concentration of 10 mg/ml with distilled water. The reaction mixture contained 1.91 ml of 20 mM sodium phosphate buffer, pH 8.5; 70 µl of ethanol; 8 µl of 50 mM NAD+; 5 µl of 0.37 mM [4-^{3}H] NADH (5 µCi) and 3 µl of ADH. The reaction was performed at 30°C and the production of NADH was monitored continuously at 340 nm until there was no further change in absorbance at this wavelength.

GDH [Sigma; G2501] was supplied as a suspension in 2 M ammonium sulphate. The protein was initially recovered by centrifuging 1 ml of this preparation at 12,000 x g for 15 minutes at 4°C. The pellet was resusupended in 2 ml of 10 mM sodium phosphate buffer, pH 7.2 and dialysed for 18 hr at 4°C against 4 l of the same buffer. The resulting material was centrifuged in a minifuge for 5 mins in order to remove any insoluble material. The reaction mixture contained 1.42 ml of 20 mM sodium phosphate buffer, pH 8.5; 500 µl of 100 mM glutamate; 8 µl of 50 mM NAD+; 5 µl of 0.37 mM [4-^{3}H] NAD$^+$ (5 µCi) and 50 µl of GDH. Formation of NADH was again monitored at 340 nm until no further change was observed.

The newly synthesised A-[4-^{3}H]NADH and B-[4-^{3}H]NADH were used immediately as cofactors for the reduction of biliverdin-IXα by biliverdin-IXα reductase.

2.2.18 (b) BVR-A Catalysed Reduction of Biliverdin-IXα in the Presence of NADH Labelled at Either the A or B Face with Tritium.

The radiolabelled A and B stereoisomers of [4-^{3}H]NADH were each, in turn, used as co-factor for the BVR-catalysed reduction of biliverdin-IXα to bilirubin-IXα. This was done simply by direct addition of assay components [biliverdin-IXα (12.5 µl from 1

mM stock); BSA (2.5 µl from 3.7 mM stock); BVR-A (37 µl from 0.85 mg/ml stock) and 425 µl of 500 mM sodium phosphate, pH 6.9] to the completed ADH and GDH reactions set up as described above. Control reactions were set up to contain all the assay components listed above with the exception of BVR-A. The reactions were conducted at 30°C and bilirubin production was monitored at 460 nm.

2.2.18 (c) Organic extraction and Scintillation Counting of Radiolabelled Bilirubin-IXα.

Once the BVR reactions had gone to completion, the contents of the cuvettes were transferred to 10 ml polypropylene tubes. Chloroform (0.9 ml) was added to each tube and the contents were mixed vigourously for 30 s. Glacial acetic acid (160µl) was added to the tubes to facilitate transfer of the bilirubin to the organic solvent. The mixture was again vortexed for 30 s. The contents were transferred to minifuge tubes and centifuged at top speed for 2 min. The organic chloroform layer containing the radiolabelled bilirubin was recovered by puncturing the bottom of the tube with a hyperdermic syringe needle, having previously inserted the needle into the lid of the tube. An eppendorf was placed underneath the tube and the organic liquid was collected. A sample of this material (300 µl) was added to 5 ml of toluene-PPO for liquid scintillation counting.

2.2.19. Crystallization of Recombinant Human BVR-A.

2.2.19 (a) Initial Screening for Crystallography Conditions.

Crystallization experiments were performed using the hanging drop vapor diffusion method in Linbro 24-well culture plates, supplied by Hampton Research Tools. A 2 µl sample of concentrated BVR-A (6 mg/ml) was added to an equal volume of structure screening reagent on a siliconized cover slip. The cover slip was inverted over a well containing 1 ml of the same reagent and this procedure was repeated for each reagent (100 in total). The screen was performed in duplicate at 4°C and 21°C.

2.2.19 (b) Preparation of Selenomethionine Derivative for Analysis by Multiwavelength Anomalous Diffraction (MAD).

A selenomethionine derivative of human BVR-A was produced using the *E.coli* methionine auxotroph strain B834 (DE3) which has the gene for bacteriophage T7 RNA polymerase integrated into it's chromosome. Cells were transformed with the

recombinant pGEX-BVR-A plasmid according to the procedures outlined in Section 2.2.4 (a). All growth experiments were performed in New Minimal Medium (NMM). This was prepared from autoclaved 1M stocks of the following salt solutions: ammonium sulphate (7.5 mM), NaCl (8.5 mM), potassium dihydrogenphosphate (22.5 mM), potassium hydrogenphosphate (50 mM), magnesium sulphate (1 mM) and glucose (20 mM). Filter-sterilized stocks of Ca^{2+}, Fe^{2+} and trace elements (Cu^{2+}, Mn^{2+}, Zn^{2+} and MoO_4) (1mg/ml) were added to the medium to a final concentration of 1 µg/ml. Aliquots of sterilized thiamine and biotin stocks (10 mg/ml) were added to a final concentration of 10 µg/ml in media. A mixture of all amino acids without Met (filter sterilized stock of 0.5 g/l in 137 mM NaCl, 2.5 mM KCl, 10 mM sodium hydrogen phosphate, 1.76 mM potassium dihydrogen phosphate, pH 7.0) was added to a final concentration of 50 mg/l. All bacterial growth was under the selective pressure of 100 mg/l ampicillin.

SeMet increases the bacterial generation time by a factor of two or more, therefore, a 5 ml overnight culture was grown initially in NMM with a limited amount of Met (0.3 mM; prepared from a 50 mg/ml stock). This culture was transferred the following day to NMM containing SeMet at a final concentration of 0.5 mM. Growth was monitored and protein expression was induced with 1 mM IPTG at an A_{600} of 1.1-1.3. The cells were harvested the following morning and the protein was purified as outlined in Section 2.2.11.

2.2.20. Transient Transfections and Reporter Gene Assays

2.2.20 (a) Cell Culture.

Mouse hepatoma cell lines expressing the wild-type Ah receptor (Hepa 1c1c7), mutant Ah receptor (Hepa C4) and the mutant Ah receptor nuclear transporter (Hepa C12) were cultured in minimal essential medium (αMEM) supplemented with 10% fetal calf serum, 100 µg/ml gentamycin and 2 mM L-glutamine and maintained at 37°C in a humidified atmosphere of 5% CO_2, in 75 or 175 cm^2 flasks. Cells were seeded at 1 x 10^5 ml^{-1} for growing in a total volume of 15 ml (75 cm^2 flask) or 35 ml (175 cm^2 flask), and passaged when 80% confluent as follows: Cell monolayers were washed with sterile PBS and incubated with 0.25 % (w/v) trypsin/EDTA at 37°C until detachment became evident (approx. 3-5 min). The flask was tapped to complete detachment and warmed medium was added (10 ml for 75 cm^2 and 20 ml for 175 cm^2 flasks) in order to terminate trypsinization. The cell suspension was centrifuged at 170 g for 5 min and the supernatant was discarded. The cell pellet was resuspended in 1 ml of medium and cell number and viability was determined by mixing a 10 µl aliquot of resuspended cells with 10 µl of trypan blue dye. After 2-3 min, the mixture was applied to a haemocytometer for

cell counting.

2.2.20 (b) Calcium Phosphate Transfection.

On the day before transfection, cells were seeded in 24-well plates at a density of 1 x 10^5 ml^{-1}. Details of the constructs used in this study are outlined in Chapter 6. Transfections were performed using the standard calcium phosphate precipitation technique as follows: 42 µl of 2.5 M $CaCl_2$ was added to the appropriate amount of plasmid DNA. The DNA/$CaCl_2$ complex was added dropwise to 210 µl of 2 x HBS buffer (280 mM NaCl; 1.5 mM $Na_2HPO_4.2H_2O$; 10 mM KCl; 12 mM dextrose; 50 mM HEPES) and left at room temperature for 30 mins. The mixture was then added dropwise to the cells at 30 µl/well. The cells were incubated under standard growth conditions for 5 hrs after which time the medium was replaced in order to ensure cell recovery. After approximately 18 hrs the cells were treated with various agents at the concentrations indicated in figure legends (Chapter 6). Where the concentration of a compound is described as '0' in legends, this corresponds to treatment with vehicle.

2.2.21 (c) Determination of Luciferase Reporter Construct Activity.

Following aspiration of the growth medium, cells were washed with 2 ml of sterile PBS (RT). The cells were lysed with the addition of 50 µl of fresh 1 X lysis buffer (Promega) and left shaking at room temperature for 15 minutes. After such time the 24 well plates were centrifuged at 1,000 x g in a bench top centrifuge, 10 µl of the supernatant fraction was incubated with 40 µl of luciferase substrate and the relative luciferase activity was determined with a multi-well plate luminometer.

Chapter 3

Cloning, Overexpression & Purification of Human Biliverdin-IXα Reductase

3.1. Amplification of hBVR-A cDNA.

Oligonucleotide primers used for amplification purposes were designed based on the published cDNA sequence for human BVR-A (Maines *et al.*, 1996) and are shown in Fig. 3.1. Base substitutions were incorporated into each primer as a means of introducing restriction sites into the 5' and 3' end of the BVR-A sequence, thereby, facilitating insertion into the appropriate expression vector. A single forward primer (Oligo 1), containing a *BamH1* restriction site, was used for cloning into the pGEX-KG and pTrcHis B vectors, however, individual oligonucleotides were designed for reverse priming as a compatible 3' restriction site was not present in the two vectors. The pGEX-KG reverse primer (Oligo 2) contains an *Nco 1* restriction site whereas the pTrcHis B primer (Oligo 3) contains a *Kpn 1* restriction site. Digestion at all three sites produces a single stranded protrusion of 5 base pairs which generally gives rise to a higher ligation efficiency. PCR products from reactions incorporating Oligos 1 and 2 and Oligos 1 and 3 are referred to as GST-BVR and hexaHis-BVR, respectively.

The cDNA library used as target in the amplification reactions was derived from the U937 monocyte cell line which has been subcloned into the pTZ18R plasmid. A PCR master mix was prepared and contained the following components: 1µl of target DNA, 1X Taq polymerase buffer, magnesium chloride at a final concentration of 2.0 mM and 3.0 mM for hexaHis- and GST-BVR, respectively; dNTPs at a final concentration of 0.2 mM; forward and reverse primers at 0.4 µM and 0.2 µM, respectively and 2.5 units of Taq polymerase in a final volume of 50 µl. Priming was effective at an annealing temperature of 58°C, the thermal cycles used for the amplification of both products are outlined in Section 2.2.5. Amplification of the GST-BVR sequence was less efficient and a denaturation step at 95°C for 5 mins, prior to the addition of *Taq* polymerase, was included in the original protocol. This is referred to as a 'hot-start' and is recommended for the amplification of difficult sequences. PCR products of the predicted size i.e. 944 bp are shown in Figs. 3.2 (a) and 3.3 (a).

3.2. Cloning of hBVR-A cDNA into the pGEX-KG Expression Vector.

The cDNA encoding hBVR-A was cloned into the pGEX-KG expression vector in an effort to produce a GST-fusion protein. The plasmid was purified by SDS-alkaline lysis and digested using *BamH1* and *Nco 1* restriction enzymes. Digestion was carried out at 37°C for 2 hrs in the presence of 1X Multicore buffer; 1 µg of plasmid DNA and 10 units of each restriction enzyme in a final volume of 20 µl. The linearized plasmid DNA was purified as outlined in Section 2.2.2. The GST-BVR PCR product was purified in the

PRIMER	DIRECTION	SEQUENCE
Oligo 1	Forward	5'- GCA.GGA.TCC.AAG.ATG.AAT.GCA.GAG -3' *BamH1*
Oligo 2	Reverse	5'-AA.CCA.AAT.GCT.GGT.GCC.ATG.GTG.GAA -3' *Nco 1*
Oligo 3	Reverse	5'- AA.CCA.AAT.GCT.GGT.ACC.ATC.TTG.GAA -3' *Kpn 1*

Figure. 3.1. Sequences of Oligonucleotides used in PCR Reactions.

same manner in order to remove any traces of *Taq* polymerase and dNTPs etc. Following digestion with both restriction enzymes, the DNA fragment was again purified using the High Pure PCR Product Purification Kit which provided better DNA yields when compared to the Agarose Gel DNA Extraction Kit.

Ligation reactions were set up as described by Sambrook *et al.* (1989) with a vector to insert molar ratio of 1:3 for sticky-ended ligations. Approximately 150 ng of insert DNA and 50 ng of vector DNA were used in subsequent ligation reactions. Initial overnight ligations using T4 DNA ligase and ligation buffer did not yield any positive transformants. Successful ligation was finally achieved using the Rapid DNA Ligation Kit (Promega) which omits the overnight step at 16°C and ligation is allowed to proceed at room temperature for a 30 minute period prior to transformation of competent cells. The ligation mixture contained the appropriate volume of vector and insert DNA, 1X DNA dilution buffer, 1X ligation buffer and 1µl of T4 DNA ligase. Competent *E.coli* cells were prepared as outlined in Section 2.2.4 and 200 µl aliquots were transformed before plating onto LB agar containing 100 µg/ml ampicillin. Positive and negative controls were included in all transformation reactions, the former consisted of circularised plasmid DNA while the latter consisted of ligation mixture containing digested plasmid DNA with no cDNA insert. Any positive transformants were replated on a master plate and screened for the presence of the hBVR-A insert.

3.3. Cloning of hBVR-A cDNA into the pTrcHis B Expression Vector.

The cDNA encoding BVR-A was also cloned into the pTrcHis B expression vector which is designed for the production of hexahistidine fusion proteins. The cloning procedure undertaken in this case was the same as that outlined above, however, digestion was carried out with *BamH1* and *Kpn 1* restriction enzymes. The pTrcHis B plasmid and the hexaHis PCR product were digested, purified and ligated for 30 minutes at room temperature before being plated on LB agar supplemented with ampicillin. All positive transformants were screened for the presence of the BVR-A insert.

3.4. Screening for the Presence of the hBVR-A Insert.

Plasmid DNA from putative expression clones was purified according to the method of Holmes and Quigley (1981). The isolated DNA was compared to control DNA i.e. vector containing no insert, and any plasmids that appeared larger than the control were

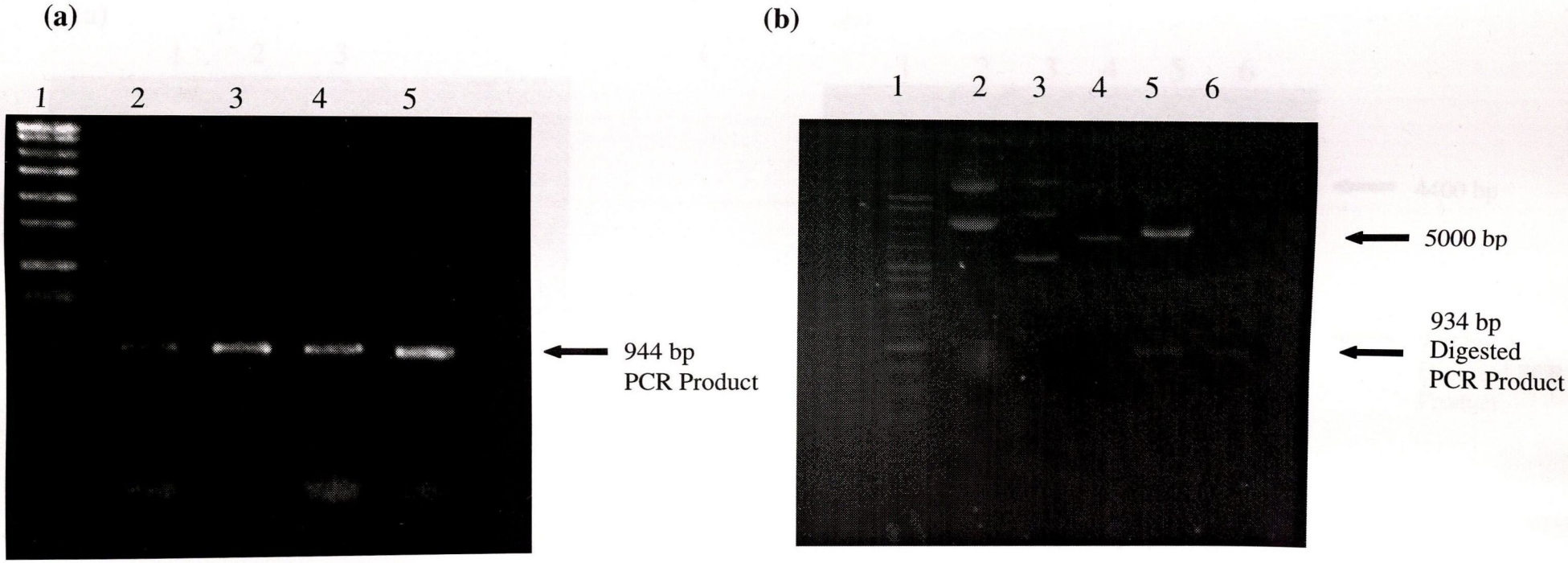

Figure 3.2. Cloning of hBVR-A cDNA into the pGEX-KG Expression Vector.

(a) The cDNA encoding hBVR-A was amplified according to the procedures outlined in Section 2.2.5 with Oligos 1 and 2 (Fig. 3.1.). Lane 1 contains DNA molecular weight markers no. VII, Boehringer Mannheim (see Appendix) while lanes 2 to 5 contain 1/5 the total reaction volumes of 100 µl PCR samples.

(b) The pGEX-BVR-A construct was identified by visualisation on a 1% agarose gel following restriction digest analysis. Lane 1 contains DNA molecular weight markers no. VII, Boehringer Mannheim (see Appendix). Lane 2 contains undigested pGEX-KG with no insert. Lane 3 contains undigested pGEX-BVR-A isolated from positive transformants following ligation into the pGEX-KG expression plasmid. Lanes 4 and 5 contain samples of pGEX-KG and pGEX-BVR-A, respectively, following double digest with *BamH1* and *Nco1*. A control PCR product of the correct size is shown in lane 6.

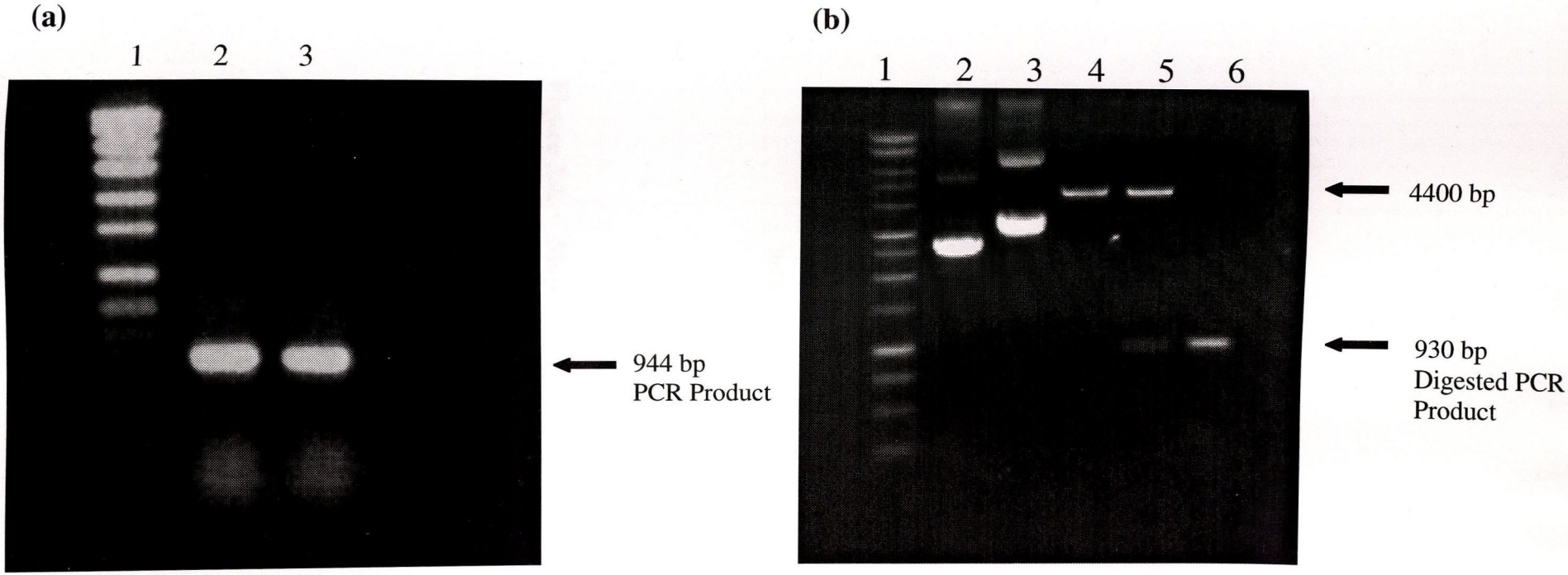

Figure 3.3. Cloning of hBVR-A cDNA into the pTrc His B Expression Vector.

(a) The cDNA encoding hBVR-A was amplified according to the procedures outlined in Section 2.2.5 with Oligos 1 and 3 (Fig. 3.1.). Lane 1 contains DNA molecular weight markers no. VII, Boehringer Mannheim (see Appendix) while lanes 2 and 3 contain 1/5 the total reaction volumes of 100 µl PCR samples.

(b) The pTrc-BVR-A construct was identified by visualisation on a 1% agarose gel following restriction digest analysis. Lane 1 contains DNA molecular weight markers no. VII, Boehringer Mannheim (see Appendix). Lane 2 contains undigested pTrc-His B with no insert. Lane 3 contains undigested pTrc-BVR-A isolated from positive transformants following ligation into the pTrcHis B expression plasmid. Lanes 4 and 5 contain samples of pTrcHisB and pTrc-BVR-A, respectively, following double digest with *BamH1* and *Kpn1*. A control PCR product of the correct size is shown in lane 6.

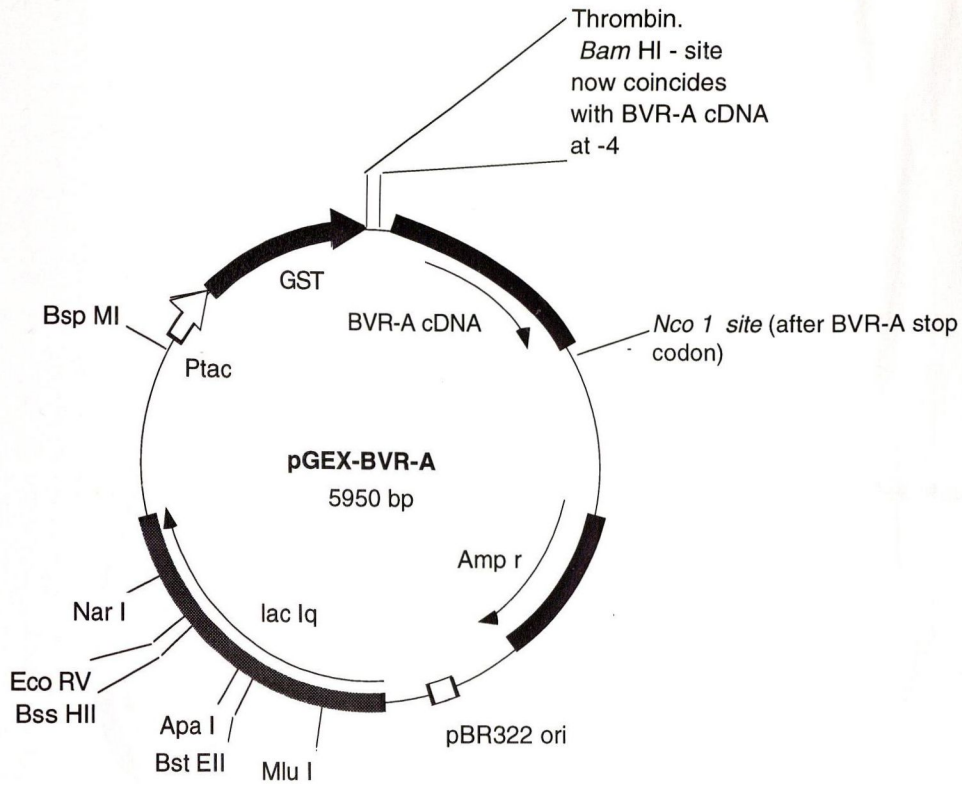

Figure 3.4. Map of the pGEX-BVR-A construct.

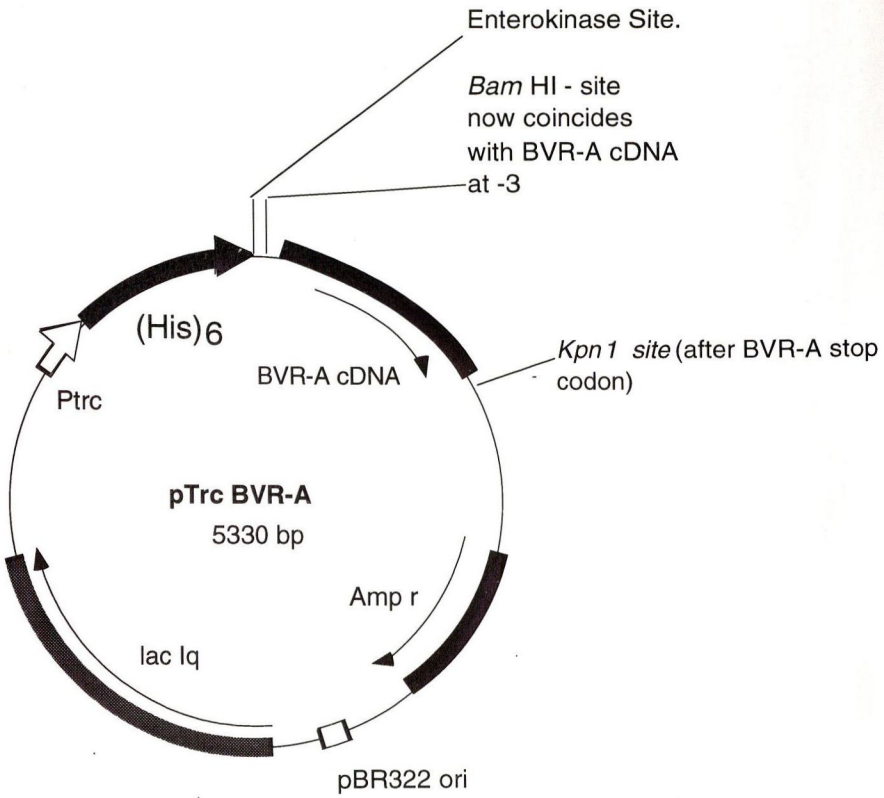

Figure. 3.5. Map of the pTrc-BVR-A Construct.

Figure 3.6. Overexpression of hBVR-A in *E.coli* TG1 Cells.

(a) Timecourse of IPTG Induction.

Lane 1 contains prestained molecular weight standards from NEB (expressed as kilodaltons). Lanes 2, 3 and 4 contain lysate from transformed cells following induction for 1, 4 and 16 hrs, respectively. Lane 5 to 7 are as described for lanes 2 to 4, however, in this case cells were transformed with the pTrc-BVR-A expression plasmid.

(b) The Effect of Glucose on expression of the GST-fusion Protein.

Lane 1 contains prestained molecular weight standards. Lane 2 contains lysate from cells grown overnight (- IPTG) in the presence of 2% glucose. Lane 3 contains lysate prepared from cells grown overnight (+ IPTG) in the presence of 2% glucose. As is evident from the gel, the *tac* promoter is effectively repressed when glucose is included in the growth medium.

(a)

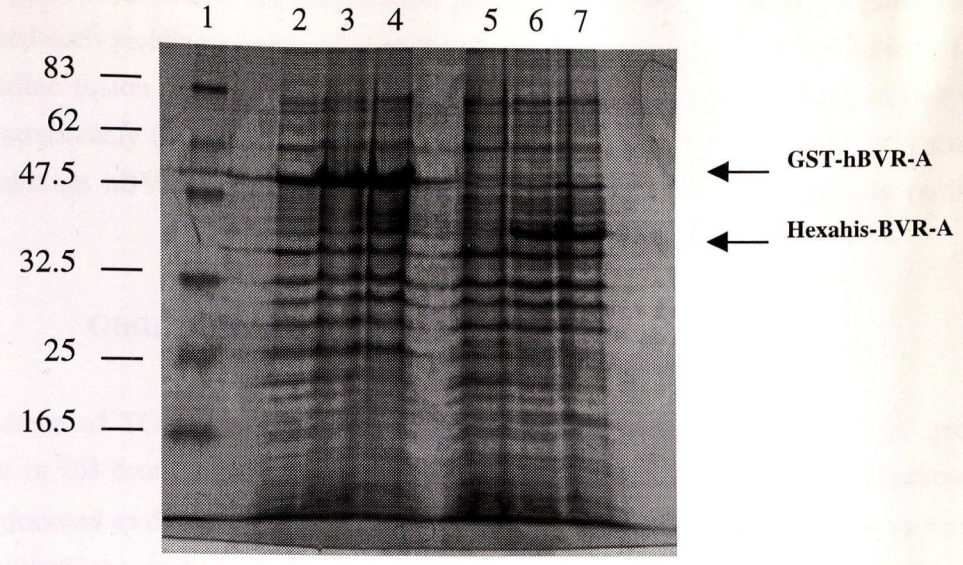
1
2
3
4
5
6
7
83
62
47.5
32.5
25
16.5
GST-hBVR-A
Hexahis-BVR-A

(b)

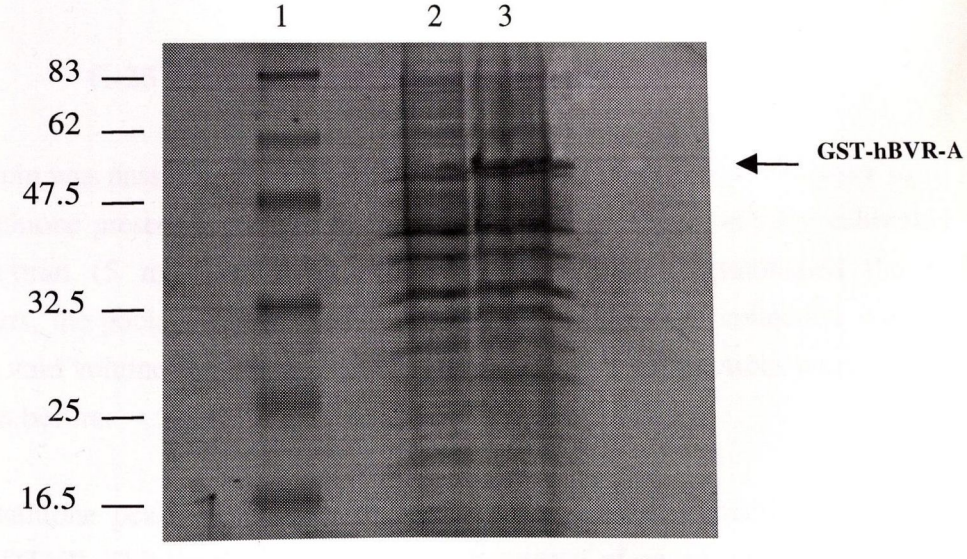
1
2
3
83
62
47.5
32.5
25
16.5
GST-hBVR-A

3.6. Purification of Recombinant hBVR-A.

In initial purification trials, the GST-fusion protein was affinity purified on glutathione-Sepharose beads yielding a preparation that was approximately 90% pure. Elution of the hexahistidine-fusion protein from a nickel-affinity resin produced a preparation that was only approximately 60% pure, therefore, the GST-fusion protein was used as a source of recombinant hBVR-A throughout this study. The purification procedure is outlined below.

3.6.1. Glutathione-Sepharose Affinity Chromatography.

A 2 l culture of TG1 cells transformed with the pGEX-BVR-A plasmid was grown overnight in LB broth supplemented with ampicillin (100 μg/ml). The cell supernatant was fractionated as described in Section 2.2.11 (a) and the cleared cell lysate was loaded onto a glutathione-sepharose affinity column (20 x 2 cm). The column was washed extensively in PBS and the straight through fractions were monitored for BVR-A activity. Having established that the fusion protein was in fact binding to the column, elution was carried with 10 mM glutathione in 50 mM Tris-HCl. The A_{280} of the eluted fractions was recorded and enzyme assays were performed to identify the peak fractions. The elution profile is shown in Fig. 3.7.

3.6.2. G-25 Gel Filtration Chromatography.

The protein was passed down a Sephadex G-25 gel filtration column in order to remove the glutathione present in the eluted fractions. The column was initially calibrated with Blue Dextran (5 mg) and dinitrophenol (5 mg). Having established the column parameters, the pooled protein sample was loaded and fraction collection was initiated once the void volume had run through. The protein containing fractions were assayed and pooled as before.

The glutathione peak was located by reacting the remaining fractions with the thiol reagent, DTNB. This reaction is based on the formation of an adduct between the DTNB disulphide group and the thiol group of glutathione, releasing NTB which is yellow and absorbs strongly at 410 nm. As shown in Fig. 3.8, the glutathione is effectively separated from the GST-fusion protein at this stage of the purification procedure.

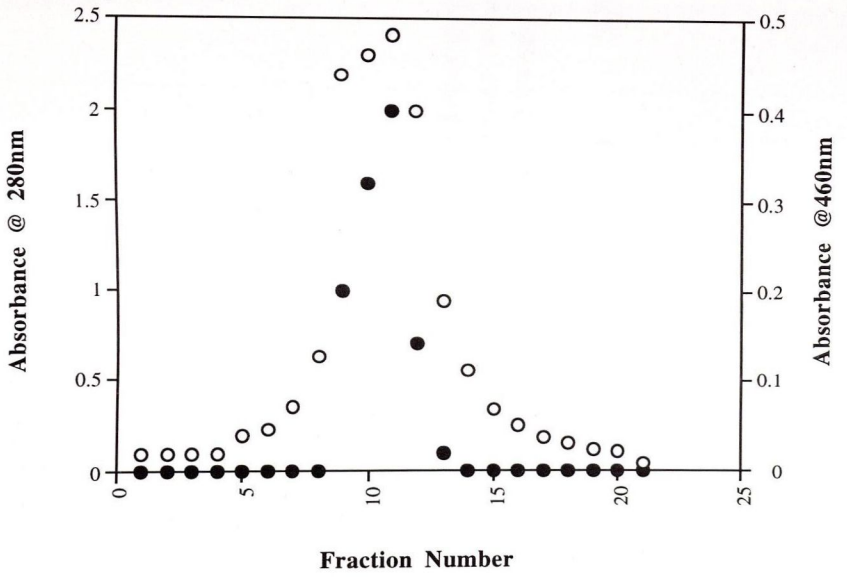

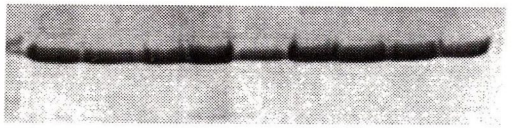

Figure 3.7. Elution of Fusion Protein from Gluathione Sepharose.

The GST-hBVR-A fusion protein was purified on a glutathione-sepharose affinity column as outlined in Section 2.2.11 (a). Fractions were assayed for protein (O) and BVR-A activity (●) before being analysed on a 15% SDS-gel as shown above.

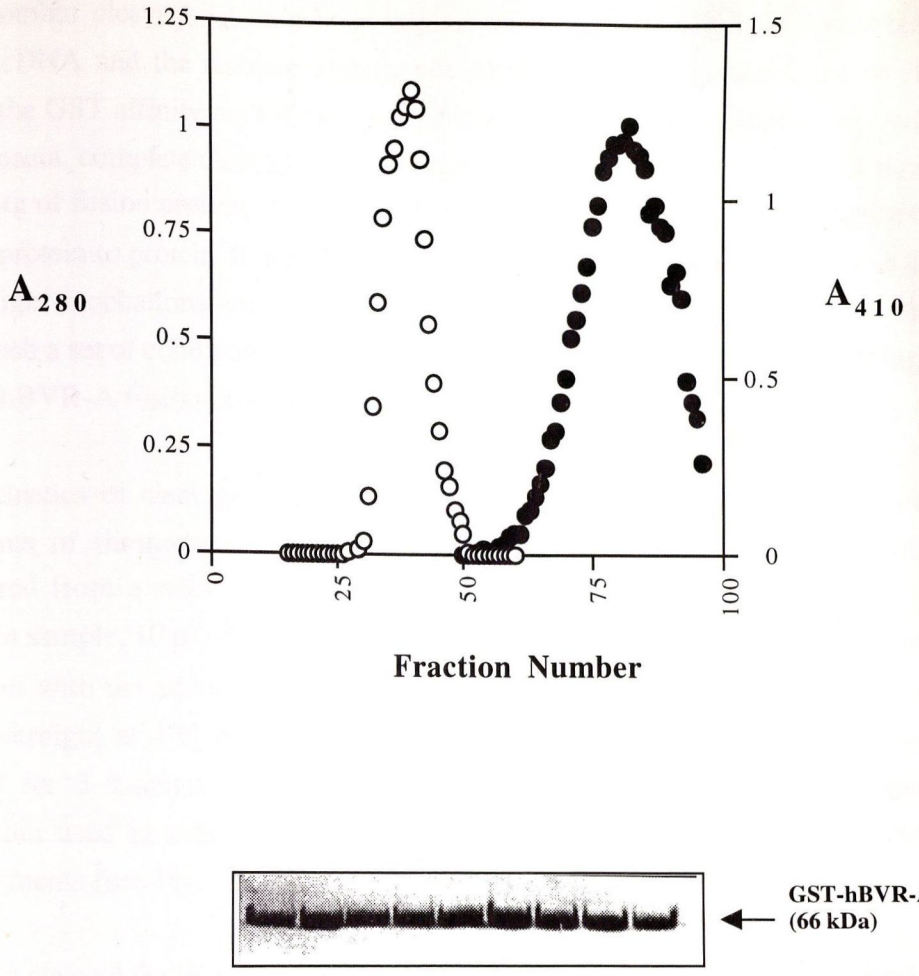

Figure 3.8. **G-25 Gel-filtration Elution Profile.**

The GST-fusion protein was separated from the glutathione by fractionation on a G-25 gel filtration column as outlined in Section 2.2.11 (d). The glutathione peak was detected following reaction with 2 mM DTNB.

3.7. Thrombin Cleavage of the GST-fusion Protein.

A thrombin cleavage site has been engineered into the pGEX-KG vector between the GST cDNA and the multiple cloning site such that cloned proteins can be dissociated from the GST affinity tag following purification on glutathione-Sepharose. According to Pharmacia, complete cleavage should occur overnight at 22°C with 1 unit of thrombin per 100 μg of fusion protein, however, the conditions and kinetics of cleavage tend to vary from protein to protein. In addition, it is preferable to keep protein solutions at 4°C where overnight incubations are involved. A series of experiments were set up in order to establish a set of conditions culminating in the complete removal of the GST tag from the GST-hBVR-A fusion protein.

The kinetics of cleavage were initially investigated at room temperature with varying amounts of thrombin over a 10 minute period. A series of 10-fold dilutions were prepared from a stock solution of thrombin comprising 1 unit/μl. To each 100 μg of protein sample, 10 μl of diluted thrombin was added. The reaction was stopped after 10 minutes with the addition of 5X SDS sample buffer. A second experiment was carried out overnight at 4°C with 0.1, 0.01 and 0.001 units of thrombin. The samples were boiled for 3 minutes at 100°C and analysed by SDS-PAGE. The concentration of thrombin used in subsequent experiments was decided, based on the results of these experiments (see Fig. 3.9).

Having cleaved the hBVR-A protein from the GST tag it was then necessary to separate both proteins such that a purified sample of hBVR-A could be obtained. Given that the hBVR-A protein was no longer attached to the GST tag it was anticipated that the two could be efficiently separated by running the sample back down the GSH column. The column was loaded and the straight through fractions were collected, assayed for BVR-A activity and analysed by SDS-PAGE. As expected, the hBVR-A protein did not bind to the column and the resulting protein was pure by SDS-PAGE as shown in Fig. 3.10 (a). Western blot analysis was performed and a single immunoreactive band was detected using antiserum raised against recombinant rat BVR-A. [See Fig. 3.10 (b)].

3.8. Sequence Analysis of cDNA Insert in Plasmid pGEX-BVR-A.

DNA sequencing was carried out by MWG Biotech using standard M13 primers. The results are shown if Fig. 3.11. Comparison of the sequence with that reported by Maines *et al.* (1996) indicated that the sequence of the insert differed at 6 base positions (see Fig. 3.12).

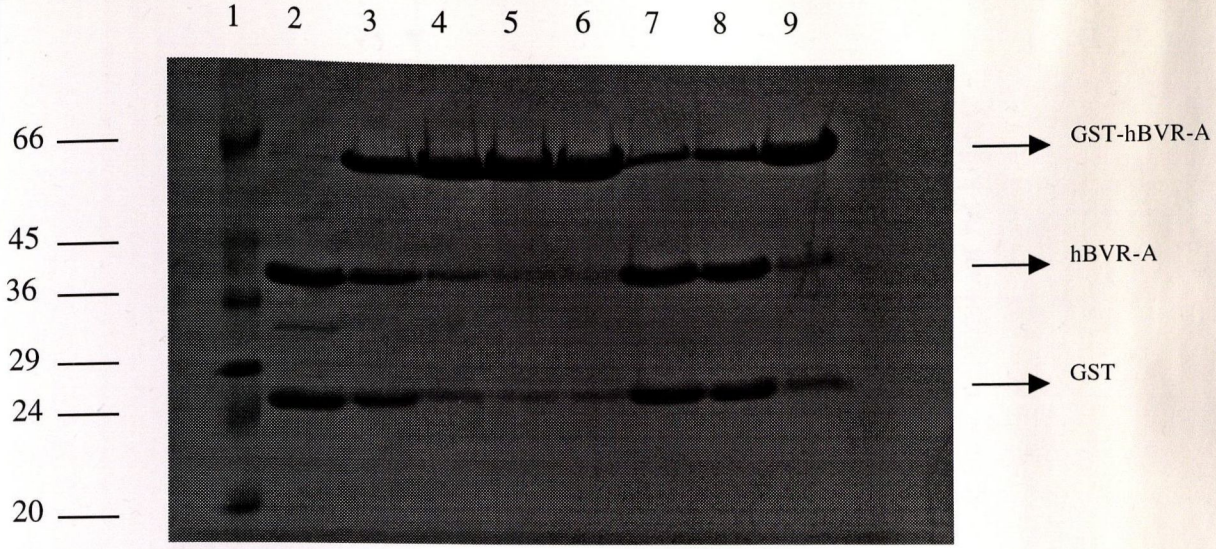

Figure 3.9. Kinetics of Thrombin Cleavage.

Thrombin cleavage experiments were carried out under various conditions as described in Section 2.2.8 (c). Lane 1 contains molecular weight standards (expressed as kilodaltons). Lanes 2 to 6 contain samples of GST-fusion protein cleaved for 10 mins at room temperature with 10, 1, 0.1, 0.01 and 0.001 units of thrombin, respectively. Lanes 7 to 9 contain samples cleaved overnight at 4°C with 0.1, 0.01 and 0.001 units of thrombin respectively.

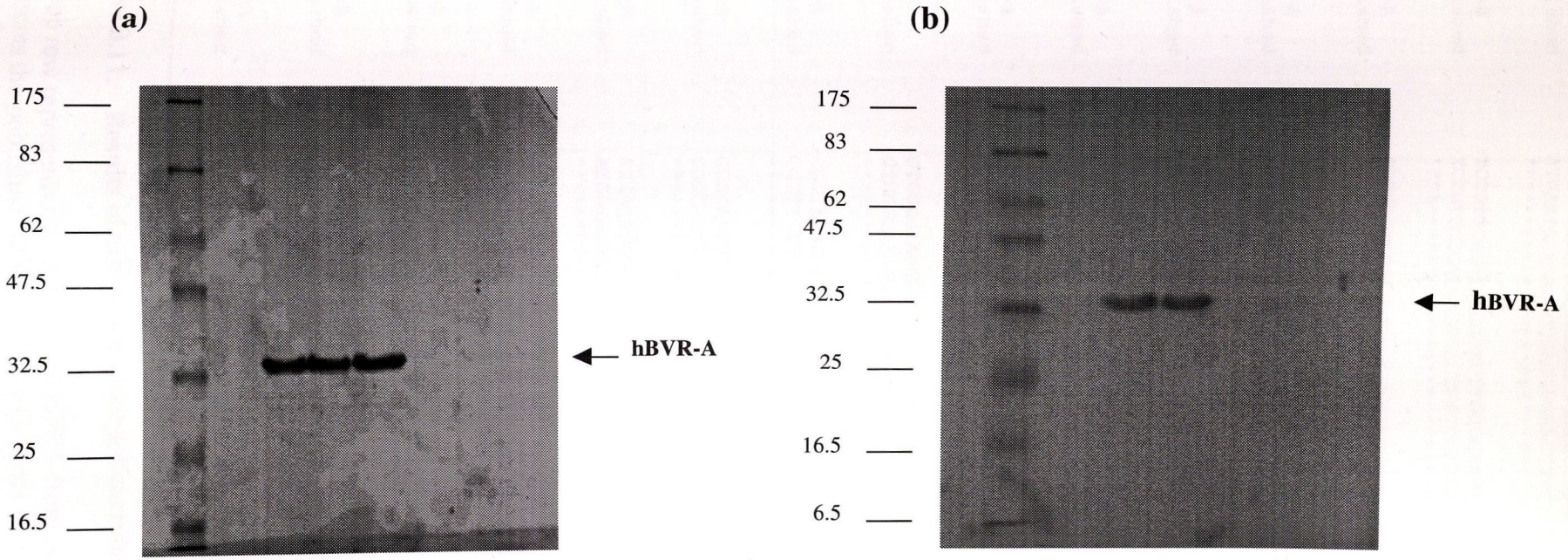

Figure 3.10. Analysis of hBVR-A Following Thrombin Cleavage.

Following removal of the GST-affinity tag, the purified hBVR-A protein was analysed on a 15% SDS-PAGE gel (**a**). The protein was subsequently immunodetected using antisera raised against recombinant rat kidney BVR-A (**b**).

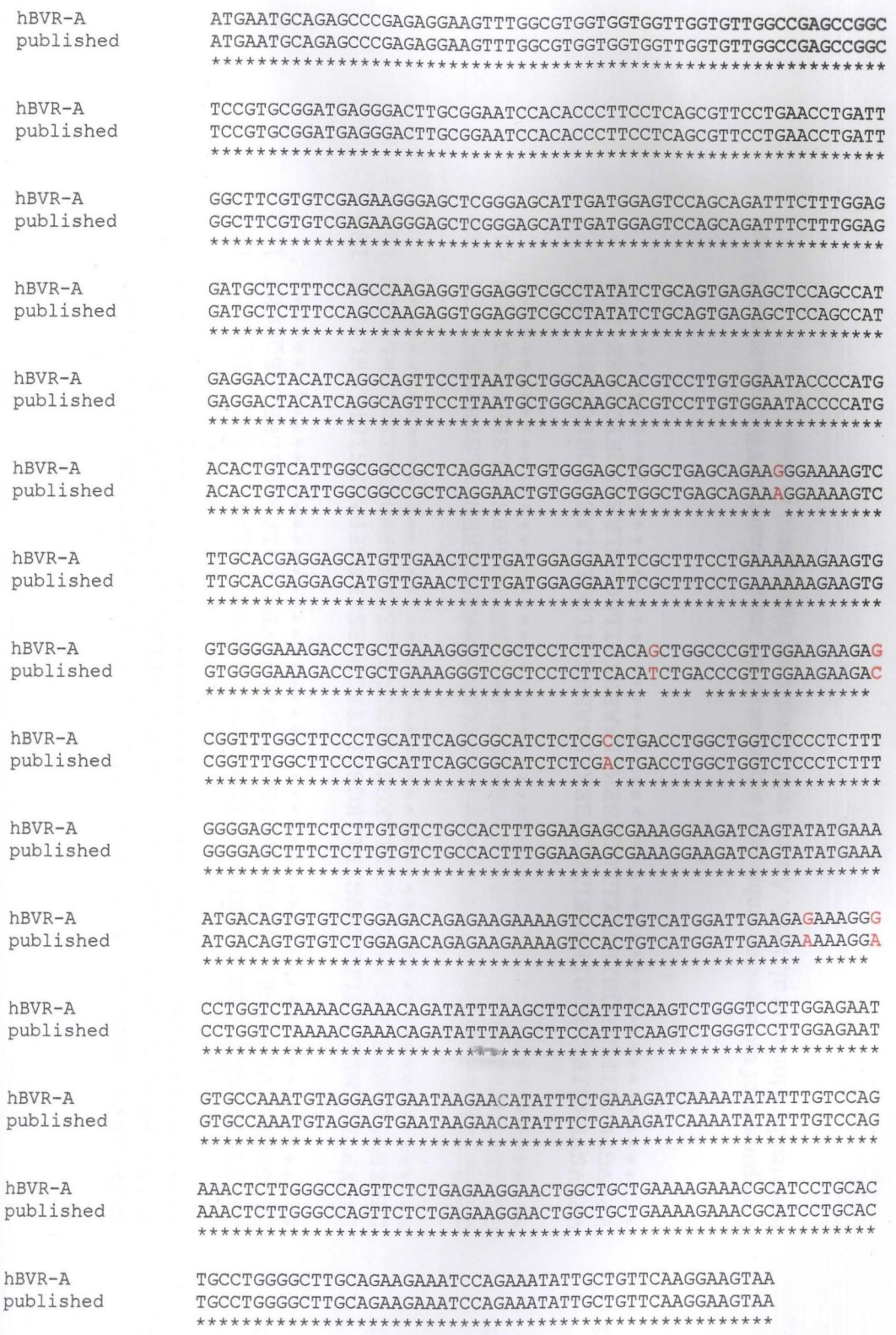

Figure 3.11. Results of cDNA Sequencing Reactions.

The top row represents the recombinant cDNA from pGEX-BVR-A. The bottom row represents the published cDNA sequence (Maines *et al.*, 1996). Base changes are highlighted in red.

```
hBVR-A      MNAEPERKFGVVVVGVGRAGSVRMRDLRNPHPSSAFLNLIGFVSRRELGSIDGVQQISLE 60
Published   MNAEPERKFGVVVVGVGRAGSVRMRDLRNPHPSSAFLNLIGFVSRRELGSIDGVQQISLE 60
            ************************************************************

hBVR-A      DALSSQEVEVAYICSESSSHEDYIRQFLNAGKHVLVEYPMTLSLAAAQELWELAEQKGKV 120
Published   DALSSQEVEVAYICSESSSHEDYIRQFLNAGKHVLVEYPMTLSLAAAQELWELAEQKGKV 120
            ************************************************************

hBVR-A      LHEEHVELLMEEFAFLKKEVVGKDLLKGSLLFTAGPLEEERFGFPAFSGISRLTWLVSLF 180
Published   LHEEHVELLMEEFAFLKKEVVGKDLLKGSLLFTSDPLEEDRFGFPAFSGISRLTWLVSLF 180
            **********************************:.****:********************

hBVR-A      GELSLVSATLEERKEDQYMKMTVCLETEKKSPLSWIEEKGPGLKRNRYLSFHFKSGSLEN 240
Published   GELSLVSATLEERKEDQYMKMTVCLETEKKSPLSWIEEKGPGLKRNRYLSFHFKSGSLEN 240
            ************************************************************

hBVR-A      VPNVGVNKNIFLKDQNIFVQKLLGQFSEKELAAEKKRILHCLGLAEEIQKYCCSRK 296
Published   VPNVGVNKNIFLKDQNIFVQKLLGQFSEKELAAEKKRILHCLGLAEEIQKYCCSRK 296
            ********************************************************
```

Figure 3.12. Comparison of the expected amino acid sequence of the recombinant hBVR-A protein with that reported by Maines *et al*, 1996. Amino acid changes are highlighted in blue.

3.9. Mass Spectroscopic Analysis of Recombinant hBVR-A.

On SDS-PAGE, recombinant hBVR-A migrates with a mobility corresponding to a molecular mass of 40 kDa. Similar behaviour has been reported for the native human enzyme (Rigney *et al.*, 1988; Maines & Trakshel, 1993). This is in contrast to the behaviour of the rat, mouse and ox enzymes which exhibit a molecular mass of 34 kDa on electrophoresis (Rigney *et al.*, 1988). Given that the rat enzyme contains 295 amino acids and the human enzyme contains 296 amino acids, mass spectroscopy was carried out by Dr. Ian Campazanu (University of Southampton) in order to determine the true relative molecular mass of hBVR-A. The results are shown in Fig. 3.13. The major peak at 34,330 represents the hBVR-A protein while the additional peak at 34,030 is most likely a breakdown product.

3.10. Preparation of SeMet Substituted hBVR-A for use in MAD Analysis.

The recombinant pGEX-hBVR-A expression plasmid was transformed into the *E.coli* methionine auxotroph strain B834(DE3) according to the procedures outlined in Section 2.2.4 (a). LB broth was replaced by New Minimal Medium [Section.2.2.19 (b)] for expression purposes. The recombinant protein was purified in a 3-step process as described in Section 3.5. As shown in Fig. 3.14, a homogeneous preparation of hBVR-A was obtained, however, protein yields decreased from 80 mg to 20 mg per 2 l culture using this modified method suggesting that the presence of SeMet in the culture medium exerted toxic effects on the cells.

(a)

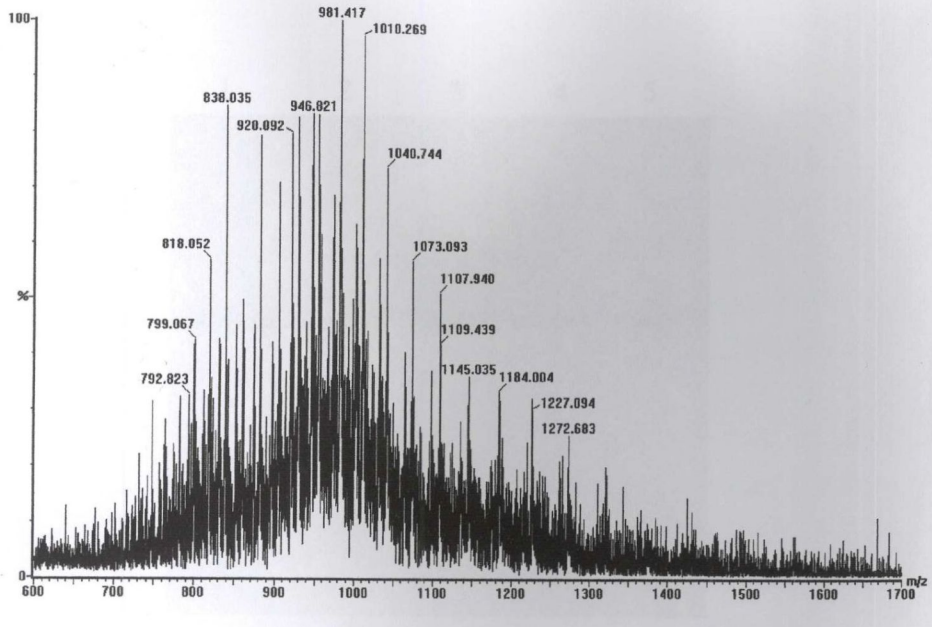

(b)

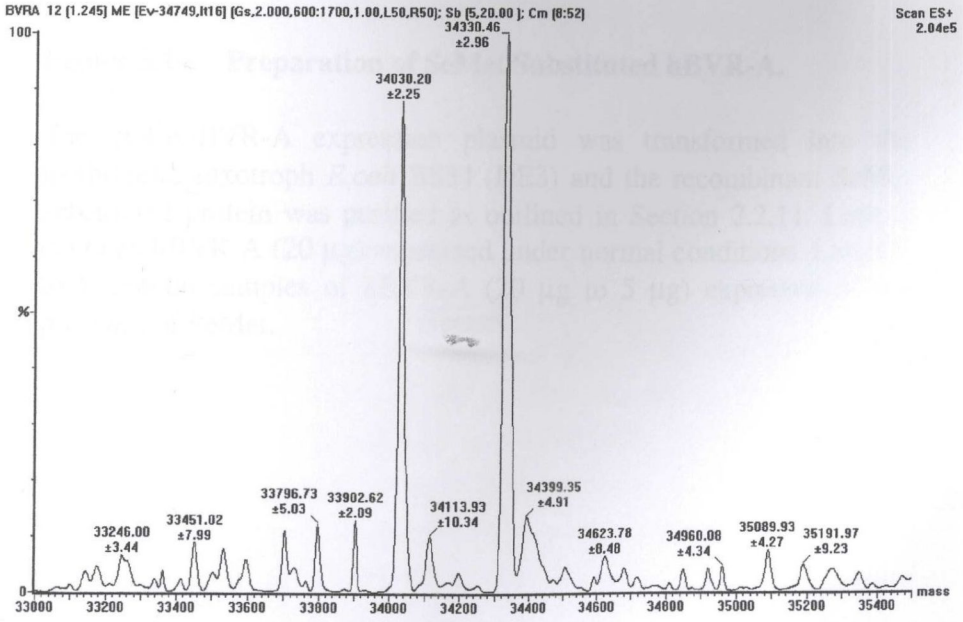

Figure 3.13. Mass Spectroscopic Analysis of Recombinant hBVR-A.

(a) Raw data obtained from ES-MS analysis of 2 μg of hBVR-A

(b) Deconvoluted spectrum of multiply charged envelope.

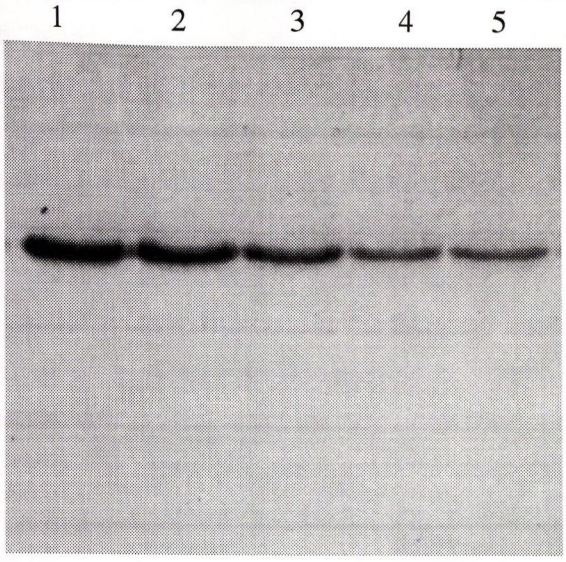

Figure 3.14. Preparation of SeMet Substituted hBVR-A.

The pGEX-BVR-A expression plasmid was transformed into the methionine auxotroph *E.coli* B834 (DE3) and the recombinant SeMet substituted protein was purified as outlined in Section 2.2.11. Lane 1 contains hBVR-A (20 μg) expressed under normal conditions. Lanes 2 to 5 contain samples of hBVR-A (20 μg to 5 μg) expressed in the presence of SeMet.

Discussion.

The full length cDNA encoding human BVR-A was amplified from a monocyte cDNA library and subsequently cloned into the pGEX-KG and pTrcHis B expression vectors. In both cases, induction of transformed cultures with IPTG resulted in the expression of a recombinant protein which displayed the appropriate molecular weight and was immunologically cross-reactive with antisera raised against recombinant rat kidney BVR-A. The enzyme was catalytically active in the form of a GST and hexahistidine fusion, however, expression levels were lower in the case of the GST-fusion which is most likely attributed to the size of the affinity tag (26 kDa). This problem was overcome by growing cells at 30°C (as opposed to 37°C) overnight in the presence of 2% glucose which serves to repress any background protein expression that may be deleterious to the cells. The presence of the purification tags had no apparent effect on BVR-A activity and both proteins exhibited a high affinity for the biliverdin substrate. Sequence analysis of the recombinant pGEX BVR-A expression plasmid revealed that the cDNA insert differed at 6 base positions to the sequence reported by Maines *et al.* (1996). This may have arisen due to polymorphisms or base misincorporations during the PCR cycles. Alternatively, there may be errors in the original sequence reported in the literature. The predicted amino acid changes are highlighted in Fig. 3.12 and appear to have no effect on enzyme activity. The overexpression protocol described in the present work produced an average of 80 mg of GST-fusion protein from a 2 l culture. A homogeneous preparation of enzyme was obtained in a 3-step process the GST moiety was subsequently removed following digestion with thrombin.

Rat and human BVR-A are substantially similar at the nucleotide and amino acid levels and differ in the number of amino acids by only one residue (295 for the rat versus 296 for the human enzyme). Although sequence divergence for short regions such as the 11 carboxyterminal amino acids can be as low as 45%, overall the predicted peptides and nucleotide sequences share 83% identity. On SDS-PAGE, the rat enzyme displays an apparent mass of 34 kDa (Kutty & Maines, 1981), however, the human enzyme migrates as a 40 kDa protein. It has been suggested that this difference in molecular mass reflects differential post-translational modification (Maines *et al.*, 1996), therefore, mass spectroscopic analysis was undertaken in order to determine the true molecular mass of hBVR-A. A value corresponding to 34,330 kDa was obtained, therefore, it can be concluded that hBVR-A runs anomalously on SDS-PAGE and is not subject to significant post-translational modification as has been suggested previously.

Attempts to solve the three-dimensional structure of hBVR-A in collaboration with Dr. Darren Thompson, University of Southampton are ongoing. Crystals diffracting at 3Å

have recently been obtained (see overleaf) and efforts are underway to improve this resolution. A selenomethionine derivative of the recombinant protein has also been prepared for use in Multiwavelength Anomalous Diffraction (MAD) experiments. Cowie and Cohen (1957) demonstrated for the first time that methionine (Met) could be replaced to high level by selenomethionine (SeMet) in *E.coli*. Two different approaches have been utilised; bacteria may be either grown in sulphur free media with a limited source of selenate or selenite or bacterial strains auxotrophic for methionine may be grown in minimal media supplemented with SeMet instead of Met. This second approach is the method of choice and it has since been demonstrated that $tRNA^{Met}$ is charged with SeMet, which is subsequently incorporated into polypeptides *in vivo* (McConnell & Hoffmann, 1972). The MAD method does require the special properties of synchrotron radiation, but it has advantages in that isomorphism is perfect and all data can be measured from a single crystal. Telluromethionine (TetMet) has also been used in an analogous approach, however it is highly toxic and difficult to synthesise chemically.

A preliminary crystallographic study of recombinant rat BVR has been reported in the literature (Sun *et al.*, 2000). In a personal communication from Dr. Akihiro Kikuchi, it has been confirmed that the nicotinamide cofactor binds, as predicted from sequence alignments, to a conserved glycine rich region in the N-terminal domain of the protein termed the "Rossmann" fold (Rossmann *et al.*, 1974). This βαβ fold is common to the nucleotide binding domains of many proteins. It is centered around a highly conserved glycine-rich region (Gly-X-Gly-X-X-Gly), where X is any amino acid that constitutes a tight turn at the end of the first strand of a β-sheet and marks the beginning of the succeeding α-helix (Weirenga *et al.*, 1985). The first glycine residue is essential for the tightness of the turn, the second (at the N-terminus of the helix) allows the dinucleotide to be bound without obstruction from the amino acid side chain at this position and the third seems to provide space for a close interaction between the β-strand and the α-helix. Figure 3.15 shows the relevant region of the hBVR-A sequence aligned with a number of proteins of known structure. Numbers are included to indicate the position in the primary structure of the first residue shown for each sequence. Fig. 3.16 shows the aligned N-terminal sequence of BVR-A enzyme from a number of species. This region appears to be conserved.

McCoubrey and Maines (1994) have carried out site-directed mutagenesis on the three cysteine residues (amino acids 73, 280 and 291) of rat BVR-A, in order to examine their roles in substrate and co-factor binding. Modification of the amino-proximal cysteine (Cys^{73}) which is contained within the stretch of amino acids 64 to 115, shown in Fig. 3.17, completely inactivated the enzyme with NADH and NADPH. Although modification of either of the two cysteines located near the C-terminus significantly reduced activity

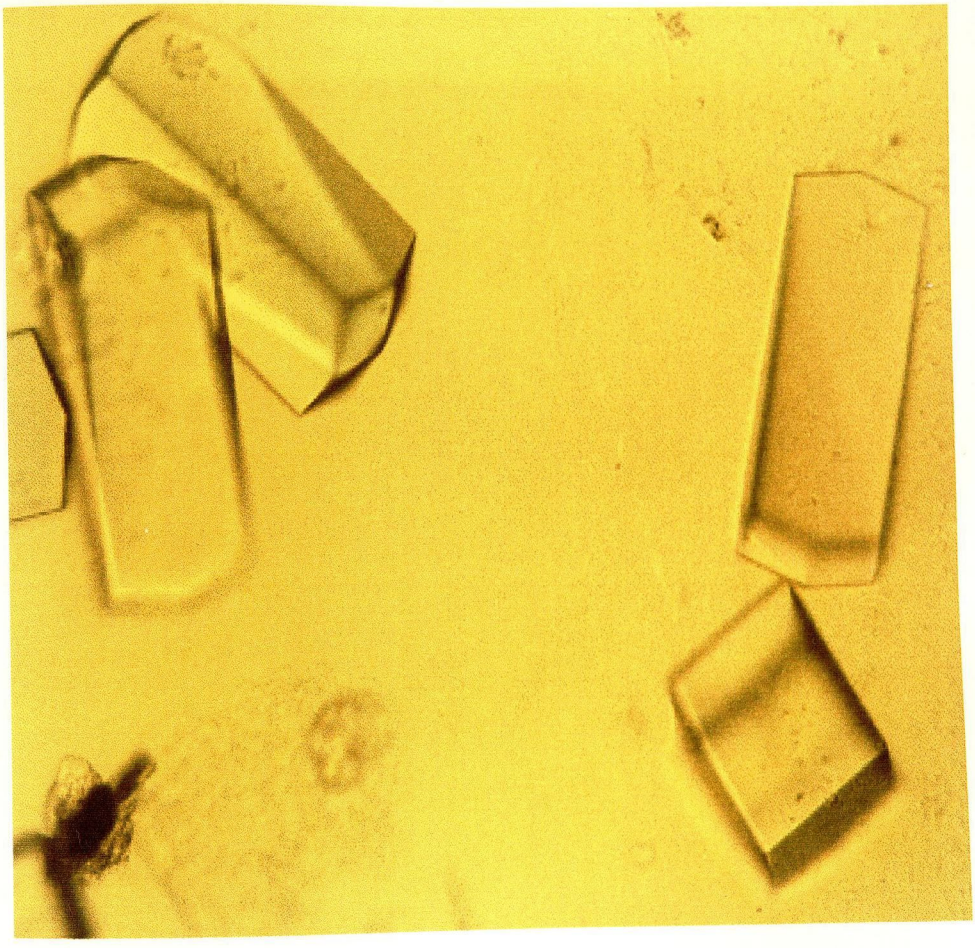

Figure 3.15. **Amino acid sequences of nicotinamide coenzyme-binding enzymes around the βαβ dinucleotide binding fold.**

Sequences **1** to **5** are from known structures used to derive the fingerprint for either NAD or FAD binding. Proteins **1** to **3** bind NAD, **4** and **5** bind FAD. The remaining dinucleotide binding regions have been predicted from amino acid sequeence information. Proteins **1 1** and **1 2** are rat kidney and human liver BVR-A, respectively. (The numbers in brackets indicate the amino acid residue to which these stretches correspond).

	β	α	loop	β	
1	T C A V F G L	G G V G L S V I M G C K A A G A A	- -	R I I G V D I	(194-224)
2	K I T V V G V	G A V G M A C A I S I L M K D L A	D -	E V A L V D V	(22-53)
3	K I G I D G F	G R I G R L V L R A A L S C G A Q	- -	V V A V N D P	(2-32)
4	D Y L V I G G	G S G G L A S A R R A A E L G A	- - -	R A A V V E S	(22-51)
5	Q V A I I G A	G P S G L L L G Q L L H K A G I	- - -	D N V I L E R	(4-32)
6	V I F V A G L	G G I G L D T S K Q L L K R D L	K - -	N L V I L D R	(9-38)
7	T F A V Q G F	G N V G L H S M R Y L H R F G A	K - -	C V A V G E S	(246-275)
8	K V C I V G S	G D W G S A I A K I V G G N A A	- - -	Q L A Q F D P	(4-33)
9	T V G V L G S	G H A G T A L A A W F A S R H V	P T A	L W A P A D H	(34-45)
10	H V T V I G G	G L M G A G I A Q V A A A T G H	- - -	T V V L V D Q	(17-45)
11	G V V V V G V	G R A G S V R L R D L K D P R S	A A - -	V S R R E L	(10-46)
12	G V V V V G V	G R A G S V R M R D L R N P H P	S S - -	V S R R E L	(10-48)

1 Horse liver alcohol dehydrogenase (Eklund *et al.*, 1981; Jornvall, 1970).

2 Dogfish muscle lactate dehydrogenase (Taylor, 1977; Eventoff *et al.*, 1977).

3 Lobster glyceraldehyde-3-phosphate dehydrognase (Davidson *et al.*, 1967; Moras *et al.*, 1975).

4 Human erythrocyte glutathione reductase (Krauth-Siegel *et al.*, 1982; Schulz *et al.*, 1982).

5 *Pseudomonas fluorescens* *p*-hydroxybenzoate hydroxylase (Weijer *et al.*, 1982; Weirenga *et al.*, 1979).

6 Drosphilia alcohol dehydrogenase (Kreitman, 1983).

7 Bovine glutamate dehydrogenase (Moon & Smith, 1973).

8 Rabbit muscle glycerol-3-phosphate dehydrogenase (Cole *et al.*, 1978).

9 *Agrobacterium tumefaciens* nopaline synthase (Depicker *et al.*, 1982).

10 Pig L-3-hydroxyacyl-CoA-dehydrogenase (Bitar *et al.*, 1980).

11 Rat kidney biliverdin-IXα reductase (Fahkrai & Maines, 1992).

12 Human liver biliverdin-IXα reductase (Maines *et al.*, 1996).

Predicted secondary structure is indicated in blue. The conserved basic or hydrophilic residue found at the start of the consensus sequence has been highlighted in cyan. There are six positions at which conserved small, hydrophobic residues are usually found, and these have been highlighted in green. The characteristic glycine residues and the conserved acidic residue have been highlighted in magenta.

Figure 3.16. **N-terminal amino acid sequences of BVR-A from a number of species.**

Human	A E P R K F G V V V V G V G R A G S V R M R D L R N P H P S	*a*
Rat	A E P R K F G V V V V G V G R A G S V R L R D L K D P R S A	*b*
Ox	A E P R K F G V V V V G V G R A G S V R L R	*c*
Salmon	- - - - - F G V V V V G I G - - - - - - L A P L P S X X - -	*d*

a Maines *et al.*, 1996.

b Fahkrai & Maines, 1992.

c Rigney, 1989.

d Elliot, 1996.

Figure 3.17. Sequence Comparison of Human liver BVR-A (amino acids 65 - 116) with that of Rat Kidney BVR-A (amino acids 64 -115).

Human	E S E V A Y I C S E S S S H E D Y I R Q F L N A G K H V L V E Y P M T L S L A A A Q E L W E L A E Q
Rat	E I D V A Y I C S E S S S H E D Y I R Q F L Q A G K H V L V E Y P M T L S F A A A Q E L W E L A E Q

The amino acid sequences shown are those deduced from the cDNA sequences as reported by Fahrai and Maines (1992) for the rat enzyme and by Maines *et al.* (1996) for the human enzyme (confirmed in this study). Amino acids in the rat sequence that differ at the same position from the human sequence are highlighted in red.

with both co-factors, these mutations did not inactivate the enzyme. These workers concluded that Cys^{73} plays a central role in substrate or co-factor binding. O'Carra and Collerhan (1970) reported that the NADH and NADPH-dependent activities of BVR-A are competitive, suggesting that these co-factors bind to the same site. Given that the N-terminus contains a Rossman fold-like sequence that represents the co-factor binding region, it is tempting to speculate that the downstream region, at amino acids 64 to 115, represents an important part of the substrate-binding catalytic site.

Contrary to the majority of known pyridine nucleotide-dependent dehydrogenases studied to date, BVR-A and BVR-B are monomeric enzymes. It has been postulated that monomeric $NAD(P)^+$-linked oxidoreductases may represent a link between a hypothetical ancestral dehydrogenase, as proposed by Rossmann *et al.* (1974) and the diversified oligomeric forms that predominate today (Wermuth *et al.*, 1977). While the monomeric pyridine nucleotide enzymes still comprise a minority amongst dehydrogenase and reductase enzymes, the number being characterised is growing steadily. Some of the better known examples include dihydrofolate reductase (Batley & Morris, 1977) and some forms of aldehyde reductase (Davidson *et al.*, 1978; Turner & Tipton, 1972). A number of distinct protein superfamilies are now emerging based on structural differences/similarities between monomeric dehydrogenase families. For example, the mammalian hydroxysteroid dehydrogenases (HSDs) include at least two distinct protein families; the aldo-keto reductase superfamily (Bohren *et al.*, 1989) and the short-chain alcohol dehydrogenase family. Crystallographic studies on recombinant human placental aldose reductase was the first demonstration of a NADH/NADPH-binding domain consisting solely of as β/α barrel (Wilson *et al.*, 1992). Conversely, the 3.0 Å-resolution X-ray crystal structure of 3α-hydroxysteroid/dihydrodiol dehydrogenase (3α-HSD) folds into a α/β barrel motif (Pawlowski *et al.*, 1991). Deviations from the classic Rossman fold are not uncommon. Examples include mercuric reductase (Browne *et al.*, 1983) and *S.cerevisiae* alcohol dehydrogenase (Wills & Jornvall, 1977) as shown in Fig. 3.18.

Efforts are also being made to solve the 3-dimensional structure of the cyanobacterial biliverdin reductase from *Synechocystis* sp. PCC 6803 (kindly supplied by Dr. Wendy Schluchter, University of California). The enzyme was identified in 1997 in the first demonstration of bilirubin formation in a bacterium (Schluchter & Glazer, 1997). The enzyme bears 22% sequence similarity to the rat and human enzyme with residues 92 - 134 being the most highly conserved. The kinetic profile of the enzyme differs from it's mammalian counterpart in that optimal activity is seen at pH 5.8 for both NADPH and NADH (as opposed to 6.5 for NADH and 8.7 for NADPH), suggesting that the enzyme may be localised in an acidic cell compartment such as the intrathylakoidal space. It has been suggested that the conversion of biliverdin to bilirubin in cyanobacteria is important

Figure 3.18. Examples of proteins with a classic Rossmann fold that deviate in sequence (highlighted in red) from the consensus primary sequence usually found in this region.

	consensus sequence (where * = any hydrophobic residue)	* * G X G X X G	
1	mercuric reductase, FAD-binding domain (Brown *et al.*, 1983)	A V I G S G G A A M A	(102-112)
2	mercuric reductase, NADP-binding domain (Brown *et al.*, 1983)	A V I G S S V V A L E	(274-284)
3	alcohol dehydrogenase (Saccharomyces cerevisiae) (Wills & Jornvall ,1977)	R V L G I D G G E G K	(196-207)

for normal phycobiliprotein biosynthesis. Phycobiliproteins are the major light harvesting proteins in cyanobacteria and red-algae. These proteins carry linear tetrapyrrole prosthetic groups (phycobilins) and biliverdin-IXα is believed to be the common precursor to all of the phycobilins. The phycobiliproteins of Synechocystis sp. PCC 6803 contain only phycocyanobilin (PCB) which is produced from the precursor 15, 16-dihydrobiliverdin. BVR mutants, producing no bilirubin, synthesised approximately 85% of the normal amount of phycobilisome cores containing phycocyanobilin-bearing core peptides but no detectable phycocyanin. It has been suggested that bilirubin directly modulates the flux of biliverdin into the biosynthetic pathway and/or influences the transcription of phycocyanin structural genes. Alternatively, the lack of phycocyanin in response to the absence of bilirubin (which is believed to be a physiologically relevant scavenger of reactive oxygen species) may be a protective mechanism as the absence of phycocyanin would lower the absorbance cross-section for photosynthesis and therefore slow electron transport resulting in decreased levels of reduced ferredoxin, a known source of reactive oxygen species. It will be of great interest to elucidate the functions of this ancient enzyme given the emerging role of haem catabolic products as antioxidants, anti-inflammatories and putative signalling molecules (see Chapter 5).

Chapter 4

Kinetic Studies on Recombinant Human Biliverdin-IXα Reductase

Kinetic studies on BVR-A have proved refractory due, in part, to the relative insolubility of the reaction product, bilirubin-IXα, which has been reported as low as 7 nM at pH 7.4 (Broderson, 1979). Internal hydrogen bonding between the propionate side chains and the terminal lactams is largely responsible for the low solubility of bilirubin-IXα in aqueous media. BSA is normally included in the assay of BVR-A activity to bind bilirubin-IXα, thereby increasing it's solubility. The extinction coefficient for bilirubin bound to BSA is 55 $mM^{-1}cm^{-1}$ and although it is difficult to obtain a reliable estimate of the extinction coefficient in the absence of a binding protein, Phillips (1981) has reported a value of 27 mM^{-1} cm^{-1}. Another complicating feature for kinetic studies of BVR-A is the potent substrate inhibition observed at relatively low concentrations of biliverdin. BSA binds to biliverdin and it's inclusion in the assay mixture alleviates the substrate inhibition to some extent by reducing the effective free concentration of biliverdin, however total concentrations of biliverdin need to be adjusted to give the free concentration when calculating kinetic constants for BVR-A. Studies on ox kidney BVR-A have been performed in the absence of BSA at pH 9 where both the apparent $K_m^{biliverdin}$ and the substrate inhibitory K_i increase substantially. Under these conditions the ox enzyme obeys an ordered BiBi mechanism with NADPH as the first substrate to bind to the enzyme and bilirubin the first product to dissociate (Rigney & Mantle, 1988). These studies revealed that substrate inhibition occurs when biliverdin binds to the enzyme-$NADP^+$ complex during the catalytic cycle (Rigney *et al.*, 1988) as shown in Figure 4.1. Inhibition was found to be partial for the ox kidney enzyme (Phillips, 1988) which is in contrast to the rat kidney enzyme where the substrate inhibition observed is total (Ennis, 1996). Product inhibition by bilirubin cannot be ruled out however it is difficult to determine due to it's limited solubility. A number of workers have estimated the apparent K_m values for biliverdin-IXα and NAD(P)H in a number of different species and tissues at neutral pH and these are summarized in Table 4.1. The biliverdin concentrations necessary to measure initial rates below the substrate inhibitory phase are in the submicromolar range. Thus it appears that for the accurate determination of steady state kinetic constants for BVR-A, at physiological pH values and in the absence of additional components (e.g. BSA), an alternative assay system needs to be developed.

Mammalian BVR-A shows a much higher affinity for NADPH than for NADH, which is reflected in the approximately 100-1000 fold lower apparent K_m value for the former (see Table 4.1). NADPH also confers on the enzyme a much higher affinity for biliverdin than does NADH and presumably promotes a tighter binding of biliverdin to the enzyme-nucleotide complex. Both $NADP^+$ and NAD^+ act as competitive inhibitors against

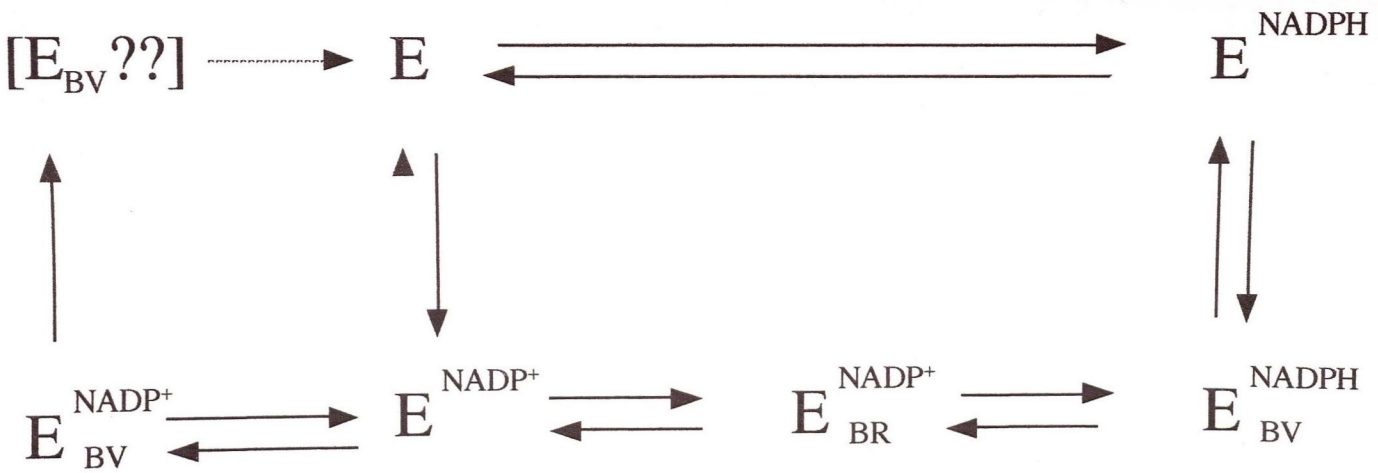

Figure 4.1. The Proposed Reaction Mechanism for Reduction of Biliverdin by BVR-A.
(Adapted from Rigney, 1986).

SUBSTRATE	CO-SUBSTRATE	GUINEA-PIG LIVER (a)	GUINEA-PIG LIVER (b)	RAT KIDNEY (c)	RAT LIVER (d)	RAT LIVER (e)	OX KIDNEY (f)	PIG SPLEEN (d)	HUMAN LIVER(g)
BILIVERDIN	NADPH	-	0.2	3.7	0.3	3	-	0.3	0.3
BILVERDIN	NADH	0.6 - 1.4	1 - 2	-	3	5	5	1 - 2	-
NADPH	BILIVERDIN	-	2 - 5	-	3	3	-	0.5	13 - 36
NADH	BILVERDIN	240	200 - 500	-	1500 - 2000	270	500	1500 - 2000	5600-8200

Table 4.1. Apparent K_m Values for Biliverdin and NAD(P)H with Biliverdin Reductase from Different Species and Tissues*

(a) Singleton & Lancaster (1965)

(b) O'Carra & Colleran (1971)

(c) Tenhunen *et al.* (1970a), assays were performed in the presence of 0.35 mg/ml BSA.

(d) Noguchi *et al.* (1979)

(e) Kutty & Maines (1981), assays were performed in the presence of 1 mg/ml BSA.

(f) Phillips (1981), assays were performed in the presence of 2.5 mg/ml BSA.

(g) Yamaguchi *et al.* (1994)

* Adapted from Rigney (1986)

(All values are expressed as μM)

NADPH and NADH and are mixed against biliverdin suggesting that the tetrapyrrole and nucleotide cofactors bind in a ternary complex. The hydride ion transfer from the C4 position of NADH was found to be stereospecific for both salmon liver and rat kidney BVR-A (Elliot, 1996; Ennis, 1996). Such stereospecificity in oxidoreductase reactions has been traditionally used to classify the enzymes involved into two distinct groups; the A-stereospecific enzymes which remove a hydride from the A-side of the pyridine ring, and the B-stereospecific enzymes which remove a hydride from the B-side of the pyridine ring (Popjak, 1970). Both the rat and salmon form of the enzyme were found to be B-side specific. Given that the stereospecificity of NAD(P)H-linked oxidoreductases is highly conserved during the course of evolution it was predicted that human BVR-A would also exhibit this behaviour.

BVR-A has the characteristic of having two distinct pH optima depending on which cofactor is used. With NADH optimal activity is seen at pH 6.7-6.9, however, with NADPH as cofactor, optimal activity is seen at pH 8.7 (Singleton & Laster, 1965; Noguchi *et al.*, 1979; Kutty & Maines, 1981; Rigney, 1986; Fahkrai & Maines, 1992). The nature of this dual pH-cofactor specificity has not been further investigated and to date no other enzyme system has been reported to exhibit this behaviour.

There is no three-dimensional structure for BVR-A although crystals have been reported for the rat enzyme (Sun *et al.*, 2000). As mentioned in Section 2.2.19, crystals of recombinant human BVR-A have been obtained in collaboration with Dr. Darren Thompson (University of Southampton). The experiments outlined in this study were designed in order to gain further insight into the kinetics and structure of the human enzyme and should provide useful predictive information when examined in the context of the anticipated crystal structure.

4.1 Kinetic Characterisation of Recombinant Human BVR-A

4.1 (a) Time-dependence of Product Formation.

Product formation as a function of time was assessed by monitoring bilirubin production (A_{460}) over a 20 minute period and the results are shown in Fig. 4.2 (a). The assay mixture contained 20 μM biliverdin; 37 μM BSA and 705 μM NADH in 100 mM sodium phosphate buffer, pH 7.2. The assay was conducted at 30°C with 100 ng of purified enzyme. The reaction was initiated by the addition of NADH, having demonstrated the absence of any increase in absorbance in the presence of all other components, and shows a linear relationship indicating that true initial rates are measured. Linear product time curves were seen using a range of enzyme concentrations (see below).

4.1 (b) The Effect of Enzyme Concentration on Initial Rate.

The relationship between enzyme concentration and the initial rate of bilirubin formation is shown in Fig. 4.2 (b). Enzyme activity was measured at pH 7.2 as described in Section 2.2.15 (b). A series of reactions (2 ml) were set up containing 1.25 - 10 μg of purified enzyme. The increase in absorbance due to bilirubin production was measured spectrophotometrically at 460 nm (normally for 30 seconds to 2 minutes). All reactions were carried out at 30°C and started by the addition of NADH to the cuvette. There is clearly a linear relationship between initial rate and enzyme concentration, implying simple kinetics i.e. no evidence for polymerisation.

4.1 (c) The Effect of Biliverdin Concentration on Initial Rate Kinetics.

A series of reactions were set up employing increasing concentrations of biliverdin-IXα in order to determine (a) if the recombinant enzyme is subject to substrate inhibition and (b) if this inhibition is alleviated in the presence of BSA. The assay solution contained 705 μM NADH and biliverdin concentrations covering the range 1 - 25 μM. The assay buffer used was 100 mM sodium phosphate, pH 7.2. The buffer was pre-warmed to 30°C, and all assays were conducted at this temperature. Bilirubin production was monitored at 460 nm in both the presence and absence of 37 μM BSA and assays were started by the addition of enzyme to the cuvette (final volume; 2 ml). The results of this experiment are show in Figs. 4.3 (a) and (b). Over the entire range of biliverdin-IXα concentrations

Figure 4.2. (a) Time-dependence of Product Formation.

Product formation as a function of time was observed by monitoring the absorbance at 460 nmthe times indicated. The line is a least squares fit to $y = m\ x$ and range is indicated where necessary ($R^2 = 0.9855$). Assays were conducted as outlined in section 4.1 (a) using 100 ng of enzyme.

Figure 4.2. (b) Effect of Enzyme Concentration on Initial Rate.

Assays were performed as described in Section 4.1 (b) using the protein concentrations iindicated. Bilirubin production was monitored at 460 nm for 30 seconds to 2 minutes to measure the initial rate. Each data point represents the mean of duplicate readings and the error bars shown represent the range of these values. (The solid line is a least squares fit to $y = m\ x$, $R^2 = 0.9971$).

(a)

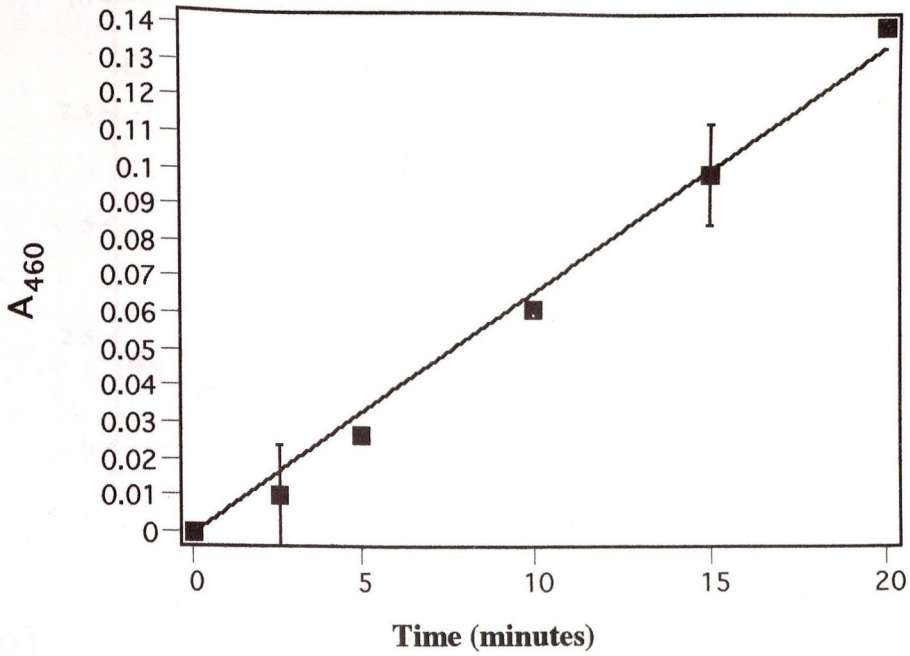
0.14
0.13
0.12
0.11
0.1
0.09
0.08
0.07
0.06
0.05
0.04
0.03
0.02
0.01
0
A460
0
5
10
15
20
Time (minutes)

(b)

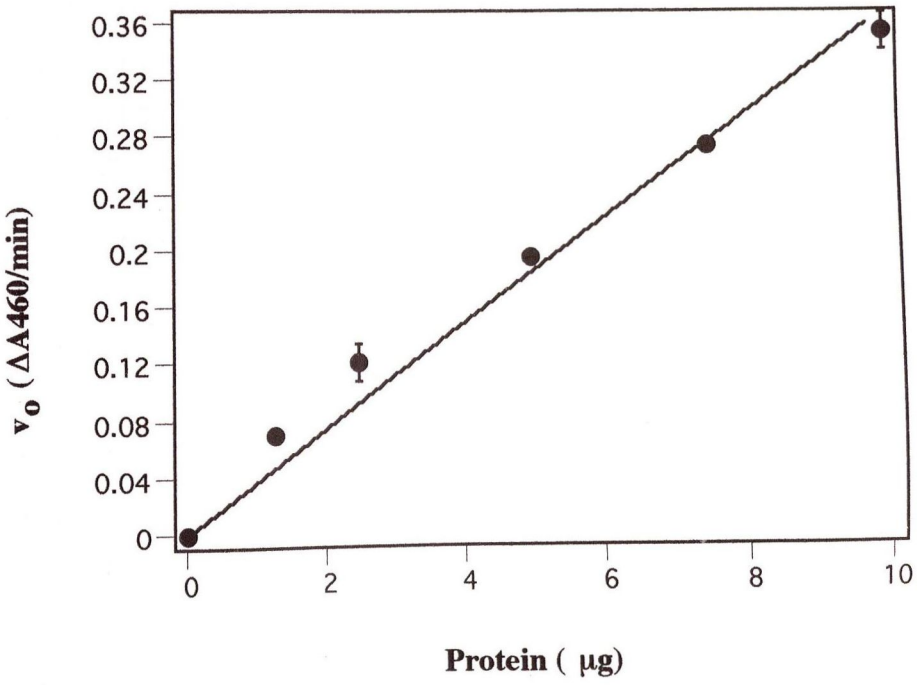
0.36
0.32
0.28
0.24
0.2
0.16
0.12
0.08
0.04
0
vo (ΔA460/min)
0
2
4
6
8
10
Protein (μg)

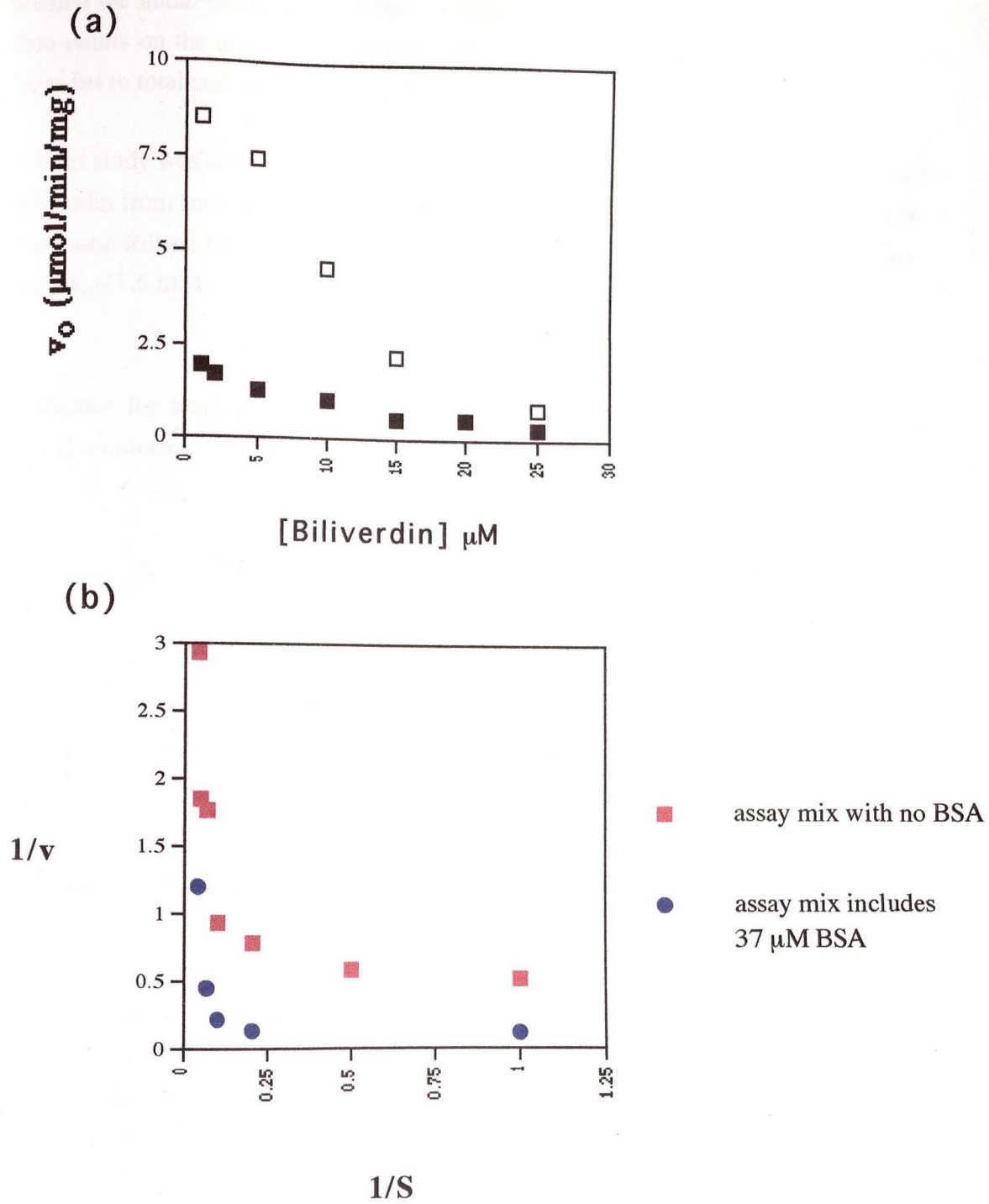

Figure 4.3. Effect of Biliverdin Concentration on Initial Rate.

(a) Assays were performed as described in section 4.1 (c) in the presence (□) and absence (■) of 37 µM BSA. Biliverdin was assayed over a concentration range of 1 - 25 µM. (Data points represent the mean of duplicate recordings).

(b) Double reciprocal plot of initial rate versus substrate concentration.

studied the initial rate declines as the substrate concentration is increased. There are no data points on the upward limb of the curve so that interpretation of kinetic parameters from fits to total and partial substrate inhibition is unreliable.

A brief study was undertaken to study the feasibility of estimating apparent K_m values for biliverdin from such data. This was in part stimulated by a personal communication from Professor Robert Eisenthal that data obtained by Ennis (1997) could be fitted to give a high K_m (1.6 mM).

Equations for total and partial substrate inhibition were used to generate "perfect" data sets (Equations 4.1. and 4.2, respectively).

$$v_0 = \frac{V_{max}\, S}{K_m + S + S^2/K_i} \qquad \text{(Eqn. 4.1)}$$

$$v_0 = \frac{V_{max1}\, S + V_{max2}\, S^2}{K_m + S + S^2/K_i} \qquad \text{(Eqn. 4.2)}$$

Figure 4.4 (a) shows a series of curves where V_{max} and K_m are set to 10 and K_i values are decreased from 100 to 1. Estimates of the kinetic parameters from a fit to total substrate inhibition yields the expected values. Similar results were obtained from fits to partial substrate inhibition. In Figure 4.4 (b), the K_m has been set to 100 and in this case neither the K_m nor K_i are apparent from values of K_i below 25. The defined values and estimates are shown in Table 4.2. Also shown in Fig. 4.5 is a data set that by visual inspection looks similar to Fig. 4.4, however a 10% error was used to adjust the data set in order to present a more realistic scenario. As before, when the K_m is low, good fits are obtained, however, at a K_m of 100 poor fits are obtained at each K_i value (Table 4.3).

When generating saturation curves for hBVR-A, no data points are present on the ascending limb of the curve. Figure 4.6 represents a data set where the number of data points on the ascending limb is decreasing. The V_{max} has been set to 10, K_m to 10 and K_i to 1. As expected good fits are obtained when all the data points are present, however, as

Figure 4.4. Determination of Kinetic Parameters Using a Perfect data Set fitted to an Equation for Total Substrate Inhibition.

This figure shows a series of curves generated using an equation for total substrate inhibition where V_{max} is set to 10 and K_i values decrease from 100 to 1. In Graph (**a**) K_m is set to 10 whereas in Graph (**b**) K_m is set to 100. The data points are those generated using Eqn.4.1 while the solid line was obtained by fitting to Eqn.4.1 using MacCurve fit. The statistically-derived estimates for the kinetic parameters K_m, V_{max} and K_i are shown in Table 4.2.

Table 4.2

Statistically-derived estimated values for K_m, V_{max} and K_i compared with defined values.

Defined K_i	Statistically-derived estimates					
	$K_m = 10$			$K_m = 100$		
	V_{max}	K_m	K_i	V_{max}	K_m	K_i
100	10	10	100	10	100	100
50	10	10	50	10	100	50
25	10	10	25	10	100	25
10	10	10	10	3	26	30
1	10	10	1	0.2	6	20

(a)

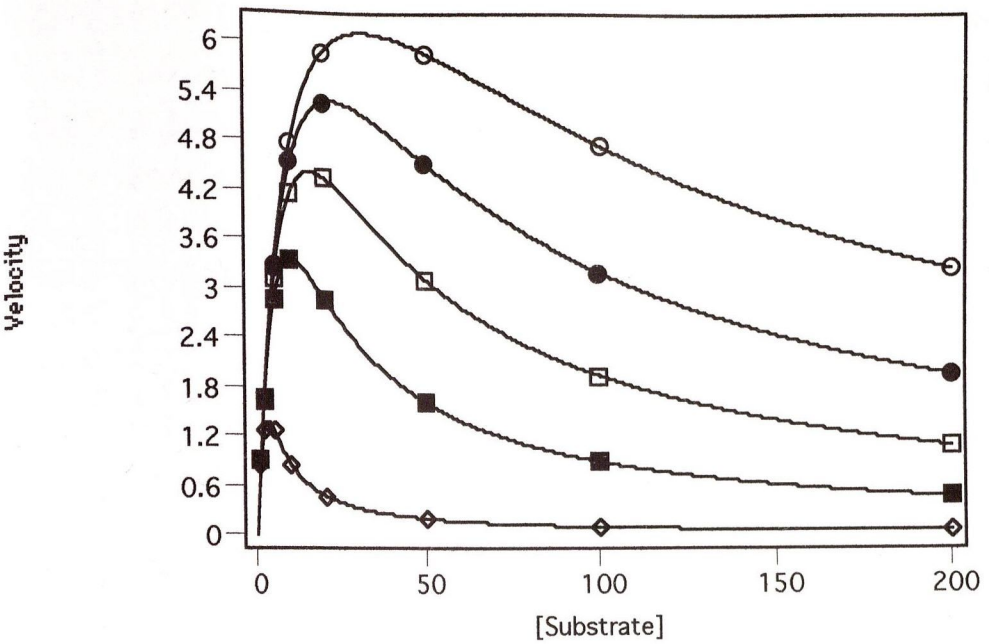
Velocity
6
5.4
4.8
4.2
3.6
3
2.4
1.8
1.2
0.6
0
0
50
100
150
200
[Substrate]

(b)

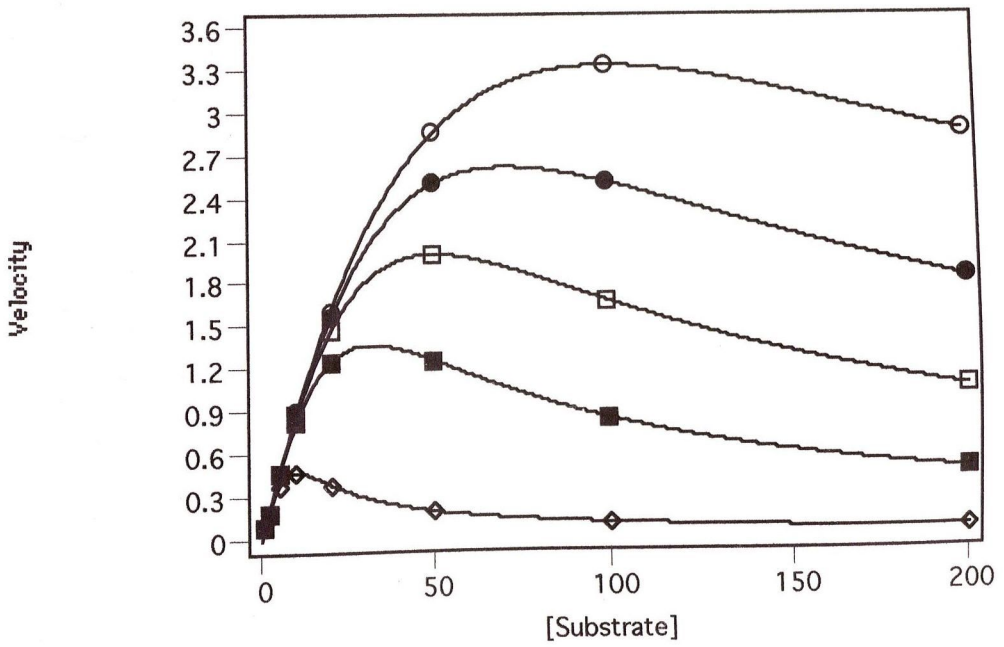
Velocity
3.6
3.3
3
2.7
2.4
2.1
1.8
1.5
1.2
0.9
0.6
0.3
0
0
50
100
150
200
[Substrate]

Figure 4.5. Determination of Kinetic Parameters with 10% Error on Data Set.

This figure shows a series of curves generated using an equation for total substrate inhibition where V_{max} is set to 10 and K_i values decrease from 100 to 1. In Graph (**a**) K_m is set to 10 whereas in Graph (**b**) K_m is set to 100. The data points are those generated using Eqn. 4.1 while the solid line was obtained by fitting to Eqn. 4.1 using MacCurve fit. The statistically-derived estimates for the kinetic parameters K_m, V_{max} and K_i are shown in Table 4.3.

Table 4.3

Statistically-derived estimated values for K_m, V_{max} and K_i compared with defined values.

Defined K_i	Statistically-derived estimates					
	$K_m = 10$			$K_m = 100$		
	V_{max}	K_m	K_i	V_{max}	K_m	K_i
100	10	10	92	19	217	12
50	10	10	45	10	110	45
25	10	10	23	7	71	35
10	10	9	10	4	34	22
1	8	8	1	0.2	5	18

(a)

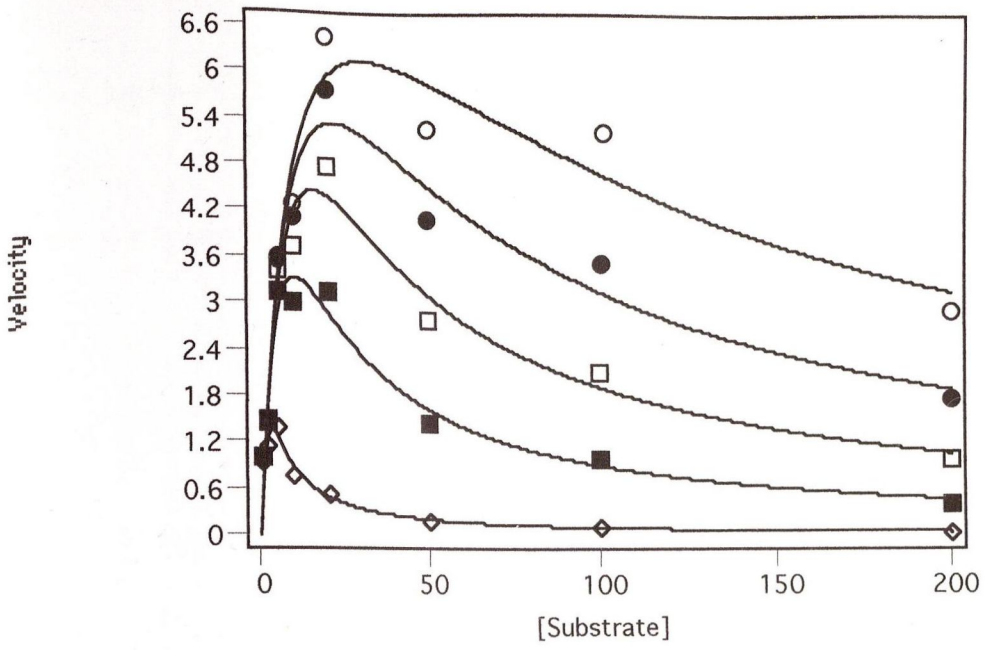
Velocity
6.6
6
5.4
4.8
4.2
3.6
3
2.4
1.8
1.2
0.6
0
0
50
100
150
200
[Substrate]

(b)

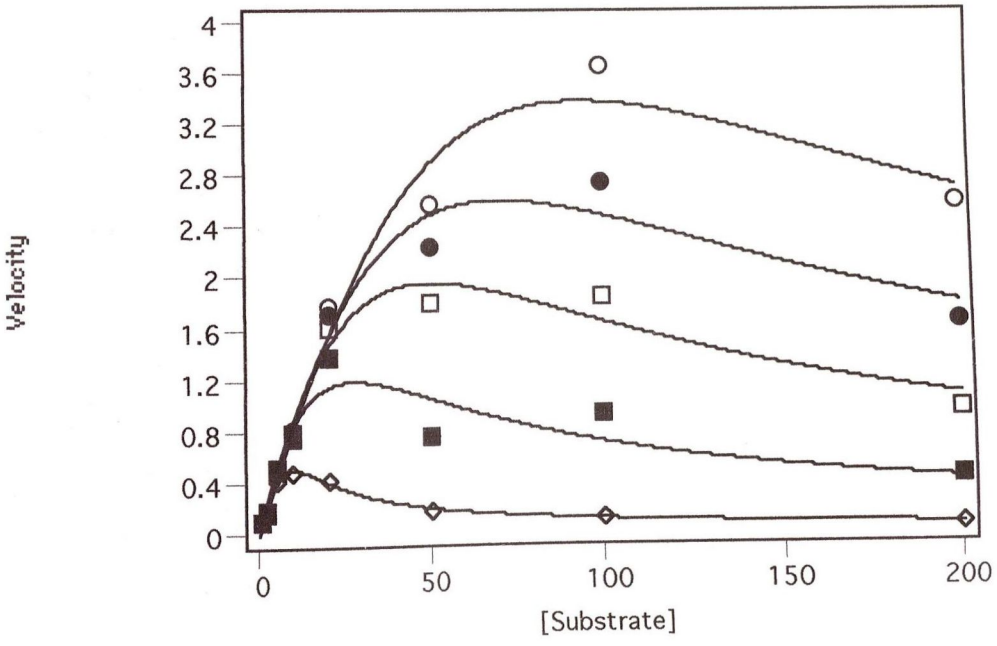
Velocity
4
3.6
3.2
2.8
2.4
2
1.6
1.2
0.8
0.4
0
0
50
100
150
200
[Substrate]

Figure 4.6. Effect of Decreasing the Data Set on the Ascending Limb of the Substrate Inhibition Curve.

In Panel 1 all of the data have been included. In panels 2, 3, and 4 the starting substrate values are 0.5, 2 and 5, respectively.

Table 4.4

Statistically derived estimates for K_m, V_{max} and K_i obtained with decreasing data sets.

		Statistically-derived Estimates			
	Defined Value	**Panel 1**	**2**	**3**	**4**
V_{max}	**10**	10	12	5	1.5
K_m	**10**	10	12	8	2.5
K_i	**1**	1	0.9	1.7	8

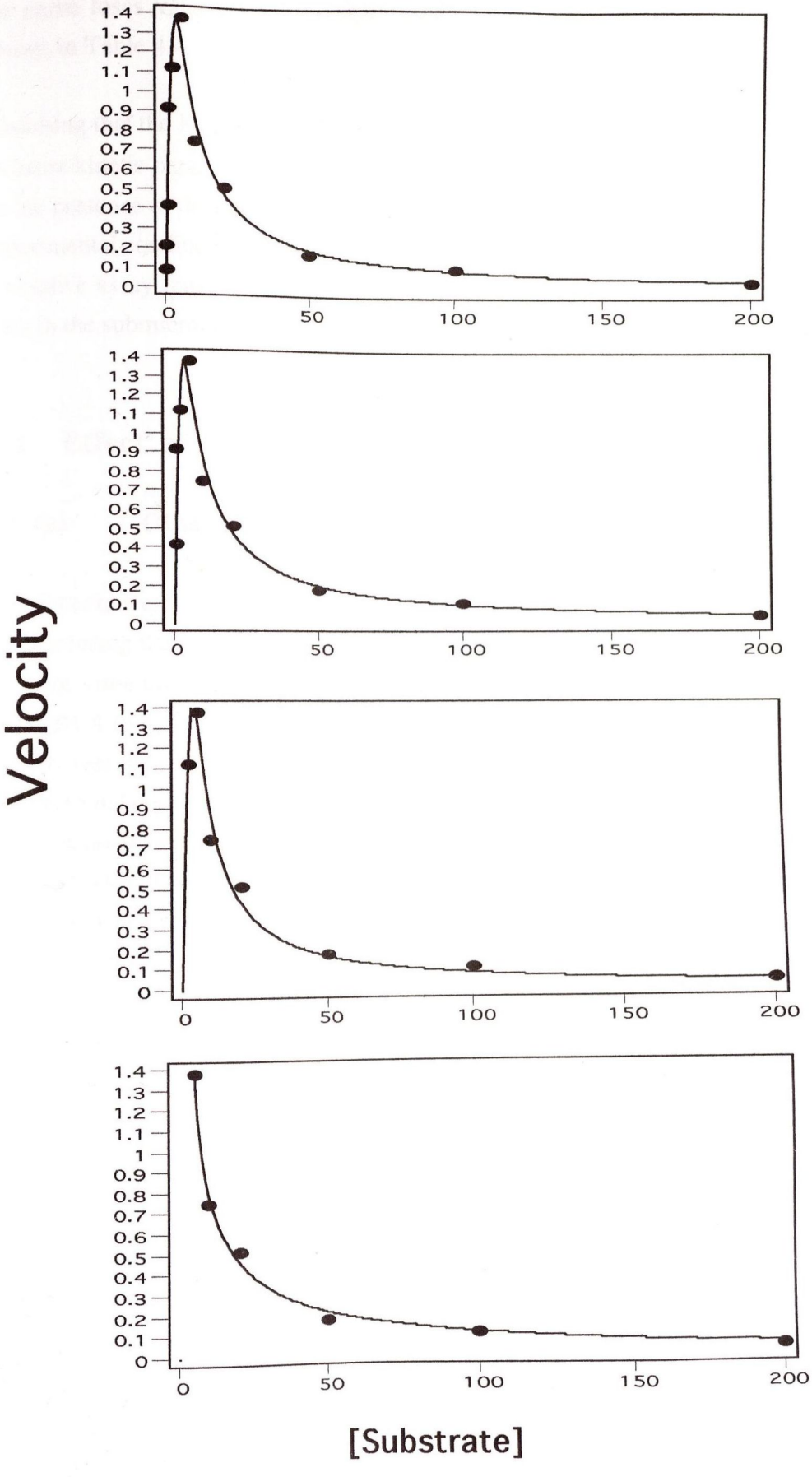
Velocity
1.4
1.3
1.2
1.1
1
0.9
0.8
0.7
0.6
0.5
0.4
0.3
0.2
0.1
0
0
50
100
150
200
[Substrate]

the curve loses values there is a dramatic effect on the estimated kinetic parameters as shown in Table 4.4.

Assuming that the K_m of hBVR-A for biliverdin-IXα is low it will be possible to reliably measure kinetic parameters using curve fitting routines, however, this is strictly dependant on the presence of data points on the ascending limb of the saturation curve. Under current experimental conditions it is not possible to obtain such values and as stated previously an alternative assay must be developed in order to allow the accurate measurement of initial rates in the submicromolar range.

4.2 Effect of pH on the Activity of hBVR-A.

4.2 (a) Observations on pH Stability.

Experiments were carried out in order to assess the stability of recombinant hBVR-A by pre-incubating the enzyme in buffer with a range of pHs. A series of buffers of different pH were made up which consisted of 100 mM sodium citrate and sodium acetate over the range pH 4 to 6, 100 mM sodium phosphate over the range pH 5.5 to 8 and 100 mM glycine over the range pH 8 to 9.5. BVR-A was diluted twenty fold in each of the buffers to give a final concentration of 0.135 mg/ml. The diluted mixtures were incubated at 30°C for 15 minutes in the buffers indicated before being extensively diluted and then assayed for hBVR-A activity at pH 7.2. For each assay, 20 µl of pre-incubated enzyme was added to a final volume of 2 ml which therefore contained 2.7 µg of enzyme. The pH was checked to ensure that the original buffer was diluted sufficiently and that the pH of the final assay mix was indeed pH 7.2. Both sodium acetate and sodium citrate were employed in the lower pH region in order to rule out a "buffer effect". As can be seen in Fig. 4.7 no adverse effects on enzyme activity are evident at the acidic or alkaline regions used. This is in contrast to the rat enzyme which is unstable at alkaline pH (Ennis, 1996).

4.2 (b) Optimum pH for hBVR-A Activity.

As mentioned previously, BVR-A can use either NADH or NADPH as cofactor in the reduction of biliverdin-IXα. This feature is common to a number of pyridine nucleotide dependant oxidoreductases, however, BVR-A is described in the literature as being unique in that it exhibits a different pH optimum with each cofactor. The recombinant human enzyme was shown also to function with both cofactors and to exhibit this dual cofactor-pH dependence.

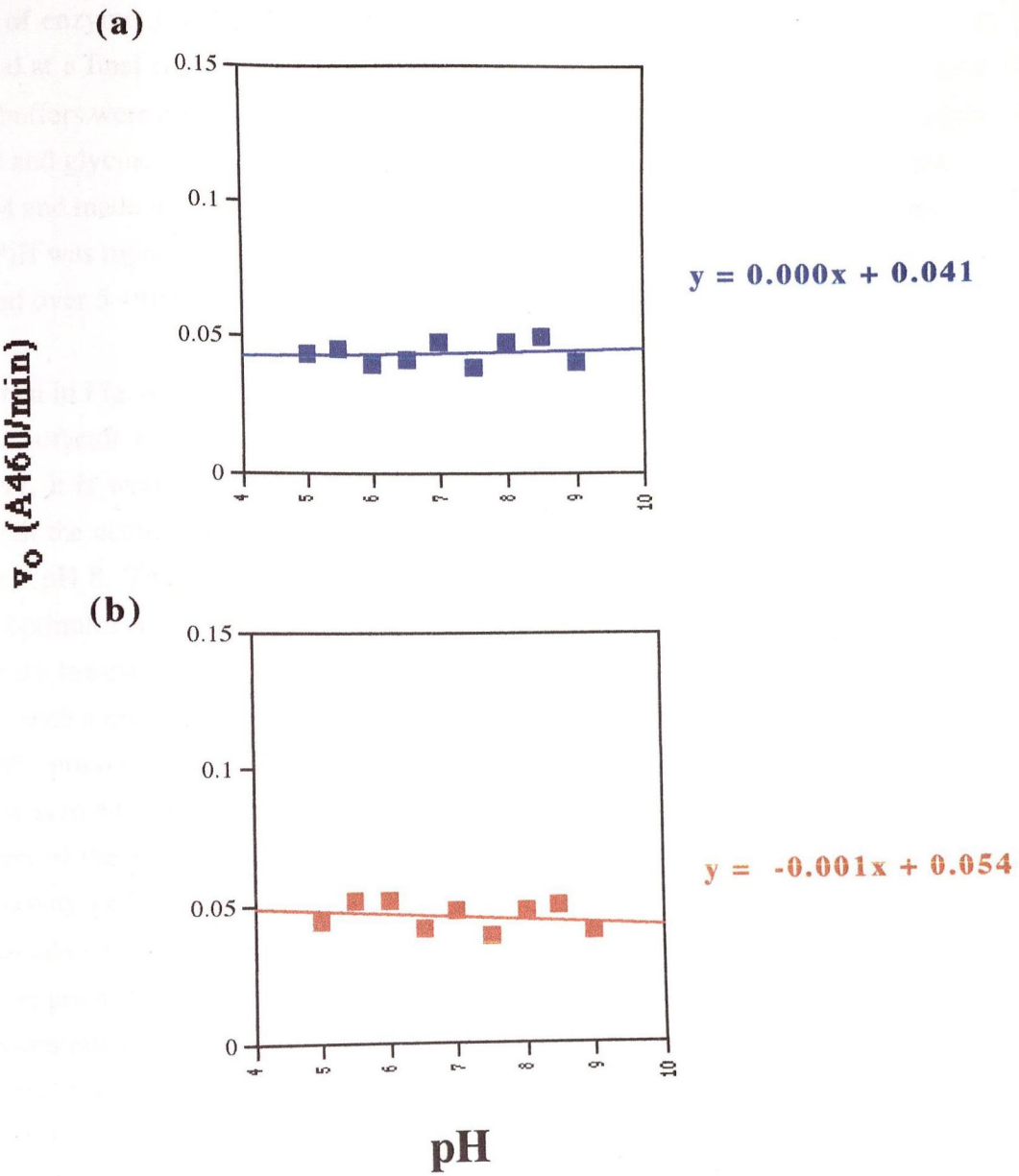

Figure 4.7. Stability of hBVR-A upon 15 minute pre-incubation at various pHs.

The stability of hBVR-A was assessed over a range of pHs as described in Section 4.2. (a). The enzyme was pre-incubated for 15 minutes in the various buffers at 30°C before being assayed for BVR activity in 100 mM sodium phosphate buffer, pH 7.2. Sodium acetate (a) and sodium citrate (b) were used as buffers in the acidic region of the pH scale.

In initial experiments on the variation of activity with pH a fixed concentration of biliverdin-IXα (20 μM) was used. The assay mixture consisted also of 37 μM BSA and 2.7 μg of enzyme. NADPH was used at a final concentration of 100 μM while NADH was used at a final concentration of 705 μM. Sodium citrate, sodium acetate and sodium lactate buffers were used over the range pH 4 to 6, sodium phosphate over the range pH 5.5 to 8 and glycine over the range pH 8 to 9 (all buffers were used at a concentration of 100 mM and made up at 0.5 pH unit intervals). As a control measure, the absorbance of NAD(P)H was monitored at 340 nm in the various buffers. No significant changes were observed over 5 - 10 minutes.

As shown in Fig. 4.8, hBVR-A exhibits a peak of activity at pH 6.5-6.7 when NADH is used as cofactor and a peak of activity at pH 8 when NADPH is used as cofactor. However, it is worth noting that with NADPH as the cofactor there is a second peak of activity in the acidic region. Indeed the rate of bilirubin formation is higher at pH 4 than the rate at pH 8. This pH range has not been examined previously in the literature where the pH optimum is described as alkaline. In addition, the rate of product formation appears to be at it's lowest at pH 6 to 7 when NADPH is used as cofactor. NADPH binds to the enzyme with a much higher affinity than NADH, however activity is generally lower with NADPH, possibly due to more pronounced substrate inhibition. This prompted the question as to whether the low activity seen at pH 6.5 with NADPH is actually caused by inhibition of the enzyme at the biliverdin concentrations used in the standard assay for BVR activity i.e. (20 μM). The peaks of activity seen in the lower and upper regions of the pH scale i.e. pH 4 - 5 and pH 8, would then be due to alleviation of this inhibition. If this assumption is correct, the activity of the enzyme would actually be higher at pH 6.5 at low concentrations of biliverdin when assayed with NADPH. In order to investigate this possibility, a series of saturation curves were generated from pH 4 to 8.5 with biliverdin as the variable substrate. Each reaction contained the standard components i.e. 100 μM NADPH, 0.135 μg of enzyme and biliverdin over the concentration range 2 to 20 μM in the various buffers.

As can be seen from Fig. 4.9, hBVR-A activity is actually higher at pH 6.5 at the lowest biliverdin concentration used (2 μM). As expected, the activity of the enzyme decreases with increasing biliverdin concentration which is indicative of substrate inhibition, therefore, at 20 μM biliverdin the rate of bilirubin production is at it's lowest. The data were fitted as described in Section 4.1 (c) in order to obtain approximate estimations of the kinetic parameters (see Fig. 4.10). At pH 4, the curve is more hyperbolic and an increase in both apparent K_m and V_{max} is observed. As the pH is increased from 4 to 4.5 the curve shifts to the left, the high V_{max} is retained and substrate inhibition is now clearly seen at biliverdin concentrations greater than 10 μM. (The substrate inhibitory K_i value decreases

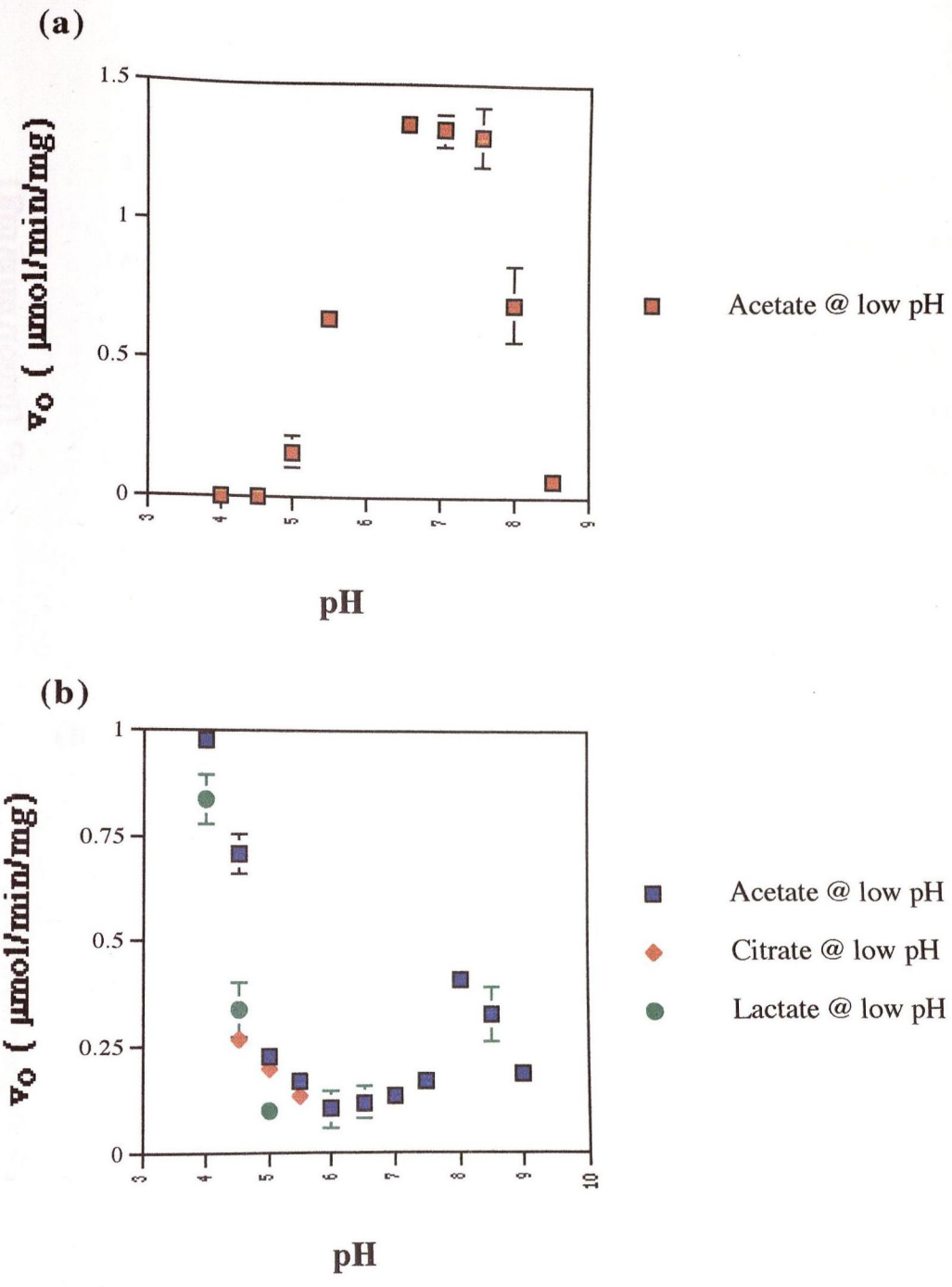

Figure 4.8. Optimum pH for hBVR-A Activity.

Bilirubin production was monitored over a range of pHs as described in Section 4.2 (b). In Fig. 4.5 (a) NADH was used as a source of reducing equivalents and activity is optimal at pH 6.5 - 7. When NADPH is used as cofactor, activity peaks at pH 8, however, an additional peak of activity is also seen in the acidic region of the pH scale [Fig. 4.5 (b)].

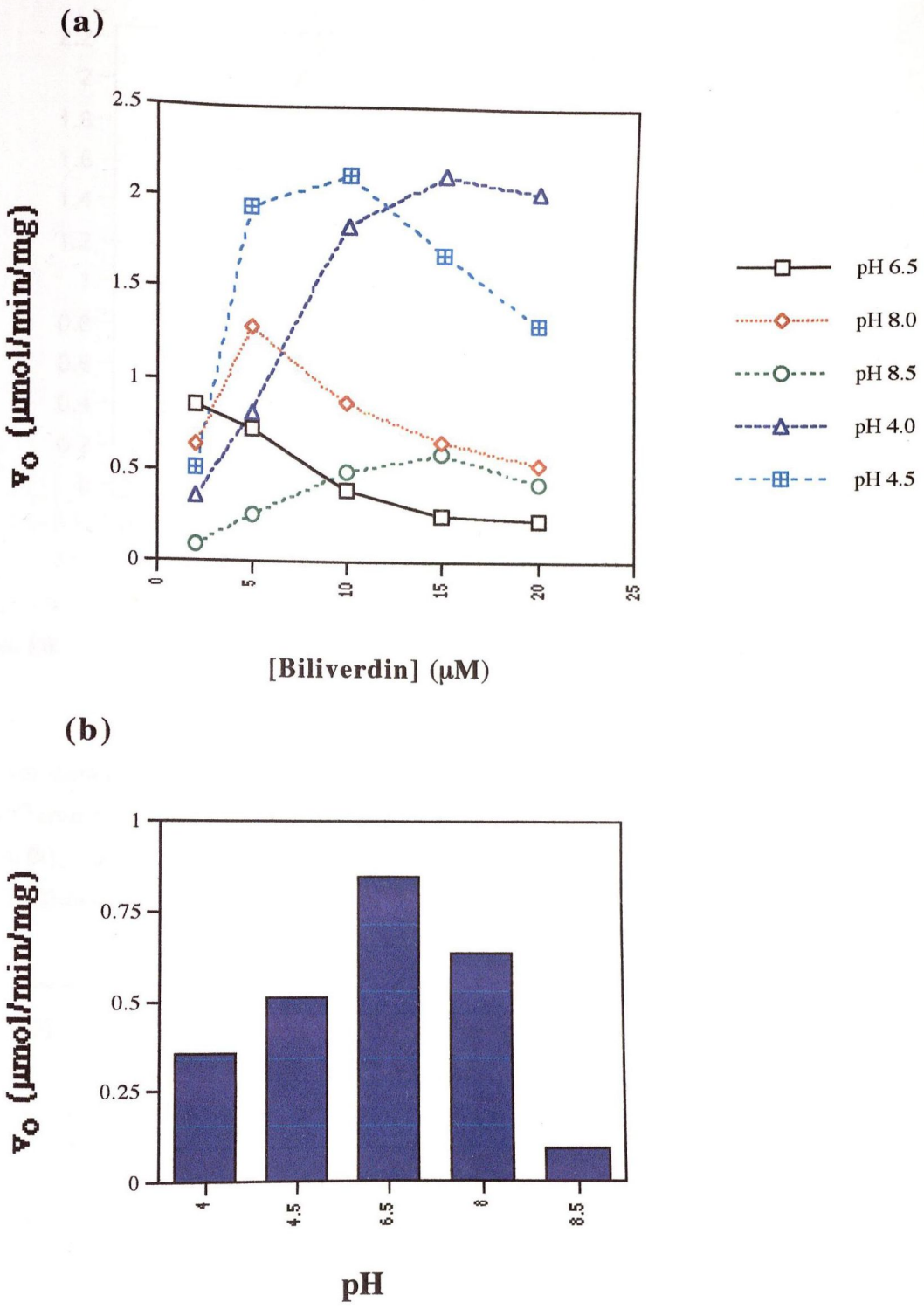

Figure 4.9. The Effect of Varying pH on the Substrate Inhibition Exhibited by hBVR-A.

(a) A series of saturation curves with biliverdin as the variable substrate were generated over a range of pHs as described in the text.

(b) The data points represent the initial rates obtained in each buffer at 2 µM biliverdin with 100 µM NADPH.

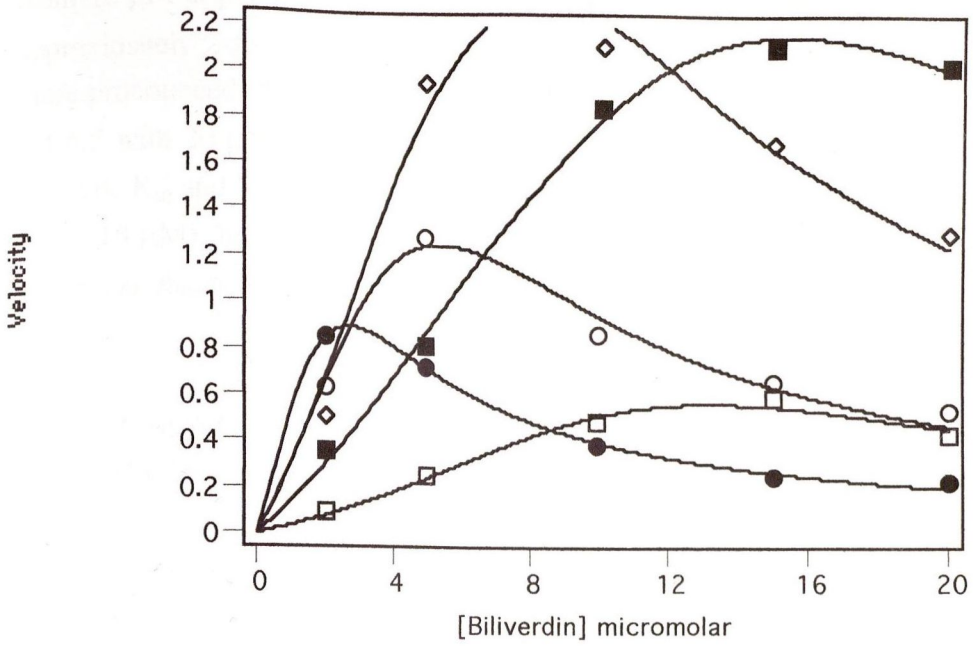

Figure 4.10. **Graphical Determination of Kinetic Constants for hBVR-A using Curve Fitting Routines.**

The data sets shown in Fig 4.9 (a) were fitted to a function for total substrate inhibition using MacCurve fit, as described in Section 4.1 (c). [pH 6.5. (●), pH 8 (○), pH 8.5 (❐), pH 4(■), pH 4.5 (◊)]. The following kinetic constants were obtained using the resulting coefficients:

pH	V_{max} (μmol/min/mg)	K_m (μM)	K_i (μM)
6.5	0.54 *	7 *	1 *
8	1.85	6.67	4.38
8.5	0.33	10.43	16.7
4	1.97	14.71	16.1
4.5	2.28	8.21	8.2

($R^2 > 0.995$ in each case).

* As mentioned in Section 4.1 (c) curve fitting routines cannot be used with confidence due the lack of data points on the ascending limb of the curve obtained at pH 6.5.

from 16 μM at pH 4 to 8 μM at pH 4.5, similarly, the apparent $K_m^{biliverdin}$ decreases approximately 2-fold). Under alkaline conditions at pH 8, substrate inhibition becomes more pronounced (K_i = 4 μM), however, the level of activity is not reduced to that seen at pH 6.5 with 20 μM biliverdin. Finally, at pH 8.5 the curve shifts to the right, there is a dramatic K_m and V_{max} effect and once again there is an alleviation of substrate inhibition (K_i = 16 μM), however, the maximal velocity seen in this case is approximately 7-fold lower than that seen under acidic conditions.

4.3 The Stereospecificity of NADH Oxidation by Human BVR-A.

As mentioned previously, the C-4 hydrogens of NAD(P)H are stereospecifically distinct in that NAD(P)H linked enzymes transfer hydrogen from either the *si* or *re* face of the dihydropyridine ring as illustrated in Fig 4.11. Experiments were performed in order to determine the stereospecificity of human BVR-A for NADH, using both A and B forms of [4-^{3}H] NADH. As mentioned in section 2.2.18 commercially available [4-^{3}H] NAD^+ was used in the enzymatic synthesis of A and B radiolabelled NADH. Yeast alcohol dehydrogenase (ADH) is an A-side specific enzyme and thus forms NADH that is labelled on the B-face ([4-^{3}H] NADH-B) while glutamate dehydrogenase (GDH) is a B-face specific enzyme producing [4-^{3}H] NADH-A. The tritiated cofactors produced in this manner were used as a source of reducing equivalents in the reduction of biliverdin-IXα and the radioactivity thus transferred to bilirubin was detected by liquid scintillation counting. The reactions involved in this procedure can be summarised as follows:

Ethanol + [4-^{3}H] NAD^+ → Acetaldehyde + [4-^{3}H] NADH-B + H^+

Glutamate + [4-^{3}H] NAD^+ → α-ketoglutarate + [4-^{3}H] NADH-A + NH_4^+

Biliverdin +[4-^{3}H] NADH-(A or B) → [^{3}H] Bilirubin + NAD^+ **or**

Bilirubin + [4-^{3}H] NAD^+

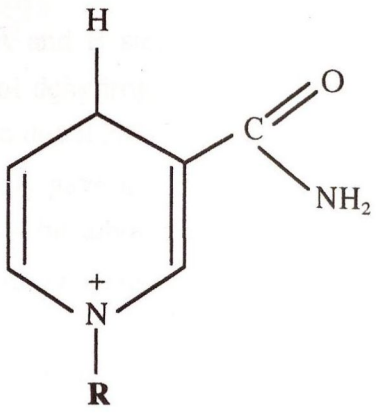

re face

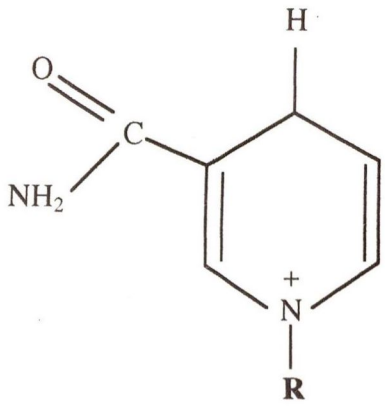

si face

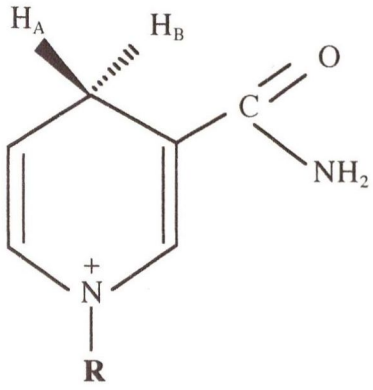

$H_A = H_R$; $H_B = H_S$

Figure 4.11. The configuration of A - face and B- face hydrogens on the C-4 carbon of the nicotinamide ring. $\mathbf{H_A}$ projects out of the plane of the page (*re* face) and $\mathbf{H_B}$ extends into the plane of the page (*si* face). (**R** represents the adenine dinucleotide structure).

4.3 (a) Synthesis of [4-^{3}H]NADH-A and [4-^{3}H]NADH-B.

The A and B stereoisomers of NADH were synthesised using the standard assays for alcohol dehydrogenase and glutamate dehydrogenase. It had been established previously that an initial NADH concentration of 100 μM could be used in the hBVR-A reaction and that this gave a specific radioactivity for [4-^{3}]NADH that allowed reliable detection of labelled bilirubin by liquid scintillation counting, having started with 5 μCi [4-^{3}]NAD$^+$ in the initial reaction for production of NADH (Ennis, 1996).

Both reactions were monitored spectrophotometrically at 340 nm and the absorbance at which no further change took place was noted. In the case of the ADH reaction, the A_{340} stopped changing appreciably at a value of 0.95. Using an extinction coefficient of 6.22 $mM^{-1}cm^{-1}$, the concentration of NADH thus produced was calculated to be 146 μM, which corresponds to a 73% conversion of the available NAD$^+$ (200 μM, starting concentration). It can be assumed that 73% of the available [4-^{3}]NAD$^+$ was converted to NADH, therefore, 3.6 μCi of [4-^{3}H]NADH-B was produced. In the case of the GDH reaction, 92 % of the available NAD$^+$ was converted to NADH indicating that 4.6 μCi of [4-^{3}H]NADH-A was produced. Dilution of the ADH and GDH reactions from 2 ml to 2.5 ml by the addition of hBVR-A reagents resulted in a final NADH concentration of 116 μM and 154 μM, respectively.

4.3 (b) hBVR-A Catalysed Reduction of Biliverdin using [4-^{3}H]NADH Stereoisomers.

The radiolabelled NADH produced in the ADH and GDH reactions was used immediately in the hBVR-A catalysed reduction of biliverdin-IXα. The standard reaction components; BSA (37 μM), biliverdin (5 μM) and BVR-A (0.85 mg/ml), were added directly to the cuvettes containing the newly synthesised NADH and bilirubin production was monitored at 460 nm. Experiments were performed in duplicate and control reactions were set up containing distilled water in place of enzyme. (These reactions represent the carry-over of non-bilirubinoid radioactivity into the organic solvent). Each 2.5 ml reaction was extracted into 900 μl of chloroform as outlined in Section 2.2.18 (c) and 300 μl of this extract was added to 5 ml of Ecosint for LSC.

The theoretical yields of label in the final reaction product were calculated as follows. In the ADH reaction, 73% of the available [4-^{3}]NAD$^+$ was converted to NADH, therefore, 3.6 μCi of [4-^{3}]NADH-B was produced. In the subsequent BVR-A reaction, biliverdin

was used at a concentration of 5 μM. This reaction was allowed to go to completion, therefore, it can be assumed that the concentration of NADH used in this reaction was also 5 μM which corresponds to 4.3 % of the total available NADH. Assuming that 4.3 % of the total radiolabelled NADH was used, it was predicted that 0.215 μCi of radiolabel was incorporated into the bilirubin product. The labelled bilirubin was organically extracted into a final volume of 900 μl, of this, a total of 300 μl was counted, therefore 1/3 of the theoretical 0.215 μCi was expected in the organic solvent (corresponding to 159,139 d.p.m.). These calculations were also performed for the GDH and control reactions and the expected versus the actual results are summarised in Table 4.5.

As illustrated in Fig. 4.12, the B-face C-4 hydrogen of NADH was clearly favoured by hBVR-A, indicating that human BVR-A is B-stereospecific. It was estimated that approximately 90,200 counts would be incorporated into the reaction product, however, the actual value is only approximately 25% of the expected value. Given that the stock [4-^{3}NAD$^+$] was found to contain the radioactivity quoted by the manufacturer, it can be postulated that the discrepancy in the expected number of counts may be due to (1) random distribution of tritium over the entire NAD$^+$ structure as opposed to just the C-4 hydrogen or (2) the presence of a contaminant that did not react and was water soluble. This seems unlikely as the contaminant would have to account for approximately 75% of the lost radioactivity.

4.4 Protein Folding Studies.

The three-dimensional structure of a protein is obtained through the folding of the polypeptide chain from an ensemble of fairly loose, disordered configurations, collectively referred to as the unfolded state. How a protein assumes it's final folded conformation is unclear, however, it has been observed that many purified proteins can spontaneously refold *in vitro* after being completely unfolded, indicating that the three-dimensional structure of a protein is ultimately determined by it's primary structure. Several models for folding have been proposed ranging from the notion that local short-range interactions throughout the polypeptide structure occur simultaneously to piece together the final configuration while other models propose a sequential pathway of folding through a limited number of intermediates. (For a detailed discussion of protein folding see Shirley, 1995). The folded state of a protein is only marginally more stable than the fully unfolded state, however, under physiological conditions the equilibrium of most proteins so greatly favors the folded state that measuring the equilibrium constant ($\mathbf{K_U}$) or free energy change ($\Delta\mathbf{G_U}$) for the folding/unfolding reaction is not possible. In the presence of denaturants

Table 4.5.

Determination of [^{3}H] Bilirubin in $CHCl_3$ extracts.

[4-^{3}H] NADH-A	% NADH produced	µCi NADH produced	Estimated d.p.m. incorp.	Actual d.p.m. incorp.	% radioact. incorp.
Test 1	92	4.58	119896	910	1 %
Test 2	92	4.58	119896	1114	
Control	92	4.58	119896	811	0.7 %

[4-^{3}H] NADH-B	% NADH produced	µCi NADH produced	Estimated d.p.m. incorp.	Actual d.p.m. incorp.	% radioact. incorp.
Test 1	73	3.66	159139	26540	14 %
Test 2	73	3.66	159139	16679	
Control	73	3.66	159139	881.7	0.6 %

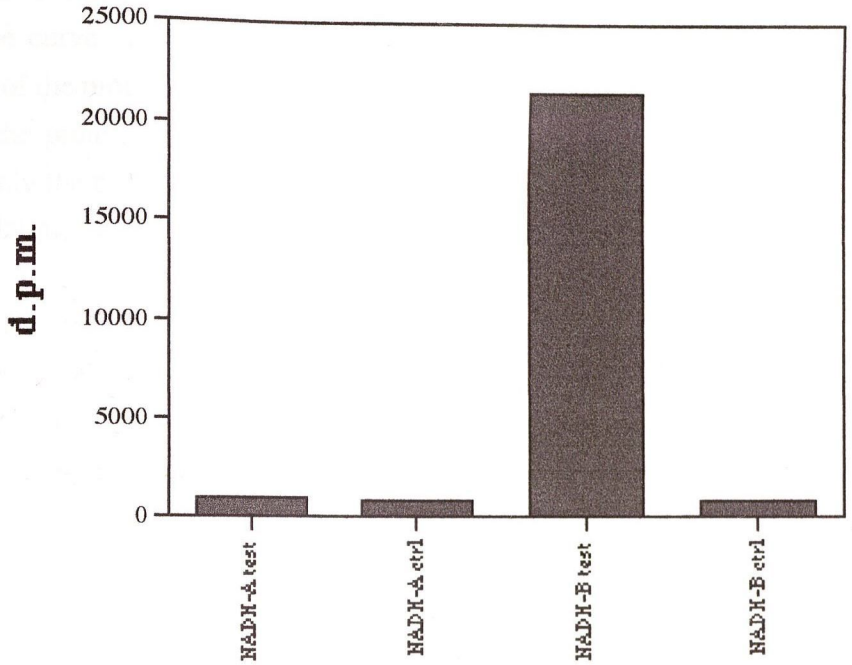

Figure 4.12. **Relative Distribution of d.p.m. in Chloroform-extracted Bilirubin Samples.**

such as urea or guanidine hydrochloride, the equilibrium will shift such that thermodynamic parameters can be accurately measured. Urea and guanidine denaturation curves are routinely used to follow the folding/unfolding reactions, a typical example is shown in Fig.4.13. The observable parameter chosen in this case to follow the unfolding reaction is fluorescence intensity, however, other spectroscopic techniques may also be used. The curve is divided into three regions; in the pre-transition region, the native structure of the protein is favoured, in the transition region, both the native and unfolded state of the protein are present in significant amounts and finally in the post-transition region, only the unfolded form of the protein is thermodynamically stable. The procedure for calculating ΔG_U for the folding/unfolding reaction is outlined in Section 4.4 (c).

The effect of denaturants on BVR-A fluorescence and activity was studied in order to gain insight into the folding/unfolding reaction of this enzyme. Denaturation curves were generated in both urea and guanidine hydrochloride and various kinetic experiments were set up to monitor changes in substrate binding and catalytic activity during the unfolding reaction.

4.4 (a) Determination of Urea and Guanidine Hydrochloride Denaturation Curves for Human BVR-A.

Guanidine hydrochloride and urea denaturation curves were determined by monitoring the fluorescence intensity of human BVR-A as a function of denaturant concentration. A separate solution was used to determine each point on the denaturation curves, therefore, stock solutions (6M guanidine hydrochloride and 8M Urea) of both denaturants were prepared initially in 100 mM sodium phosphate buffer, pH 7.2 and the remaining solutions were prepared by dilution of the stocks in the same buffer. Fluorescence emission was monitored at 340 nm (excitation at 295 nm) and the resulting profiles are shown in Fig. 4.14 and Fig. 4.15.

In order to ensure that the folding/unfolding reaction was at equilibrium, fluorescence intensity was measured over a period of 10 minutes. As can be seen from both profiles, there appears to be very little change in fluorescence intensity after approximately 1 minute. Both denaturation curves display sigmoidal behaviour, however, there are notable differences between the two profiles. For example, in the case of the urea denaturation curve, the pre-transition region is well defined and the curve enters the transition region at a concentration of approximately 3 M urea. The guanidine hydrochloride denaturation curve differs in this respect in that the pre-transition region is short-lived and the curve enters the transition region at approximately 1 M guanidine hydrochloride. Clearly, the

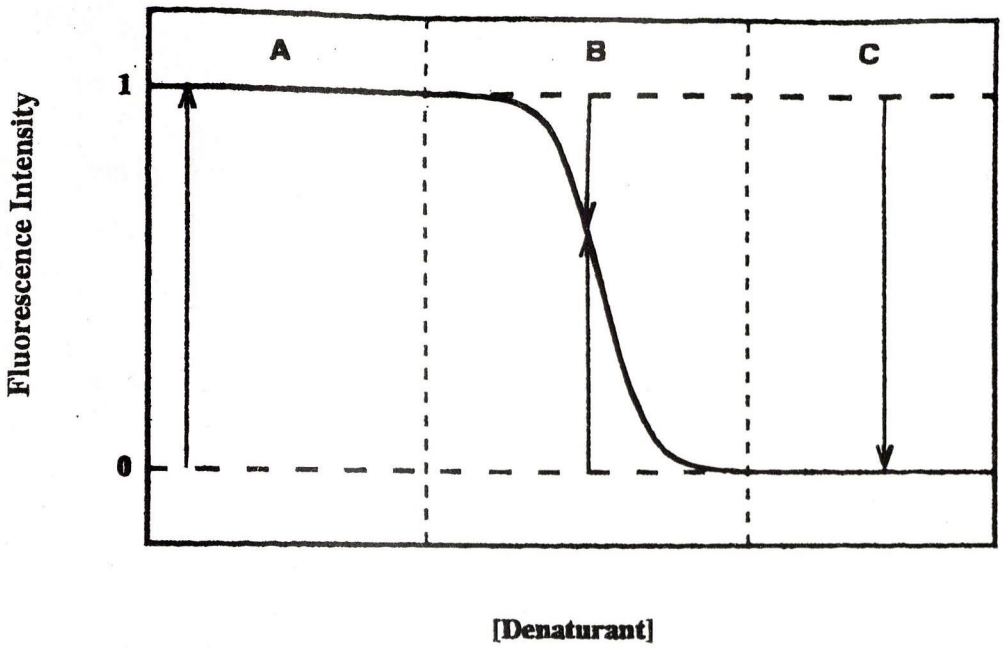

Figure 4.13

Schematic representation of a typical denaturation curve. Dashed lines are extrapolated baselines for the native and the unfolded state. In (A) the majority of the protein is in the folded state, in (B) both the folded and unfolded form of the protein are present in significant amounts and in (C) only the unfolded form of the protein is stable. (Adapted from Shirley, 1995).

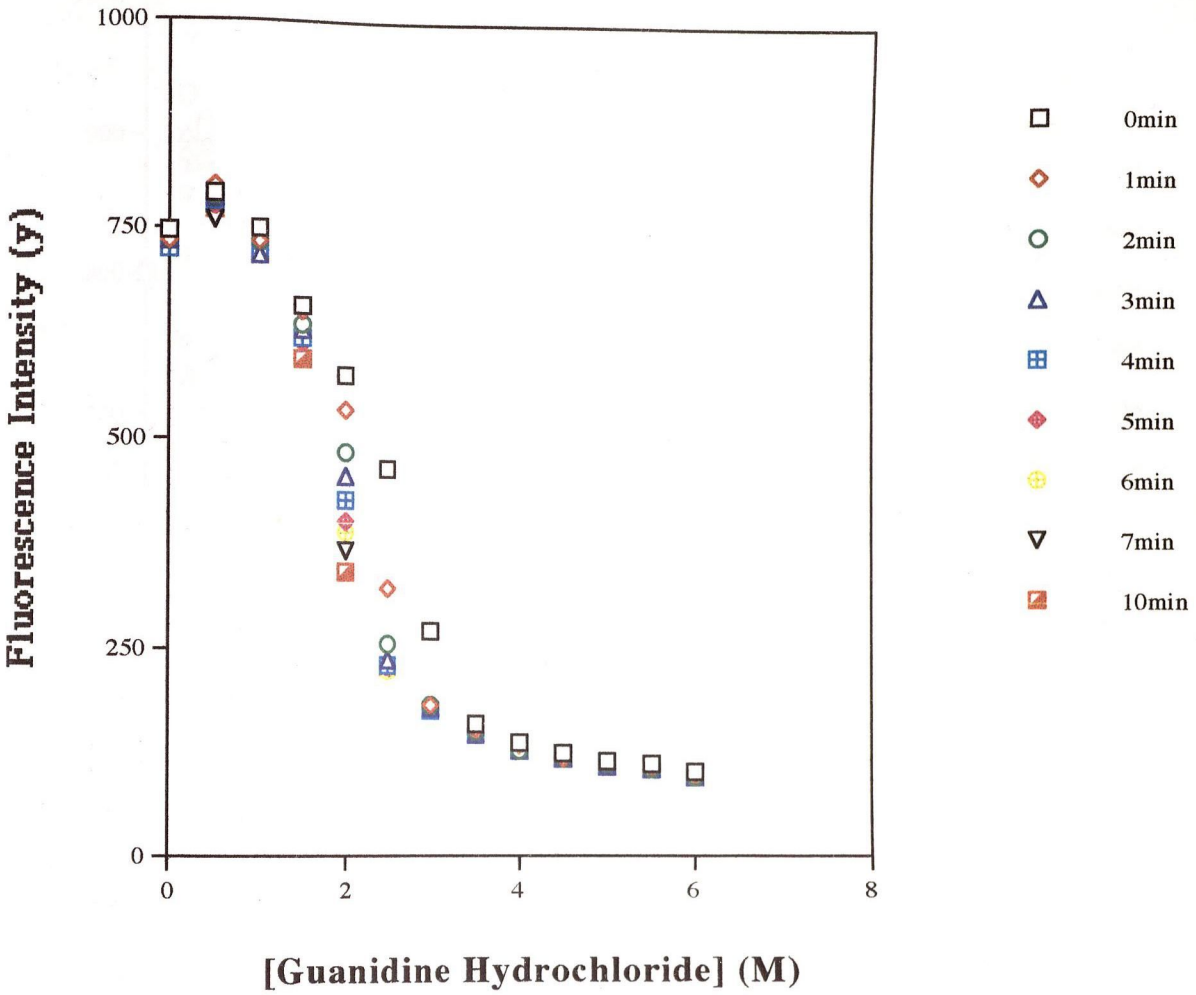

Figure 4.14. Guanidine Hydrochloride Denaturation Curve for hBVR-A.

hBVR-A was incubated in a range of guanidine hydrochloride concentrations over a ten minute period. The fluorescence intensity of each protein sample was monitored at 340 nm (excitation wavelength = 295 nm) and plotted as a function of denaturant concentration.

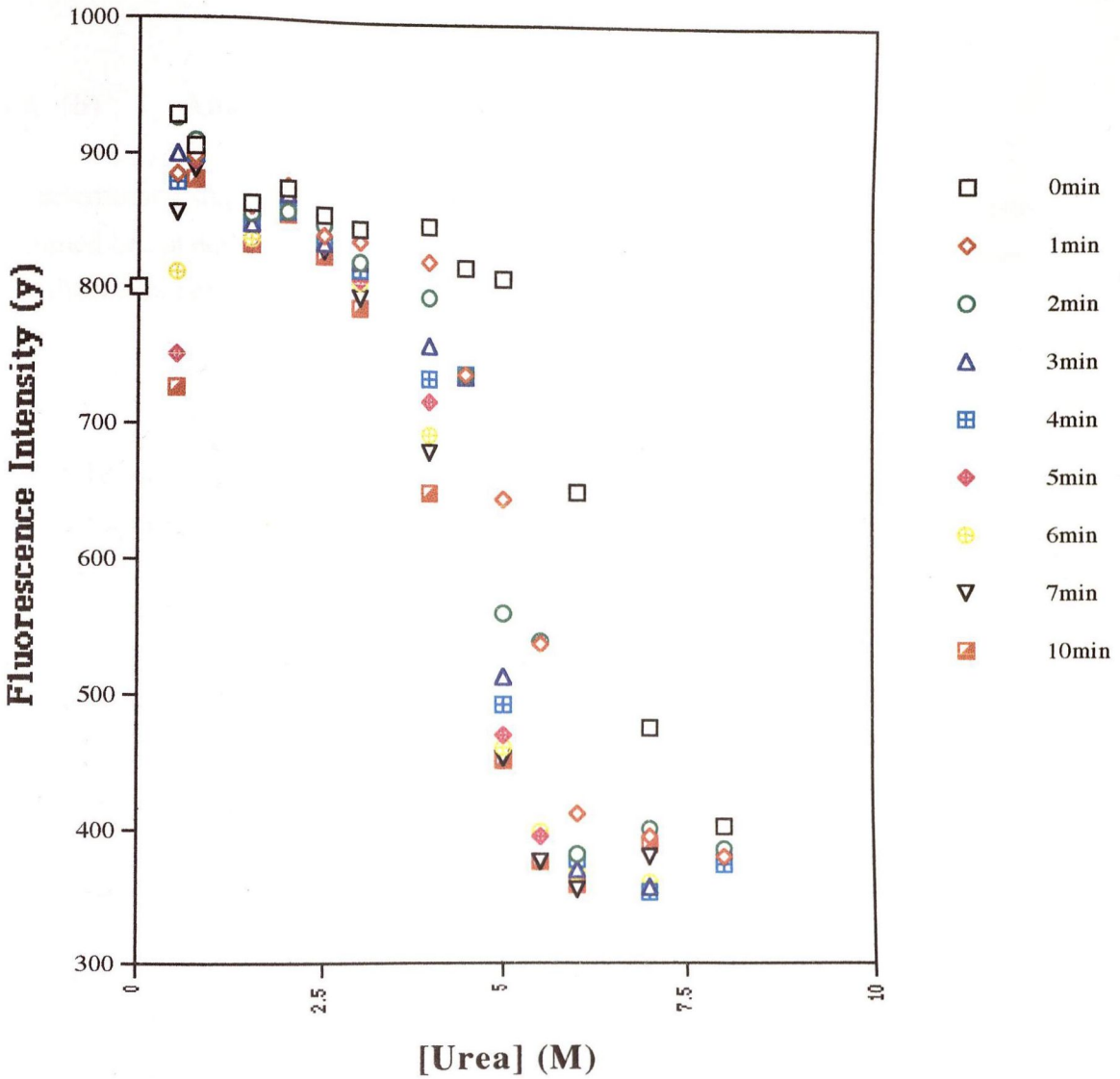

Figure 4.15. **Urea Denaturation Curve for hBVR-A.**

hBVR-A was incubated in a range of urea concentrations over a ten minute period. The fluorescence intensity of each protein sample was monitored at 340 nm (excitation wavelength = 295 nm) and plotted as a function of denaturant concentration.

unfolding behaviour exhibited by a protein is dependant on the nature of the denaturant used in the reaction. As a comparative measure, both curves were used in an attempt to determine the thermodynamic parameters.

4.4 (b) Analysis of Denaturation Curves.

In determining the ΔG_U for the folding/unfolding reaction, a two-state mechanism is assumed i.e.. at equilibrium only the fully folded and fully unfolded protein are present at significant concentrations, therefore

$$f_F + f_U = 1 \qquad \text{(Eqn. 4.3)}$$

where f_F and f_U represent the fraction of total protein in the folded and unfolded conformations, respectively. There will, undoubtedly, be intermediates present, however, for many proteins the concentration of intermediates has been found to be small relative to the concentrations of the native and denatured proteins.

The analysis of a typical denaturation curve assuming a two-state mechanism is shown in Fig. 4.16. The observed fluorescence intensity, **y**, at any point on the transition curve is given by

$$y = y_F f_F + y_U f_U \qquad \text{(Eqn. 4.4)}$$

where y_F and y_U represent the values of **y** characteristic of the folded and unfolded protein and are obtained by extrapolation of the pre- and post transition baselines, respectively.

The equilibrium constant, K_U, is a measure of the ratio of unfolded to folded protein and is used in the calculation of ΔG_U as follows

$$\Delta G_U = -RT\ln K_U \qquad \text{(Eqn. 4.5)}$$

Where **R** is the gas constant (1.987 cal/deg/mol) and **T** is the absolute temperature (K).

The guanidine hydrochloride and urea denaturation curves for hBVR-A were analysed as described above assuming a two-state mechanism. The thermodynamic parameters are summarized in Tables 4.6 and 4.7. As mentioned above, there are very few points in the pre-transition region of the guanidine hydrochloride denaturation curve making estimation

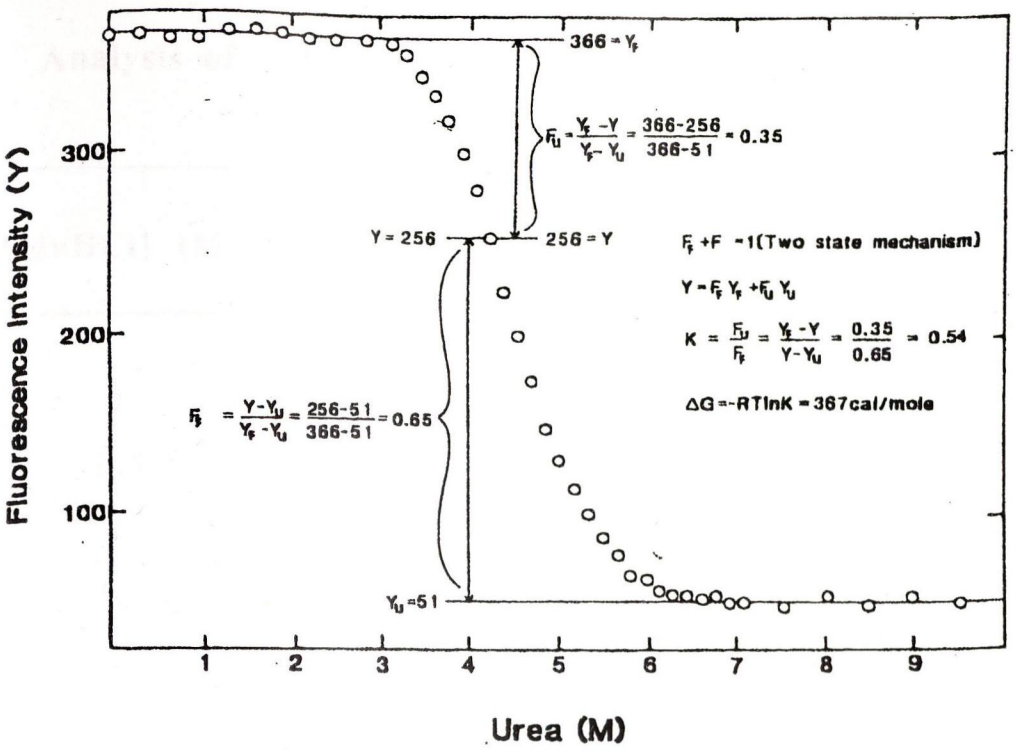

Figure 4.16. The analysis of a urea denaturation curve of Ribonuclease T1 assuming a two-state mechanism (adapted from Shirley, 1995).

Table 4.6

Analysis of Guanidine Hydrochloride Denaturation Curve

[GdnHCl] (M)[a]	f_U[b]	f_F[c]	K_U[d]	ΔG_U (cal/mol)[e]
1	0.17	0.83	0.20	932
1.5	0.35	0.65	0.52	380
2	0.71	0.29	2.43	-530
2.5	0.87	0.13	6.69	-1125
3	0.94	0.06	15.66	-1629
3.5	0.97	0.03	32.33	-2058

a Molar guanidine hydrochloride concentration.

b Fraction of total protein in the unfolded form.

c Fraction of total protein in the folded form.

d Equilibrium constant for the folding/unfolding reaction.

e Change in free energy for the folding/unfolding reaction.

Table 4.7

Analysis of Urea Denaturation Curve

Urea (M)	f_U	f_F	K_U	ΔG_U (kcal/mol)
4	0.11	0.89	0.12	1.24
4.5	0.35	0.65	0.54	0.37
5	0.61	0.39	1.57	-0.23
5.5	0.92	0.08	11.2	-1.43

of $\mathbf{y_F}$ difficult. It is clear that low concentrations of guanidine hydrochloride are sufficient to shift the equilibrium of the folding/unfolding reaction to the right.

The method most commonly used to estimate the free energy change for the folding/unfolding reaction in the absence of denaturant employs the linear extrapolation model. This model assumes that the linear dependence of ΔG_U on denaturant concentration observed in the transition region continues to zero concentration of denaturant. The value obtained using this method, $\Delta G_U(H_2O)$, is referred to as the conformation stability of the protein and is given by:

$$\Delta G_U = \Delta G_U(H_2O) - m\,[\text{denaturant}] \qquad \text{(Eqn. 4.6)}$$

where m is a measure of the dependence of free energy on denaturant concentration, and depends on the amount and composition of polypeptide that is freshly exposed to solvent on unfolding. The variation of ΔG_U with the concentration of denaturant is illustrated in Figs. 4.17 and 4.18. Estimates of $\Delta G_U(H_2O)$ for hBVR-A in guanidine hydrochloride and urea gave values of 2.2 and 8.8 kcal/mol, respectively, again suggesting that the thermodynamic parameters obtained in these studies are dependant on the denaturant used to stimulate the unfolding reaction.

4.4 (c) The Effect of Denaturant Concentration on hBVR-A Activity.

The activity of hBVR-A was measured as a function of denaturant concentration. Enzyme assays were performed as described in Section 2.2.15 (b), however, sodium phosphate buffer was replaced by buffer containing guanidine hydrochloride or urea. Each assay was started by the addition of enzyme to the cuvette and bilirubin production was monitored at 460 nm. As can be seen from Fig.4.19, there is an obvious increase in hBVR-A activity up to a concentration of 3.5 M urea, at higher urea concentrations the activity of the enzyme decays. In order to investigate the possibility that the apparent increase in activity results from alleviation of substrate inhibition, enzyme activity was measured in 3M urea with a range of biliverdin concentrations. As can be seen from Fig.4.20, the activity of hBVR-A assumes a hyperbolic dependence on biliverdin concentration in the presence of 3 M urea. This is in contrast to the kinetics observed in the absence of urea where pronounced substrate inhibition is apparent above 10 μM biliverdin.

To determine whether the "new kinetic form" seen in the presence of 3 M urea was stable, the enzyme was incubated in 3M urea for 30 minutes and 60 minutes before being

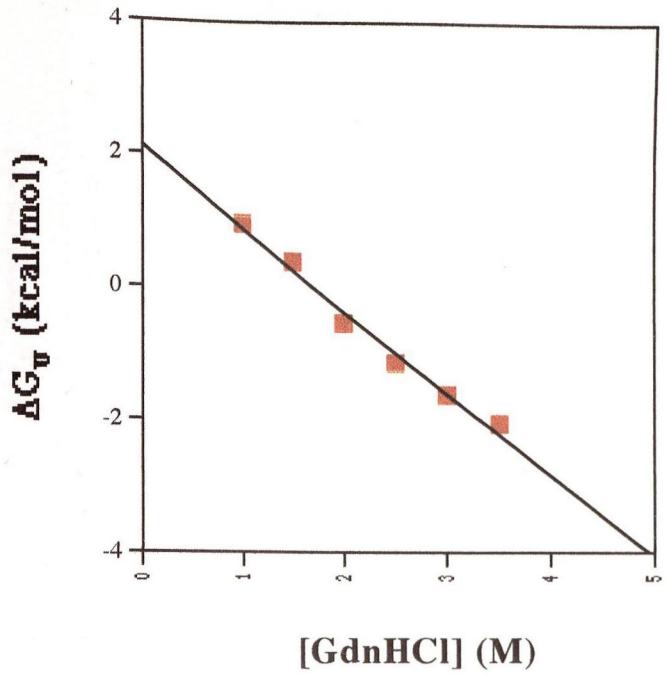

Figure 4.17. **The variation of ΔG_u with guanidine hydrochloride concentration for hBVR-A.**

The data points are from the transition region of Fig. 4.14 as analysed in Table 4.6. A least squares analysis of this data fit to Eqn. 4.6 yields: $\Delta G_U(H_2O)$ = 2.2 kcal/mol.

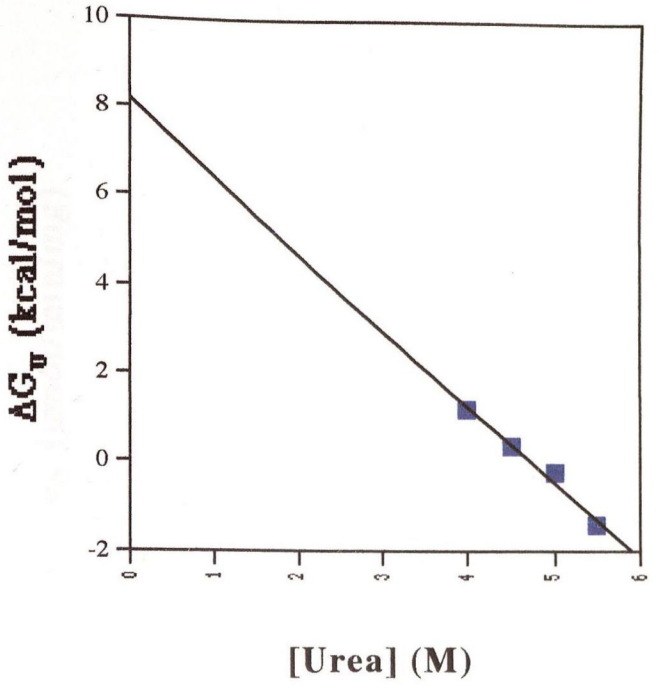

Figure 4.18. **The variation of ΔG_U with urea concentration for hBVR-A.**

The data points are from the transition region of Fig. 4.15 as analysed in Table 4.7. A least squares analysis of this data fit to Eqn. 4.6 yields: $\Delta G_U(H_2O)$ = 8.1 kcal/mol.

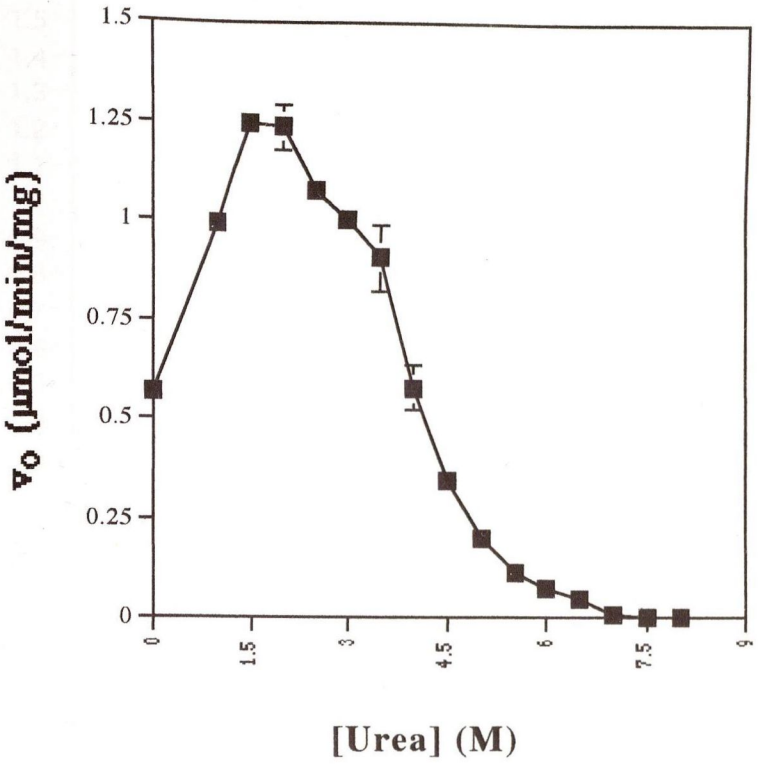

Figure 4.19. **The Effect of Denaturant Concentration on hBVR-A Activity.**

Enzyme activity was monitored at 460 nm in a range of urea concentrations. The reactions contained 705 µM NADH, 20 µM biliverdin and hBVR-A at a final concentration of 0.135 mg/ml. All assays were carried out in phosphate buffered urea solutions, pH 7.2.

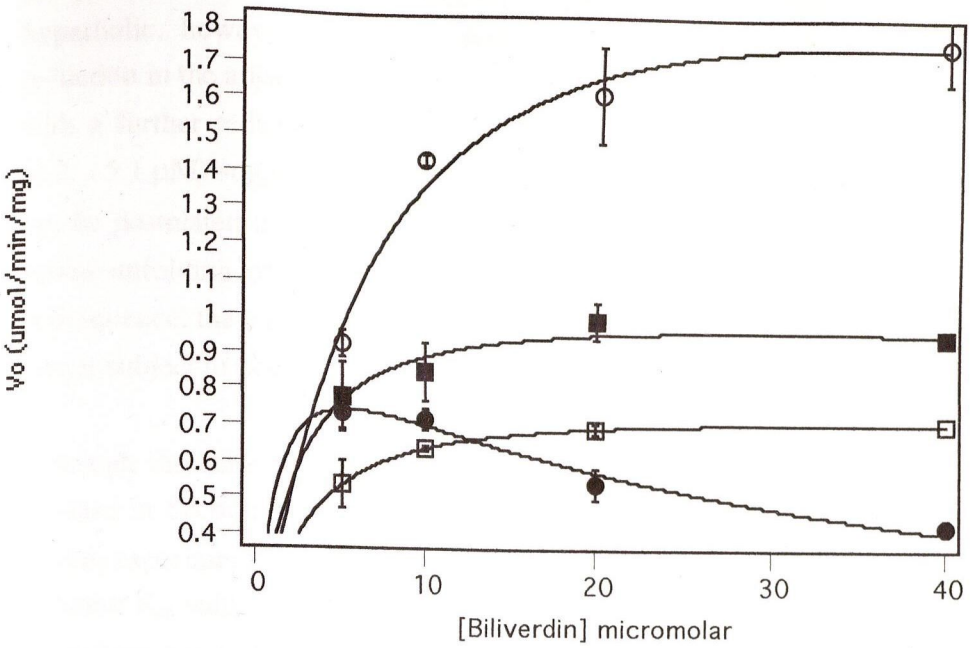

Figure 4.20. **The Substrate Inhibition Exhibited by hBVR-A is Alleviated in the Presence of 3 M Urea.**

Saturation curves with biliverdin as the variable substrate were generated in the presence (○) and absence (●) of 3 M urea as described in Section 2.2.17. The curve becomes hyperbolic in the presence of denaturant indicating that the enzyme is no longer subject to potent substrate inhibition. Additional experiments were performed where the enzyme was incubated for 30 minutes (■) and 60 minutes (❐) in 3 M urea before being assayed. Enzyme activity decays with time as the enzyme assumes the unfolded conformation. Data sets were fitted to a function describing total substrate inhibition and kinetic constants were calculated from the resulting coefficients as summarised below:

[Urea] (M)	Time (mins)	V_{max} (μmol/min/mg)	K_m (μM)	K_i (μM)
0 *	0 **	1.06	1.12	25
3	0	2.57	5.10	152
3	30	1.11	2.22	386
3	60	0.831	2.69	407

* No data points present on the ascending limb of the saturation curve.

** Zero time refers to direct assay of enzyme activity with no pre-incubation time.

assayed. At 30 minutes, the curve of activity versus biliverdin concentration remains hyperbolic, however, there is a marked decay in activity with an approximate 50% reduction in the apparent V_{max} observed. Enzyme activity decays further after 60 minutes with a further reduction in apparent V_{max}. The apparent $K_m^{biliverdin}$ is fairly constant (2.2. - 5.1 μM) suggesting that the new kinetic form decays with a $t_{1/2}$ of 36 minutes. It can be postulated that the initial increase in hBVR-A activity seen at time zero is due to partial unfolding or conformational "breathing" within the polypeptide structure. As a consequence, the enzyme will bind it's substrates with a lower affinity and is therefore no longer subject to potent substrate inhibition.

Although the substrate inhibition is relieved in the presence of 3M urea, for reasons outlined in Section 4.1 (c), it is still difficult to obtain a K_m value for biliverdin under current experimental conditions in the absence of urea. However, it is possible to obtain apparent K_m values for NADH and NADPH. Enzyme activity was, therefore, measured in the presence and absence of 3 M urea at a fixed biliverdin concentration (20 μM) with both NADH and NADPH as the variable substrate (NADH was assayed over a concentration range of 0.125 - 4 mM while NADPH was assayed over the range 0.5 to 20 μM). The results of these experiments are shown in Fig. 4.21 and Fig. 4.22. In the presence of 3 M urea there is a six-fold increase in the apparent K_m for NADH while the apparent K_m for NADPH increases nearly 3-fold. Similarly, apparent V_{max} values increase 5 and 11-fold for NADH and NADPH, respectively. The competitive binding of NAD^+ and $NADP^+$ was exploited in order to compare inhibitory K_i values in the presence and absence of urea (see Figs. 4.23 to 4.28). In the case of NAD^+, the K_i increases 5-fold in the presence of denaturant, however, the inhibitory K_i for $NADP^+$ was actually found to decrease by a factor of 5 when assayed in urea. The various kinetic constants obtained in these experiments are summarised in Table 4.8.

A series of saturation curves with NADH as the variable substrate (0.125 to 4 mM) were generated at 0.5, 1, 1.5 and 2 M urea. As shown in Fig. 4.29, the apparent K_m and V_{max} values obtained under denaturing conditions were found to increase with denaturant concentration. It was also found that the kinetic parameters obtained in 3 M urea decreased with time as the protein assumed the unfolded conformation (see Figs.4.30 and 4.31). The half life of the modified kinetic form in 3 M urea can be calculated as 9 minutes and 13 minutes for the NADH and NADPH data sets, respectively. These values are relatively close to the value of 36 minutes estimated from the "biliverdin" data set shown in Fig.4.20.

Dissociation constants (K_D) for both NADPH and $NADP^+$ binding to hBVR-A were determined by monitoring the quenching of protein fluorescence in the presence and

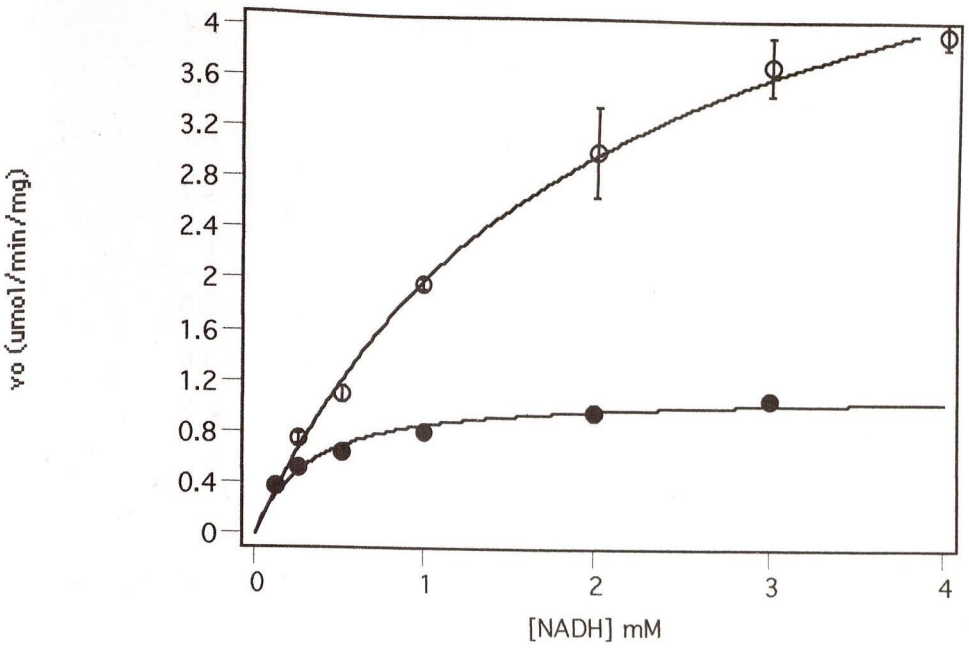

Figure 4.21. Estimation of apparent K_m and V_{max} for NADH.

Assays were carried out in the presence of 20 μM biliverdin with varying concentrations of NADH. Data points represent hBVR-A activity in the presence (○) and absence (●) of 3 M urea. K_m and V_{max} values estimated from these plots are shown below:

	K_m (mM)	V_{max} (μmol/min/mg)
- Urea	0.331 ± 0.05	1.16 ± 0.04
+ Urea	2.05 ± 0.18	6.15 ± 0.25

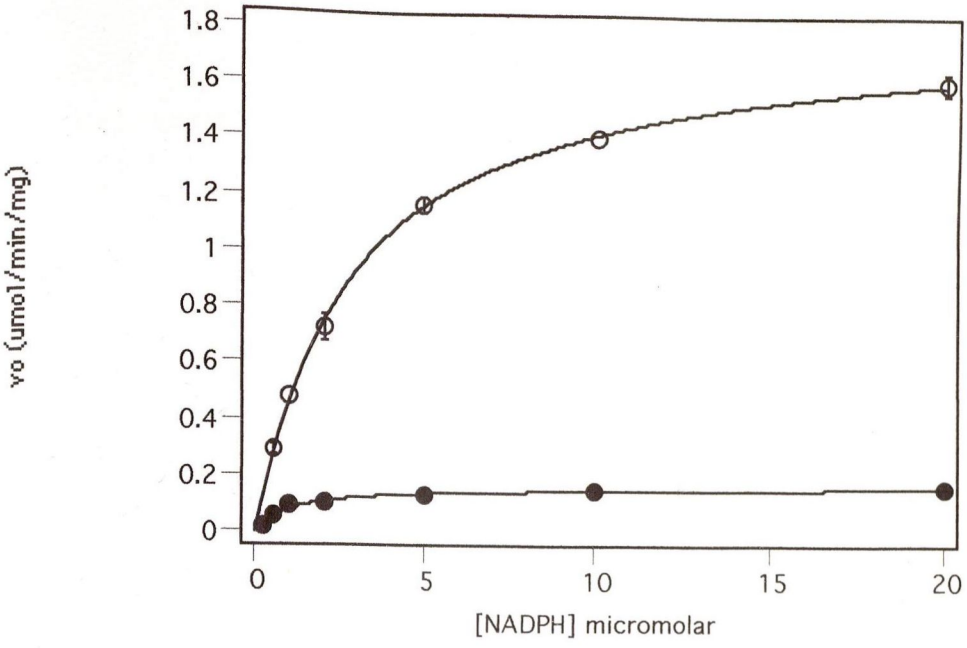

Figure 4.22. Estimation of apparent K_m and V_{max} for NADPH.

Assays were carried out in the presence of 20 μM biliverdin with varying concentrations of NADPH. Data points represent hBVR-A activity in the presence (❍) and absence (●) of 3 M urea. K_m and V_{max} values estimated from these plots are shown below:

	K_m (μM)	V_{max} (μmol/min/mg)
- Urea	1.0 ± 0.17	0.165 ± 0.01
+ Urea	3.0 ± 0.11	1.84 ± 0.02

Figure 4.23 (a) **Initial Rate Kinetics of NADH at Varying Concentrations of NAD^+.**

Results are presented as initial rate against NADH concentration at NAD^+ concentrations of 0 mM (○), 0.5 mM (●), 1 mM (❐) and 2 mM(■). Assays were performed in sodium phosphate buffer, pH 7.2 at 30°C.

Figure 4.23 (b) **Double Reciprocal Plots of Initial Rate against NADH Concentration at Varying Concentrations of NAD^+.**

Results are presented as double reciprocal plots of initial rate against NADH concentrations as described above.

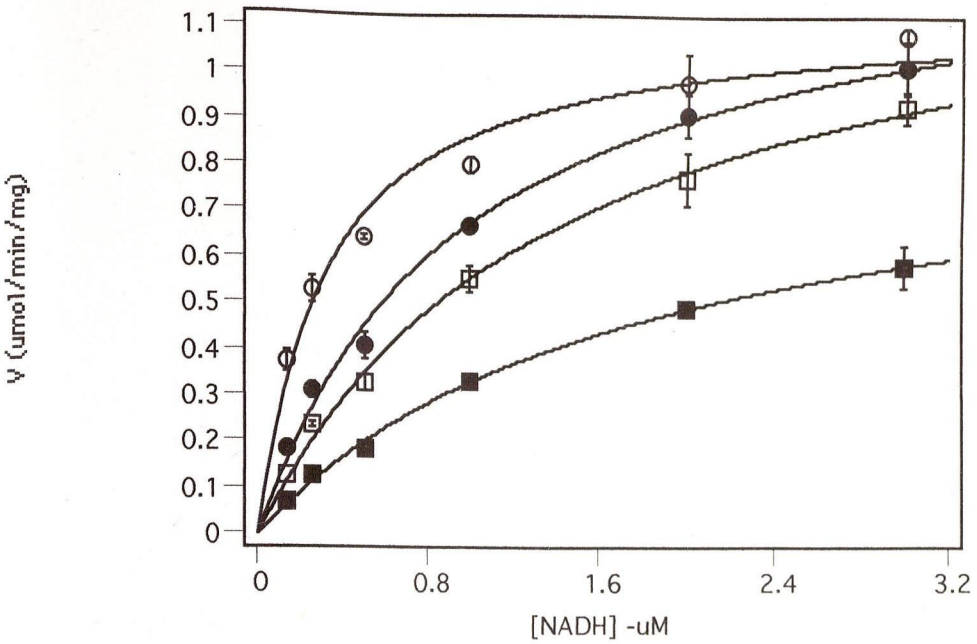
V (umol/min/mg)
1.1
1
0.9
0.8
0.7
0.6
0.5
0.4
0.3
0.2
0.1
0
0
0.8
1.6
2.4
3.2
[NADH] -uM

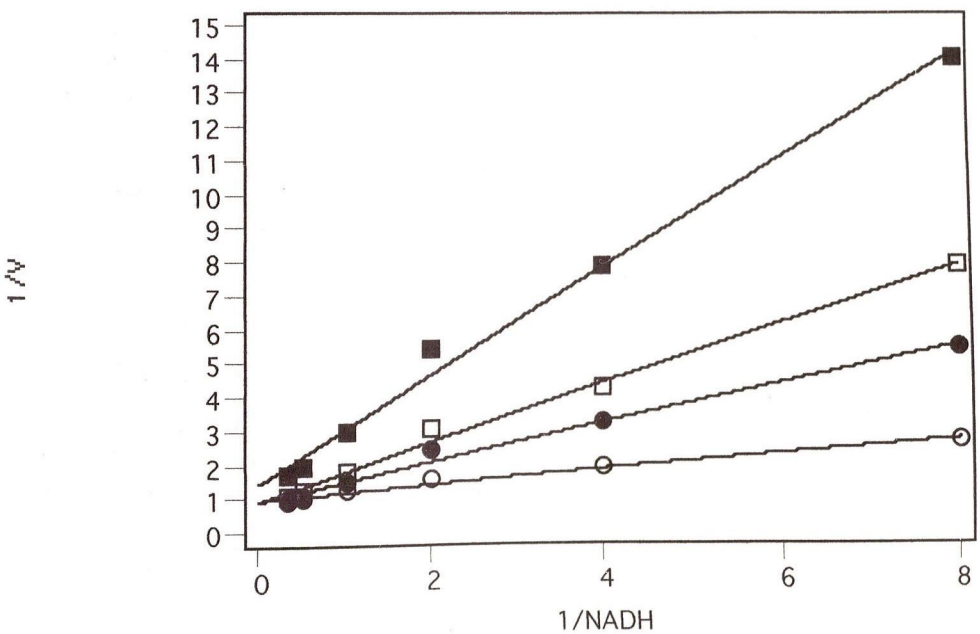
1/V
15
14
13
12
11
10
9
8
7
6
5
4
3
2
1
0
0
2
4
6
8
1/NADH

Figure 4.24 (a) **Initial Rate Kinetics of NADH at Varying Concentrations of NAD^+ in the Presence of 3 M Urea.**

Results are presented as initial rate against NADH concentration at NAD^+ concentrations of 0 mM (○), 0.5 mM (●), 1 mM (□) and 2 mM(■). Assays were performed in 3 M urea at 30°C.

Figure 4.24 (b) **Double Reciprocal Plots of Initial Rate against NADH Concentration at Varying Concentrations of NAD^+.**

Results are presented as double reciprocal plots of initial rate against NADH concentrations as described above.

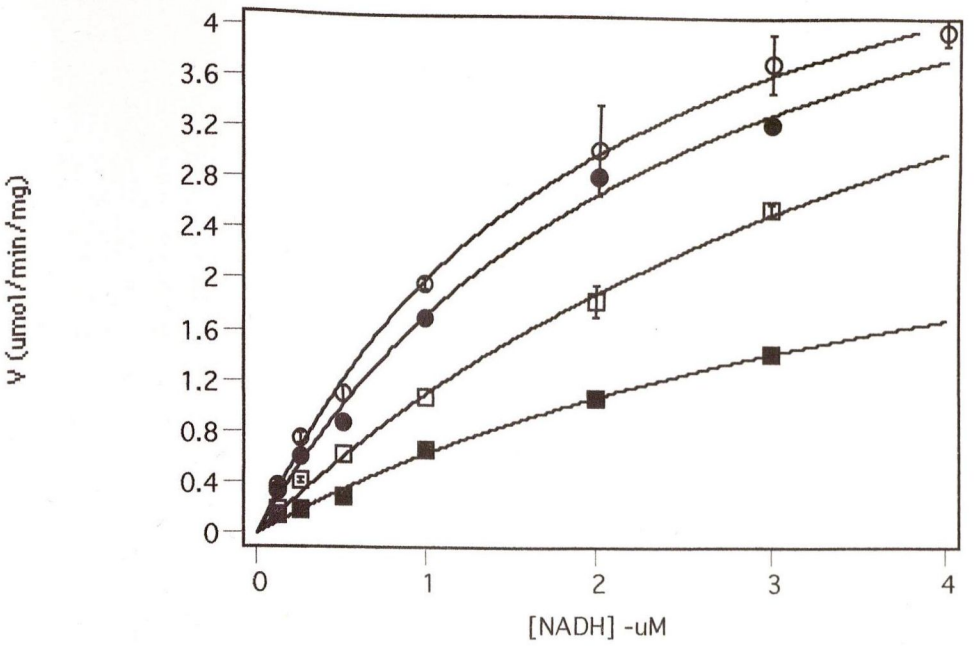
V (umol/min/mg)
4
3.6
3.2
2.8
2.4
2
1.6
1.2
0.8
0.4
0
0
1
2
3
4
[NADH] -uM

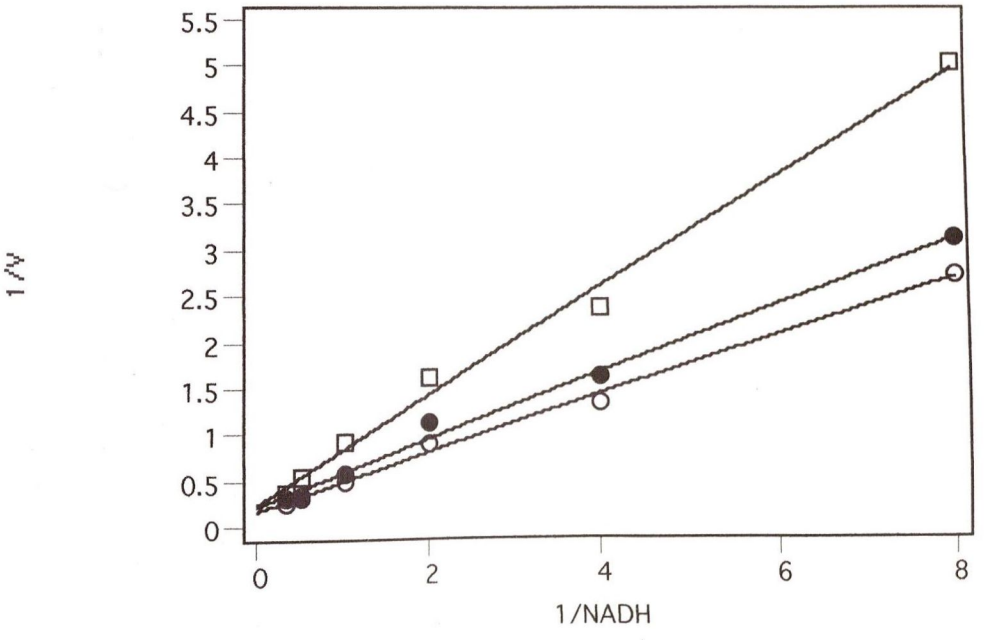
1/V
5.5
5
4.5
4
3.5
3
2.5
2
1.5
1
0.5
0
0
2
4
6
8
1/NADH

Figure 4.25 (a) **Initial Rate Kinetics of NADPH at Varying Concentrations of $NADP^+$.**

Results are presented as initial rate against NADPH concentration at $NADP^+$ concentrations of 0 μM (○), 1 μM (●), 2 μM (□) and 5 μM(■). Assays were performed in sodium phosphate buffer, pH 7.2 at 30°C.

Figure 4.25 (b) **Double Reciprocal Plots of Initial Rate against NADPH Concentration at Varying Concentrations of $NADP^+$.**

Results are presented as double reciprocal plots of initial rate against NADPH concentrations as described above.

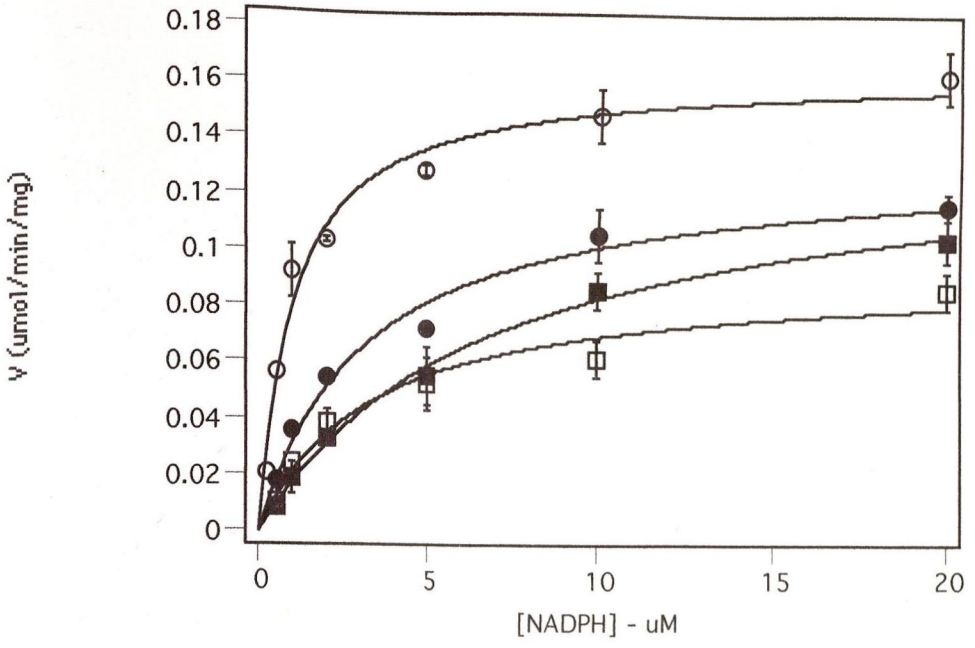
v (umol/min/mg)
0.18
0.16
0.14
0.12
0.1
0.08
0.06
0.04
0.02
0
0
5
10
15
20
[NADPH] - uM

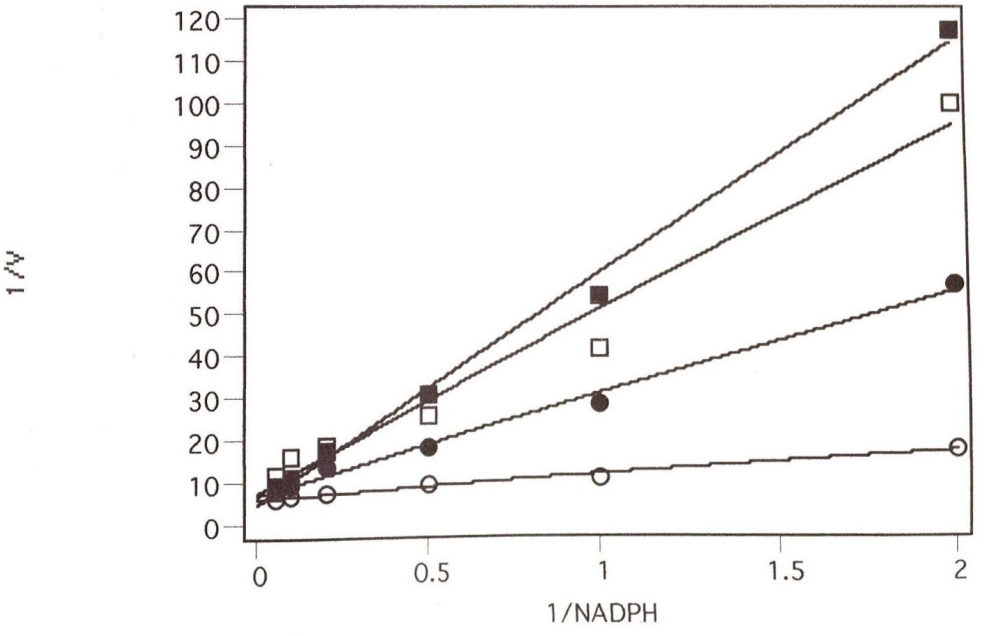
1/v
120
110
100
90
80
70
60
50
40
30
20
10
0
0
0.5
1
1.5
2
1/NADPH

Figure 4.26 (a) **Initial Rate Kinetics of NADPH at Varying Concentrations of $NADP^+$ in the Presence of 3 M Urea.**

Results are presented as initial rate against NADPH concentration at $NADP^+$ concentrations of 0 μM (○), 5 μM (●), 10 μM (□) and 20 μM(■). Assays were performed in 3 M urea at 30°C.

Figure 4.26 (b) **Double Reciprocal Plots of Initial Rate against NADPH Concentration at Varying Concentrations of $NADP^+$.**

Results are presented as double reciprocal plots of initial rate against NADPH concentrations as described above.

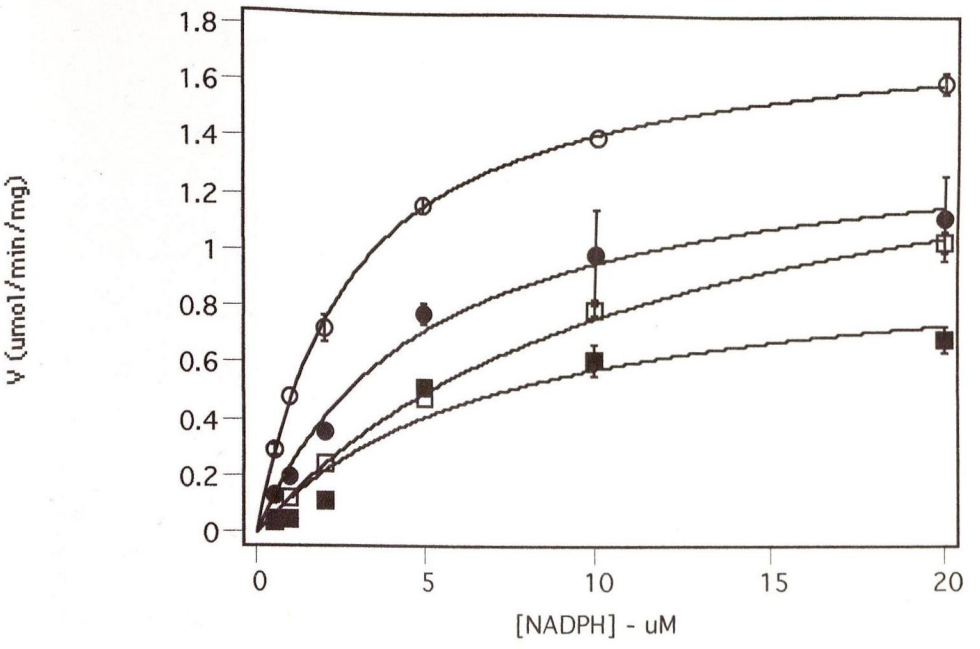
V (umol/min/mg)
1.8
1.6
1.4
1.2
1
0.8
0.6
0.4
0.2
0
0
5
10
15
20
[NADPH] - uM

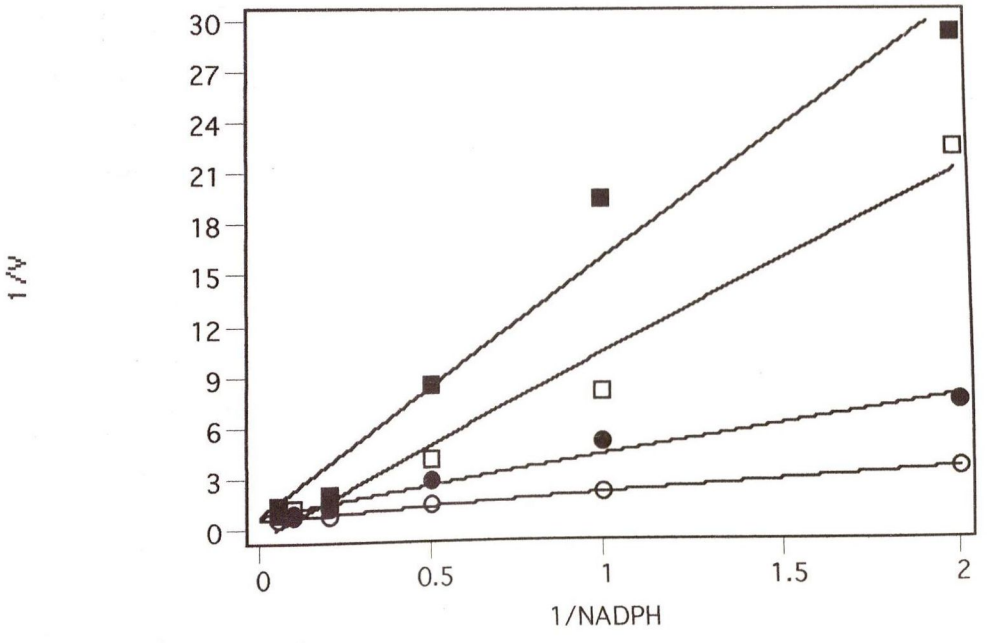
1/V
30
27
24
21
18
15
12
9
6
3
0
0
0.5
1
1.5
2
1/NADPH

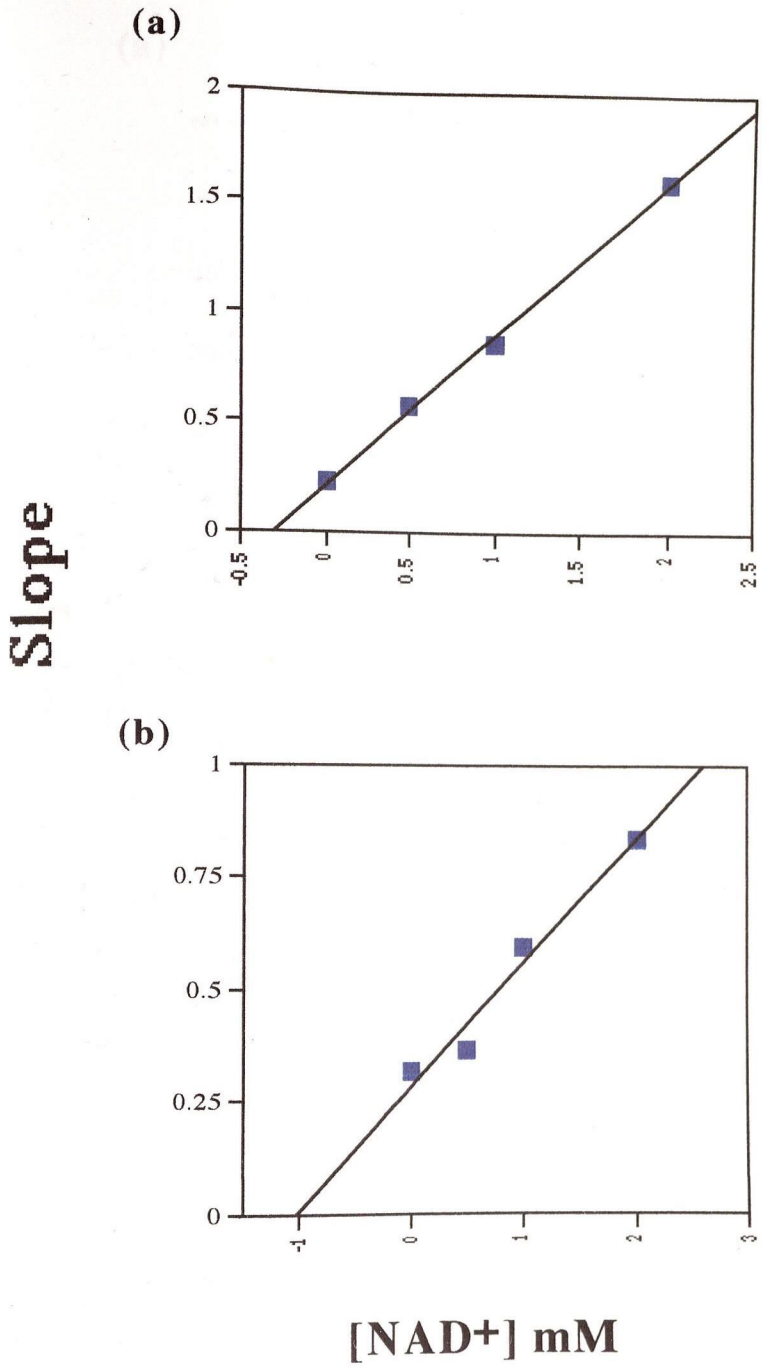

Figure 4.27. **Slope Replots for NAD^+ Inhibition in the Presence and Absence of 3 M Urea.**

The slopes were determined from the 1/v against 1/NADH plot shown in Fig. 4.23 (b) and 4.24 (b). These were replotted against NAD^+ concentration. (Graph (**a**): - Urea, Graph (**b**): + urea).

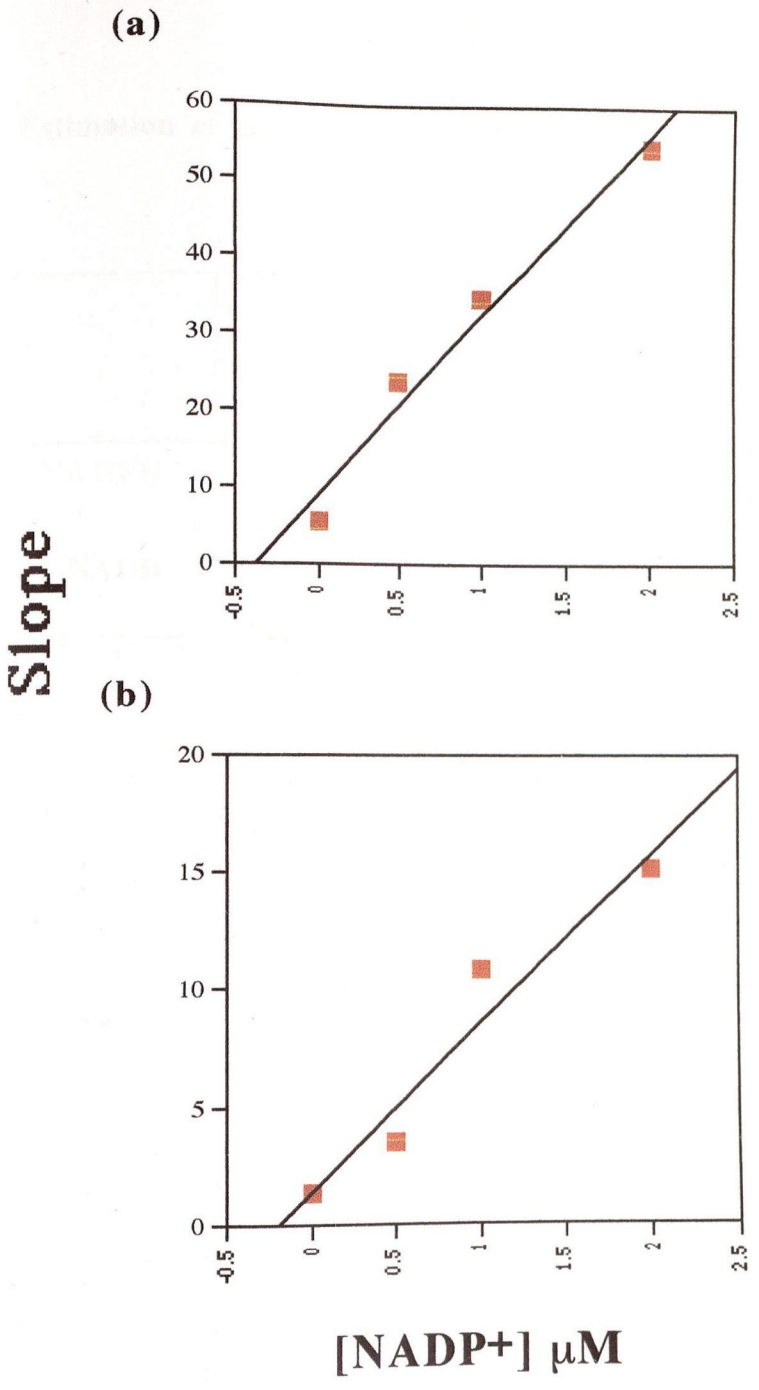

Figure 4.28. **Slope Replots for NADP$^+$ Inhibition in the Presence and Absence of 3 M Urea.**

The slopes were determined from the 1/v against 1/NADPH plot shown in Fig. 4.25 (b) and 4.26 (b). These were replotted against NADP$^+$ concentration. (Graph (**a**): - Urea, Graph (**b**): + urea).

Table 4.8 (a)

Estimation of apparent K_m and V_{max} values for hBVR-A in the presence and absence of 3 M Urea.

	- Urea		+ Urea	
	K_m	V_{max} (μmol/min/mg)	K_m	V_{max} (μmol/min/mg)
NADPH	1 μM	0.165	3 μM	1.8
NADH	0.33 mM	1.2	2 mM	6

Table 4.8 (b)

Estimation of apparent K_i and K_D values for hBVR-A in the presence and absence of 3 M Urea.

	- Urea		+ Urea	
	K_i	K_D	K_i	K_D
NADPH	-	1.92 μM	-	6.77 μM
NADP+	1.6 μM	1.85 μM	0.35 μM	5.23 μM
NAD+	0.3 mM	-	1.7 mM	-

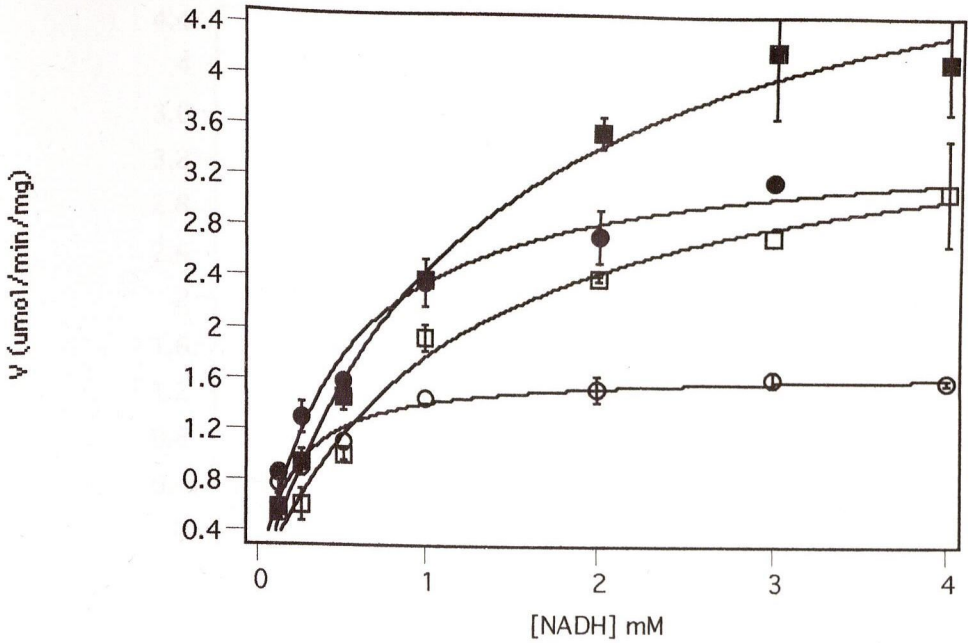

Figure 4.29. **Estimation of Apparent K_m and V_{max} of NADH in 0.5 - 2 M Urea.**

The assay was carried out in the presence of 20 μM biliverdin with varying concentrations of NADH. Data points represent hBVR-A activity in 0.5 M (○), 1 M(●), 1.5 M(□) and 2 M(■) urea. Apparent K_m and V_{max} values estimated from these plots are shown below:

[Urea] M	K_m (mM)	V_{max} (μmol/min/mg)
0	0.33 ± 0.05*	1.16 ± 0.04 *
0.5	0.20 ± 0.03	1.71 ± 0.05
1	0.50 ± 0.09	3.58 ± 0.21
1.5	1.22 ± 0.22	4.0 ± 0.27
2	1.34 ± 0.19	5.8 ± 0.32

* Taken from Fig. 4.21.

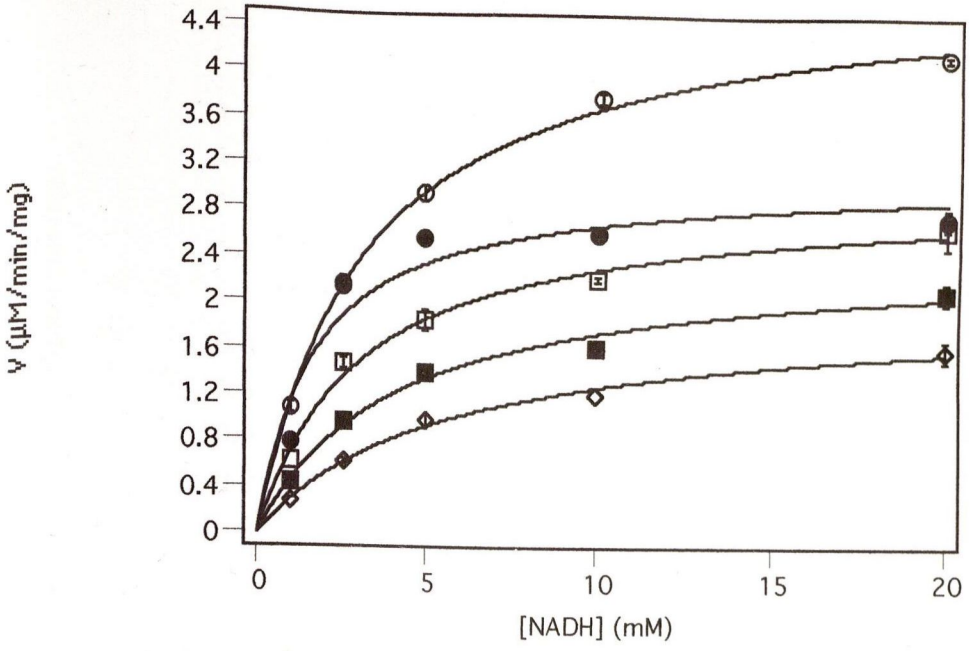

Figure 4.30. **Effect of Incubation Time in 3 M Urea on Initial Rate Kinetics.**

Samples of enzyme were incubated in 3 M urea for 0 (○), 3 (●), 6 (❐), 9 (■) and 12 (◊) minutes before being assayed for hBVR-A activity. Data points represent initial rate measurements with 20 µM biliverdin and varying concentrations of NADH. Apparent K_m and V_{max} values for NADH estimated from these plots are shown below:

Time (mins)	K_m (mM)	V_{max} (µmol/min/mg)
0	3.25 ± 0.21	4.92 ± 0.11
3	1.70 ± 0.70	3.16 ± 0.35
6	3.14 ± 0.52	3.04 ± 0.16
9	4.30 ± 0.70	2.51 ± 0.15
12	2.60 ± 0.46	2.05 ± 0.90

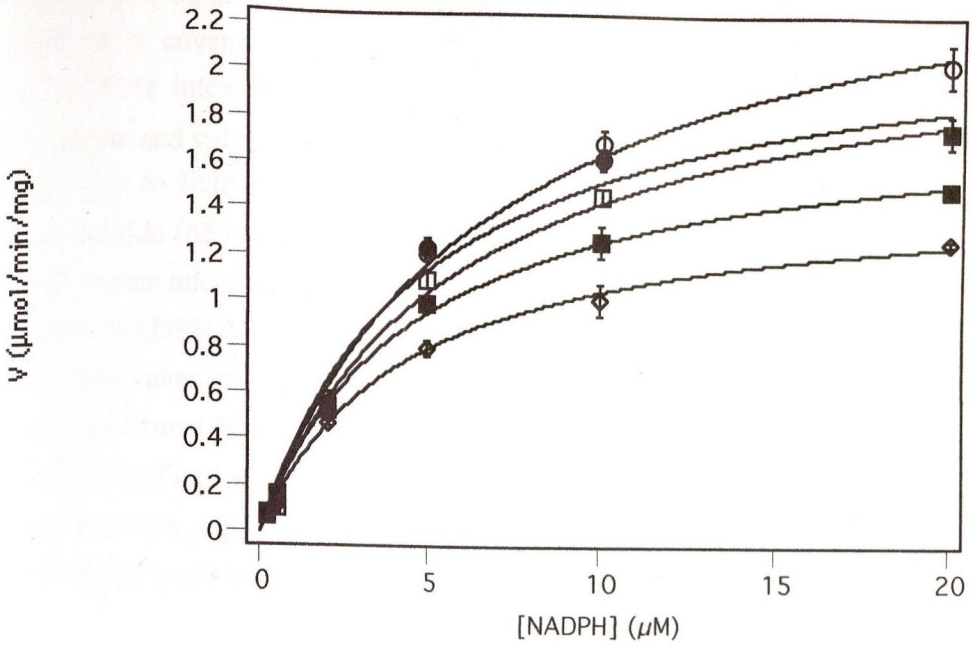

Figure 4.31. **Effect of Incubation Time in 3 M Urea on Initial Rate Kinetics.**

Samples of enzyme were incubated in 3 M urea for 0 (○), 3 (●), 6 (□), 9 (■) and 12 (◊) minutes before being assayed for hBVR-A activity. Data points represent initial rate measurements with 20 µM biliverdin and varying concentrations of NADPH. Apparent K_m and V_{max} values for NADPH estimated from these plots are shown below:

Time (mins)	**K_m (µM)**	**V_{max} (µmol/min/mg)**
0	6.89 ± 0.70	2.80 ± 0.12
3	5.04 ± 1.21	2.31 ± 0.20
6	6.09 ± 0.83	2.33 ± 0.12
9	4.84 ± 0.41	1.89 ± 0.05
12	4.64 ± 0.37	1.55 ± 0.43

absence of 3 M urea. Sequential additions of NADPH and $NADP^+$ (0 - 100 μM) were made to a cuvette containing hBVR-A at a final concentration of 1.5 μM. The fluorescence intensity (F_{meas}) of the solution was measured after each addition of nucleotide and values were corrected for the 'inner -filter' effect, as described in Section 2.2.15 (d), to yield F_{corr} values. The change in fluorescence intensity upon each addition of nucleotide (ΔF) was calculated and dissociation constants were determined from a plot of ΔF versus nucleotide concentration, as shown in Figs. 4.32 and 4.33. In the absence of urea, NADPH binds to human BVR-A with a K_D of 1.92 μM. In the presence of 3 M urea, this value increases to 6.77 μM. Similarly, the dissociation constant for $NADP^+$ increases from 1.85 μM to 5.23 μM in the presence of denaturant. It was not possible to measure the binding of NADH to human BVR-A using fluorescence spectroscopy as the concentrations required for maximal binding are in the millimolar range and the "inner-filter' effect is greatly enhanced.

4.4 (d) The Reversibility of the Unfolding Reaction.

When carrying out protein folding studies, it is necessary to establish if the unfolding reaction is reversible. The method most commonly used to monitor reversibility involves exposing the protein of interest to high concentrations of denaturant and then diluting the protein to conditions where it is assumed to regain it's native folded conformation. The reaction is said to be reversible if the chosen observable parameter (fluorescence emission, activity etc.) is identical after denaturation and refolding to the value measured under non-denaturing conditions.

A concentrated stock solution of human BVR-A was diluted 10-fold in 10 mM sodium phosphate buffer to give a final concentration of 0.27 mg/ml. A 20 μl sample of the diluted material was then assayed under standard conditions in order to calculate the rate of bilirubin formation under native conditions. A second sample of enzyme was diluted and assayed as described above, however, in this case the sodium phosphate buffer was supplemented with 3 M urea. As expected, the rate of product formation increased 10-fold due to alleviation of substrate inhibition. A third sample of enzyme was again diluted 10-fold in 3 M urea, however, on this occasion, a 20 μl sample of the diluted enzyme was assayed, and therefore diluted 100-fold (final volume in cuvette; 2 ml), in 100 mM sodium phosphate. As illustrated in Fig. 4.34, the calculated rate of bilirubin formation upon dilution of the denaturant was exactly the same as that found when the enzyme was diluted and assayed under non-denaturing conditions.

(a)

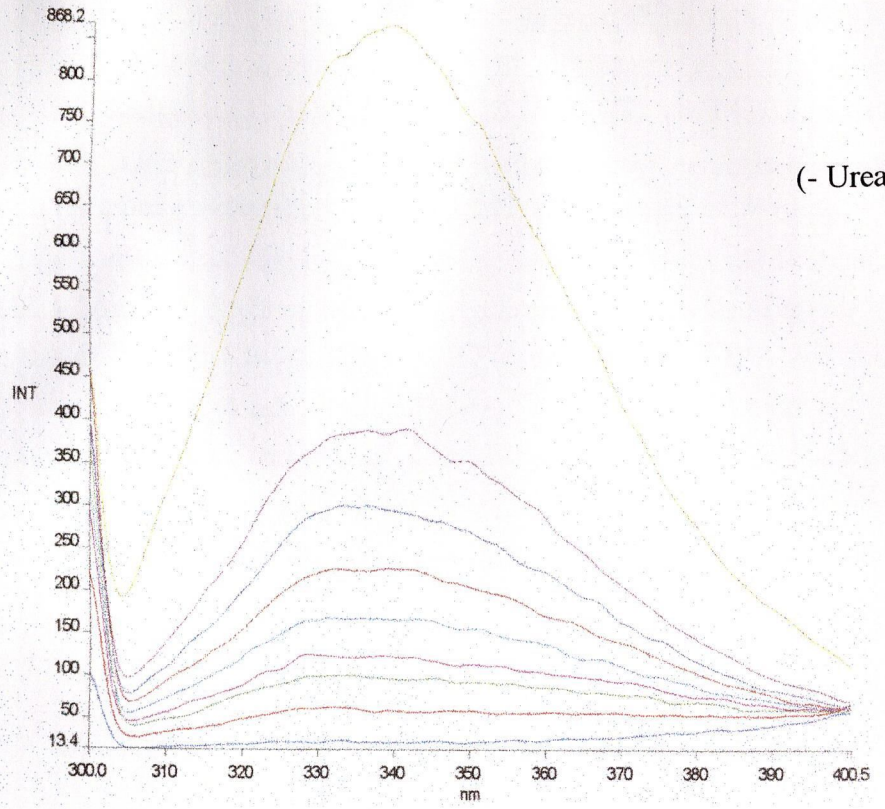
868.2
800
750
700
650
600
550
500
450
INT
400
350
300
250
200
150
100
50
13.4
300.0
310
320
330
340
350
360
370
380
390
400.5
nm

(- Urea)

(b)

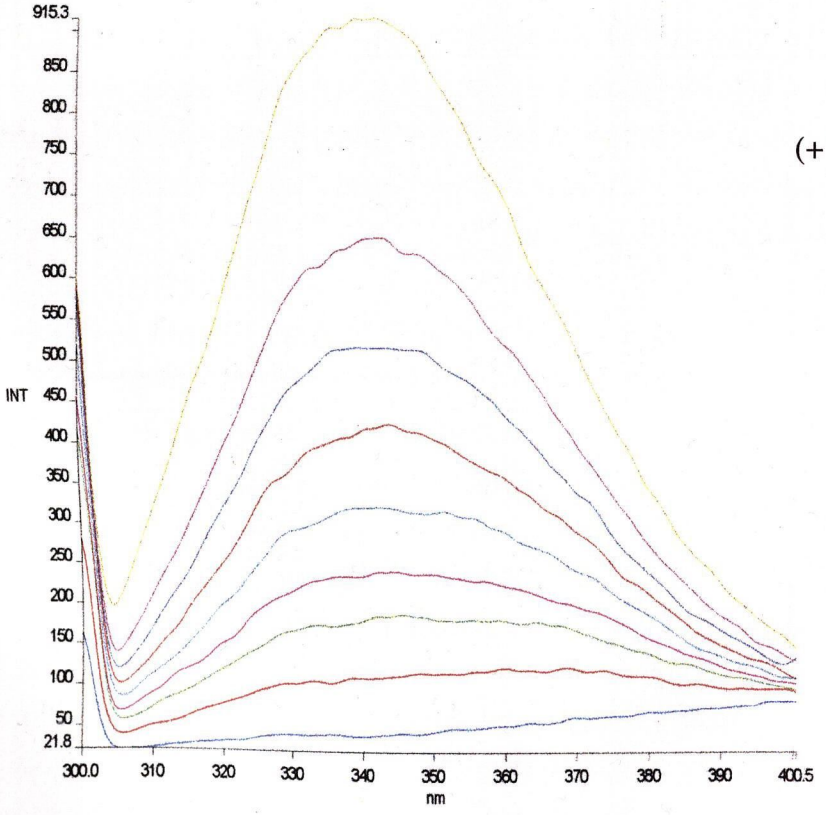
915.3
850
800
750
700
650
600
550
500
INT
450
400
350
300
250
200
150
100
50
21.8
300.0
310
320
330
340
350
360
370
380
390
400.5
nm

(+ Urea)

(c)

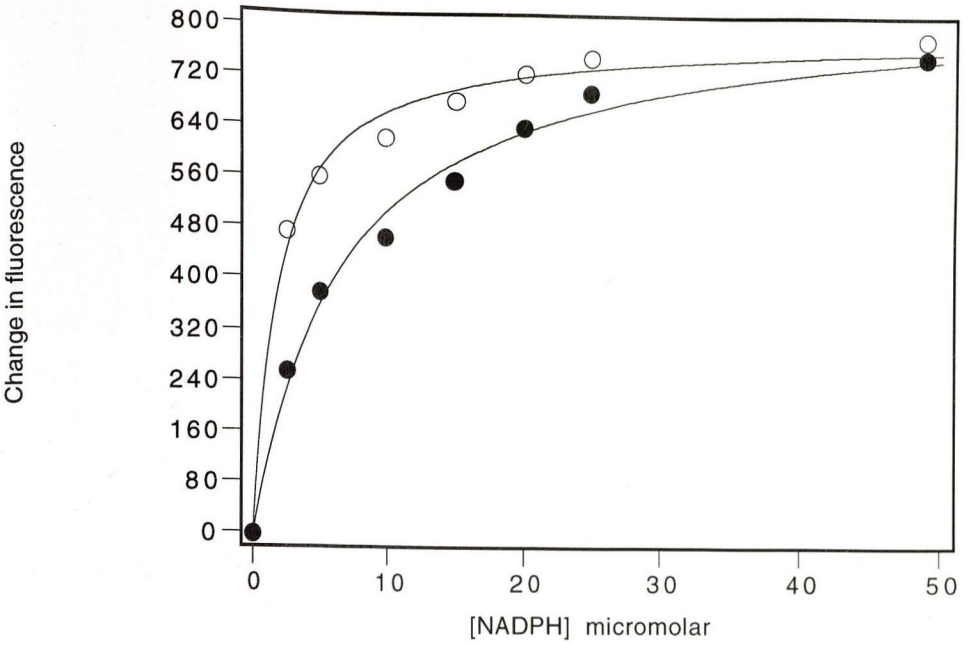

Figure 4.32. Determination of the Dissociation Constant for NADPH in the Presence and Absence of 3 M Urea.

(a) Sequential additions of NADPH were made to a cuvette containing 1.5 μM hBVR-A in sodium phosphate buffer, pH 7.2. The fluorescence intensity was measured at 340 nm (excitation 295 nm) after each addition of nucleotide.

(b) Sequential additions of NADPH were made to a cuvette containing 1.5 μM hBVR-A in 3 M urea. The fluorescence intensity was measured at 340 nm (excitation 295 nm) after each addition of nucleotide.

(c) The fluorescence intensites measured in (a) and (b) above were corrected for the 'inner-filter effect' to yield F_{corr} as described in Section 2.?. The change in fluorescence in the presence (●) and absence (○) of 3 M urea was calculated at each point by subtraction of F_{corr} from the fluorescence of the protein in the absence of nucleotide.

(a)

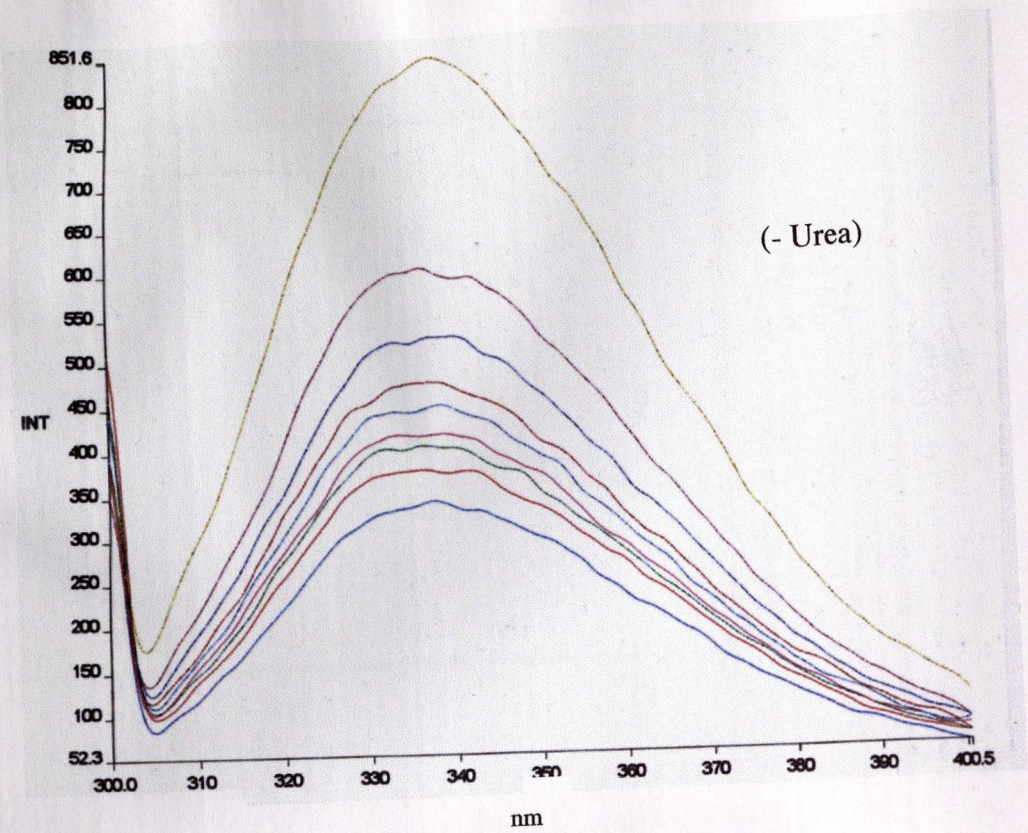
851.6
800
750
700
650
600
550
500
450
400
350
300
250
200
150
100
52.3
INT
300.0
310
320
330
340
360
370
380
390
400.5
nm
(- Urea)

(b)

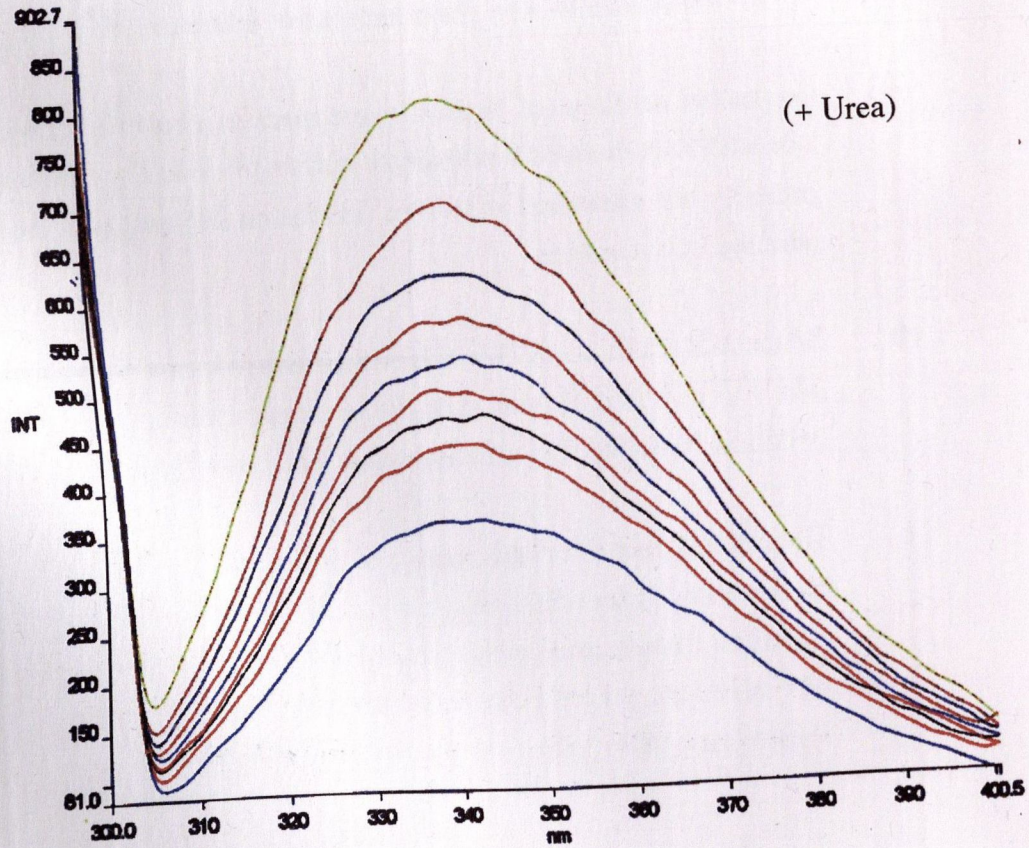
902.7
850
800
750
700
650
600
550
500
450
400
350
300
250
200
150
61.0
INT
300.0
310
320
330
340
350
360
370
380
390
400.5
nm
(+ Urea)

(c)

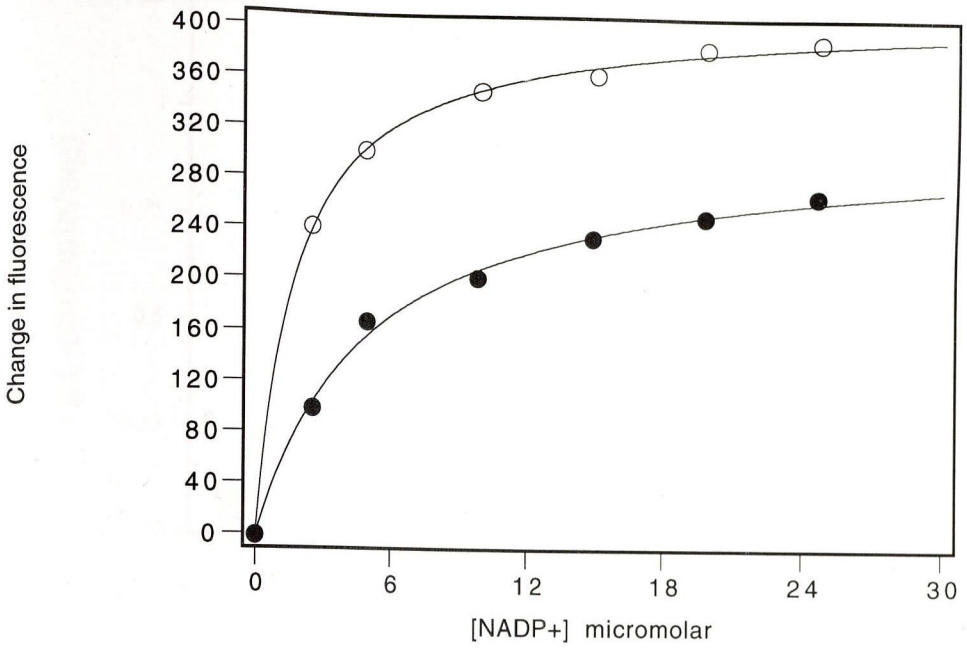

Figure 4.33. **Determination of the Dissociation Constant for $NADP^+$ in the Presence and Absence of 3 M Urea.**

(a) Sequential additions of $NADP^+$ were made to a cuvette containing 1.5 μM hBVR-A in sodium phosphate buffer, pH 7.2. The fluorescence intensity was measured at 340 nm (excitation 295 nm) after each addition of nucleotide.

(b) Sequential additions of $NADP^+$ were made to a cuvette containing 1.5 μM hBVR-A in 3 M urea. The fluorescence intensity was measured at 340 nm (excitation 295 nm) after each addition of nucleotide.

(c) The fluorescence intensites measured in (a) and (b) above were corrected for the 'inner-filter effect' to yield F_{corr} as described in Section 2.?. The change in fluorescence in the presence (●) and absence (❍) of 3 M urea was calculated at each point by subtraction of F_{corr} from the fluorescence of the protein in the absence of nucleotide.

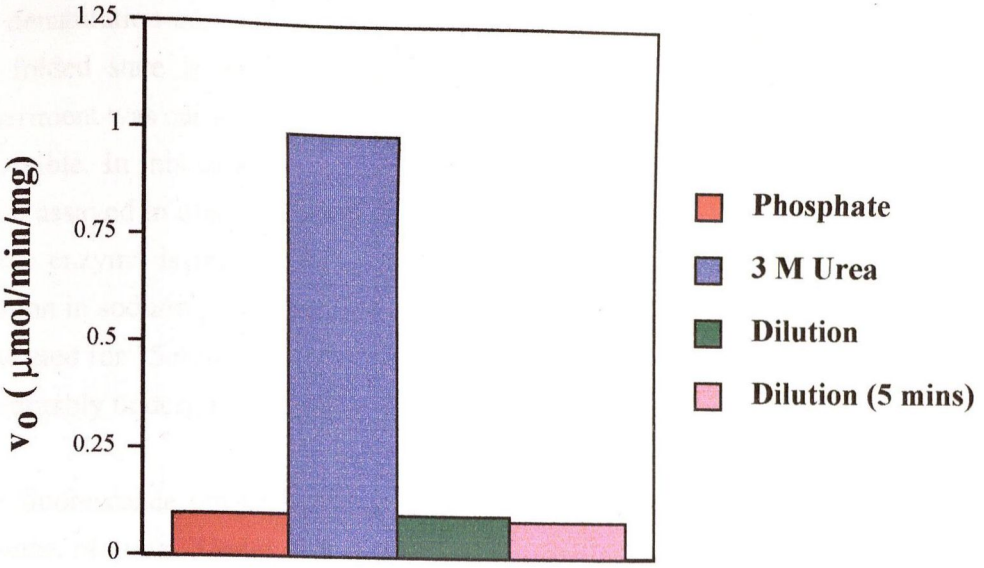

Figure 4.34. Reversibity of the Unfolding Reaction in 3 M Urea.

A stock solution of hBVR-A (2.7 mg/ml) was diluted and assayed in sodium phosphate buffer (❐) and 3 M urea (❐) at a final concentration of 0.27mg/ml. The enzyme was then incubated briefly in 3 M urea before being diluted and assayed in sodium phosphate buffer (❐). Finally, the enzyme was incubated for 5 minutes in 3 M urea before being diluted and assayed in sodium phosphate buffer (❐). The data points represent initial rate measurements with 20 μM biliverdin and 705 μM NADH. The partial unfolding seen at 3 M urea is reversible upon dilution into sodium phosphate buffer.

At high urea concentrations, the activity of human BVR-A begins to decay as can be seen from Fig.4.19. At 6 M urea there is only residual activity remaining, and the points on the denaturation curve are entering the post-transition region, the fraction of enzyme in the folded state is therefore small relative to that in the unfolded state. A similar experiment was carried out in order to determine if the unfolding seen at 6 M urea is also reversible. In this case, the activity seen upon dilution should be greater than that seen when assayed in urea. The results of this experiment are shown in Fig. 4.35. The activity of the enzyme is reduced by approximately 60% when assayed in 6 M urea. Upon dilution in sodium phosphate buffer, enzyme activity returns to normal. If the enzyme is incubated for 15 minutes in 6 M urea prior to refolding, the enzyme loses activity and is presumably undergoing complete denaturation.

The fluorescence emission of human BVR-A was also monitored in the presence and absence of urea. Under non-denaturing conditions, the emission spectrum peaks at approximately 335 nm with an F_{meas} value of 550 (see Fig.4.36). In 6 M urea, the intrinsic fluorescence of the enzyme is quenched and the spectrum shifts to the red with a F_{meas} value of 420 at 335 nm. If a sample of enzyme is added to an Eppendorf containing 6 M urea, mixed briefly and then immediately diluted into sodium phosphate buffer such that the final protein concentration after dilution matches that in the previous measurements, the emission spectrum shifts to the left and is virtually superimposable on the spectrum obtained in sodium phosphate buffer, hence the initial quenching observed in the presence of denaturant is reversible upon dilution.

In all of the above experiments, the final concentration of urea after dilution was less than 0.06 M. At this concentration of the denaturant, the observable parameters did not differ significantly from those seen under non-denaturing conditions. As shown in Fig. 4.15 and 4.19, changes were observed in both the activity and fluorescence of BVR-A at 0.5 M urea, therefore, an experiment was carried out in order to determine if the unfolding seen at a higher urea concentration could be reversed to that seen at 0.5 M urea. A concentrated stock solution of BVR-A (2.7 mg/ml) was diluted to 0.135 mg/ml and assayed in 2M urea. A second sample was then diluted and assayed in 0.5 M urea. As expected, the rate of bilirubin production seen at 2 M urea was higher than that observed at 0.5 M urea due to increased alleviation of substrate inhibition. A third sample of enzyme was diluted in 2 M urea, however, in this case the enzyme was assayed (and therefore diluted) in 0.5 M urea. As shown in Fig. 4.37, the rate of product formation in going from 2 M urea to 0.5 M urea was virtually the same as that seen when the enzyme was assayed directly in 0.5 M urea. Finally, the enzyme stock was diluted in 2 M urea and assayed in 10 mM sodium phosphate buffer. In this instance, the rate of product formation was comparable to that seen in the absence of denaturant.

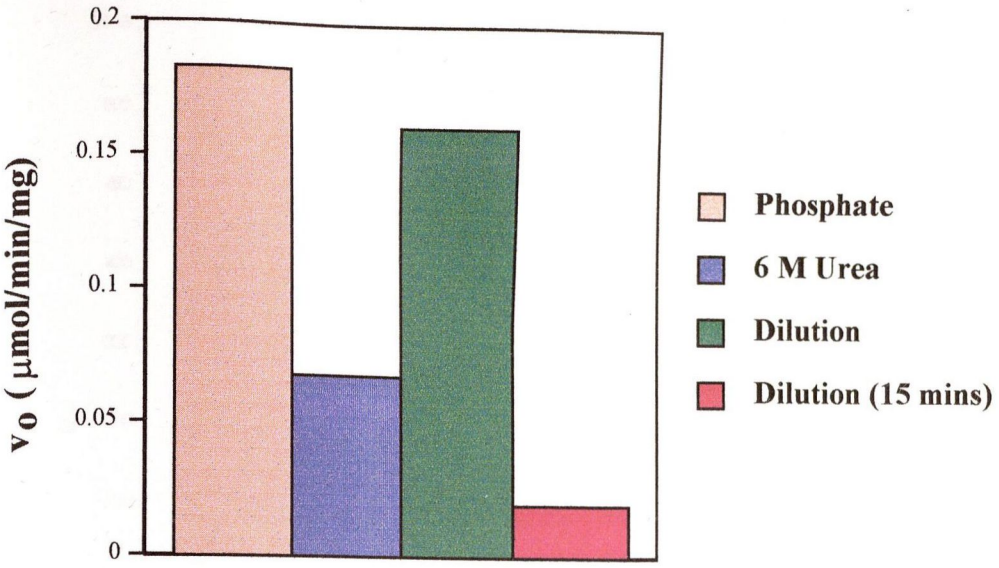

Figure 4.35. Reversibity of the Unfolding Reaction in 6 M Urea.

A stock solution of hBVR-A (2.7 mg/ml) was diluted and assayed in sodium phosphate buffer (❐) and 6 M urea (❐) at a final concentration of 0.27 mg/ml. The enzyme was then incubated briefly in 6 M urea before being diluted and assayed in sodium phosphate buffer (❐). Finally, the enzyme was incubated for 15 minutes in 6 M urea before being diluted and assayed in sodium phosphate buffer (❐). The data points represent initial rate measurements with 20 μM biliverdin and 705 μM NADH. The partial unfolding seen at 6 M urea is reversible upon dilution into sodium phosphate buffer, however, the enzyme does not regain activity after a 15 minute incubation period in the denaturant.

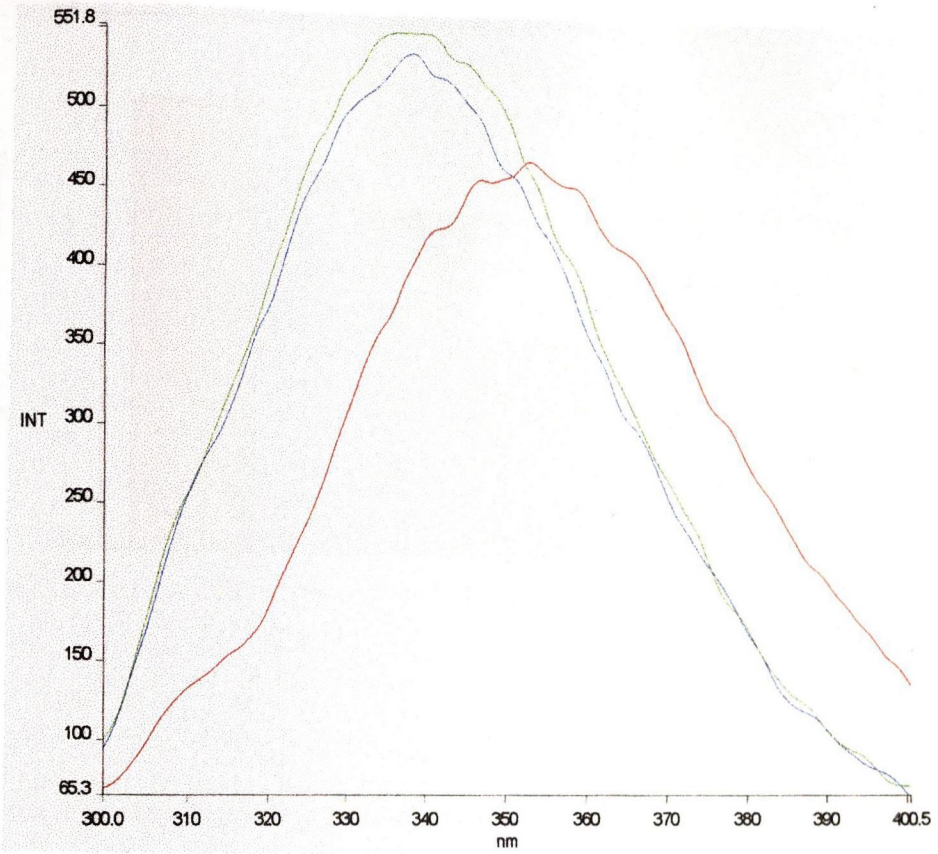

Figure 4.36. Reversibility of the Unfolding Reaction in 6 M Urea.

The fluorescence emission of hBVR-A was monitored under native conditions and in the presence of 6 M urea as outlined in Section 4.4 (d). A sample of enzyme was then pre-incubated briefly in 6 M urea before being diluted into sodium phosphate buffer and the fluorescence emission was again measured.

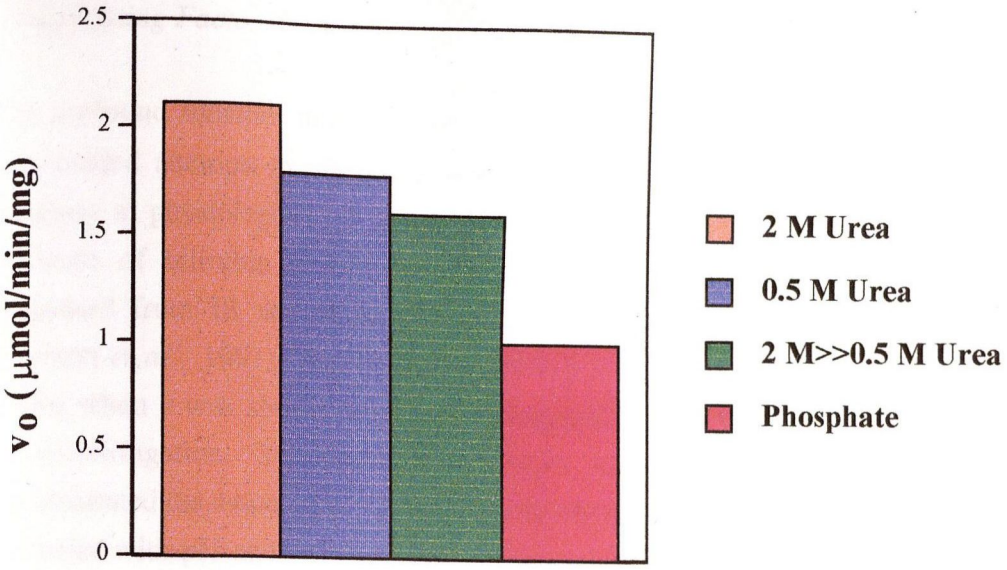

Figure 4.37. The Unfolding Intermediate Formed in 2 M urea can Partially Refold to a Distinct Intermediate seen at 0.5 M Urea.

A stock solution of hBVR-A (2.7 mg/ml) was diluted and assayed in 2 M Urea (❐) and 0.5 M urea (❐). A sample of enzyme was diluted from 2 M urea to 0.5 M urea and activity was measured as before (❐). Finally, the enzyme was diluted and assayed in sodium phosphate buffer, pH 7.2 (❐). The data points represent initial rate measurements with 20 mM biliverdin and 705 mM NADH. The partial unfolding seen at 2 M urea is reversible to that seen at 0.5 M urea suggesting the frormation of distinct kinetic intermediates during the unfolding process.

Complicating Factors in the Study of hBVR-A Kinetics.

The profound substrate inhibition and the insolubility of the product bilirubin-IXα has confounded attempts to determine kinetic constants for hBVR-A with any degree of accuracy at physiological pH values in the absence of serum albumin. The compact structure of bilirubin formed as a result of intramolecular hydrogen-bonding was suggested from IR and NMR observations and confirmed by X-ray crystallography (Bonnett *et al.*, 1991). Association of albumin with bilirubin was first detected in the 1930s when it was shown that bilirubin migrated with albumin on electrophoresis and ultracentrifugation. Subsequent confirmation came when Martin *et al.*, (1949) demonstrated the association of bilirubin with crystalline albumin. The affinity of binding increases with pH and decreases with chloride ion concentration, indeed both of these factors have been shown to have an effect on BVR-A kinetics.

In the standard assay for BVR-A activity there is a linear relationship between product concentration (A_{460}) and time when BSA (37 μM) is incorporated into the assay mixture. However, in the absence of BSA, product-time curves deviate from linearity at the start of the reaction as the enzyme begins to turnover. Thus it is not possible to record reliable data at sub-inhibitory concentrations of biliverdin-IXα in the absence of BSA. Previous workers (Phillips, 1981; Rigney, 1985) have attempted to define a physical basis for the increase in ΔA_{460} seen on addition of BSA to the assay mixture. Based on the assumption that the effect of the addition of BSA is simply to double the extinction co-efficient of bilirubin, it is possible to interpret the change in initial rate obtained upon addition of BSA as due to sequestering of biliverdin by BSA. If rates are normalised on the basis of the extinction coefficient and it is assumed that the rate in the presence and absence of BSA is due to identical concentrations of biliverdin, then the bound and free concentrations of biliverdin can be calculated for any particular concentration of BSA. Unfortunately, the work of Phillips is consistent with the physically unreasonable conclusion that there are a large number of binding sites (N = 10) with very low affinities for biliverdin binding (0.5 mM).

hBVR-A exhibits marked substrate inhibition by biliverdin-IXα, a phenomenon widely documented for a number of $NADP^+$ dependent oxidoreductases. Substrate inhibition (where the initial rate plateaus and then decreases as the concentration of substrate is increased) can be explained by two distinct physical models. Both involve substrate binding twice during the catalytic cycle. Earlier models achieved this by simply allowing two molecules of substrate to bind, the first to form a catalytically active ES complex

while the second formed a dead-end non-productive ES_2 complex (Scheme I).

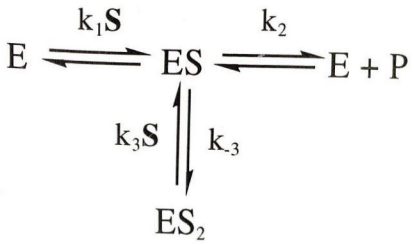

Scheme I

This notion was further refined by Murray (1930), who suggested that if the active site of an enzyme consisted of two or more subsites with affinities for different parts of the substrate molecule, then unproductive crowding of the two molecules of the substrate might occur (Scheme II). This notion was later adopted by Wilson and Cabib (1956) to explain the inhibition of acetylcholinesterase by excess choline.

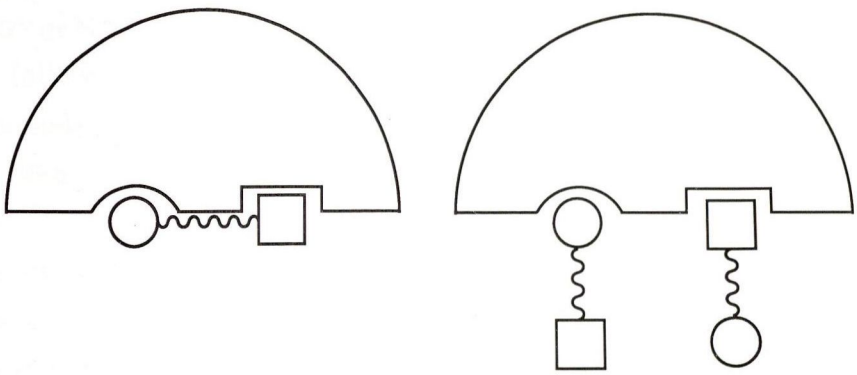

Scheme II

An alternative scheme, where two molecules of substrate bound to the enzyme during the catalytic cycle but without the formation of an ES_2 complex, was first proposed by Raval and Wolfe (1963) to explain the inhibition of malate dehydrogenase at high concentrations of oxaloacetate (OAA). In this case oxaloacetate normally combines with the E-NADH complex to form the productive ternary complex E-NADH-OAA. However, it may also react with the free enzyme in competition against NAD^+ and NADH, or react with the E-NAD complex in competition against malate. In each case a dead-end complex

is formed at high concentrations of substrate (Scheme III).

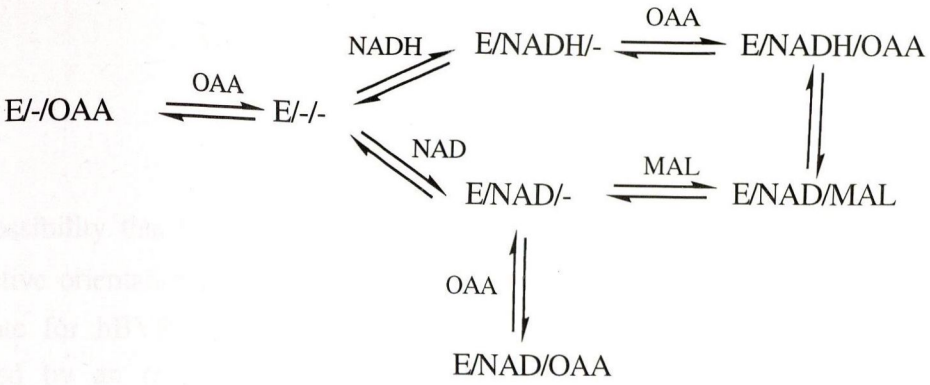

Scheme III

The enzyme-OAA complex can be competed by high concentrations of NAD^+ (or NADH) however, formation of the enzyme-NAD-OAA complex cannot be overcome by high NAD^+ or NADH and is responsible for the observed substrate inhibition. hBVR-A probably follows a similar mechanism with biliverdin-IXα binding to the enzyme-$NADP^+$ complex. Evidence for such a mechanism has been described for the ox enzyme (Rigney, 1986).

Inhibition by substrate may also occur if the substrate can bind in a number of orientations, only one of which is productive. Westley (1969) has shown that although the behaviour is competitive (Scheme IV) the rate equation (Eqn. 4.7) predicts an uncompetitive pattern. Increasing the substrate concentration cannot overcome the inhibition and the apparent K_m is lower than would be the case if the non-productive orientation did not occur.

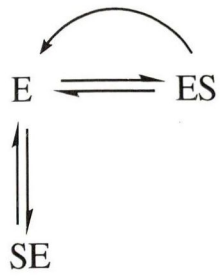

Scheme IV

$$vo = \frac{V_{max}S}{K_m + S\,(1 + K_m/K_i)} \qquad \text{(Eqn. 4.7)}$$

The possibility that biliverdin-IXα can bind to the enzyme-NADH complex in a non-productive orientation cannot be ruled out. Studies on the specificity of the tetrapyrrole substrate for hBVR-A and hBVR-B (see Chapter 5) have revealed that hBVR-B is inhibited by an α-isomer of biliverdin. hBVR-B cannot catalyse the reduction of biliverdin-IXα and given that this inhibition is competitive with respect to FMN it seems likely that the tetrapyrrole is rotated such that the reducible C-10 methene bridge is no longer in close proximity to the nicotinamide cofactor. Indeed the recent solution of the crystal structure of hBVR-B complexed with biliverdin-IXα confirms that this rotation occurs (Pereira, personal communication). Although a non-productive orientation of biliverdin-IXα binding to hBVR-A cannot be ruled out, it cannot be adapted to explain the substrate inhibition of BVR-A for the reasons discussed previously. However it may be that the BVR-A mechanism actually conforms to a mechanism of the type:

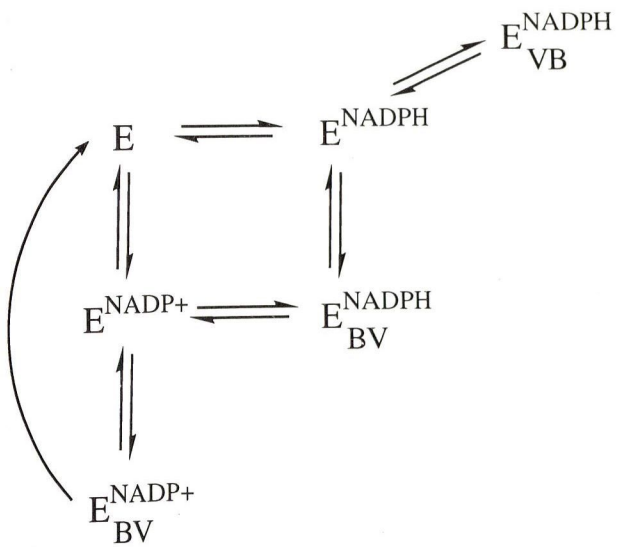

Further studies will be neccesary to examine this hypothesis.

A number of curve fitting routines for substrate inhibition were performed in order to test the reliability of using such methods to determine kinetic constants for hBVR-A. A series

of data sets were generated using equations describing total and partial substrate inhibition. As a general rule, accurate estimations of K_m, V_{max} and K_i could be made at low K_m values. However, as the K_m is increased errors arise during least squares analysis of this type of data. In addition, curve fitting routines could only be used with confidence when there was a sufficient number of data points on the ascending limb of the saturation curve. Under current experimental conditions it is not possible to obtain initial rates for hBVR-A in the sub-inhibitory phase. A measure of the physiological concentration of biliverdin-IXα in tissues in which BVR-A is expressed has not yet been achieved. It may be that the concentrations of biliverdin used for *in vitro* studies are in excess of the normal physiological levels. This is especially true in light of the fact that biliverdin interacts with serum albumin and other intracellular binding proteins *in vivo*. Also worthy of consideration in the interpretation of kinetic data are the facts that both biliverdin and bilirubin bind to serum albumin, bilirubin may be sequestered in lipid micelles *in vivo* and BVR-A enzyme may interact directly with members of the micosomal haem oxygenase system *in vivo*.

An alternative assay using ^{32}P -labelled NADPH is currently being developed and is based on the fact that $NADP^+$ and NADPH can be separated using ion-exchange methods. It should be possible to measure initial rates at low concentrations of biliverdin using a discontinuous method whereby oxidised [^{32}P]-$NADP^+$ is separated from the reaction mixture and counted. The quantity of NADPH oxidised can then be correlated to the amount of biliverdin reduced to bilirubin.

Even with NADH as cofactor, the K_m for biliverdin is at the limit of the linear range of the spectrophotometric assay. The K_m for NADPH is far lower than that for NADH, suggesting that NADPH may be preferentially utilised as co-factor for the reduction of biliverdin under physiological conditions. It has been suggested that NADPH is usually the physiologically relevant cofactor in such cases of cytosolic enzymes, since in this location, $NADP^+$ is predominantly in the reduced form and NAD^+ is in the oxidised form (Siess *et al.*, 1977; Williamson *et al.*, 1967).

Stopped-flow studies monitoring the quenching of protein fluorescence by NADPH in the pre-steady state demonstated that NADPH binds to hBVR-A with an initial encounter K_D of 8.4 μM (see Fig. 4.38). However, a K_D of 1.9 μM was calculated from equilibrium protein fluorescence quenching experiments. This suggests that the initial binding of nucleotide to the enzyme is followed by isomerization to a 'nucleotide-induced' conformation.

Stopped-flow kinetic studies also revealed an initial burst of bilirubin production at 460

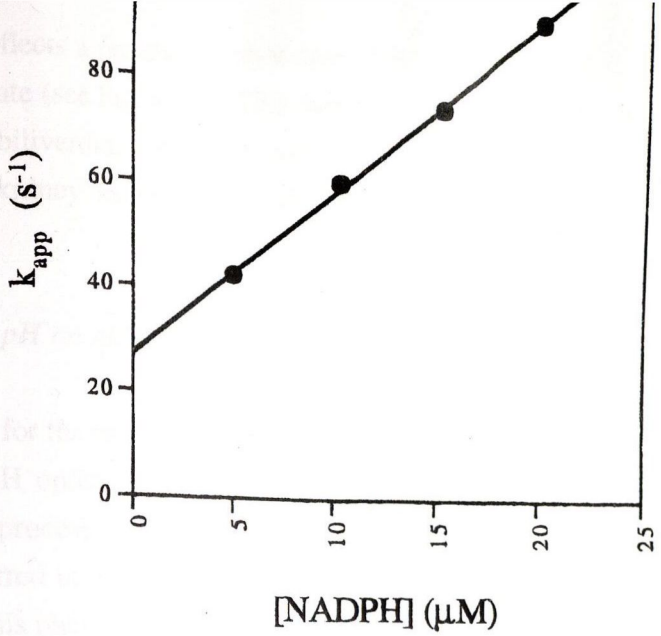

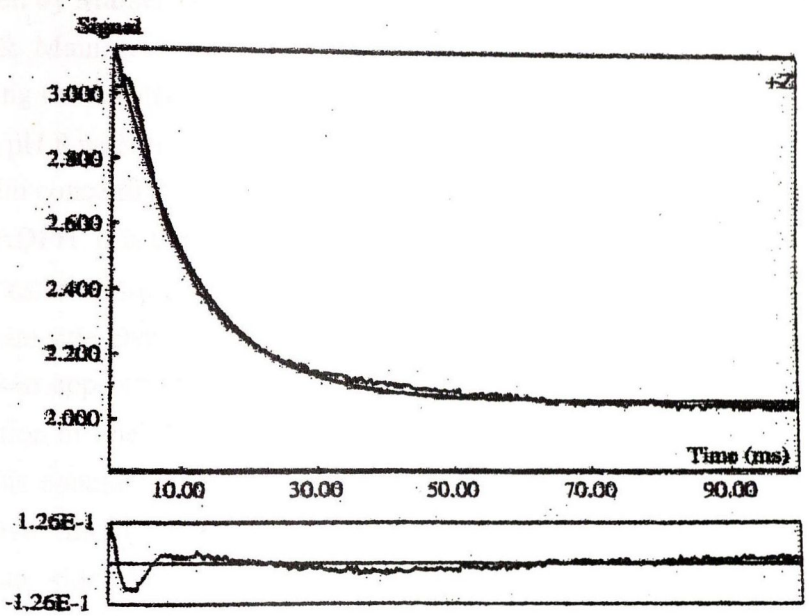

Figure 4.38. Determination of the dissociation constant for NADPH binding to hBVR-A in the pre-steady state.

Fluorescence quenching experiments were performed as outlined in Section 2.2.15 (e). A dissociation constant of 8.4 μM was calculated from the plot of k_{pp} versus nucleotide concentration ($k - 1 = 27\ s^{-1}$; $k + 1 = 3.2 \times 10^6\ M^{-1}\ s^{-1}$).

nm, which reflects a pre-steady state rate of bilirubin formation that is greater than the steady-state rate (see Fig. 4.39). This suggests that the rate limiting step occurs after the reduction of biliverdin, consistant with the findings of Rigney *et al.*(1989) and Ennis (1996) on ox kidney and rat kidney BVR-A, respectively.

The Effect of pH on hBVR-A Kinetics.

As is the case for the native enzyme, recombinant hBVR-A has the characteristic of having two distinct pH optima depending on whether NADH or NADPH is used as cofactor in the reductive process. This feature has been highlighted in the literature and the enzyme has been referred to as "unique" among all oxidoreductases. However, as highlighted in Section 4.2, this phenomenon is clearly dependent on the experimental conditions used to assess the relationship between pH and activity. The "dual cofactor/pH behaviour" described by Maines and other workers (Singleton & Laster, 1965; Noguchi *et al.*, 1979; Kutty & Maines, 1981; Rigney, 1986; Fahkrai & Maines, 1992) is clearly seen by restricting the substrate concentration monitored to 20 μM. Under these conditions activity peaks a pH 8 with NADPH although there is an additional peak of activity at pH 4. At low biliverdin concentrations, in this case 2 μM, enzyme activity is actually highest at pH 6.5 with NADPH. It is tempting to ascribe the increase in apparent K_m and K_i under alkaline conditions to deprotonation of a basic residue involved in binding one of the biliverdin propionate side chains as an ion-pair. A similar argument can be advanced to explain the increase in apparent K_m and K_i for biliverdin-IXα as the pH is decreased. In this case, protonation of one of the propionate side chains on the tetrapyrrole may weaken the ion-pair. This conclusion is further supported by the work of Colleran and O'Carra (1970) who have described a reduction in biliverdin reductase activity on esterifying one propionate side chain indicating that interaction between a monocarboxylate biliverdin anion and the enzyme is less favourable than the interaction involving the dicarboxylate form of the enzyme.

The Stereospecificity of NADH Oxidation by HBVR-A.

The effect of incubating hBVR-A with biliverdin and [4-^{3}H]NADH labelled on the A face and the B face with GDH and ADH, repectively, showed clearly that hBVR-A is B-face-specific. The GDH and ADH converted 92% and 73% of the NAD^+ to NADH, respectively and the subsequent BVR-A reactions were allowed to go to completion. Under these conditions the incorporation of ^{3}H into bilirubin for the B-face reaction was essentially quantitative (21,600 d.p.m. compared with 1,012 d.p.m.with NADH labelled

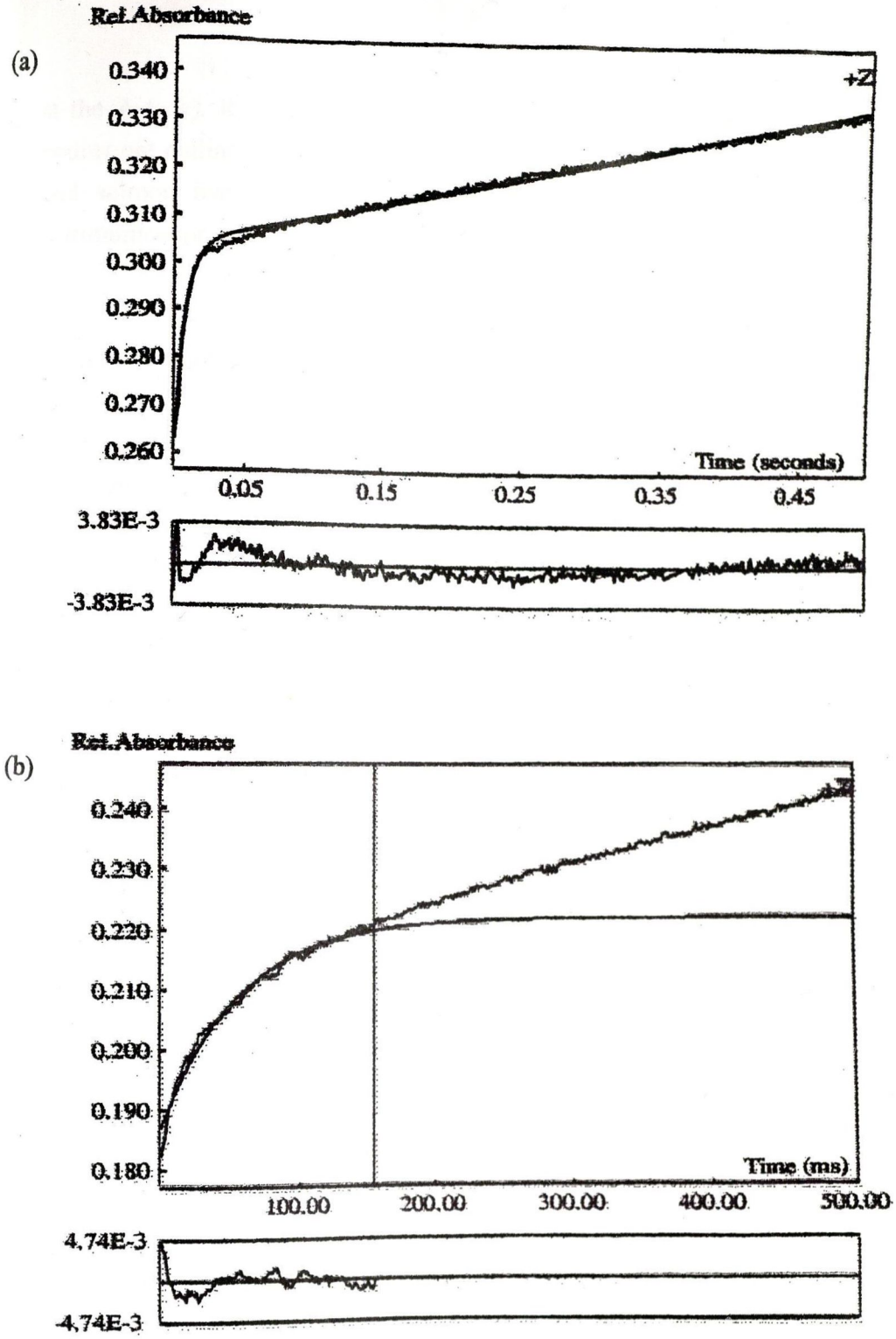

Figure 4.39. Measurement of bilirubin production in the pre-steady state.

Stopped flow experiments were carried out as outlined in Section 2.2.15 (c). An initial burst of bilirubin production was recorded, which reflects a pre-steady state rate of formation of bilirubin that is greater than that observed in the steady state. Bilirubin production was monitored at 460 nm using both NADPH (a) and NADH (b) as cofactor.

at the A-face). Reasons for the discrepency in the actual versus expected number of counts are outlined in Section 4.3 (b). Similar results have been obtained for rat kidney and salmon liver BVR-A and more recently for human BVR-B (Darcy, personal communication).

Protein Folding Studies.

Denaturation with guanidine hydrochloride or urea is one of the primary ways of measuring the conformational stability of proteins. Despite their widespread use in measuring the free energies of unfolding, the mode of action of these two agents is not completely understood. It has been proposed that denaturants induce unfolding by stabilizing the unfolded state of proteins over the folded state, either through direct interaction with the protein molecule or indirectly by changing the properties of the solvent. Wu *et al.* (1999) have recently presented evidence suggesting that the effect of urea on the activity of ribonuclease A and papain can be well described by the denaturant binding model. In addition, Mande *et al.* (2000) have recently solved crystal structures of hen egg-white lysozyme complexed with dimethyl sulfoxide and guanidine chloride complexes. In the present study, both guanidine hydrochloride and urea were used over a range of concentrations to evaluate the unfolding free energy change for hBVR-A. The linear extrapolation model, which assumes that only the denatured and native states are significantly populated, yielded values of 2.2 and 8 kcal/mol for guanidine hydrochloride and urea, respectively. Further studies will be required to confirm if the value obtained is dependant on the nature of the denaturant used to induce the unfolding event.

The presence of intermediates in the unfolding pathway cannot be ruled out. In 3 M urea, the activity of hBVR-A was found to increase substantially. Initial rate studies with biliverdin as the variable substrate revealed that the profound substrate inhibition exhibited by the enzyme is alleviated in the presence of 3 M urea in a manner analogous to that observed under acidic and alkaline conditions. Apparent K_m and substrate inhibitory K_i values increased substantially as did the dissociation constants for nucleotide binding. The partial unfolding seen in 3 M urea was also found to be reversible. Dilution of the protein to conditions where it assumes the native folded conformation resulted in a return to the substrate inhibited kinetics characteristic of this enzyme. In 6 M urea, the activity of the enzyme decayed substantially indicating that the enzyme was undergoing complete denaturation. Immediate removal of the denaturant resulted in the enzyme regaining activity, however, it was not possible to refold the enzyme following a 15 minute pre-incubation period at this concentration of denaturant.

The effect of urea on the kinetics of hBVR-A could be attributed to the denaturant acting as a competitive inhibitor of the enzyme, however, this seems unlikely as similar results were obtained with guanidine hydrochloride. In addition, the results obtained in kinetic experiments can be correlated with those obtained from experiments monitoring the effect of denaturants on the intrinsic fluorescence of the hBVR-A protein.

Chapter 5

Studies on the Specificity of the Tetrapyrrole Substrate for Human Biliverdin-IXα Reductase and Human Biliverdin-IXβ Reductase

Introduction

The formation of linear tetrapyrroles by haem catabolism in mammals has, until recently, been discussed in terms of the IXα isomers of biliverdin and bilirubin as both haem oxygenases I and II (HO-1 and HO-2), and BVR-A are reported to exhibit such specificity. When assayed with the four isomeric biliverdins (Fig. 5.1) that can be derived by cleavage of haem IX, BVR-A showed a very clear-cut, but not absolute, specificity for the α-isomer (Colleran & O'Carra, 1977). Just as BVR-A does not have an absolute specificity for the α-isomer, BVR-B does not have an absolute specificity for biliverdin-IXβ. Table 5.1 shows the relative rates of reduction of the four biliverdin-IX isomers in NADPH-dependent reactions, by the biliverdin reductase isozymes purified from human liver by Yamaguchi *et al.* (1994). For the two BVR-B isozymes (isozymes I and II), the relative rates were as follows: For isozyme I, taking the initial rate of reduction of the biliverdin-IXβ isomer as 100%, the relative rates of reduction of the -IXα, -IXγ and -IXδ isomers were 0, 109 and 133%, respectively. For isozyme II, the relative rates of reduction of the biliverdin-IXα, -IXγ and -IXδ isomers were 0, 129 and 157%, respectively.

The chemical synthesis of the four isomers of biliverdin, cleaved at the α, β, δ and γ positions using ascorbate -mediated coupled oxidation of pyridine-haem is not amenable to large scale production. The vinyl side chains of biliverdin are also quite unstable making these compounds difficult to work with. The early work by Colleran and O'Carra (1977) demonstrated that replacement of the vinyl side chains by ethyl side chains (defined as mesobiliverdins) had little effect on substrate affinity. A series of synthetic symmetrical mesobiliverdins with propionates at various positions along the tetrapyrrole backbone (kindly supplied by Professor David Lightner, University of Nevada) were used to assess further the substrate specificity of hBVR-A and hBVR-B. The structures of the verdin isomers are shown in Fig. 5.2 they have been assigned to three different groups according to their structures. Group I represents a series of biliverdins which have propionate side chains "moving" from a bridging position across the central methene bridge, as in biliverdin-IXα, to a "γ-configuration". Group II represents a series of biliverdins which are based on the mesobiliverdin-XIIIα structure but the propionate side chains have been modified. The Group III biliverdins are analogs of mesobiliverdin-XIIIα which have substitutions made at the C_{10} position, i.e. the position at which BVR-A reduces the biliverdin to produce bilirubin.

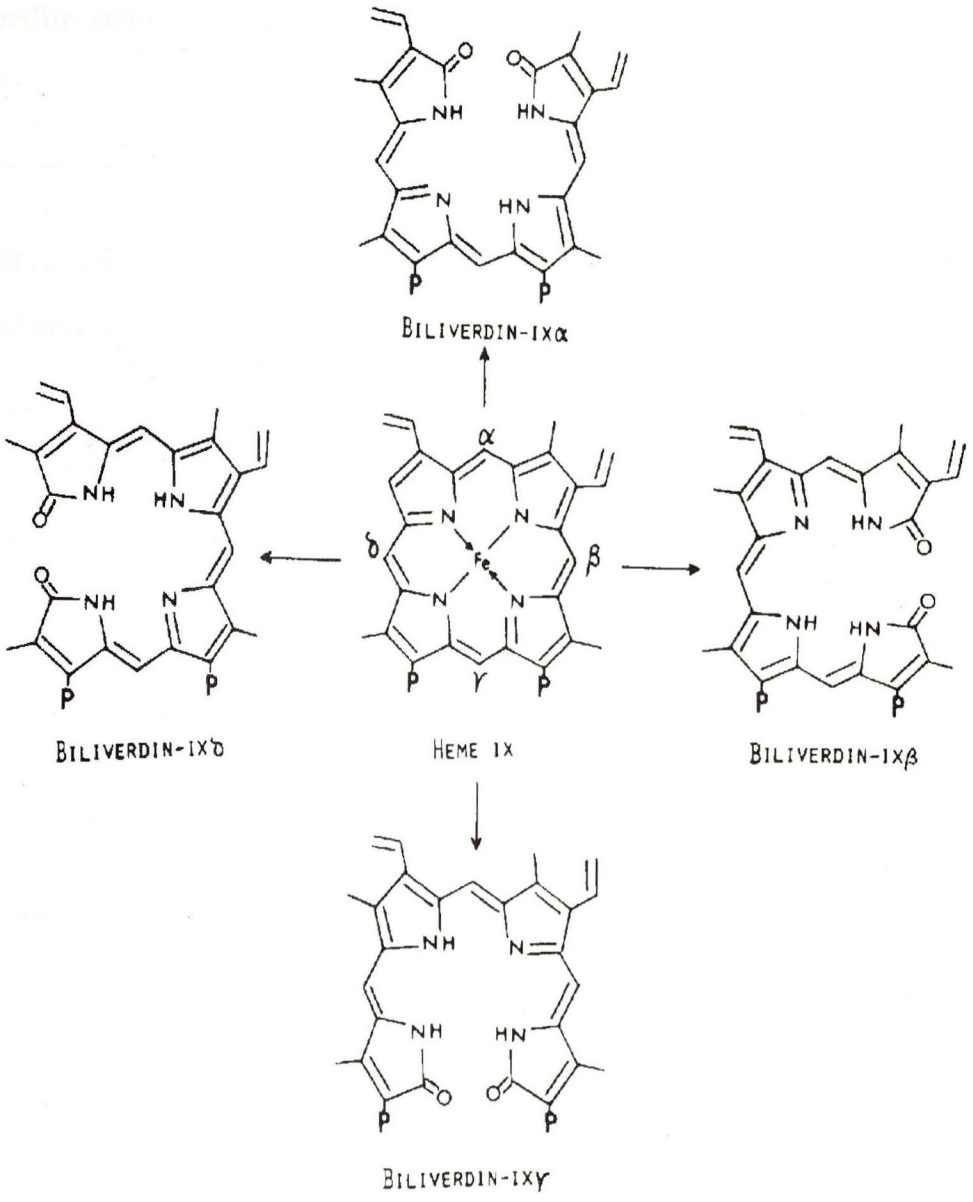

Figure 5.1. Biliverdin Isomers Resulting From Haem Cleavage.

Four possible isomers of biliverdin can result from the cleavage of haem because of the nonequivalence of the four methene bridge positions α, β, δ and γ (P = $-CH_2CH_2COOH$).

Table 5.1.

The relative initial rates of reduction of biliverdin-IX isomers by human biliverdin reductase isozymes (Yamaguchi *et al.*, 1994).

Biliverdin Reductase	biliverdin-IXα	biliverdin-IXβ	biliverdin-IXγ	biliverdin-IXδ
isozyme I *	0	100	109	133
isozyme II *	0	100	129	157
isozyme III **	100	0.3	0.3	0.6
isozyme IV **	100	0.4	0.3	0.6

* Taking the initial rate of reduction of the -IXβ isomers as 100%, the relative initial rates of reduction of the other isomers (-IXα, -IXγ and -IXδ) were calculated.

** Taking the initial rate of reduction of the -IXα isomers as 100%, the relative initial rates of reduction of the other isomers (-IXβ, -IXγ and -IXδ) were calculated.

(The relative rates are expressed as percentages)

GROUP I BILIVERDINS

1 Biliverdin-IXα

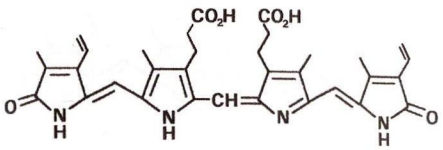

2 Mesobiliverdin-XIIIα

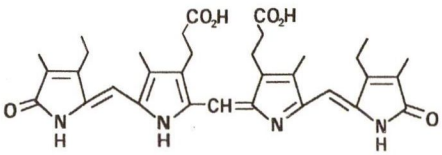

3 Mesobiliverdin-IVα

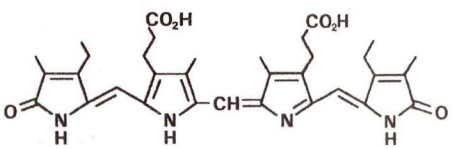

4 12-ethyl-Mesobiliverdin-XIIIα

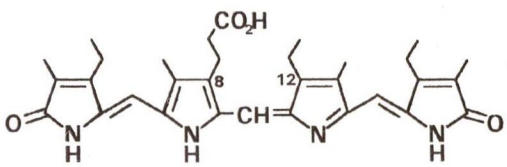

5 12-ethyl-13-methyl-
Mesobiliverdin-IVα

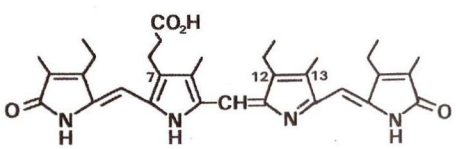

6 Mesobiliverdin-XIIIγ

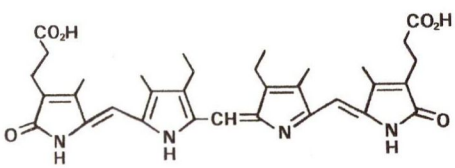

7 Mesobiliverdin-XIIγ

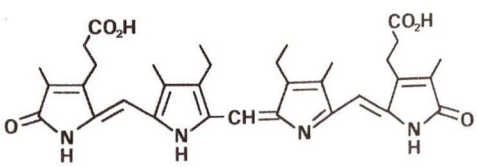

8 8,12-dimethyl-
Mesobiliverdin-XIIγ

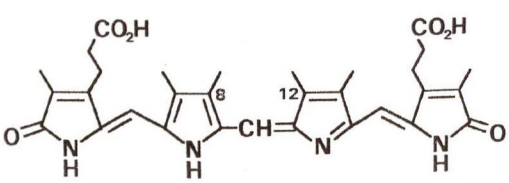

GROUP II BILIVERDINS

9 α,α,α',α'-tetramethyl-
Mesobiliverdin-XIIIα

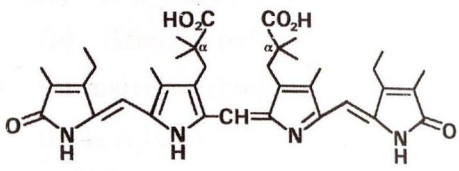

10 α,α'-dimethoxy-
Mesobiliverdin-XIIIα

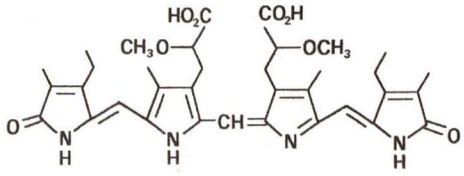

11 (n=3)-Mesobiliverdin-XIIIα

12 (n=5)-Mesobiliverdin-XIIIα

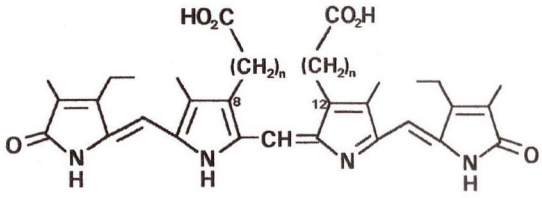

GROUP III BILIVERDINS

13-16 Basic structure: Mesobiliverdin-XIIIα

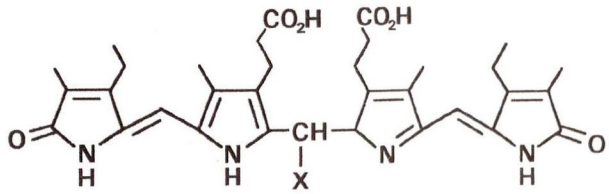

13: x=tertiary butyl

14: x=adamantyl

15: x=phenyl

16: x=methyl

Figure 5.2. Structures of Synthetic Biliverdin Isomers.

5.1. Preparation of Partially Pure Native Biliverdin-IXα Reductase and Biliverdin-IXβ Reductase.

In order to compare the activities of the native and recombinant enzymes, hBVR-A and hBVR-B were partially purified from human erythrocytes as described in Section 2.2.16 (a). Briefly, red blood cell lysate was applied to a DEAE-cellulose column. After extensive washing in 10 mM sodium phosphate, pH 7.2., the two activities were eluted using a 10 to 350 mM sodium phosphate gradient. The protein fractions were monitored at 280 nm and assayed for BVR-A activity using 5 μM biliverdin-IXα, 37 μM BSA and 705 μM NADH. The fractions were also assayed for flavin reductase activity using 25 μM NADPH and 150 μM FMN in 100 mM KH_2PO_4, pH 7.5. The elution profile is shown in Fig. 5.3(a) and reveals complete separation of the two activities. This was subsequently confirmed by immunoblotting [Fig. 5.3(b)].

5.2. Preliminary Plate Assays.

Given the colorimetric nature of the BVR assay, it was possible to carry out an initial analysis using a multi-well plate format. Figure 5.4 shows the result of an overnight incubation of all the verdin isomers with recombinant hBVR-A (row C) and hBVR-B (row E) and the native forms of human BVR-A (row B) and BVR-B (row D) isolated from red blood cells. The incubations were carried out in the presence of NADPH (50 μM), BSA (1 mg/ml) and 100 mM potassium phosphate buffer, pH 7.5. Rows A and F are control incubations containing no enzyme. It is clear that the recombinant enzymes exhibit identical behaviour to the native enzymes and that all of the Group I and Group II structures are substrates for BVR-A. In these two groups, those isomers that contained bridging propionates (**1**, **2**, **4**), modified bridging propionates (**9**, **10**) and extended bridging carboxylate side chains (butyrate, **11**; hexanoate, **12**) were not reduced by BVR-B (either native or recombinant). In this discussion, bridging propionates refers to propionate side chains at positions C_8 and C_{12}, effectively bridging the central methene bridge (C_{10}).

The verdins substituted at C_{10} (**13**, **14**, **15** & **16**) showed no change in the visible spectrum. Unfortunately, none of these compounds are particularly effective inhibitors of BVR-A or BVR-B (which might have been a starting point for anti-hyperbilirubinaemia therapy). The methyl derivative (**16**) was the most potent, exhibiting modest inhibition at 25 μM.

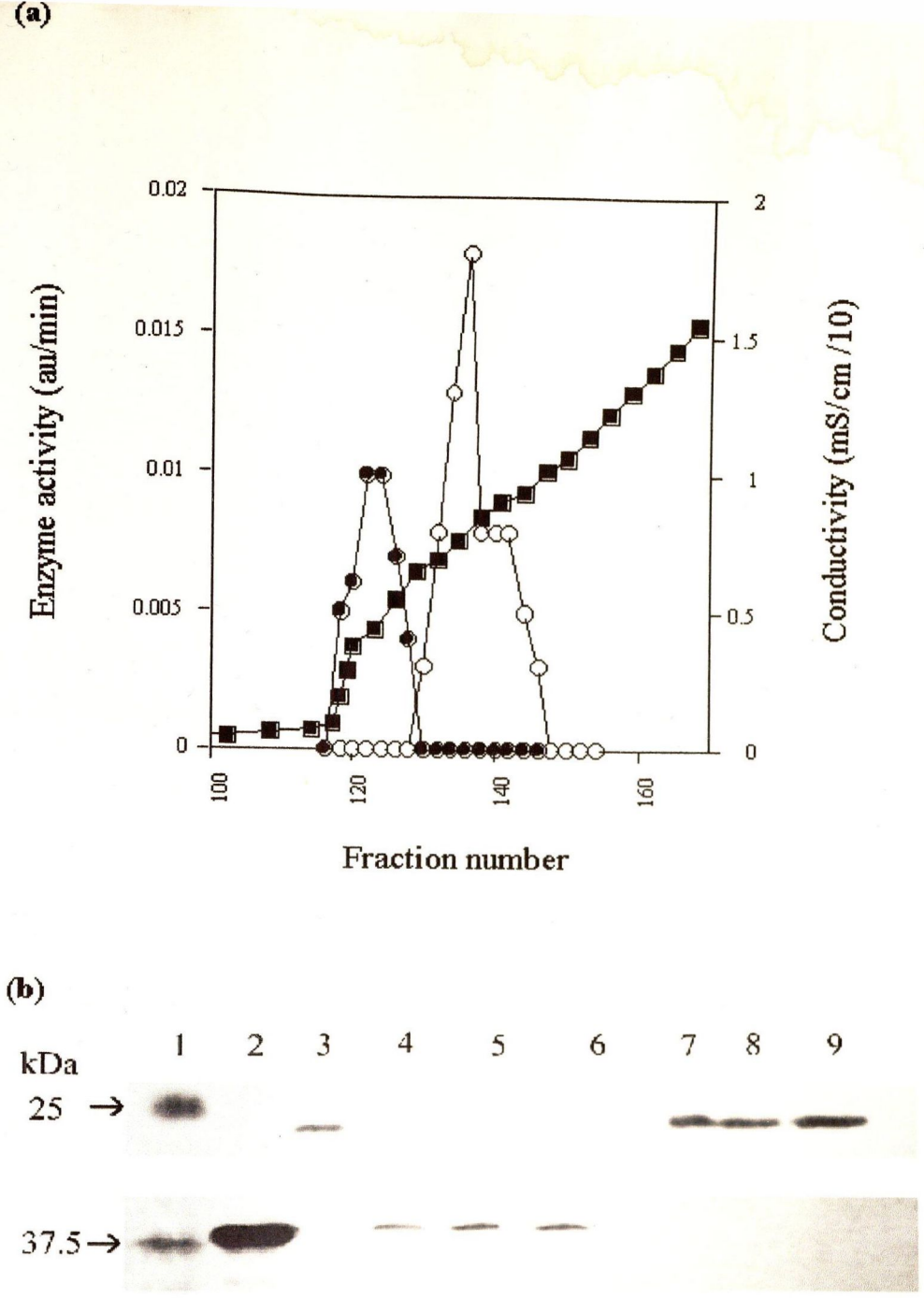

Figure 5.3. Separation of native human BVR-A and BVR-B on DEAE- cellulose.

(**a**) Human BVR-A and BVR-B isolated from erythroyctes were separated using ion-exchange chromatography. Fractions were assayed for flavin reductase activity (●), BVR-A activity (○) and conductivity (■). (**b**) Western-blot analysis was carried out on fractions over the peak of BVR-A activity (lanes 4, 5 and 6) and over the peak of flavin reductase activity (lanes 7, 8 and 9) using antisera raised against BVR-A and BVR-B, respectively. Lane 1, molecular mass markers; lane 2, BVR-A standard (5 μg); lane 3, BVR-B standard (5 μg).

Figure 5.4. A comparison of the substrate specificity of native and recombinant human BVR-A and human BVR-B.

Incubations were carried out in the presence of NADPH (50 μM), BSA (1 mg/ml) and 100 mM potassium phosphate, pH 7.5. Rows A and F do not contain enzyme. Rows B and C contain native and recombinant BVR-A, respectively. Rows D and E contain native and recombinant BVR-B, respectively. Numbers 1 to 16 represent the various verdin structures illustrated in Fig. 5.2.

(a) GROUP I BILIVERDINS

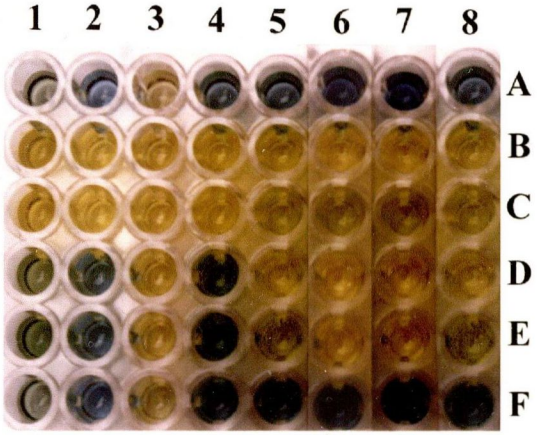

(b) GROUP II BILIVERDINS

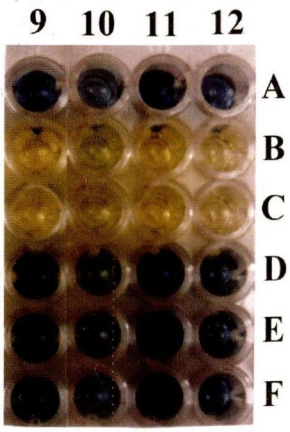

(c) GROUP III BILIVERDINS

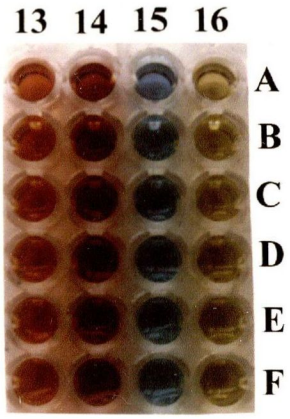

5.3. Initial Rate Studies on hBVR-A with Various Isomers of Biliverdin.

Although the overnight plate incubations allow a crude definition of whether or not the various compounds behave as substrates for the two enzyme forms, it yields little information about the relative rates of reaction. Initial rate measurements with biliverdin as the variable substrate were made by monitoring biliverdin consumption at 660 nm in the presence and absence of BSA (1 mg/ml) using the extinction coefficients given in Table 5.2. No co-solvents or detergents were added to the assay mixture (Beer Lambert's law was obeyed over the concentration range used). All assays were conducted in 100 mM potassium phosphate buffer, pH 7.5 and contained NADPH at a saturating concentration of 50 μM. The initial rate kinetics for compounds **1**, **2**, **3**, **4**, **5**, **6**, **8** and **9** with recombinant hBVR-A are shown in Fig. 5.5. It is clear that the addition of BSA has a pronounced effect on the activity with mesobiliverdin-IVα (**3**), however, for biliverdin-IXα (**1**) and 12-ethyl mesobiliverdin-XIIIα (**4**) the effect is mainly on sequestration of substrate.

The initial rate data were fitted to equations for simple hyperbolic kinetics and total and partial substrate inhibition as described in Section 4.1 (c). Most data sets showed potent substrate inhibition, where few data points were on the upward limb and fitting (to either total or partial substrate inhibition) produced negative coefficients or large errors. For this reason estimates of the kinetic parameters were obtained by manually generating saturation curves for total substrate inhibition (using, where possible, initial estimates from the curve fitting routines) and visually checking the theoretical line against the data set. For several of the substrates with BVR-B the substrate inhibition is so potent that the only kinetic parameter obtainable was the substrate inhibitory K_i value, obtained by plotting the reciprocal of the initial rate against the concentration of the tetrapyrrole. For those substrates exhibiting partial substrate inhibition only the linear part of the vo^{-1} versus [biliverdin] curve were used to obtain the substrate inhibitory K_i value.

As the kinetics of BVR-A involve pronounced substrate inhibition, since the effect of albumin on the initial rate is not clear and, as the present work shows, these effects vary depending on the substrates used, for the present discussion, good substrates are defined as those which, when assayed in the presence of BSA, exhibit an apparent K_m for biliverdin of less than 10 μM and which exhibit a maximal initial rate of greater than 5 μmol/min/mg. Poor substrates are defined as those which exhibit a an apparent K_m for biliverdin greater than 20 μM and which exhibit a maximal initial rate no greater than 1 μmol/min/mg. It is clear that the compounds with a bridging propionate are all good substrates (compounds **1**, **2** and **4**) with two propionates being preferred (i.e. biliverdin-

TABLE 5.2

Calculated extinction coefficients for synthetic biliverdin isomers at maximum absorbance.

Biliverdin Isomer	**Extinction Coefficient** ($l\ mol^{-1}\ cm^{-1}$)
Mesobiliverdin IXα	1.2×10^4
Mesobiliverdin-X111α	1×10^4
Mesobiliverdin- IVα	2.2×10^3
12-Ethyl Mesobiliverdin-XIIIα	9.9×10^3
12-Ethyl-13-Methyl Mesobiliverdin-IVα	1.4×10^4
Mesobiliverdin XIIIγ	1.54×10^4
Mesobiliverdin-XIIγ	1.16×10^4
8,12-Dimethyl Mesobiliverdin-XIIγ	1.31×10^4
α,α,α',α'-Tetramethyl-Mesobiliverdin-XIIIα	7.78×10^3
α,α' -Dimethoxy-Mesobiliverdin-XIIα	1.48×10^4
Mesobiliverdin-XIIIα -(n=3)	1.36×10^4
Mesobiliverdin-XIIIα -(n=4)	1.78×10^4

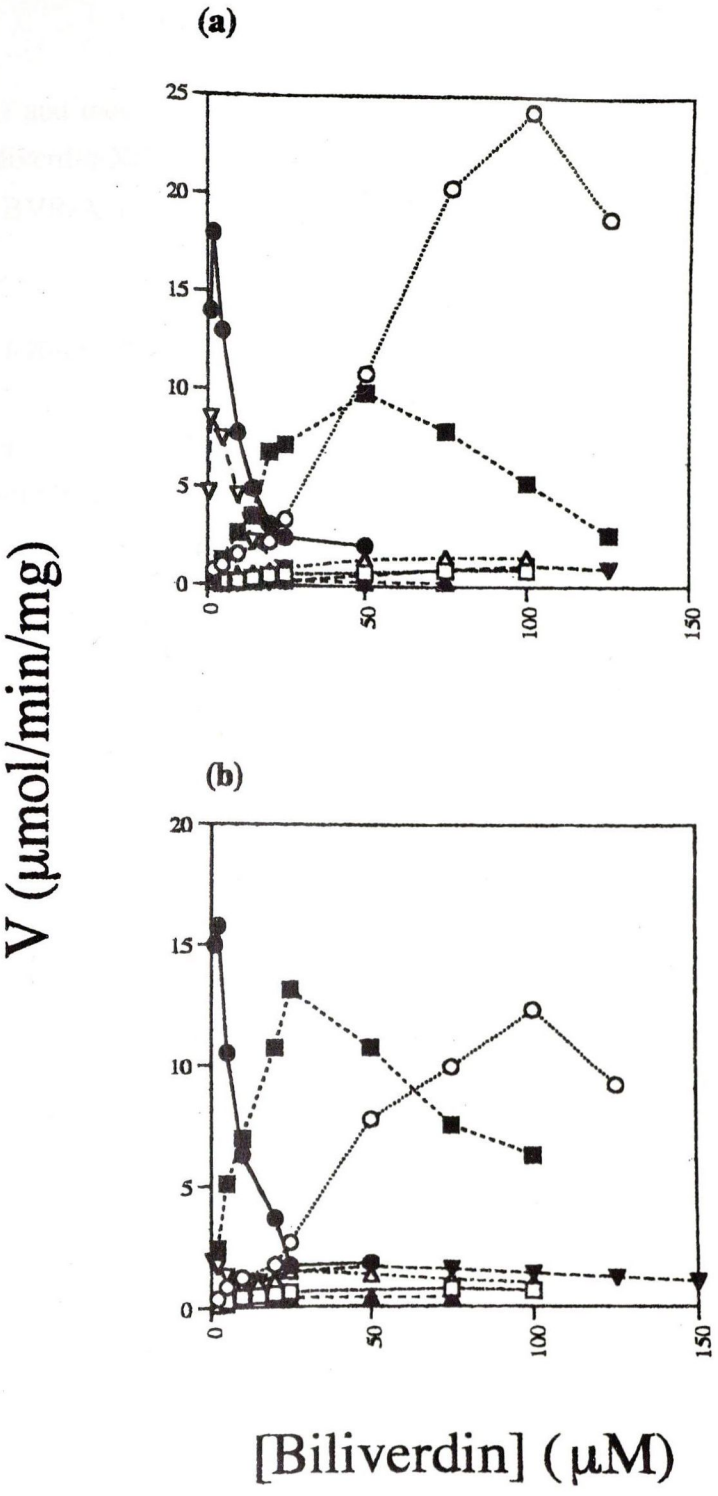

Figure 5.5. Initial rate studies on BVR-A with various isomers of biliverdin.

The substrate specificity of recombinant human BVR-A was examined in **(a)** the presence and **(b)** the absence of BSA. Consumption of verdins 2 (●), 3 (○), 4 (■), 5 (□), 8 (▲), 9 (Δ), 6 (▼), and 1 (∇) was monitored at 660 nm and initial rates were calculated using the extinction coefficients given in Table 5.2.

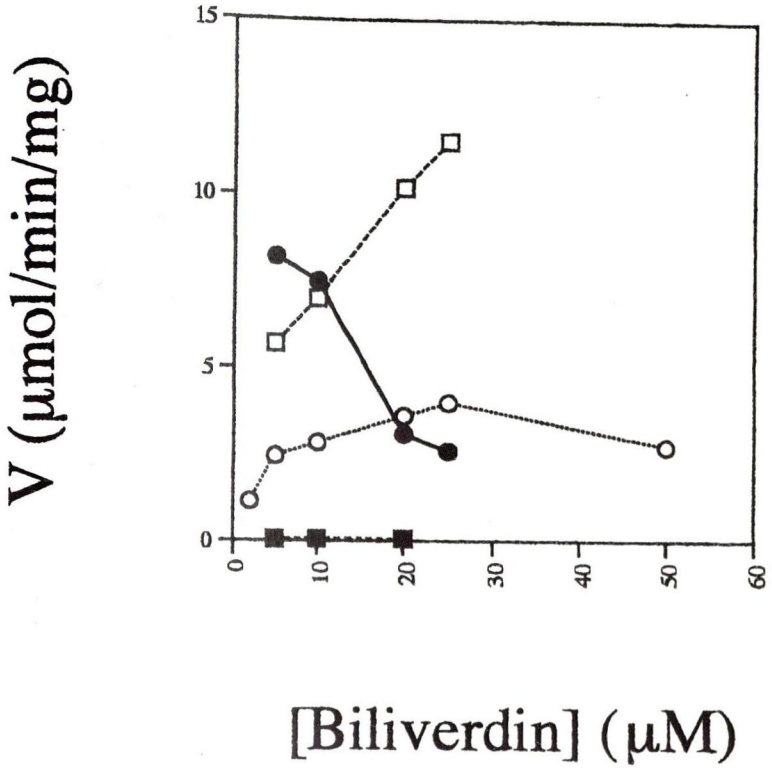

Figure 5.6. Effect of carboxylic acid chain length on human BVR-A activity.

BVR-A activity was measured using mesobiliverdin-XIIIα where the propionate side chains at positions 8 and 12 have been substituted to produce a dimethoxy (□),butyrate (○), and hexanoate (■) derivative (verdins 10, 11 and 12, respectively) as shown in Fig. 5.2. The reduction of biliverdin IXα is also included in this figure (●).

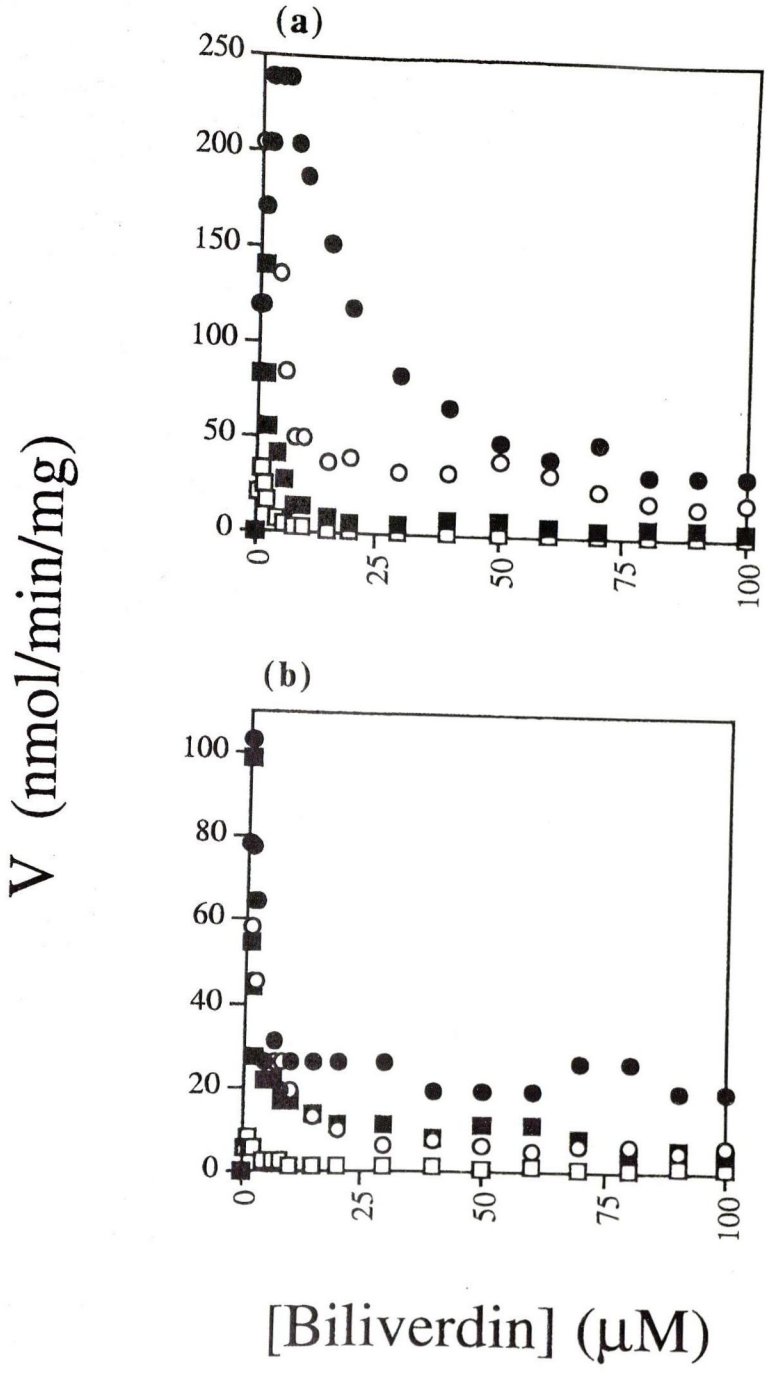

Figure 5.7. Initial rate studies on BVR-B with various isomers of biliverdin.

The substrate specificity of recombinant BVR-B was examined using **(a)** verdins 7 ((●) + BSA, (○) - BSA)) and 5 ((■) + BSA , (□) - BSA) and **(b)** verdins 8 ((●) + BSA, (○) - BSA) and 6 ((■) + BSA , (□) - BSA).

TABLE 5.3

Kinetic parameters for human BVR-A and human BVR-B.

Verdin Isomer	**BVR-A**			**BVR-B**
	K_m^{app} (μM)	k_{cat}^{app} (sec^{-1})	K_i^{app} (μM)	K_i^{app} (μM)
Biliverdin-IXα	7	44	0.7	
Mesobiliverdin-XIIIα	11	114	0.4	
Mesobiliverdin-IVα	76	34	169	
12-Ethyl Mesobiliverdin-XIIIα	200	45	10	
12-Ethyl-13-Methyl Mesobiliverdin-IVα	31	0.6		0.3
Mesobiliverdin-XIIIγ	79	0.9	213	0.5
8,12-Dimethyl Mesobiliverdin-XIIγ	26	0.5	30	0.8
α,α,α',α'-Tetramethyl Mesobiliverdin-XIIIα	37	1		
Mesobiliverdin-XIIγ				3

Discussion

Both hBVR-A and hBVR-B exhibit a fairly broad specificity in terms of the tetrapyrrole substrate, with human BVR-A able to reduce all of the structures tested. Early work on partially purified preparations of guinea pig BVR-A (that may have been contaminated with BVR-B) also suggested that although the IXα isomer was preferred, the β, γ, and δ- isomers were also substrates for the enzyme, which suggests that significant binding energy may be associated with an interaction between the carboxylate side chains and a residue(s) on the enzyme (presumably lysine or arginine). The observation that those compounds with two bridging propionates (**1** and **2**) have lower apparent $K_m^{biliverdin}$ values than the monopropionate verdin substrates (12-ethyl-mesobiliverdin-XIIIα ; **4**) is consistent with the hypothesis that BVR-A may utilise two basic residues to stabilise tetrapyrrole binding (Fig. 5.8). BVR-B is most distinct in that the bridging propionate rule for BVR-A is the antithesis in this case. The hypothesis that, in contrast to BVR-A, there may be a pair of negatively charged residues in BVR-B that do not permit the IXα isomer to bind productively (as shown in Fig. 5.9) has recently been shown to be incorrect (Pereira, personal communication). The crystal structure of BVR-B simply does not have space in the hydrophobic tetrapyrrole/flavin pocket to accommodate propionate side chains (see Fig. 5.10). In agreement with the competitive kinetics observed for mesobiliverdin-XIIIα against FMN, the IXα isomers can bind to BVR-B in a non-productive mode by rotating through 90°C as illustrated in Fig. 5.11.

The number of compounds known to interact with BVR-B/FR now includes a wide range of biliverdin isomers in addition to pyrroloquinoline quinone (Xu *et al.*, 1993), various haems, fatty acids and porphyrins (Xu *et al.*, 1992). As mentioned previously, crystals of hBVR-A have also been obtained and the two in conjunction should allow the accuracy of both models to be tested.

It is worth noting that rat liver BVR-A has also been reported to convert the phytochrome chromophore precursor, 3-E-phytochromobilin and the phycobiliprotein chromophore precursors, 3-E-phycocyanobilin and 3-E-phycoerythrobilin, to novel bilirubinoid products (Terry *et al*, 1993). As shown in Fig. 5.12, all three bilins have propionate side chains at the C_8 and C_{12} positions. In addition, the bilins each contain the reduced A-ring with an ethylidene substituent, a structural feature which appears to be required for proper assembly with their respective apoproteins (Li & Lagarias, 1992; cited in Terry *et al.*, 1993). Phytochromobilin and phycocyanobilin are particularly good substrates for BVR-A with K_m and V_{max} values similar to those of biliverdin-IXα indicating that the ethylidene moiety does not directly influence substrate binding to the enzyme. The ethylidene moiety is, however, required for the formation of the thioether linkage to

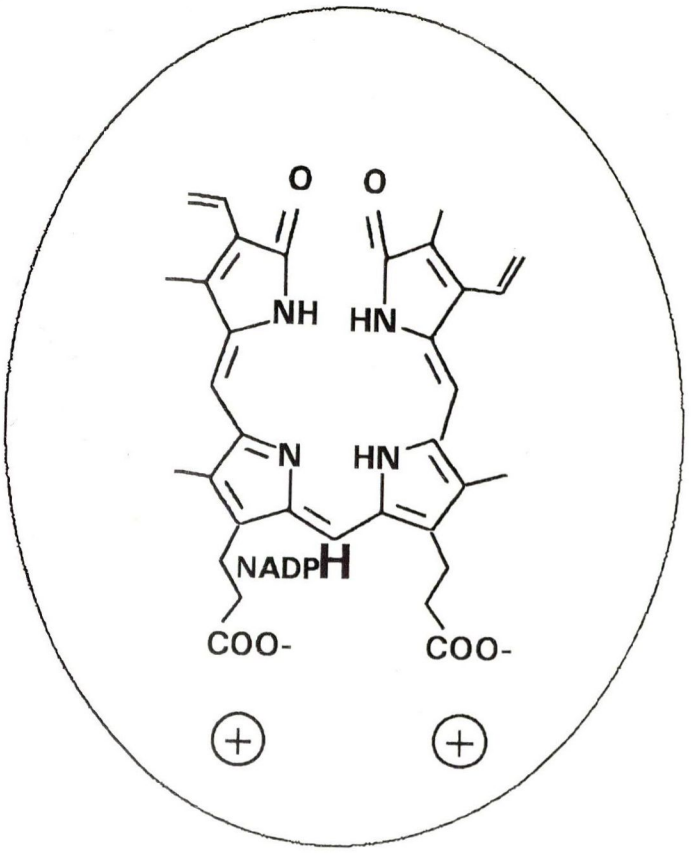

Figure 5.8. Proposed BVR-A Binding Site for Biliverdin-IXα.

It is proposed that the propionate side chains bridging the C_{10} position on the tetrapyrrole interact with the two positively charged residues on BVR-A to promote binding and subsequent catalysis. NADPH is included in the figure to indicate the methene bridge which is reduced by BVR-A.

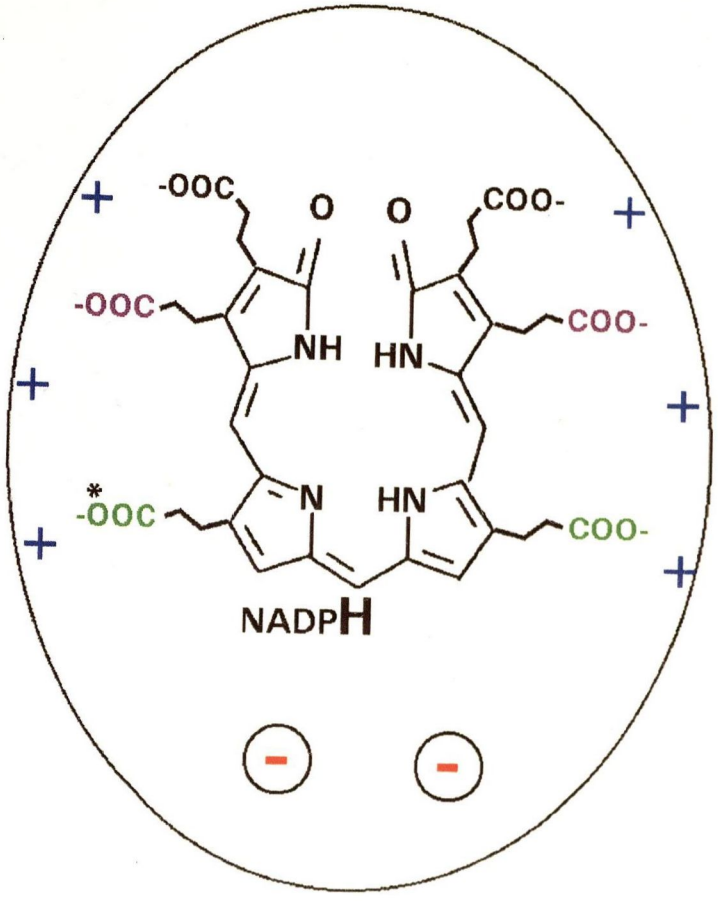

Figure 5.9. Early Model of the BVR-B Binding Site for Biliverdin (Cunnigham *et al*, 2000).

It was proposed that two negatively charged residues within the active site of the enzyme prevented the binding of biliverdin isomers with propionate side chains bridging the central methene bridge. Binding of the non-alpha isomers can be rationalised, if in addition to the two negatively charged residues, there were a series of positively charged residues around the tetrapyrrole binding site of the enzyme that interacted electrostatically with the propionate side chains of mesobiliverdin-IVα (*green*), 8,12-dimethyl-mesobiliverdin-XIIIγ and mesobiliverdin-XIIγ (*magenta*) and mesobiliverdin-XIIIγ (*black*). The *asterisk* indicates the position of a single carboxyl group in the 12-ethyl-13-methyl-mesobiliverdin-IVα.

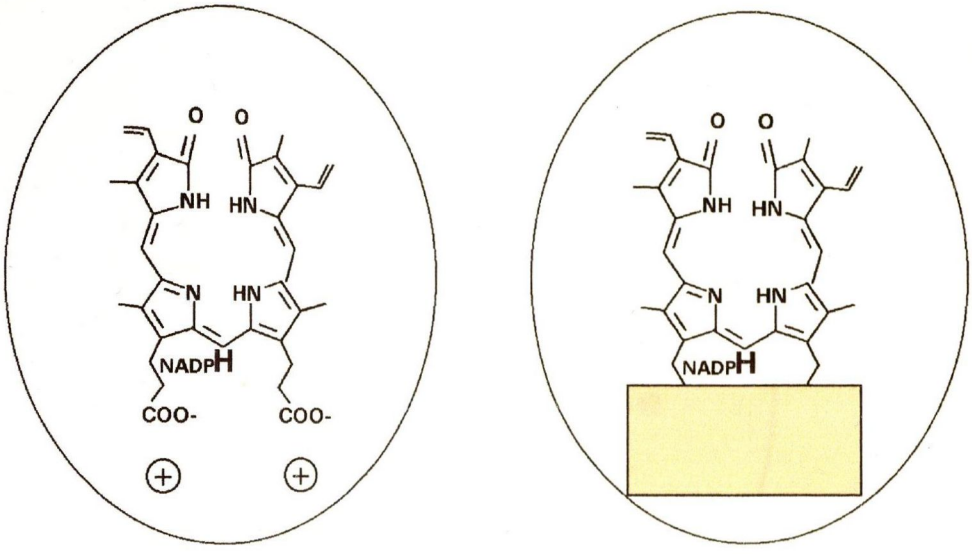

Figure 5.10. BVR-B cannot accommodate propionate side chains due to a hindrance (*orange*) domain within the enzyme active site.

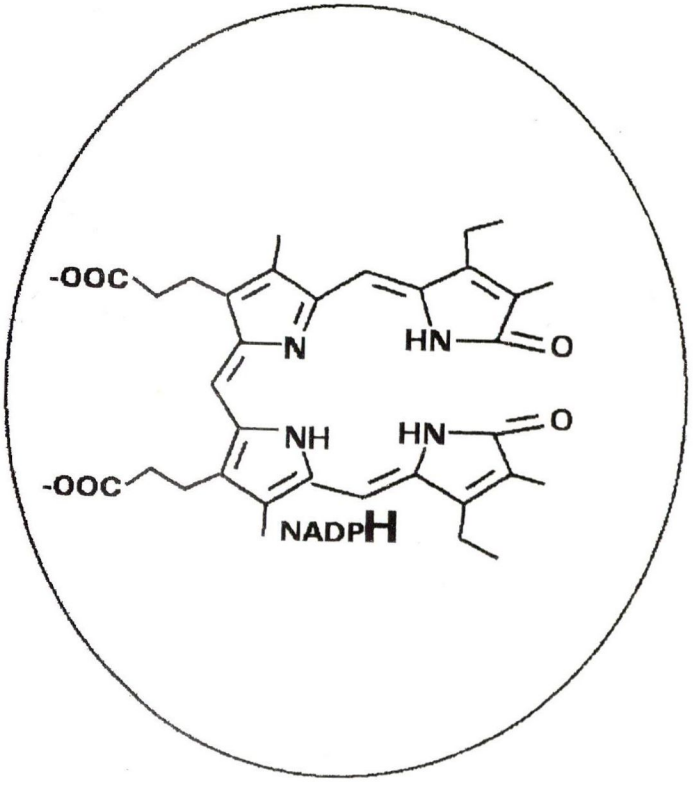

Figure 5.11. Mesobiliverdin-XIIIα Inhibition of BVR-B.

This figure illustrates how mesobiliverdin-XIIIα, with it's propionate side chains, orientates itself in the BVR-B tetrapyrrole binding site. It's C_{10} carbon is no longer orientated in the correct position for reduction, therefore, the isomer cannot act as a substrate for BVR-B.

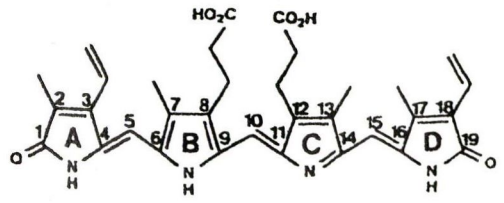

biliverdin (BV)

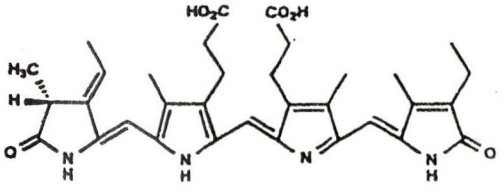

phycocyanobilin (PCB)

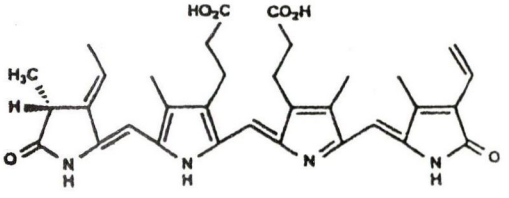

phytochromobilin (PΦB)

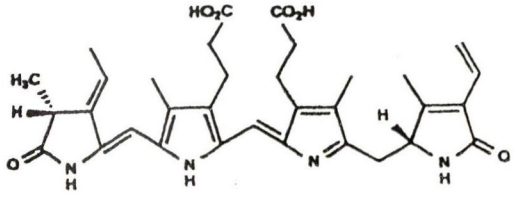

phycoerythrobilin (PEB)

Figure 5.12. Structures of biliverdin-IXα, phycocyanobilin, phytochromobilin and phycoerythrobilin.

apophytochrome. *In vitro* phytochrome assembly experiments demonstrated that the phytorubin products produced by BVR-A did not form photoactive adducts with recombinant apophytochrome. It has been proposed that the structural configurations of the phytorubins are poorly suited to the chromophore pocket of apophytochrome (possibly due to extensive H-bonding as in the case of bilirubin-IXα). Transgenic expression of BVR-A in *Arabadopsis thaliana* has since been shown to alter light mediated growth and development and offers great potential for the experimental manipulation of photomorphogenetic responses in plants.

Chapter 6

Studies on Linear Tetrapyrrole Signalling

Introduction.

The Aryl hydrocarbon receptor (AhR) is a ligand activated basic helix-loop-helix transcription factor which regulates many of the toxic and biological effects of a variety of polyhalogenated and polycyclic aromatic hydrocarbons such as 2,3,7,8-tetrachlorodibenzo-*p*-dioxin (TCDD) and related compounds. Unliganded AhR is localised in the cytoplasm of cells in an inactive multiprotein complex that contains hsp90 (a heat shock protein of 90 kDa). Upon ligand binding, the AhR complex dissociates from hsp90 and translocates to the nucleus where it subsequently dimerizes with the AhR nuclear transporter (ARNT) to mediate gene regulation through direct binding to xenobiotic response element (XRE) enhancer sequences. XREs with the core sequence "GCGTG" (Denison *et al.*, 1988) are found in the promoter regions of several genes involved in xenobiotic metabolism, including members of the cytochrome P450 family (Cyp1a1, Cyp1a2 and Cyp1b1), UDP-glucuronyl transferase and NADPH quinone reductase. Binding to these enhancer sequence causes a change in chromatin structure that facilitates the binding of the basal transcription machinery. TCDD toxicity observed in animal models includes tumor promotion, immune suppression, embryotoxicity, epithelial hyperplasia and a severe wasting syndrome resulting ultimately in death (Schmidt & Bradfield, 1996).

For years many researchers entertained the hypothesis that an endogenous ligand for the AhR existed. The constitutively elevated expression of Cyp1a1/2 in congenitally jaundiced Gunn rats (the animal model for human Crigler-Najjar syndrome type-1) led workers to investigate if the haem degradation product, bilirubin, could act as an endogenous activator of Cyp1a1/2 expression. Sinal and Bend (1997) later reported that in mouse hepatoma cells, bilirubin induces Cyp1a1 gene expression through a direct activation of the AhR, while its metabolic precursors biliverdin and hemin appeared to induce Cyp1a1 indirectly by serving as precursors for enzymatic formation of bilirubin. The ability of bilirubin to directly bind to the AhR and induce gene expression was subsequently demonstrated in a variety of other species (Phelan *et al.*, 1998).

The transcription of Cyp1a1/2 is also regulated by cytokines. TNF-α and IL-1β have been shown to suppress TCDD-mediated induction of Cyp1a1/2 in hepatocytes (Barker *et al.*, 1992). Both cytokines are strong inducers of the pleiotropic transcription factor NF-κB which participates in many of the physiological responses adversely affected by xenobiotics. Tian *et al.* (1999) later reported that AhR and NF-κB signalling pathways interact and that this interaction is associated with mutual functional modulation of gene expression controlled by both transcription factors. More specifically, the p65 (RelA) subunit of the classic NF-κB p65/p50 heterodimer was shown to physically interact with

the AhR but not ARNT. One possibility is that the AhR and RelA form an inactive complex, thereby preventing each other from binding to their respective enhancer sequences. It has also been postulated that the AhR and NF-κB compete for the transcriptional coactivator p300/CBP which serves as an integrator for many signalling pathways. The glucocorticoid receptor has also been shown to repress NF-κB activity (Caldenhoven *et al.*, 1995). Inhibition in this case was found to be mediated in part through induction of IκBα, however, there is no evidence to support an analogous mechanism in the case of the AhR. The negative cross-talk between the AhR and NF-κB may underlie important aspects of the pathophysiological responses to xenobiotics, for example, TCDD-induced immune suppression could be a result of AhR-induced suppression of NF-κB. Conversely, transrepression of AhR activity by NF-κB may be the underlying mechanism responsible for the suppression of Cyp1a1/2 gene expression by cytokines and other agents capable of inducing NF-κB.

Haem oxygenase-1 (HO-1), the rate limiting enzyme in haem catabolism, is upregulated several fold in response to a variety of stimuli including pro-inflammatory cytokines and reactive oxygen species. In a carageenin induced model of inflammation elevation of HO-1 resulted in a striking suppression of the inflammatory response, whereas, inhibition of this enzyme led to potentiation of the inflammatory response (Willis *et al.*, 1996). Carageenin was injected into the pleural cavity of rats resulting in the development of an acute complement-dependent inflammatory response which was maximal after 24 hours (as characterised by inflammatory cell number and exudate volume). HO-1 activity increased as inflammation proceeded and was found to be maximal as the inflammation was resolving. Administration of the HO inhibitor, tin protoporphyrin (SnPP) led to a potentiation of the response whereas administration of ferriprotoporphyrin IX chloride (FePP), a potent inducer of HO-1, resulted in a dose-dependent suppression of inflammatory cell number and exudate volume. The factor responsible for mediating this effect had not been identified. NF-κB plays a crucial role in the regulation of gene expression in response to injury and inflammatory stimuli, therefore, a series of experiments were carried out in order to test the hypothesis that the haem catabolite, bilirubin, may be responsible for down regulating the immune response through activation of the AhR with subsequent suppression of NF-κB activity. The proposed model is illustrated in Fig. 6.1.

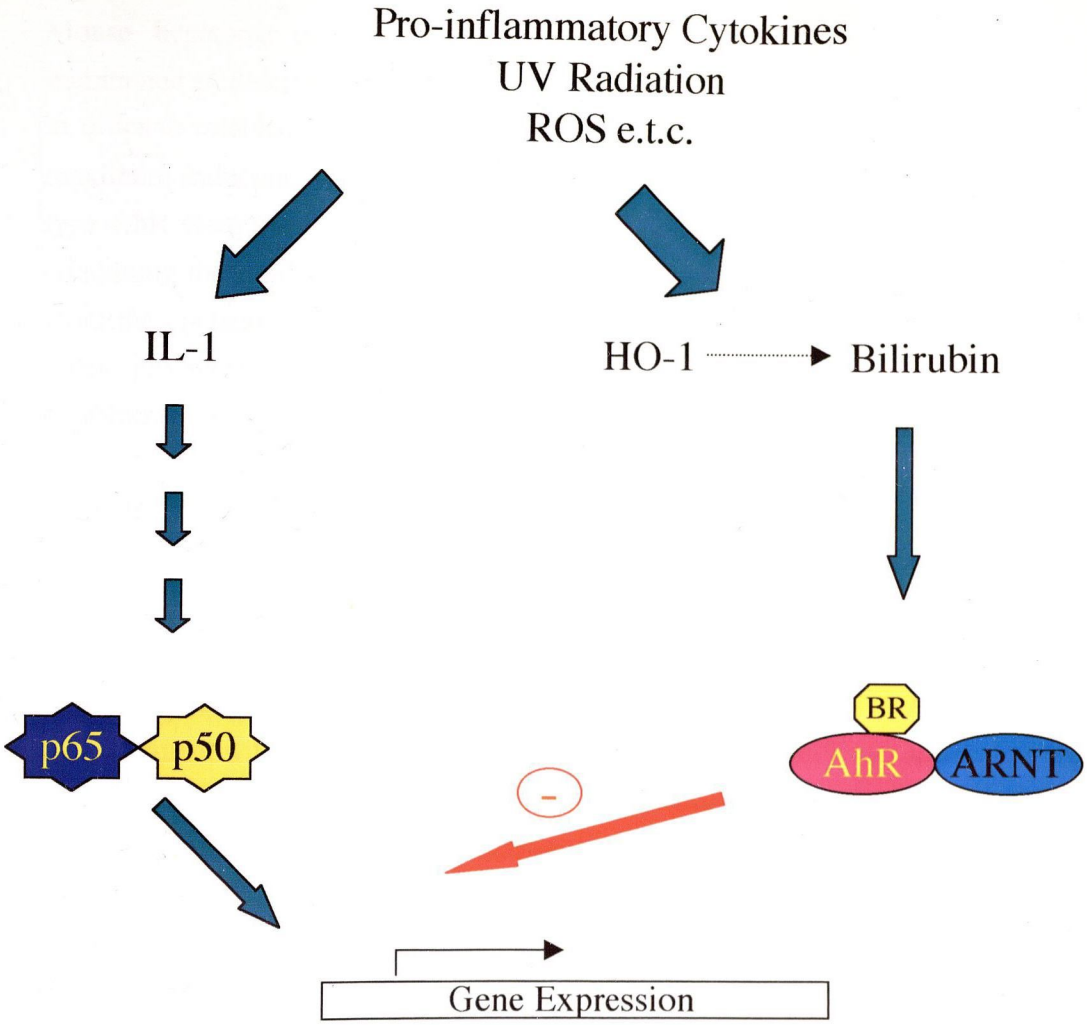

Figure 6.1. Proposed model for the regulation of NF-κB-mediated transriptional activation by the Aryl Hydrocarbon Receptor as a consequence of HO-1 upregulation.

6.1 Induction of XRE-luciferase Activity in Hepa1c1c7 Cells.

Mouse hepatoma cells (Hepa1c1c7) expressing wild type AhR were grown and maintained as described in Section 2.2.20 (a). Preliminary experiments were carried out in order to establish the concentration of biliverdin-IXα and bilirubin-IXα required for maximum induction of the luciferase reporter gene. The cells, which express the wild-type AhR were transiently transfected with a XRE-driven reporter gene (pGud-Luc6.1) containing the firefly luciferase gene under the control of four XRE segments derived from the upstream region of the murine CYP1A1 gene and the mouse mammary tumor virus promoter. The cells were then treated with the AhR ligands at various concentrations or Me_2SO (solvent control) for 18 hours before harvest for determination of luciferase activity. A pEF-LacZ β-galactosidase control vector was included for normalisation of transfection efficiency and β-napthoflavone (BNF) which is a strong inducer of AhR-dependent transcriptional activation was used at a concentration of 200 nM as a positive control for luciferase induction.

The results of these experiments are shown in Fig. 6.2. Previous studies have reported that treatment with 100 μM biliverdin and bilirubin induces luciferase activity 12 and 16-fold, respectively, over untreated cells. In this experiment, treatment with biliverdin-IXα induced luciferase expression in a dose-dependent manner, however, the concentrations required for significant stimulation exceeded those used by previous workers. As shown in Fig. 6.2 (a), luciferase activity is induced only 5-fold over control cells at a concentration of 400 μM. Treatment of the cells with 100 μM bilirubin resulted in a 2-fold activation of the XRE-driven luciferase reporter gene [Fig. 6.2 (b)]. The reason for this discrepancy is unclear at present. At higher concentrations, bilirubin comes out of solution and exerts toxic effects on the cells, therefore, biliverdin was used as a ligand for the AhR in subsequent experiments. Hepa1c1c7 cells constitutively express biliverdin-IXα reductase activity (Sinal & Bend, 1997), therefore, it seems likely that following uptake biliverdin is converted to bilirubin and that activation of the AhR is actually mediated by the latter.

6.2 Induction of κB-luciferase Activity in Hepa1c1c7 Cells.

Hepa1c1c7 cells were transiently transfected with an NF-κB-luciferase reporter plasmid (pNF-κB-Luc) (100 ng) before being treated with TNF-α and PMA at a series of concentrations as described in the text. As shown in Fig. 6.3, treatment with TNF-α, which is a strong inducer of NF-κB, failed to drive the κB-dependent promoter to a great extent. Similar results were obtained on treatment with PMA (see Fig. 6.4), p65 and IL-

(a)

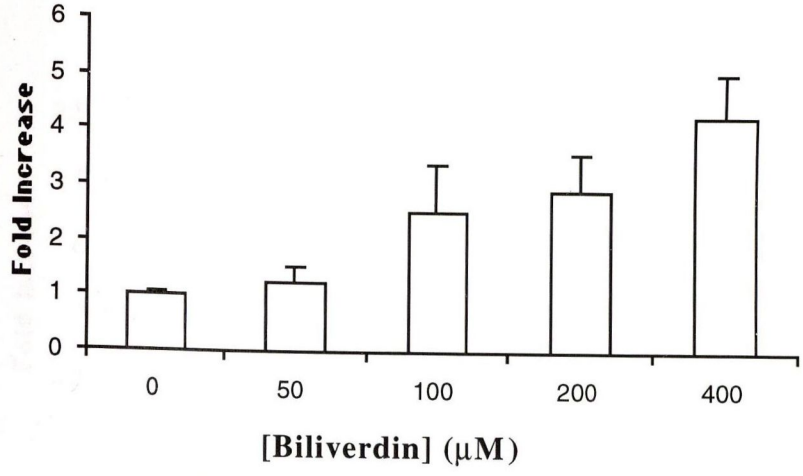

(b)

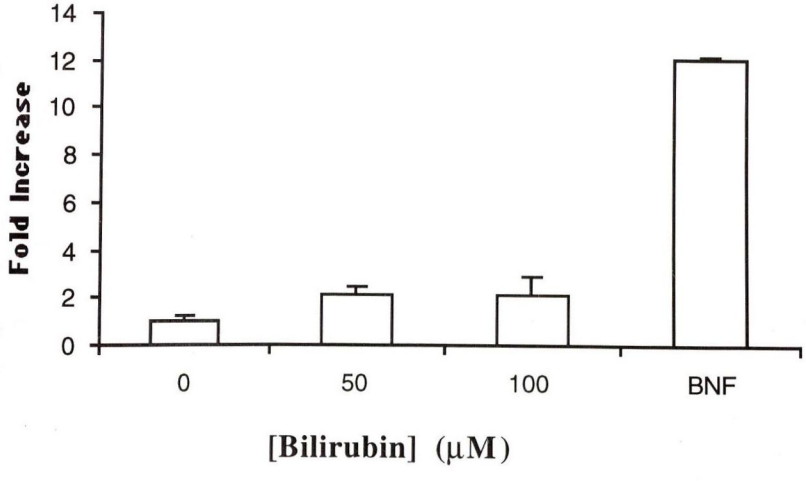

Figure 6.2. Dose dependent Increase in XRE-luciferase Reporter Construct Activity.

Hepa1c1c7 cells were transiently transfected with 100 ng pGudLuc1.1 as described in Section 2.2.20 before being treated with biliverdin (**a**) and bilirubin (**b**) for 16 hours. BNF (0.2 mM) was used as a positive control for luciferase induction. Fold increase represents luciferase activity, corrected for transfection efficiency, relative to vehicle treated cells.

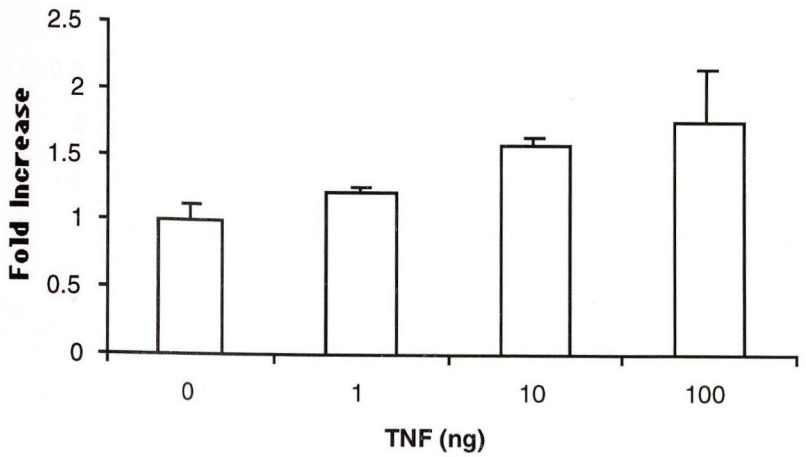

Figure 6.3. Dose-dependent Increase in κB-luciferase Reporter Construct Activity.

Hepa1c1c7 cells were transiently transfected with pκB-Luc as described in Section 2.2.20. After 12 hours the cells were treated with TNF-α for 5 hours, and the activity of the reporter gene was determined. Fold increase represents luciferase activity, corrected for transfection efficiency, relative to vehicle treated cells.

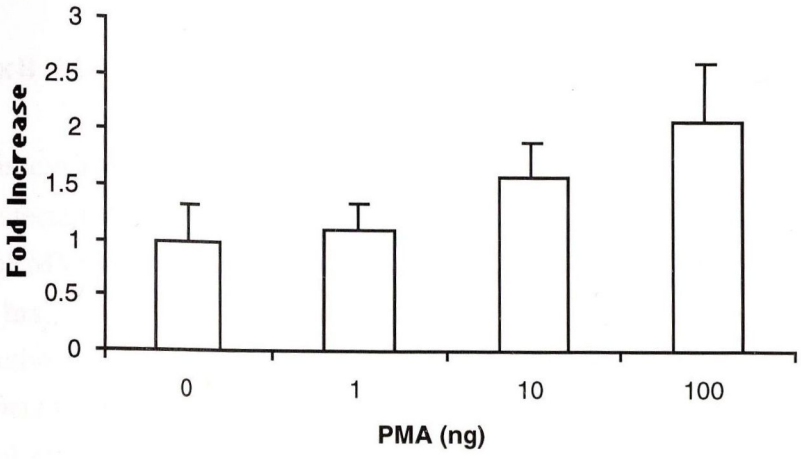

Figure 6.4. Dose-dependent Increase in κB-luciferase Reporter Construct Activity.

Hepa1c1c7 cells were transiently transfected with pκB-Luc as described in Section 2.2.20. After 12 hours the cells were treated with PMA for 5 hours, and the activity of the reporter gene was determined. Fold increase represents luciferase activity, corrected for transfection efficiency, relative to vehicle treated cells.

1β. Basal NF-κB levels were found to be high in untreated cells indicating that Hepa1c17 cells express high background levels of NF-κB activity. Reduction in the concentration of reporter plasmid used for transfection experiments failed to reduce this basal activity. Reduction of the concentration of FCS in the culture medium also failed to reduce background reporter construct expression levels.

6.3 NF-κB Mediated Suppression of AhR Transcriptional activation.

In order to assess the effect of NF-κB on AhR mediated transcription, Hepa1c1c7 cells were co-transfected with the pGud-Luc6.1 reporter gene and increasing amounts (50 ng - 200 ng) of pCMV65 (which expresses the p65/RelA) before being treated with 200 nM BNF for 16 hrs. As expected, transfection of increasing amounts of the p65 expression plasmid effectively suppressed BNF-induced XRE-dependent promoter activity (see Fig. 6.5). Treatment with TNF-α has also been reported to suppress NF-κB mediated transcriptional activation (Tian *et al*, 1999), however, cytokine treatment was found to have no effect in this case as shown in Fig. 6.6.

In an analogous experiment, Hepa1c1c7 cells were co-transfected with both plasmids before being treated with 400 μM biliveridn-IXα. As shown in Fig. 6.7, co-transfection of pCMV65 also represses biliverdin-induced AhR transcriptional activation.

6.4 AhR-Mediated Suppression of NF-κB Transcriptional activation.

As mentioned above, Hepa1c1c7 cells express high background levels of NF-κB activity, therefore it was not possible to carry out induction experiments using this cell line. An experiment was carried out in order to assess whether activation of the AhR could suppress the basal activation of NF-κB. Cells were transfected with pNF-κB-Luc before being treatment with 1 μM and 10 μM BNF for 16-18 hrs. As shown in Fig. 6.8, treatment of the cells with 10 μM BNF resulted in a 5-fold decrease in the basal activation of the κB-reporter plasmid.

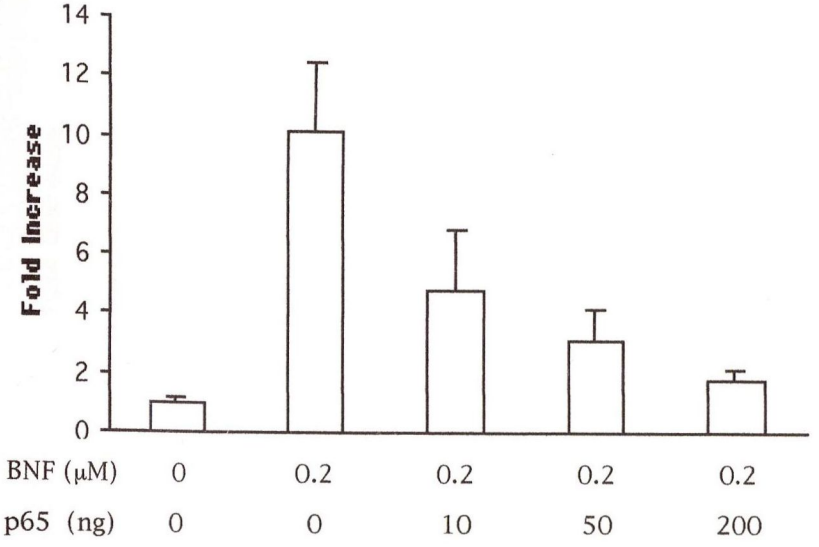

Figure 6.5. p65 Suppression of AhR-Mediated Transcriptional Activation.

Hepa1c1c7 cells were co-transfected with pGud.Luc1.1 (100 ng), increasing amounts of pCMV65 (10 - 200 ng) and the appropriate amount of empty vector (pCMV). After 12 hours the cells were treated with BNF (0.2 μM) for 16 hours before being processed for determination of luciferase activity.

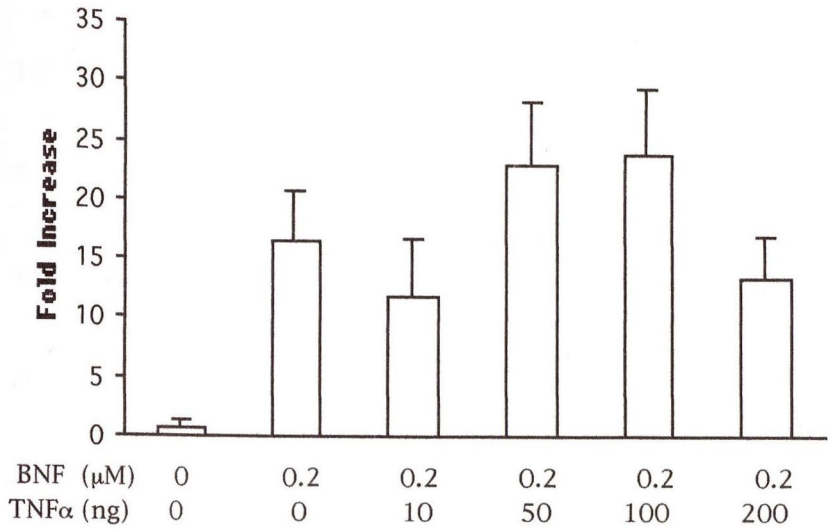

Figure 6.6. TNFα does not Inhibit AhR-mediated Transcriptional Activation.

Hepa1c1c7 cells were transiently transfected with pGud.Luc1.1 (100 ng) as described in the text. After 12 hours the cells were treated with BNF (0.2 μM) and TNFα at the concentrations indicated for 16 hours before being processed for determination of luciferase activity.

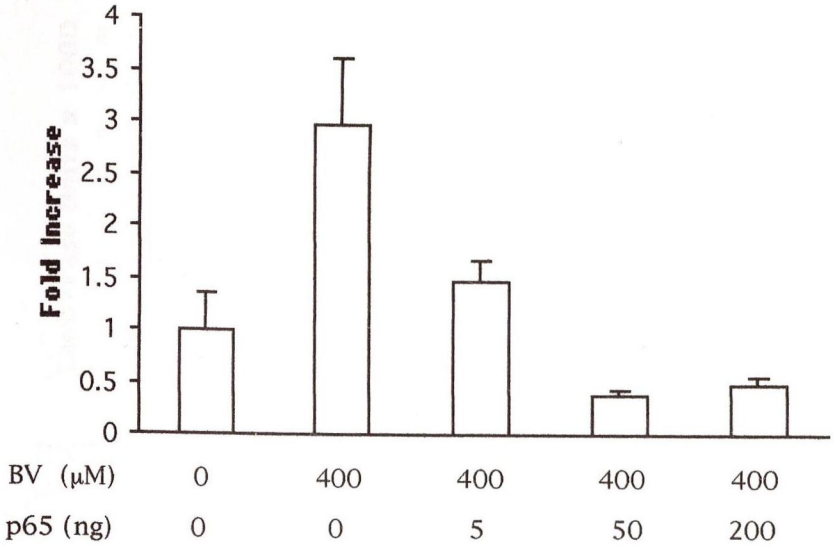

Figure 6.7. p65-mediated Suppression of AhR Transcriptional Activation.

Hepa1c1c7 cells were co-transfected with pGud.Luc1.1 (100 ng) and increasing amounts of pCMV65 (5 - 200 ng) and the appropriate amount of empty vector (pCMV). After 12 hours the cells were treated with biliverdin (400 μM) for 16 hours before being processed for determination of luciferase activity.

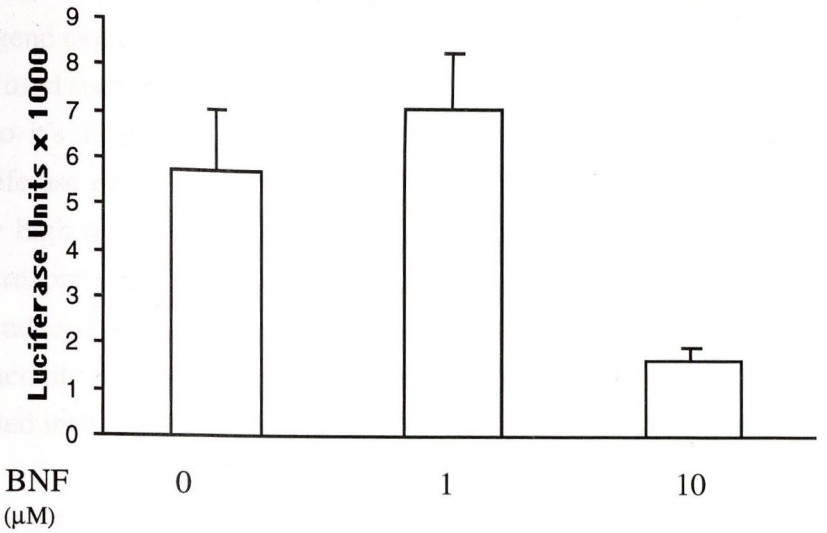

Figure 6.8. AhR-mediated Suppression of Basal NF-κB Activation.

Hepa1c1c7 cells were transfected with pGud.Luc1.1 (100 ng) as described in the text. After 12 hours the cells were treated with 1 μM and 10 μM BNF for 16 hours before being processed for determination of luciferase activity.

Discussion.

Activation of the AhR signalling pathway by physiological concentrations of endogenous haem metabolites has been demonstrated by two independent groups. In this study, the concentrations of biliverdin and bilirubin required for the induction of XRE-driven luciferase gene expression in transiently transfected Hepa1c17 cells exceeded the doses previously used such that bilirubin could not be used as a ligand for the activation of the AhR due to it's limited solubility. While the concentrations of biliverdin used did not induce luciferase expression to the levels previously reported, the fold increase was sufficiently high to permit inhibition studies to be carried out. In a transient transfection assay, overexpression of increasing amounts of p65 effectively suppressed BNF and biliverdin-induced XRE-dependent promoter activity. Inhibition of BNF-induced XRE luciferase activity has been demonstrated previously, however this is the first report of a p65-mediated inhibition of biliverdin-induced AhR transcriptional activation.

The ultimate aim of this study was to deduce if high levels of bilirubin/biliverdin could inhibit NF-κB activity. It was envisaged that the cytokine induced activation of NF-κB could be inhibited by treatment with the tetrapyrroles in a manner analogous to the suppression of NF-κB by treatment with TCDD. Unfortunately, the basal NF-κB activity was particularly high in the cell line used in this study, therefore, treatment with TNF-α, PMA or IL1-β did not drive the κB-dependent promoter sufficiently over control vehicle treated cells. However, it was possible to inhibit the basal NF-κB activity in a dose-dependent manner using BNF at concentrations of 1 and 10 μM. In order to assess the effect of AhR ligands on cytokine-induce κB activity, future studies will employ an AhR expression plasmid that will be transfected into cell lines routinely used to monitor NF-κB activity such as Hela or Cos-7 cells. In addition, the underlying mechanism for the transrepression between the AhR and NF-κB will be further investigated. As mentioned previously, earlier studies have revealed that AhR and p65 are physically capable of associating with each other in total cell lysates. It has been proposed that this association results in the formation of an inactive complex. A similar mechanism has been proposed to explain the mutual repression of the hormone-activated progesterone receptor and the p65 subunit of NF-κB (Kalkhoven *et al.*, 1996).

The possibility that ligand-activated AhR and p65 are competing for a common transcriptional coactivator cannot be ruled out. Several such transcriptional cofactors have been identified, examples include CBP (Chivia *et al.*, 1993), and p300 (Echner*et al.*, 1994). These cofactors can act as coactivators or corepressors depending on their transcriptional properties. CBP was originally identified as a coactivator for CREB (cAMP-responsive element-binding protein) however, it is now known to be a common

activator for numerous DNA-binding transcription factors including AP1 and steroid hormone receptors (Kamei *et al.*, 1996). CBP does not directly bind to DNA, rather it mediates transcriptional effects from the sequence-specific transcription factors to the general transcription machinery. Kobayashi *et al.* (1997) reported that ARNT interacts with CBP via it's C-terminal activation domain and that overexpression of adenovirus E1A, which complexes with CBP, repressed the inducible expression of Cyp1a1. Similarly, the N- and C-terminal domains of CBP interact with the transactivation domain of p65 as demonstrated by mammalian two-hybrid systems (Gerritsen *et al.*, 1997). When E-selectin and VCAM-1 reporter constructs were cotransfected with both the CBP and p65 expression plasmids, the activities of the reporter constructs were raised 3- to 5-fold above those seen with p65 expression plasmid alone. It should be possible to test whether the AhR and p65 are competing for CBP by co-transfecting Hepa1c1c7 cells with p65, the XRE-reporter construct and increasing concentrations of CBP. If the two transcription factors are competing for CBP, overexpression of the latter should rescue the inhibition of XRE-driven reporter activity by p65. Conversely, inhibition of κB-dependent reporter activity by BNF will be rescued by cotransfection of CBP if this hypothesis is correct.

As mentioned in Chapter 5, a series of synthetic biliverdin isomers have been produced with propionates at various sites along the pigment backbone. The ability of these analogs and indeed the respective bilirubin isomers to activate the AhR will be examined. It will be of particular interest to assess the effect of bilirubin-IXβ, which appears to be a uniquely foetal metabolite, on AhR function. It is conceivable that a function for the IXβ isomer may be related to foetal suppression of the maternal immune system. One important function of progesterone during pregnancy is to prevent activation of an immune response directed against the embryo. It has been proposed that the immunosuppressive action of this hormone during pregnancy is partly due to the inhibition of the transcriptional activity of NF-κB by the progesterone receptor (Kalkhoven *et al.*, 1996). Intriguingly, the recent suggestion that indoleamine dioxygenase may be involved in foetal suppression of the maternal immune response (Munn *et al.*, 1998) could also support Ah receptor involvement as tryptophan metabolites are also known to bind to and activate this transcription factor (Health-Paglinso *et al.*, 1998).

It will also be of interest to assess the effect of AhR ligands on HO-1 gene expression. The 5' untranslated region of this gene contains binding sites for both NF-κB and AP1 transcription factors. Several members of the nuclear hormone receptor family have been reported to inhibit AP-1 activity and inhibition is the apparent result of competition for limiting amounts of CBP/p300 (Kamei *et al.*, 1996). HO-1 is the rate limiting enzyme in

haem catabolism and can be upregulated as much as 200-fold in response to pro-inflammatory stimuli. It is possible that activation of the AhR by haem catabolites will act as a negative feedback loop to down regulate HO-1 expression as the inflammatory response is resolving. The cDNA encoding the enzyme has been cloned into the pGEX-KG expression vector and antibodies to the enzyme are currently being prepared (Dunne & Mantle, unpublished work) in order to test this hypothesis. The proposed model is illustrated in Fig. 6.9.

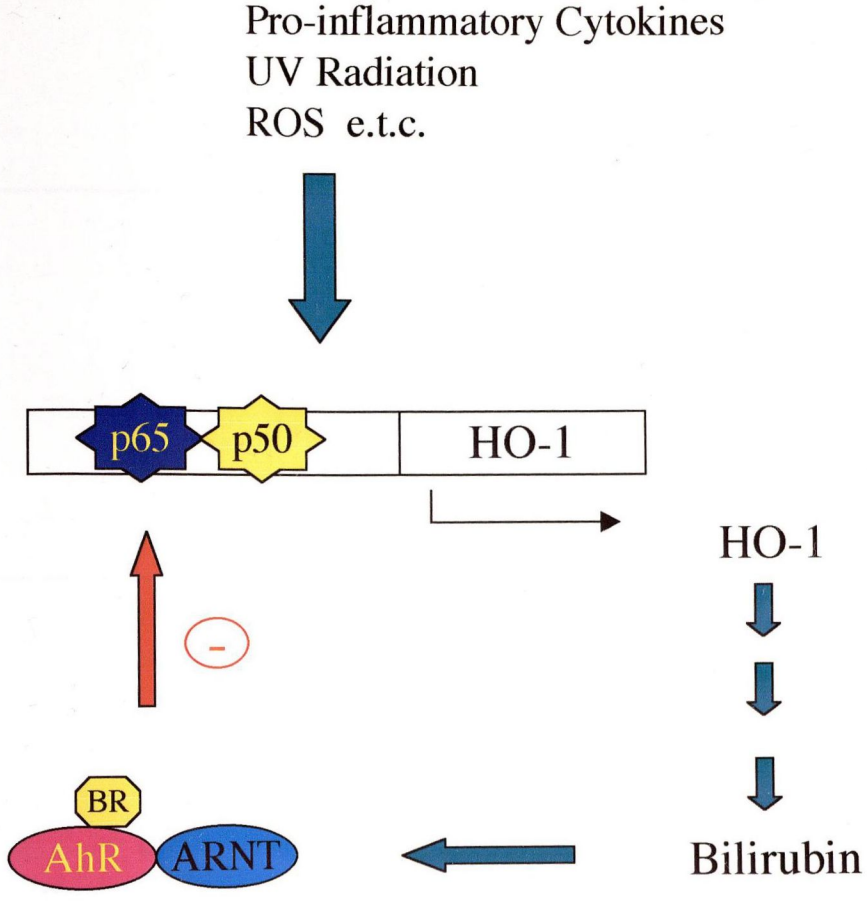

Figure 6.9. Proposed model for the inhibition of HO-1 gene expression by bilirubin-bound AhR.

Chapter 7

General Discussion

For many years the microsomal haem-oxygenase system has been recognised as being responsible for catalysing the degradation of haem to biliverdin-IXα. Since the IXα isomers of biliverdin and bilirubin are the predominant isomers found in adult mammalian systems, and the haem oxygenase system acts stereospecifically on haem to produce only the IXα isomer of biliverdin, this was considered for the most part to be the only haem catabolic process of any physiological significance. In light of the existence of a second biliverdin reductase, BVR-B, with selectivity directed towards other isomers of biliverdin and in view of the observations made by a number of workers regarding the relative proportions of different biliverdin isomers in foetal tissues compared with adult tissues, it is clear that a broader approach is required to understand the overall process of haem degradation.

The physiological relevance of the apparent switch in haem degradation from a IXβ pathway *in utero* to a IXα pathway is unclear, although it may be coupled to a switch from foetal to adult haemoglobin. The α-chains of human adult haemoglobin (HbA) and foetal haemoglobin (HbF) are identical, however, HbA contains two β-chains whereas HbF is composed predominantly of tetramers of two α and two γ-chains. The β-chains differ from the α-chains by 39 amino acid residues (Frier & Perutz, 1977) and it is conceivable that these changes in amino acid sequence result in different proportions of biliverdin isomers being produced either by direct coupled oxidation or possibly through the action of a novel haem oxygenase. With regards to the former hypothesis, coupled-oxidation *in vivo* may be mediated by the chain-breaking antioxidant, ascorbate. Dehydroascorbate (DHA), the two-electron oxidised form of vitamin C is rapidly sequestered by erythrocytes and reduced to ascorbate by GSH in a direct chemical reaction (May, 1998). The ascorbate can then pass slowly from the erythrocyte back into the plasma via the GLUT 1 transporter. It is concievable that biliverdin-IXβ is formed *in vivo* by a coupled oxidation of foetal haemoglobin with ascorbate serving as the reductant.

The existence of a novel haem oxygenase capable of directing cleavage exclusively towards the B-methene bridge of the haem molecule cannot be ruled out. The possibility arises that BVR-B itself is capable of acting as a haem oxygenase. Recent studies have shown that BVR-B is capable of binding haem (Cunningham, 1998), however, incubation of the enzyme with haem and NADPH had no effect on the visible spectrum of haemin. The lack of catalytic activity in this case may have been due to the absence of NADPH-cytochrome c reductase, a known source of reducing equivalents in the HO-1 catalysed oxidation of haem. NADPH-cytochrome c reductase alone has been shown to be capable of degrading haem *in vitro*, although there is some evidence to suggest that the products of this reaction are dipyrrole compounds and not tetrapyrroles (Yoshinaga,

1982).

It has recently been reported that human BVR-B/FR, like the *E.coli* FR, exhibits ferric reductase activity and this activity requires both NADPH and FMN (Cunningham *et al.*, 2000). An apparent K_m of 2.56 μM for ferric iron was observed. It is intriguing that an enzyme functionally coupled to haem cleavage should be capable of reducing both the linear tetrapyrrole and the ferric iron produced. The HO-1 catalysed conversion of haem to biliverdin-IXα is accompanied by the release of ferrous iron (Liu & Ortiz de Montellano, 2000). The release of iron in the reduced state may be physiologically important as ferrous iron is suitable for uptake into normal transport and storage sites, whereas ferric iron has a low solubility and must be reduced before it can be similarly processed (Poss & Tonegawa, 1997). The ability of BVR-B to reduce ferric iron may also be functionally significant if, as mentioned above, the enzyme possesses intrinsic HO activity or indeed if the reaction mechanism of the putative 'foetal haem oxygenase' does not involve reduction of Fe^{3+}•biliverdin to Fe^{2+}•biliverdin.

BVR-A has been reported to interact *in vitro* with HO and NADPH-cytochrome c reductase 1:1:1 ternary complex (Yoshinaga *et al.*, 1982). Both HO and NADPH-cytochrome c reductase are bound to the endoplasmic reticulum, whereas BVR-A is a cytosolic enzyme leading to the suggestion that BVR-A binds at the membrane/cytosol interface, perhaps near the active site of HO which is known to be exposed to the cytoplasm. Liu & Ortiz de Montellano (2000) have shown that BVR-A accelerates biliverdin release from HO-1 and proposed that this increased dissociation rate is caused by allosteric weakening of the binding of biliverdin to HO-1 or even the direct transfer of biliverdin from HO-1 to BVR-A. The crystal structure of a truncated form of HO-1 lacking the C-terminal membrane anchor has recently been solved (Schuller *et al.*, 1999) and indicates that haem is bound in a cleft with an edge exposed to the solvent. The electrostatic potential of the amino acids surrounding the cleft and the exposed haem edge is positive. NADPH-cytochrome c reductase, on the other hand, is negatively charged (Wang *et al.*, 1997)) suggesting that the enzyme binds over the exposed haem edge. Based on these findings it has been proposed that BVR-A binds in a similar manner and participates in the extraction of the biliverdin product. Attempts by these workers to detect a stable BVR-A:HO-1 complex have thus far been unsuccessful. During the course of this study, the truncated form of human HO-1 was cloned and overexpressed as a GST-fusion protein and will be used in future GST-pull down experiments in order to further investigate the possibility that HO-1 and BVR-A are interacting *in vivo*. Efforts will also be made to investigate the co-localization of these two proteins, and indeed NADPH-cytochrome c reductase with the use fluorescent protein tags. The possibility that BVR-B is interacting with a novel haem oxygenase will also be investigated in a similar manner

using cord blood as a source of foetal haemoglobin.

The fact that bilirubin conjugating activity in neonates is not fully functional until full-term has already been discussed (see Section 1.?). In the developing foetus, the highest level of glucuronyl transferase activity reaches less than 1% of that in normal adults (Kawade & Onishi, 1981). This activity is required for the excretion of bilirubin-IXα from the liver to the bile. The IX-β isomer of bilirubin is hydrophilic, therefore, the production of bilirubin-IXβ by the foetus allows excretion of bilirubin without the requirement for a conjugating system. It will be of interest to determine if this form of bilirubin exhibits antioxidant activity. Reactions of bilirubin-IXα involving toxic oxygen reaction products have been well documented and several researchers have found that experimental upregulation of HO-1 affords protection against subsequent oxidative challenges. More recently it has been demonstrated that mice lacking HO-1 are susceptible to the accumulation of free radicals and to oxidative injury (Poss & Tonegawa, 1997), thus establishing that the haem catabolon is an important enzymatic antioxidant system.

Both biliverdin-IXα and bilirubin-IXα have also been implicated as modulators of the immune system. The possibility that this effect is mediated through activation of the AhR, has been discussed in Chapter 6. Intriguingly, it has also been suggested that bile pigments act as nonvisual photoreceptors that mediate circadian responses to a light-dark cycle known as the circadian clock. For many years it was accepted that visual pigments mediate light's primary effects on biological clock systems. However, mice homozygous for the autosomal recessive allele *rd* (retinally degenerate), which have no electrophysiological or behavioural visual responses to light, can be entrained to a light-dark cycle (Foster *et al.*, 1991; cited in Cambell & Murphy, 1998). Cambell & Murphy have shown that the endogenous clock of humans can be entrained by light application to an unexpected spot, the popliteal region (the back of the knees). This model postulates that haem moieties could serve as photoreceptors and that tetrapyrrole -based pigments, such as bilirubin in mammals, act as counterparts to the tetrapyrrole-based, primary light-sensitive plant pigments of chlorophyll and phytochrome to mediate light's chronobiological effects. Many vertebrates and non-vertebrate species have multiple photoreceptor systems through which circadian entrainment may be achieved. In the house sparrow, three different pathways through which circadian entrainment may be achieved have been identified (Menaker, 1968; cited in Cambell & Murphy, 1998). Similarly, a number of fish, amphibian, and reptile species have extraocular pathways for circadian light transduction (Alder, 1976; cited in Cambell & Murphy, 1998), thus it is possible that bilirubin acts as the mammalian counterpart of these phototransducing receptors. Interestingly, both the AhR and ARNT proteins contain PAS repeats which are

involved in protein-protein interactions and have also been associated with light reception, light regulation and clock proteins (Zhulin, *et al*, 1997).

Although O'Carra & Colleran (1977) considered the suggestion that BVR-A may have arisen and been retained accidentally, they pointed out that this is unlikely because the enzyme has a very high affinity for biliverdin and specificity for the IXα isomer. The possibility that BVR-A may have some additional function, as yet unrecognised, cannot be ruled out. Indeed, BVR-B was previously characterised by workers as having a variety of other activities including flavin reductase, methaemoglobin reductase and more recently ferric reductase. The recombinant hBVR-A described in this work did not exhibit any flavin reductase activity and in view of it's inability to reduce flavin it is unlikely that the enzyme is a ferric reductase. As mentioned previously, human BVR-A has recently been described as a zinc-metalloprotein (Maines *et al*, 1996) and it has been suggested that BVR-A may have functions, other than catalytic activity, that pertain to it's association with Zn. For example, BVR-A may serve as a Zn storage protein or more intriguingly as a regulator of gene expression. With respect to the latter, the basic residues, Arg and Lys, that flank the postulated Zn coordination site at the carboxy-terminus of the protein (see Fig.1.8) may be of significance. Positively charged residues adjacent to the zinc-finger motif are postulated to make points of contact with DNA. It is worth noting also that BVR-A from the cyanobacteria *Synechocystis* sp PCC 6803 has been reported to act as a putative regulator of phycobiliprotein biosynthesis. As mentioned in Chapter 3, crystals of both proteins have been obtained. A comparison of the 3-dimensional structures will aid in the identification of structural domains that are of functional significance in both the human enzyme and it's ancestral counterpart.

It is clear that significant progress has been made in the area of haem catabolism. Previous studies on BVR-A have been hampered by lack of enzyme. The present study has described a protocol for producing large quantities of purified hBVR-A in a three-step process. The recombinant enzyme has been made available for crystallographic studies and it is hoped that an X-ray structure for this enzyme will soon become available in view of the recent resolution of the hBVR-B crystal structure. Kinetic studies have revealed the basis of the dual pH/cofactor specificity exhibited of this enzyme and comparison of the initial rate kinetics for hBVR-A and hBVR-B with a series of synthetic biliverdin analogs has revealed characteristic behaviour that allow us to propose distinct models for the two active sites. Structural studies have revealed that the stereospecificity of NADH oxidation by hBVR-A is B-side specific and denaturant-induced unfolding has demonstated that hBVR-A can reversibly unfold to a kinetically distinct intermediate that no longer exhibits substrate inhibited kinetics. Finally, activation of the AhR by haem catabolites has been demonstrated and potential experiments that may further define a role for bile pigments in

modulation of the immune response have been outlined.

References

A

Alam, J., Cai, J. & Smith, A. (1994) J. Mol. Biol. **269**, 1001-1009. Isolation and Characterisation of the Mouse Heme Oxygenase-1 Gene. Distal 5' Sequences are Required for Induction by Heme or Heavy Metals.

Aono,S., Adachi, Y., Uyama, E., Yamada, Y., Keino, H., Nanno, T., Koiwai, O. & Sato, H. (1995) Lancet. **345**, 958-959. Analysis of Genes for Bilirubin UDP-Glucuronosyltransferase in Gilbert's Syndrome.

Aono,S., Yamada, Y., Keino, H., Sassaoka, Y., Nakagawa, T., Onishi, S., Mimura, S., Koiwai, O. & Sato, S. (1994) Pediatr. Res. **35**, 629-632. A New Type of Defect in the Gene for Bilirubin Uridine 5'-Diphosphate-Glucuronosyltransferase in a Patient with Crigler-Najjar Syndrome Type I.

Askari, F., Hitomi, E., Thiney, M. & Wilson, J.M. (1995) Gene Ther. **2**, 203-208. Retrovirus-Mediated Expression of HUG Br 1 in Crigler-Najjar Syndrome Type I Human Fibroblasts and Correction of the Genetic Defect in Gunn rat Hepatocytes.

B

Barker, C.W., Fagan, J.B. & Pasco, D.S. (1992). J. Biol. Chem. **267**, 8050-8055. Interleukin-1 Beta Suppresses the Induction of P4501A1 and P4501A2 mRNAs in Isolated Hepatocytes.

Batley, K.E. & Morris, H.R. (1977) Biochem. Biophys. Res. Commum. **75**, 1010-1014. Dihydrofolate Reductase from Lactobacillus casei: N-terminal Sequence and Comparison with the Substrate Binding Region of Other Reductases.

Beale, S.I. & Castelfranco, P.A. (1974) Plant Physiol. **53**, 297-303. The Biosynthesis of δ-Aminolevulinic Acid in Higher Plants.II. Formation of ^{14}C-δ-Aminolevulinic Acid from Labeled Precursors in Greening Plant Tissues.

Beer, H. & Bernard, K. (1959) Chimia. **13**, 291-292. Influence of Bilirubin and Vitamin E on Oxidation of Unsaturated Fatty Acids by Ultraviolet Radiation.

Berk, P.D., Howe, R.B., Bloomer, J.R. & Berlin, N.I. (1969) J. Clin. Invest. **48**, 2176-2190. Studies of Bilirubin Kinetics in Normal Adults.

Bitar, K.G., Perez-Aranda, A. & Bradshaw, R.A. (1980) FEBS Lett. **116**, 196-198. Amino Acid Sequence of L-3-Hydroxyacyl CoA Dehydrogenase from Pig Heart Muscle.

Bohren, K.M., Bullock, B., Wermuth, B. & Gabbay, K.H. (1989) J. Biol. Chem. **264**, 9547-9551. The Aldo-Keto Reductase Superfamily: cDNAs and Deduced Amino Acid Sequences of Human Aldehyde and Aldose Reductases.

Bonnet, R., Davis, J.E. & Hursthouse, M.B. (1976) Nature **262**, 326-328. Structure of Bilirubin.

Bosma, P.J., Chowdhury, J.R., Bakker, C., Gantla, S., de Boer, A., Oostra, B.A., Lindhout, D., Tytgat, G.N., Jansen, P.l., Oude Elferink, R.P. (1995) N. Eng. J. Med. **333**, 1171-1175. The Genetic basis of the Reduced Expression of Bilirubin UDP-Glucuronosyltransferase 1 in Gilbert's Syndrome.

Broderson, R. & Bartels, P. (1969) Eur. J. Biochem. **10**, 468-473. Enzymatic Oxidation of Bilirubin.

Broderson, R. (1979) J. Biol. Chem. **254**, 2364-2369. Bilirubin: Solubility and Interaction with Albumin and Phospholipid.

Brown, N.L., Ford, S.J., Pridmore, R.D. & Fritzinger, D.A. (1983) Biochemistry **22**, 4089-4095. Nucleotide Sequence of a Gene from the *Pseudomanas* Transposon Tn501 Encoding Mercuric Reductase.

C

Campbell, S.S. & Murphy, P.J. (1998) Science **279**, 396-398. Extraocular Circadian Phototransduction in Humans.

Caldenhoven, E., Liden, J., Wissink, S., Van der Stolpe, A., Raaijmakers, J., Koenderman, L., Okret, S., Gustafsson, J.A., and Van der Saag, P.T. (1995) Mol.Endocrinol. **9**, 401-412. Negative Crosstalk Between RelA and the Glucorticoid Receptor: A Possible Mechanism for the Anti-Inflammatory Action of Glucocorticoids.

Chivia, J.C., Kwok, R., Lanb, N., Hagiwara, M., Montmony, M. & Goodman, R. (1993) Nature **365**, 855-859. Phosphorylated CREB Binds Specifically to the Nuclear Protein CBP.

Cole, E.S., Lepp, C.A., Holohan, P.D. & Fondy, T.P. (1978) J. Biol. Chem. **253**, 7952-7959. Isolation and Characterisation of Flavin-Linked Glycerol-3-Phosphate Dehydrogenase from Rabbit Skeletal Muscle Mitochondria and Comparison with the Enzyme from Rabbit Brain.

Colleran, E. & O'Carra, P. (1977) in "Chemistry and Physiology of Bile Pigments", (eds Berk, P.D. & Berlin, N.I., DHEW Publication No. (NIH) 77-1100, Fogarty International Centre Proceedings No.35) p69-80.

Cowie, D.B. & Cohen, G.N. (1957) Biochim. Biophys. Acta **26**, 252-261. Biosynthesis by *Eschericia coli* of Active Altered Proteins Containing Selenium Instead of Sulphur.

Crigler, J.F. & Najjar, V.A. (1952) Pediatrics. **10**, 169-180. Conjenital Familial Nonhaemolytic Jaundice with Kernicterus.

Cunningham, O., Gore, M.G. & Mantle, T.J. (2000) Biochem. J. **345**, 393-399. Initial-rate Kinetics of the Flavin Reductase Reaction Catalysed by Human Biliverdin-IXβ Reductase (BVR-B).

Cunningham, O. (1998) Ph.D. Thesis, University of Dublin. Studies on Human Liver Biliverdin-IXβ Reductase.

D

Davidson, B.E., Saigo, M., Noller, H.F. & Harris, J.I. (1967) Nature **216**, 1181-1185. Amino Acid Sequence of Glyceraldehyde-3-Phosphate Dehydrogenase from Lobster Muscle.

Davidson, W.S., Walton, D.J. & Flynn, T.G. (1978) Comp. Biochem. Physiol. **60B**, 309-315. A Comparative Study of the Tissue and Species Distribution of NADPH-Dependent Aldehyde Reductase.

Depicker, A., Stachel, S., Dhaese, P., Zambryski, P. & Goodman, H.M. (1982) J. Mol. Appl. Genet. **1**, 561-573. Nopaline Synthase: Transcript Mapping and DNA Sequence.

Denison, M.S., Fisher, J.M. & Whitlock, J.P. (1988) J. Biol. Chem. **263**, 17221-

17224. The DNA Recognition Site for the Dioxin-Ah Receptor Complex.

E

Echner, R., Ewen, M., Newsome, D., Gerdes, M., DeCaprio, J., Lawrence, J. & Livingston, D. (1994) Genes Dev. **8**, 869-884. Molecular Cloning and Functional Analysis of the Adenovirus E1A-associated 300-kDa Protein Reveals a Protein with Properties of a Transcriptional Adaptor.

Eklund, H., Samana, J.P., Wallen, L., branden, C.I., Akeson, A. & Jones, T.A. (1981) J. Mol. Biol. **146**, 561-587. Structure of a Triclinic Ternary Complex of Horse Liver Alcohol Dehyrogenase at 2.4 Å Resolution.

Elliot, G. (1996) Ph.D. Thesis, University of Dublin. Studies on Salmon Liver Biliverdin reductase.

Ennis, O. (1996) Ph.D. Thesis, University of Dublin. Mammalian Biliverdin Reduction: The Cloning and Overexpression of Rat Kidney Biliverdin-IXα Reductase in *Escherichia coli*.

Eventoff, W., Rossmann, M.G., Taylor, S.S., Torff, H.J., Meyer, H., Keil, W. & kiltz, H.H. (1977) Proc.Natl.Acad.Sci. **74**, 2766-2681. Structural Adaptations of Lactate Dehydrogenase Isozymes.

F

Fahkrai, H. & Maines, M.D. (1992) J. Biol. Chem. **267**, 4023-4029. Expression and Characterisation of a cDNA for Rat Kidney Biliverdin Reductase; Evidence Suggesting the Liver and Kidney Enzymes are the Same Transcript Product.

Frydman, R.B., Tomaro, M.L., Buldain, G., Awruch, J., Diaz, L. & Frydman, B. (1981) Biochemistry **20**, 5177-82. Specificity of Heme Oxygenase: A Study with Synthetic Hemins.

Frier, J.A. & Perutz, M.F. (1977) J. Mol. Biol. **112**, 97-112. Structure of Human Foetal DeoxyHaemoglobin.

G

Gibson, K.D., Laver, W.G. & Neuberger, A. (1958) Biochem. J. **70**, 71-81. Initial Stages in the Biosynthesis of Porphyrins.

Gerritsen, M.E., Williams, A.J., Neish, A.S., Moore, S., Shi, Y. & Collins, T. (1997) Proc. Natl. Acad. Sci. USA. **94**, 2927-2932. CREB-Binding Protein/p300 are Transcriptional Coactivaors of p65.

Gordon, E.R., Schaffer, E.A. & Sass-Kortsak, A. (1976) Gasteroenterology. **70**, 761-765. Bilirubin Secretion and Conjugation in the Crigler-Najjar Syndrome Type II.

Goreski, C.A., Gordon, E.F., Schaffer, E.A., Pare, P., Carassavas, D. & Aronoff, A. (1978) Clin. Sci. Mol. Med. **55**, 63-71. Definition of a Conjugation Dysfunction in Gilbvert's Syndrome; Studies of the Handling of Bilirubin Loads and the Pattern of Bilirubin Conjugates Secreted in Bile.

Granick, S. & Beale, S.I. (1978) Advan. Enzymol. **40**, 33-203. Hemes, Chlorophylls and Related Compounds; Biosynthesis and Metabolic Regulation.

Guan, K.L. & Dixon, J.E. (1991) Anal.Biochem. **192**, 262-267. Eukaryotic Proteins Expressed in *Escherichia coli*; An Improved Thrombin Cleavage and Purification procedure of fusion Proteins with Glutathione S-Transferase.

Gunn, C.K. (1938) J. Hered. **29**, 137-139. Hereditary Acholuric Jaundice in a New Mutant Strain of Rats.

H

Hayes, J.D., Strange, R.C. & Percy-Robb, I.W. (1981) Biochem. J. **197**, 491-502. A Study of the Structures of the Y_aY_a and Y_aY_c Glutathione S-Transferases from Rat Liver Cytosol. Evidence that the Y_c Monomer is Responsible for Lithocholate-Binding Activity.

Health-Palinso, S., Rogers, W.J., Tullis, K., Seidel, S.D., Cenijn, P.H., Brouwer, A. & Denison, M.S. (1998) Biochemistry **37**, 11508-11515. Activation of the Ah receptor by Tryptophan and Tryptophan Metabolites.

Heyman, E., Ohlessson, A. & Girschek, P. (1989) N. Engl. J. Med. **320**, 256. Retinopathy of Prematurity and Bilirubin.

Holmes, D.S. & Quigley, M. (1981) Anal. Biochem. **114**, 193-197. A Rapid Boiling Method for the purification of Bacterial Plasmids.

J

Jacobson, J. & Fedders, O. (1970) Scand. J. Clin. Lab. Invest. **26**, 237-241. Determination of Non-Albumin-Bound Bilirubin in Human Serum.

Jansen, P.L.M., Chowdhury, J.R., Fischberg, E.B. & Arias, I.M. (1977) J. Biol. Chem. **252**, 2710-2716. Enzymatic Conversion of Bilirubin Monoglucuronide to Diglucuronide by Rat Plasma Membranes.

Jornvall, H. (1970) Eur.J.Biochem. **16**, 41-49. Horse Liver Alcohol Dehyrogenase. On the Primary Structure of the Isoenzymes.

K

Kalkhoven, E., Wissink, S., van der Saag, P.T. & van der Burg, B. J. Biol. Chem. **271**, 6217-6224. Negative Interaction Between the RelA (p65) Subunit of NF-κB and the Progesterone Receptor.

Kamei, Y., Xu, L., Heinzel, T., Torchia, J., Kurokawa, R., Gloss, B., Lin, S., Heyman, R.A., Rose, D.W., Glass, C.K. & Rosenfeld, M.G. (1996) Cell **85**, 403-414. A CBP Integrator Complex Mediates Transcriptional Activation and AP-1 Inhibition by Nuclear Receptors.

Kannangara, C.G. & Gough, S.P. (1977) Carlsberg Res.Commun. **42**, 441-457, cited in "Biosynthesis of Tetrapyrroles", ed. P.M. Jordon, general editors, A. Neurberger & L.L.M. Van Deenan. New Comprehensive Biochemistry , Volume 19. Elsevier. 1991.

Kawada, N. & Onishi, S. (1981) Biochem. J. **196**, 257-260. The Prenatal and Postnatal Development of UDP-Glucuronyltransferase Activity Towards Bilirubin and the Effect of Premature Birth on this Activity in Human Liver.

Kikuchi, G., Kumar, A., Talmage, P. & Shemin, D. (1958) J. Biol. Chem. **233**, 1214-1219. The Enzymatic Synthesis of δ-aminolevulinic Acid.

Kivlahan, C. & James, E.J. (1984) Pediatrics. **74**, 362-370. The Natural History of Neonatal Jaundice.

Kobayashi, A., Numayama-Tsuruta, N., Sogawa, K. and Fujii-Kuriyama, Y.J. (1997) Biochem. **122**, 703-710. CBP/p300 Functions as a Possible transcriptional Coactivator of Ah Receptor Nuclear Translocator (Arnt).

Koiwai, O., Nishizawa, M., Hasada, K., Aono, S., Adachi, Y., Mamiya, N. & Sato, H. (1995). Hum. Mol. Genet. **4**, 1183-1186. Gilbert's Syndrome is Caused by a Heterozygous Missense Mutation in the Gene for Bilirubin UDP-Glucuronyltransferase.

Kornberg, A. (1942) J. Clin. Invest. **21**, 299. Latent Liver Disease in Persons Recovered from Catarrhal Jaundice and in Otherwise Normal Medical Students as Revealed by the Bilirubin Excretion Test.

Krauth-Siegel, R.L., Blatterspiel, R., Saleh, M., Schilz, E., Schirmer, R.H. & Untucht-Grau, R. (1982) Eur. J. Biochem. **121**, 259-267. Glutathione Reductase from Human Erythrocytes: Amino Acid Sequence of the Structurally known FAD-Binding Domain.

Kreitman, H. (1983) Nature. **304**, 412-417. Nucleotide Polymorphisms at the Alcohol Dehydrogenase Locus of *Drosphilia melanogaster*.

Kutty, R.K., Kutty, G., Roderiguez, I.R., Chader, G.J. & Wiggert, B. (1994) Genomics. **20**, 513-516. Heme-Oxygenase-1 (HMOX1) Maps to Chromosome 22q12 and Heme Oxygenase-2 (HMOX2) Maps to Chromosome 16p13.3.

Kutty, R.K. & Maines, M.D. (1981) J. Biol. Chem. **256**, 3956-3960. Purification and Characterisation of Rat Liver Biliverdin Reductase.

L

Lamar, C.A., Mahesh, V.B. & Brann, D.W. (1996) Endocrinolgy **137**, 790-793. Regulation of Gonadotrophin-Releasing Hormone (GnRH) Secretion by Heme Molecules: A Regulatory Role for Carbon Monoxide?

Lathe, G.H. (1972) in "*Essays in Biochemistry*" (eds. Cambell, P.N. & Dickens, F.) The Biochemical Society and the Academic Press, London. Vol. 8, 107-148.

Lemberg, R. & Legge, J.W. (1949) "Haematin Compounds and Bile Pigments", Wiley-Interscience Publishers Inc., New York.

Lemberg, R. (1956) Rev. Pure. Appl. Chem. **6**, 1-23. Chemical Mechanism of Bile Pigment Formation.

Lemberg, R. & Wyndham, R.A. (1936) Biochem. J. **30**, 1147-1170. Reduction of Biliverdin to Bilirubin in Tissues.

Levine, R.L. (1977) Clin. Chem. **23**, 2292-2301. Fluorescence Quenching Studies of the Binding of Bilirubin to Albumin.

Liu, L., & Otiz de Montellano (2000) J. Biol. Chem. **275**, 5297-5307. Reaction Intermediates and Single Turnover Rate Constants for the Oxidation of Heme by Human Heme Oxygenase-1.

London, J.M., West, R., Shemin, D. & Rittenberg, D. (1950) J. Biol. Chem. **184,** 351-358. On the Origin of Bile Pigment in Normal Man.

Lowry, C.V. & Zitomer, R.S. (1988) Mol. Cell. Biol. **8**, 4651-4658. ROX1 Encodees a Heme-Induced Repression Factor Regulating ANB1 and CYC7 of *Saccharomyces cerevisiae*.

M

Mack, C.P., Hultquist, D.E. & Schlafer, M. (1995) Biochem. Biophys. Res. Comm. **212**, 35-40. Myocardial Flavin Reductase and Riboflavin: A Potential Role in Decreasing Reoxygenation Injury.

Mande, S.C. & Sobhia, M.E. (2000) Protein Eng. **13**, 133-141. Structural Charaterization of Protein-Denaturant Interactions: Crystal Structures of Hen Egg-White Lysizyme in Complex with DMSO and Guanidinium Chloride.

Maines, M.D., Polevoda, B.V., Huang, T.J. & McCoubrey Jr., W.K. (1996) Eur. J. Biochem. **235**, 372-381. Human Biliverdin-IXα Reductase is a Zinc-Metalloprotein;

Characterisation of Purified and *E.coli* expressed Enzymes.

Maines, M.D., Trakshel, G.M. & Kutty, R.K. (1986) J. Biol. Chem . **261**, 411-419. Characterisation of Two Constitutive Forms of Rat Liver Microsomal Heme Oxygenase. Only One Molecular Species of the Enzyme is Inducible.

Maines, M.D. (1988) FASEB J. **2**, 2557-2568. Haem-Oxygenase: Function, Multiplicity, Regulatory Mechanisms and Clinical Applications.

Maines, M.D. & Trakshel, G.M. (1993) Arch. Biochem. Biophys. **300**, 320-326. Characterisation and Purification of Human Biliverdin Reductase.

May, J.M. (1998) Front. Biosci. **3**, 1-10. Ascorbate Function and Metabolism in the Human Erythrocyte.

McConnell, K.P. & Hoffmann, J.L. (1972) FEBS Lett. **24**, 60-62. Methionine-Selenomethionine Parallels in Rat Liver Polypeptide Chain Synthesis.

McCoubrey, W.K.Jr., Huang, T.J. & Maines, M.D. (1997) Eur. J. Biochem. **247**, 725-732. Isolation and Characterisation of a cDNA from the Rat Brain that Encodes Hemoprotein Heme Oxygenase-3.

McCoubrey, W.K.Jr., Cooklis, M.A. & Maines, M.D. (1995) Gene **160**, 235-240. The Structure, Organisation and Differential Expression of the Rat Gene Encoding Biliverdin Reductase.

Meera-Khan, P., Wijnen, L.M., Wijnen, J.T. & Grzeschnik, K.H. (1983) Biochem. Genet. **21**, 123-133. Electrophoretic Characterisation and Genetics of Human Biliverdin Reductase (BLVR; EC 1.3.1.24); Assignment of BLVR to the p14 Leads to cen Region pf Human Chromosome 7 in Mouse-Human Somatic cell Hybrids.

Menken, M., Waggoner, J.G. & Berlin, N.I. (1966) J. Neurochem. **13**, 1241-1248. The Influence of Bilirubin on Oxidative Phosphorylation and Related Reactions in Brain and liver Mitochondria: Effects of Protein-Binding.

Moon, K. & Smith, E.L. (1973) J. Biol. Chem. **248**, 3082-3088. Sequence of Bovine Liver Glutamate Dehydrogenase. 8 Peptides Produced by Specific Chemical Cleavages; The Complete Sequence of the Protein.

Moras, D., Olsen, K.W., Sabesan, M.N., Buehner, M., Ford, G.C. & Rossmann, M.G. (1975) J. Biol. Chem. **250**, 9137-9162. Studies of Asymmetry in the Three-Dimensional Structure of Lobster D-Glyceraldehyde-3-Phosphate Dehydrogenase.

Muir, H.M. & Neuberger, A. (1950) Biochem. J. **47**, 97-104. The Origin of the Methene Carbon Atoms.

Muller-Eberhard, U. (1970) N. Engl. J. Med. **283**, 1090-1094. Hemopexin.

Munn, D.H., Zhou, M., Attwood, J.T., Bondarev, I., Conway, S., Marshall, B., Brown, C. & Mellor, A.L. (1998) Science **281**, 1191-1193. Prevention of Allogenic Fetal Rejection by Tryptophan Catabolism.

Murray, D.R.P. (1930) Biochem. J. **24**, 1890.

N

Nakagami, S.T., Toyamura, K., Kinoshita, T. & Morisawa, S. (1993) Biochim. Biophys. Acta. **1156**, 189-193. A Beneficial Role of Bile Pigments as an Endogenous Tissue Protector: Anti-Complement Effects of Biliverdin and Conjugated Bilirubin.

Nakijima, H., Takemura, T., Nakijima, O. & Yamaoka,K. (1963) J. Biol. Chem. **238**, 3784-3796. Studies on Heme α-Methenyl Oxygenase. I. The Enzymatic Conversion of Pyridine-Hemichromogen and Hemoglobin-Haptoglobin into a Possible Precursor of Biliverdin.

Neuzil, J. & Stocker, R. (1994) J. Biol. Chem. **269**, 16712-16719. Free and Albumin Bound Bilirubin are Efficient Co-Antioxidants for α-Tocopherol, Inhibiting Plasma and Low density Lipoprotein Lipid Peroxidation.

Noguchi.M., Yoshida, T. & Kikuchi, G. (1979) J. Biochem. **86**, 833-848. Purification and Properties of Biliverdin Reductases from Pig Spleen and Rat Liver.

O

O'Carra, P. & Colleran, E. (1970a) J. Chromatogr. **50**, 458-468. Separation and Identification of Biliverdin Isomers and Isomer Analysis of Phycobilins and Bilirubin.

O'Carra, P. & Colleran, E. (1970b) Biochem. J. **119**, 42-43. Methene-Bridge Specificity of the Coupled Oxidation of Myoglobin and Haemoglobin with Ascorbate.

O'Carra, P. & Colleran, E. (1971) Biochem. J. **125**, 110. Properties and Kinetics of Biliverdin Reduction.

P

Parkes, D., Kasckow, J. & Vale, W. (1994) Brain Res. **646**, 315-318. Carbon Monoxide Modulates Secretion of Corticotropin-Releasing Factor from Rat Hypothalamic Cell Cultures.

Pawlowski, J.E., Huizinga, M. & Penning, T.M. (1991) J. Biol. Chem. **266**, 8820-8825. Cloning and Sequencing of the cDNA for Rat Liver 3a-Hydroxysteroid/Dihydrodiol Dehydrogenase.

Phelan, D., Winter, G.M., Rogers, W.J., Lam, J.C. & Denison, M.S. (1998) Arch. Biochem. Biophysics. **357**, 155-163. Activation of Ah Receptor Signal Transduction Pathway by Biliverdin and Bilirubin.

Phillips, O. & Mantle, T.J. (1981) Biochem. Soc. Trans. **9**, 275-278. Some Kinetic and Physical Properties of Biliverdin Reductase.

Phillips, O. (1981) Ph.D. Thesis, University of Dublin. Studies on Biliverdin Reductase and its Role in Haem Catabolism.

Popjak, G. 91970) in " The Enzymes" (ed. Boyer, P.D.) Vol. II pp 116-214. Academic Press, London.

Porra, R.J. & Falk, J.E. (1961) Biochem. Biophys. Res. Commun. **5**, 179-184. Protein-Bound Porphyrins Associated with Protoporphyrin Biosynthesis.

Poss, K.D. & Tonegawa, S. (1997) Proc. Natl. Acad. Sci. U.S.A. **94**, 10919-10924. Heme Oxygenase 1 is Required for Mammalian Iron Reutilization.

R

Raval, D.N. & Wolfe, R.G. (1963) Biochemistry **2**, 220-224. Malic Dehydrogenase;

Kinetic Studies of Substrate Inhibition by Oxaloacetate.

Rigney, E. (1986) Ph.D. Thesis, University of Dublin. Kinetic Studies of Ox Kidney Biliverdin Reductase.

Rigney, E., Phillips, O. & Mantle, T.J. (1988) Biochem. J. **255**, 431-435. Some Physical and Immunological Properties of Ox Kidney Biliverdin Reductase.

Rigney, E. & Mantle, T.J. (1988) Biochim. Biophys. Acta. **957**, 237-242. The Reaction Mechanism of Bovine Kidney Biliverdin reductase.

Robinson, S.H., Tsong, M., Brown, B.W. & Schmid, R. (1966) J. Clin. Invest. **45**, 1569. The Sources of Bile Pigment in the Rat: Studies of the "Early Labelled" Fraction.

Rossmann, M.G. & Liljas, L.J. (1974) J. Mol. Biol. **85**, 177. (Letters to the editor) Recognition of Structural Domains in Globular Proteins.

S

Sambrook, J., Fritsch, E.F. & Maniatis, T. (1989) "Molecular Cloning, A Laboratory Manual", 2nd edn., Cold Spring Harbour Lab Press.

Sano, S. & Granick, S. (1961) J. Biol. Chem. **236**, 1173-1180. Mitochondrial Coproporphyrinogen Oxidase and Protoporphyrin Formation.

Scharsmidt, B.F. & Gollan, J.L. (1979) in "Progress in Liver Disease" (eds. Popper, H. & Schaffner, F.). Vol.VI, pp. 187-212. Grune & Stratton, New York.

Schluchter, W.M. & Glazer, A.N. (1997) J. Biol. Chem. **272**, 13562-13569. Characterization of Cyanobacterial Biliverdin Reductase.

Schmid, R. (1972) in "The Metabolic Basis of Inherited Disease" (eds. Stanbury, J.B., Wyngarden, J.B. & Fredrickson, D.S.), 3rd edn., McGraw Hill, New York, p1141.

Schmidt, J. & Bradfield, C.A. (1996) Ann. Rev. Cell. Dev. Biol. **12**, 55-89. Ah Receptor Signaling Pathways.

Schoolingin-Jordon, P. (1994) Curr. Opin. Structural. Biol. **4**, 902-911. Highlights in Haem Biosynthesis.

Schuller, D., Wilks, A., Ortiz de Montellano, P.R. & Poulos, T. (1999) Nat. Struct. Biol. **6**, 860-867. Crystal Structure of Human Heme Oxygenase-1.

Schulz, G.E., Schirmer, R.H. & Pai, E.F. (1982) J. Mol. Biol. **160**, 287-308. FAD-Binding Site of Glutathione Reductase.

Schwertner, H.A., Jackson, W.G. & Tolan, G. (1994) Clin. Chem. **40**, 18-23. Association of Low Serum Bilirubin with Increased Risk of Coronary Artery Disease.

Seppen, J., Bosma, P.J., Goldhoorn, B.G., Bakker, C., Chowdhury, J.R., Chowdhury, N.R., Jansen, P.l. & Oude Elferink, R.P. (1994) J. Clin. Invest. **94**, 2385-2391. Discrimination Between Crigler-Najar Type I and II by Expression of Mutant Bilirubin Uridine Diphosphate-Glucuronosyltransferase.

Shemin, D. & Rittenburg, D. (1945) J. Biol. Chem. **159**, 567-568. The Utilisation of Glycine for the Synthesis of a Porphyrin.

Shemin, D., London, I.M. & Rittenburg, D. (1950) J. Biol. Chem. **183**, 757-765. The Synthesis of Protoporphyrin *In Vitro* by Red Blood Cells of the Duck.

Shemin, D. & Russell, C.S. (1953) J. Am. Chem. Soc. **75**, 4873-4875. δ-Aminolevulinic Acid; Its Role in the Biosynthesis of Porphyrins and Purines.

Sherlock, S. (1968) Disease of the Liver and Bilary System. Fourth Edition. Oxford, Blackwell Scientific Publications.

Shibahara, S., Muller, R.M. & Taguchi, H. (1987) J. Biol. Chem. **262**, 12889-12892. Transcriptional Control of Rat Heme Oxygenase by Heat Shock.

Shirley, B. (1995) Protein Folding and Stability. Series: Methods in molecular Biology. Humana Press Inc, Totowa, New Jersey.

Sinal, C.J. & Bend, J.R. (1997) Pharmacology **52**, 590-599. Aryl hydrocarbon Receptor-Dependent Induction of Cyp1a1 by Bilirubin in Mouse Hepatoma Hepa 1c1c7 Cells.

Singleton, J.W. & Laster, L. (1965) J. Biol. Chem. **240**, 4780-4789. Biliverdin Reductase of Guiney Pig Liver.

Shalloe, F., Elliot, G., Ennis, O. & Mantle, T. (1996) Biochem. J. **316**, 385-387. Evidence that Biliverdin-IXβ Reductase and Flavin Reductase are Identical.

Stevens, B. & Small, R.D., Jr. (1976) Photochem. Photobiol. **23**, 33-36. The Photoperoxidation of Unsaturated Organic Molecules. Quenching by Biliverdin and Bilirubin.

Stocker, R., Glazer, A.N. & Ames, B.N. (1987a) Proc. Natl. Acad. Sci. USA. **84**, 5918-5922. Antioxidant Activity of Albumin-Bound Bilirubin.

Stocker, R., Yamamoto, Y., McDonagh, A.F., Glazer, A.N. & Ames, B.N. (1987b) Science **235**, 1043-1046. Bilirubin is an Antioxidant of Possible Physiological Importance.

Stocker, R. & Ames, B.N. (1987c) Proc. Natl. Acad. Sci. USA. **84**, 8130-8134. Potential Role of Conjugated Bilirubin and Copper in the Metabolism of Lipid Peroxides in Bile.

Sun D., Sato, M., Yoshida,T., Shimizu, H., Miyatake, H., Adachi, S., Shiro, Y. & Kikuchi, A. (2000) Acta Cyst. **D56**, 1180 - 1182. Crystallization and Prelimnary X-Ray Diffraction Analysis of a Rat Biliverdin Reductase.

T

Taylor, S.S. (1977) J. Biol. Chem. **252**, 1799-1806. Amino Acid Sequence of Dogfish Muscle Lactate Dehydrogenase.

Tenhunen, R., Marver, H.S. & Schmid, R. (1970) J. Lab. Clin. Med. **75**, 410-421. The Enzymatic Catabolism of Hemoglobin: Stimulation of Microsomal Heme Oxygenas by Hemin.

Terry, M.J., Maines, M.D., & Lagarias C.J. (1993) J. Biol. Chem. **268**, 26099-26106. Inactivation of Phytochrome- and Phycobiliprotein-Chromophore Precursors by Rat Liver Biliverdin Reductase.

Tomoro, M.L., Frydman, R.B., Awruch, J., Valasinas, A., Frydman, B., Pandey, R.K. & Smith, K.M. (1984) Biochem. Biophys. Acta **791**, 350-356. The Specificity of Biliverdin Reductase: A Study with two Biliverdin Types.

V

Verma, A., Hirsch, D.J., Glatt, C.E., Ronnett, G.V. & Snyder, S.H. (1993) Science 259, 381-384. Carbon monoxide: A Putative Nueronal Messenger.

W

Wang, M., Roberts, D.L., Paschke, R., Shea, T.M., Masters, B.S.S. & Kim, J.J.P. (1997) Proc. Natl. Acad. Sci. U.S.A. **94**, 8411-8416. Three Dimentional Structure of NADPH-Cytochrome P450 Reductase: Prototype for FMN- and FAD-Containing Enzymes.

Weijer, W.J., Hofsteenge, J., Vereijken, J.M., Jekel, P.K. & Beintema, J.J. (1982) Biochem. Biophys. Acta. **704**, 385-388. Primary Structure of *p*-Hydroxybenzoate Hydroxylase from *Pseudomonas fluorescens.*

Weatherill, P.J., Kennedy, S.M.E., Burchell, B. (1980) Biochem. J. **191**, 155-163. Immunochemical Comparison of UDP-Glucuronyltransferase from Gunn- and Wistar-Rat Livers.

Wermuth, B., Munch, J.D.B. & von Wartburg, J.P. (1977) J. Biol. Chem. **252**, 3821-3828. Purification and Properties of NADPH-dependent Reductase from Human Liver.

Westley, J. (1969) in "Enzymic Catalysis" (eds. Halvorson, H.O., Herschel, R.L. & Bell, E.), Harper & Row, New York, Evanson and London. p42-61.

Wierenga, R.K., De Maeyer, M.C.H. & Hol, W.G.J. (1985) Biochemistry. **24**, 1346-1357. Interaction of Pyrophosphate Moieties with α-helices in Dinucleotide Binding Proteins.

Wierenga, R.K., De Jong, R.J., Kalk, K.H., Hol, W.G.J. & Drenth, J. (1979) J. Mol. Biol. **131**, 55-73. Crystal Structure of *p*-Hydroxbenzoate Hydroxylase.

Wilks, A., & Otiz de Montellano (1993) J. Biol. Chem **268**, 22357-22362. Rat Liver

Heme Oxygenase.

Willis, D., Moore, A., Frederick, R. & Willoughby, D.A. (1996) Nature Medicine **2**, 87-90. Heme-Oxygenase: A Novel Target for Modulation of the Inflammatory Response.

Wills, C. & Jornvall, H. (1977) Eur. J. Biochem. **99**, 323-331. The Two Major Isozymes of Yeat Alcohol Dehydrogenase.

Wilson, D.K., Bohren, K.M., Gabbay, K.H. & Quiocho, F.A. (1992) Science **257**, 81-84. An Unlikely Sugar Substrate Site in the 1.65 Å Structure of the Human Aldose Reductase Holoenzyme Implicated in Diabetic Complications.

Wu, J.W. & Wang, Z.X. (1999) Protein Sci. **8**, 2090-2097. New Evidence for the Denaturant Binding Model.

X

Xu, F., Mack, C.P., Quandt, K.S., Schlafer, M., Massey, V. & Hultquist, D.E. (1993) Biochem. Biophys. Res. Comm. **193**, 434-439. Pyrrolquinoline Quinone Acts with Flavin Reductase to Reduce Ferryl Myoglobin *In Vitro* and Protects Isolated Heart from Re-Oxygenation Injury.

Xu, F., Quandt, K.S. & Hultquist, D.E. (1992) Proc. Natl. Acad. Sci. U.S.A. **89**, 2130-2134. Characterization of NADPH-dependent Methaemoglobin Reductase as a Heme-Binding Protein Present in Erythrocytes and Liver.

Y

Yamaguchi, T., Komada, Y. & Nakajima, H. (1994) J. Biol. Chem. **269**, 24343-24348. Biliverdin-IXα Reductase and Biliverdin-IXβ Reductase from Human liver; Purification and Characterisation.

Yamaguchi, T., Komuro, A., Nakano, Y., Tomita, M. & Nakajima, H. (1993) J. Biol. Chem. **197**, 1518-1523. Complete Amino Acis Sequence of Biliverdin-IXβ Reductase from Human liver.

Yamaguchi, T., Horio, F., Hashizume, T., Tanaka, M., Ikeda, S., Kakinuma, A. &

Nakajima, H. (1995) Biochem. Biophys. Res. Comm. **214**, 11-19. Bilirubin is Oxidised in Rats Treated with Endotoxin and Acts as a Physiological Antoxidant Synergistically with Ascorbic Acid *In Vivo*.

Yoshinaga, T., Sassa, S. & Kappas, A. (1982) J. Biol. Chem. **257**, 7794-7802. A Comparitive Study of Heme Degradation by NADPH-Cytochrome c Reductase Alone and by the Complete Heme Oxygenase System.

Yubisui, T., Matsuki, T., Takeshita, M. & Yoneyama, Y. (1979) J. Biochem. (Tokyo) **85**, 719-728. Characterisation of the Purified NADPH-Flavin Reductase of Human Erythrocytes.

Z

Zhulin, I.B., Taylor, B.L. & Dixon, R. (1997) TIBS **22**, 331-333. PAS Domain S-Boxes in Achaea, Bacteria and Sensors for Oxygen and Redox.

APPENDIX I

Addresses of Suppliers

Amersham International Plc.
U.K. & Export Sales Officer
Valentine House
Lincoln Place
Aylesbury
Buckinghamshire, HP20 2TP.

BDH Laboratory Supplies
Poole
BH15 ITD
England.

BDH; Whatman
c/o Lennox Chemicals
J.F. Kennedy Drive
Nass Road
Dublin 12.
Ireland.

Beckman-RIIC Ltd.
Progress Road
Sands Industrial Estate
High Wycombe
Bucks HP12 4JL
U.K.

BIO 101 Inc.
P.O. Box 2284
La Jolla
CA 92038-2284
U.S.A.

Boehringer Mannheim Ireland
Valentine House
Temple Road
Blackrock
Co. Dublin.

Costar Scientific Corporation
Suppliers: Brownes
Laboratory Consumables Division
Sandyford Industrial Estate
Foxrock
Dublin 18.

Hoefer Scientific Instruments U.K.
P.O. Box 351
Newcastle
Staffs
ST5 OTT
U.K.

Nalgene Company
Subsidary of Sybron Corp.
Rochester
NY 14602-0365
U.S.A.

New England Biolabs
32 Tozer Road
Beverly
MA 10915-5599
U.S.A.

MWG Biotech U.K.
Waterside House
Peartree Bridge
Milton Keynes
MK63BY.

Sigma Chemical Co. Ltd.
Fancy Road
Poole
Dorset
U.K.

Promega Corporation (MSC)
Unit 9
Santry Hall Industrial Estate
Santry
Dublin 9.

APPENDIX II

DNA Molecular Weight Standards VII (Boehringer Mannheim).

Marker sizes in basepairs:

8510	1510
7350	1390
6110	1160
4840	980
3950	720
2810	480
1950	360
1860	

1Kb DNA Molecular Weight Standards (Promega).

Marker sizes in basepairs:

10000	2000
8000	1500
6000	1000
5000	750
4000	500
3000	250,253
2200	

APPENDIX III

Low Molecular Weight Protein Standards.

Marker sizes in kilodaltons:

66	24
45	20
36	14.2
29	

Prestained Molecular Weight Protein Standards.

Marker sizes in kilodaltons:

175	32.5
83	25
62	16.5
47.5	6.5

THE JOURNAL OF BIOLOGICAL CHEMISTRY

Vol. 275, No. 25, Issue of June 23, pp. 19009–19017, 2000
Printed in U.S.A.

Studies on the Specificity of the Tetrapyrrole Substrate for Human Biliverdin-IXα Reductase and Biliverdin-IXβ Reductase

STRUCTURE-ACTIVITY RELATIONSHIPS DEFINE MODELS FOR BOTH ACTIVE SITES*

Received for publication, December 8, 1999, and in revised form, March 2, 2000

Orla Cunningham‡§¶, Aisling Dunne‡§‖, Portia Sabido, David Lightner**‡‡, and Timothy J. Mantle‡**

*From the ‡Department of Biochemistry, Trinity College, Dublin 2, Ireland and the **Departments of Chemistry & Biochemistry, University of Nevada, Reno, Nevada 89557-0020*

A comparison of the initial rate kinetics for human biliverdin-IXα reductase and biliverdin-IXβ reductase with a series of synthetic biliverdins with propionate side chains "moving" from a bridging position across the central methene bridge (α isomers) to a "γ-configuration" reveals characteristic behavior that allows us to propose distinct models for the two active sites. For human biliverdin-IXα reductase, as previously discussed for the rat and ox enzymes, it appears that at least one "bridging propionate" is necessary for optimal binding and catalytic activity, whereas two are preferred. All other configurations studied were substrates for human biliverdin-IXα reductase, albeit poor ones. In the case of mesobiliverdin-XIIIα, extending the propionate side chains to hexanoate resulted in a significant loss of activity, whereas the butyrate derivative retained high activity. For human biliverdin-IXα reductase, we suggest that a pair of positively charged side chains play a key role in optimally binding the IXα isomers. In the case of human biliverdin-IXβ reductase, the enzyme cannot tolerate even one propionate in the bridging position, suggesting that two negatively charged residues on the enzyme surface may preclude productive binding in this case. The flavin reductase activity of biliverdin-IXβ reductase is potently inhibited by mesobiliverdin-XIIIα and protohemin, which is consistent with the hypothesis that the tetrapyrrole and flavin substrate bind at a common site.

The formation of linear tetrapyrroles by heme catabolism in mammals has, until recently, been discussed in terms of the IXα isomers of biliverdin and bilirubin as both heme oxygenases I and II (HO-1 and HO-2),[1] and biliverdin-IXα reductase (BVR-A) are reported to exhibit such specificity (1, 2). However, 87% of the bilirubin in human fetal bile has been reported to be the IXβ isomer (3). Yamaguchi *et al.* (4) purified a novel enzyme from human liver that catalyzes the reduction of the IXβ, IXγ, and IXδ isomers of biliverdin to the corresponding rubin (4). We have shown that this enzyme, biliverdin-IXβ reductase (BVR-B), is identical to NAD(P)H-linked flavin reductase (5). The source of fetal biliverdin-IXβ has not yet been determined; however, this appears to be a pathway that is only operative at any significant level in the fetus. The physiological relevance of the apparent switch in heme degradation from a IXβ pathway *in utero* to a IXα pathway at birth is unclear, although it may be coupled to the switch from fetal to adult hemoglobin. O'Carra and Colleran (6) have shown that nonenzymic ascorbate-mediated coupled oxidation of "free" heme (pyridine-heme complexes) produces all four isomers of biliverdin-IX (Scheme 1), in approximately equimolar amounts, whereas coupled oxidation of adult hemoglobin produces a mixture of IXα (65%) and IXβ (35%) isomers of biliverdin. The nature of the protein binding the heme is important because ascorbate-mediated coupled oxidation of myoglobin produces 95% biliverdin-IXα (6). It is not known which isomers of biliverdin-IX are produced by ascorbate-mediated coupled oxidation of fetal hemoglobin, although, in preliminary experiments, we cannot support BVR-B-dependent NADPH oxidation using the products of this reaction.[2]

Whereas nonenzymic coupled oxidation is demonstrable in *vitro*, it is clear that at least two forms of heme oxygenase (HO-1 and HO-2) function in *vivo*. Both of these enzymes produce the IXα isomer of biliverdin exclusively; however, the nature of the isomer produced by the recently described HO-3 (7) is not known. Quantitative flux through these three HO pathways in mammals has not been studied, although there is considerable interest that there is a requirement for a functioning HO-1 for effective reutilisation of iron in mammals (8).

The discovery that the IXα isomer of bilirubin is a ligand for the aryl hydrocarbon (Ah) receptor (9, 10) may explain the transcriptional up-regulation of the rat GST A5 gene in congenital hyperbilirubinaemia (11) and allows us to suggest that a function for the IXβ isomer (which appears to be a uniquely fetal metabolite) may be related to fetal suppression of the maternal immune system. The Ah receptor is known to be involved in immunosuppression, and, during pregnancy, there is an increased susceptibility to certain types of infection (12–14). Both biliverdin-IXα and bilirubin-IXα have been implicated as modulators of the immune system (15, 16). Intriguingly, the recent suggestion that indoleamine dioxygenase (EC 1.13.11.42) may be involved in fetal suppression of the maternal immune response (17) could also support Ah receptor involvement as tryptophan metabolites are also known to bind to and activate this transcription factor (18).

High levels of the IXα isomer of bilirubin are generally seen

* The costs of publication of this article were defrayed in part by the payment of page charges. This article must therefore be hereby marked "*advertisement*" in accordance with 18 U.S.C. Section 1734 solely to indicate this fact.

§ These authors contributed equally to this work.

¶ Supported by the Health Research Board, Ireland.

‖ Supported by the Irish National Pharmaceutical Biotechnology Center. To whom correspondence should be addressed. Tel.: 353-1-6083410; Fax: 353-1-6772400; E-mail: aidunne@tcd.ie.

‡‡ Supported by the National Institutes of Health.

[1] The abbreviations used are: HO, heme oxygenase; BVR-A, biliverdin-IXα reductase; BVR-B, biliverdin-IXβ reductase; GST, glutathione *S*-transferase; BSA, bovine serum albumin; FR, flavin reductase; PAGE, polyacrylamide gel electrophoresis.

[2] O. Cunningham and T. J. Mantle, unpublished observations.

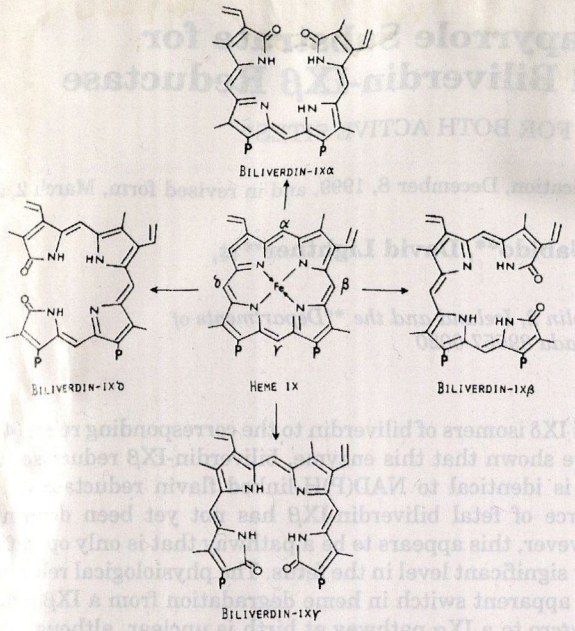

SCHEME 1. **Biliverdin isomers resulting from haem cleavage.** Four possible isomers of biliverdin can result from the cleavage of haem because of the nonequivalence of the four methene bridge positions α, β, γ, and δ (P = -CH_2CH_2COOH).

at birth (so-called physiological jaundice of the newborn) and are potentially cytotoxic if the protective binding capacity of serum albumin (19, 20) is exceeded. However, this is a period when the infant lung experiences a massive increase in the partial pressure of oxygen (21), and the transient increase in serum bilirubin levels seen at this time may represent a temporary boost in the levels of a physiologically significant antioxidant. Indeed, several workers have presented evidence that bilirubin-IXα functions as an antioxidant, both in its free form (22) and bound to albumin (23), and low serum bilirubin-IXα has been shown to correlate with increased risk of coronary artery disease in two independent studies (24, 25).

It is conceivable that linear tetrapyrroles may play significant biological roles in mammals, both as antioxidants and as anti-inflammatory agents, and it is therefore important to extend our knowledge of the substrate specificity of the two human enzymes currently known to catalyze the formation of bilirubin isomers. Further study will need to identify the origin of biliverdin-IXβ *in utero* and also to define any other linear tetrapyrroles that may occur in the adult and/or the fetus.

The chemical synthesis of the four isomers of biliverdin, cleaved at the α, β, γ, and δ positions using ascorbate-mediated coupled oxidation of pyridine-heme is not amenable to large scale production. Early work by Colleran and O'Carra (26) demonstrated that replacement of the vinyl side chains by ethyl side chains (defined as mesobiliverdins) had little effect on substrate affinity. We have therefore developed a method of producing symmetrical synthetic mesobiliverdins with propionic acid groups at varying sites along the pigment backbone (Group I verdins, Refs. 27–29; Group II verdins, Refs. 30–32; Group III verdins, Refs. 33 and 34) and report here the initial rate kinetics of these verdins with recombinant human BVR-A and BVR-B. These structure-activity relationships allow us to propose models for the active site structures of these two enzymes.

EXPERIMENTAL PROCEDURES

Cloning and Overexpression of Human Biliverdin-IXα Reductase and Human Biliverdin-IXβ Reductase

Oligonucleotide primers used to amplify the cDNA encoding human BVR-A were designed based on the cDNA sequence reported by Maines *et al.* (35). The forward (5′-GCAGGATCCAAGATGAATGCAGAG-3′) and reverse (5′-AACCAAATGCTGGTGCCATGGTGGAA-3′) primers contained *Bam*HI and *Nco*I restriction sites, respectively (underlined). A cDNA library derived from the U937 monocyte cell line was used as target in subsequent amplification reactions. The resulting 960-base pair fragment was digested and ligated into the pGEX-KG expression vector to produce the pGEX-BVR-A plasmid. *Escherichia coli* strain TG1 was transformed according to procedures described in Sambrook *et al.* (36).

E. coli cells for large scale purification of the recombinant GST fusion protein were cultured as follows. 10-ml cultures were grown in Luria-Bertani medium overnight at 30 °C in the presence of 2% glucose and 100 μg/ml ampicillin. Two-liter cultures were inoculated with the overnight cultures, grown at 30 °C to an A_{600} of 0.4–0.5, and induced with isopropyl-1-thio-β-D-galactopyranoside at a final concentration of 0.2 mM. After 18 h the cells were harvested by centrifugation (7,700 × *g* for 10 min) and lysed by sonication in the presence of lysozyme (200 μg/ml). Following centrifugation at 12,000 × *g* for 45 min, the cell supernatant was passed through a glutathione-Sepharose affinity column, and the fusion protein was eluted with 10 mM glutathione in 50 mM Tris-HCl, pH 8.0. Excess glutathione was removed by gel filtration, and the fusion protein was cleaved overnight at 4 °C with 20 units of thrombin (1 unit/μl). The liberated BVR-A was separated from the GST tag by passage through the glutathione affinity column. The approximate yield of purified BVR-A from a 2-liter culture is 30 mg. Recombinant human biliverdin-IXβ reductase was prepared as described previously by thrombin cleavage of a GST-BVR-B fusion protein (37).

Mass Spectroscopic Analysis of Recombinant Biliverdin-IXα Reductase and Biliverdin-IXβ Reductase

On SDS-PAGE, recombinant human BVR-A migrates with a mobility corresponding to a molecular mass of 40 kDa. Similar behavior has been reported for the native human enzyme (38, 39). This is in contrast to the behavior of the rat, mouse and ox enzymes which exhibit a molecular mass of 34 kDa on electrophoresis (38). Given that the rat enzyme contains 295 amino acids and the human enzyme contains 296 amino acids, mass spectroscopy was carried out to determine the relative molecular mass of human BVR-A. Similar analysis was conducted for BVR-B.

TABLE I
Calculated extinction coefficients for synthetic biliverdin isomers at maximum absorbance

Biliverdin isomer	Extinction coefficient
	liters mol^{-1} *cm*$^{-1}$
Mesobiliverdin IXα	1.2×10^4
Mesobiliverdin-XIIIα	1×10^4
Mesobiliverdin-IVα	2.2×10^3
12-Ethyl mesobiliverdin-XIIIα	9.9×10^3
12-Ethyl-13-methyl mesobiliverdin-IVα	1.4×10^4
Mesobiliverdin XIIIγ	1.54×10^4
Mesobiliverdin-XIIγ	1.16×10^4
8,12-Dimethyl mesobiliverdin-XIIγ	1.31×10^4
α,α,α′,α′-Tetramethyl-mesobiliverdin-XIIIα	7.78×10^3
α,α′-Dimethoxy-mesobiliverdin-XIIα	1.48×10^4
Mesobiliverdin-XIIIα (n = 3)	1.36×10^4
Mesobiliverdin-XIIIα (n = 4)	1.78×10^4

TABLE II
Kinetic parameters for human BVR-A and human BVR-B

Verdin isomer	BVR-A			BVR-B
	K_m^{app}	k_{cat}^{app}	K_i^{app}	K_i^{app}
	μM	s^{-1}	μM	μM
Biliverdin-IXα	7	44	0.7	
Mesobiliverdin-XIIIα	11	114	0.4	
Mesobiliverdin-IVα	76	34	169	
12-Ethyl mesobiliverdin-XIIIα	200	45	10	
12-Ethyl-13-methyl mesobiliverdin-IVα	31	0.6		0.3
Mesobiliverdin-XIIIγ	79	0.9	213	0.5
8,12-Dimethyl mesobiliverdin-XIIγ	26	0.5	30	0.8
α,α,α′,α′-Tetramethyl mesobiliverdin-XIIIα	37	1		
Mesobiliverdin-XIIγ				3

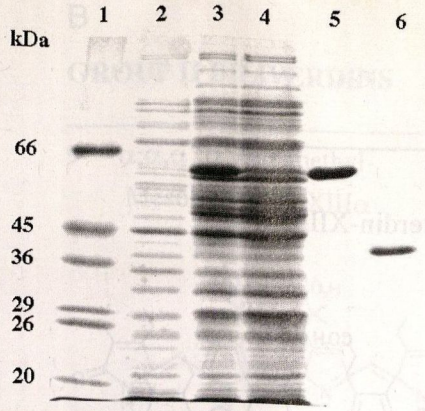

FIG. 1. **SDS-PAGE of recombinant human biliverdin-IXα reductase.** *Lane 1*, molecular mass markers (sizes indicated); *lane 2*, lysate from cells transformed with control vector (pGEX-KG with no insert); *lane 3*, lysate from cells transformed with pGEX-BVR-A (with isopropyl-1-thio-β-D-galactopyranoside); *lane 4*, lysate from cells transformed with pGEX-BVR-A (without isopropyl-1-thio-β-D-galactopyranoside); *lane 5*, purified GST-BVR-A (5 μg); *lane 6*, cleaved BVR-A (5 μg).

Stock solutions of both proteins were diluted in 200 μl of distilled water to give a final concentration of 0.6 mg/ml, and buffer was exchanged into 50 mM ammonium acetate, pH 6.0, through a pre-equilibrated PD-10 column. Samples containing BVR-A and BVR-B were pooled and adjusted to 0.4 and 0.6 mg/ml, respectively. The buffer composition was finally adjusted to 50% (v/v) acetonitrile and 1% (v/v) formic acid. Mass analysis was carried out using a Micromass triple quadrupole electrospray mass spectrometer. A 10-μl sample was introduced into the electrospray mass spectrometer via a Rheodyne injector valve fitted with a 10-μl injection loop. Analysis was carried out in positive ion mode. Raw data were collected between a mass-to-charge ratio of 600–1700 *m/z*, at a cone voltage of 30 V, HV lens of 0.22 kV, and a capillary voltage of 3.60 kV. The raw data were subjected to maximum entropy analysis according to the Micromass schedule.

Preparation of Partially Pure Native Biliverdin-IXα Reductase and Biliverdin-IXβ Reductase

Human erythrocytes were centrifuged at 4,000 × *g* for 10 min at 4 °C, and the supernatant was removed. The erythrocytes were gently resuspended in three volumes of ice-cold 0.9% (w/v) sodium chloride. Centrifugation was carried out as described above. This washing step was repeated twice. The packed erythrocytes were lysed by the addition of three volumes of ice-cold distilled water. The pH was adjusted to 6.4 using 5 M HCl. The suspension was centrifuged at 10,000 × *g* for 1 h at 4 °C. The pH was finally adjusted to 7.2 with 5 M KOH. The lysate was dialyzed against 20 liters of 10 mM sodium phosphate, pH 7.2, overnight and then loaded onto a DEAE-cellulose column (5 × 30 cm) equilibrated in 10 mM sodium phosphate, pH 7.2. The column was washed until the A_{280} was below 0.1, and the two forms of biliverdin reductase were then eluted with a 10–350 mM gradient (2 × 250 ml) of sodium phosphate, pH 7.2. The fractions were assayed for biliverdin-IXα reductase and flavin reductase activity as described below, and the peak fractions were subjected to immunoblotting with antisera raised against the recombinant BVR-A and BVR-B enzymes.

Enzyme Assays

Biliverdin Reductase Assays—The biliverdin isomers used in this study were synthesized from mono- and dipyrrole components as described previously (27–34). Dried preparations were dissolved in Me_2SO to give a final stock concentration of 1 mM. The final concentration of Me_2SO in the assay was shown to have no effect on enzyme activity.

Preliminary plate assays were conducted at 30 °C in 100 mM potassium phosphate buffer, pH 7.5, containing 50 μM NADPH and the respective biliverdin isomers at a concentration of 20 μM. Initial rate measurements with biliverdin as the variable substrate were made by monitoring biliverdin consumption at 660 nm in the presence and absence of BSA (1 mg/ml) using the extinction coefficients given in Table I. No co-solvents or detergents were added to the assay mixture (Beer Lambert's law was obeyed over the concentration range used). All assays were conducted in 100 mM potassium phosphate buffer, pH 7.5, and contained NADPH at a saturating concentration of 50 μM (the K_m^{NADPH} for BVR-A and BVR-B is 1 μM with biliverdin-IXα and FMN, respectively).

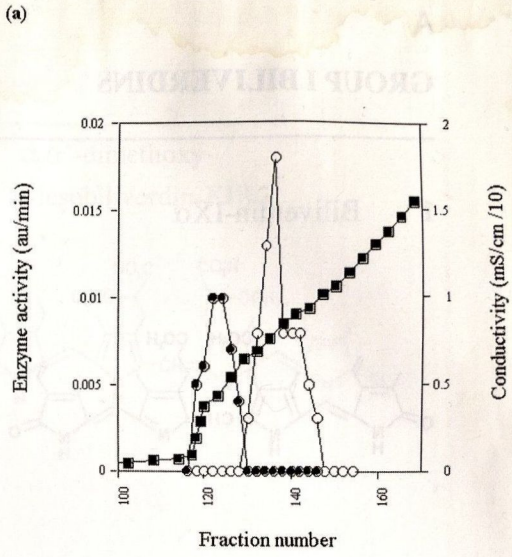

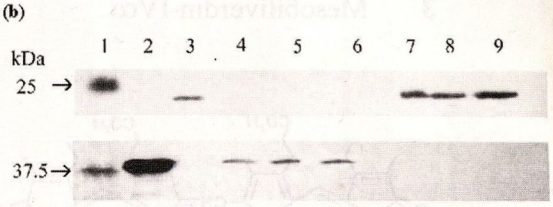

FIG. 2. **Separation of native human biliverdin-IXα reductase and biliverdin-IXβ reductase on DEAE-cellulose.** *a*, human BVR-A and BVR-B isolated from erythroyctes were separated using ion exchange chromatography. Fractions were assayed for flavin reductase activity (●), biliverdin-IXα reductase activity (●), and conductivity (■). *b*, Western blot analysis was carried out on fractions over the peak of BVR-A activity (*lanes 4-6*) and over the peak of flavin reductase activity (*lanes 7–9*) using antisera raised against BVR-A and BVR-B, respectively. *Lane 1*, molecular mass markers; *lane 2*, BVR-A standard (5 μg); *lane 3*, BVR-B standard (5 μg).

Flavin Reductase Assay—The flavin reductase activity of BVR-B was measured using the method described by Yubisui *et al.* (40). Initial rate studies were carried out under saturating concentrations of FMN (150 μM) and NADPH (50 μM) in 100 mM potassium phosphate, pH 7.5. Activity was monitored by following the decrease in absorbance of NADPH at 340 nm. Inhibition of flavin reductase (FR) activity was determined under the same conditions using mesobiliverdin-XIIIα (1 nM to 1 μM), lumichrome (5 to 75 μM), and protohemin (1 nM to 10 μM).

Treatment of Data

The initial rate data were fitted to equations for simple hyperbolic kinetics and total and partial substrate inhibiton (41). Most data sets showed potent substrate inhibition, where few data points were on the upward limb, and fitting (to either total or partial substrate inhibition) produced negative coefficients or large errors. For this reason estimates of the kinetic parameters (Table II) were obtained by manually generating saturation curves for total substrate inhibition (using, where possible, initial estimates from the curve fitting routines) and visually checking the theoretical line against the data set. For several of the substrates with BVR-B, the substrate inhibition is so potent that the only kinetic parameter obtainable was the substrate inhibitory K_i value, obtained by plotting the reciprocal of the initial rate against the concentration of the tetrapyrrole. For those substrates exhibiting partial substrate inhibition only the linear part of the v_o^{-1} *versus* [biliverdin] curve were used to obtain the substrate inhibitory K_i value. All experiments conducted in this study used 50 μM NADPH. More extensive kinetic studies, for example varying NADPH concentration, require the development of an assay that will allow initial rates to be determined at low concentrations of the tetrapyrrole substrate to allow curve fitting routines to be used with confidence.

A

GROUP I BILIVERDINS

1 Biliverdin-IXα

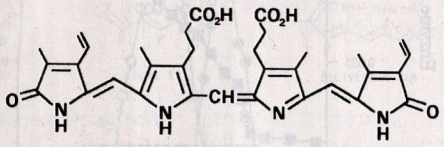

2 Mesobiliverdin-XIIIα

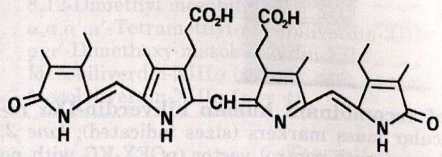

3 Mesobiliverdin-IVα

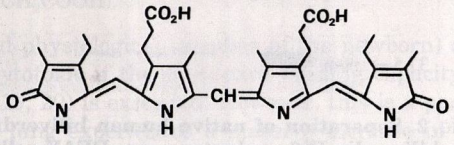

4 12-ethyl-Mesobiliverdin-XIIIα

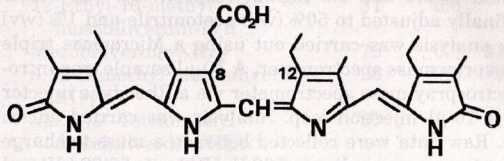

5 12-ethyl-13-methyl-Mesobiliverdin-IVα

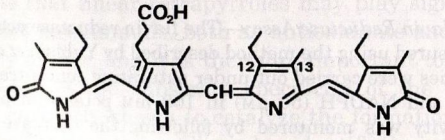

6 Mesobiliverdin-XIIIγ

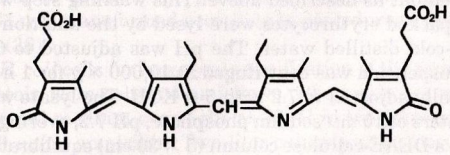

7 Mesobiliverdin-XIIγ

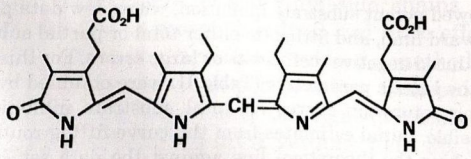

8 8,12-dimethyl-Mesobiliverdin-XIIγ

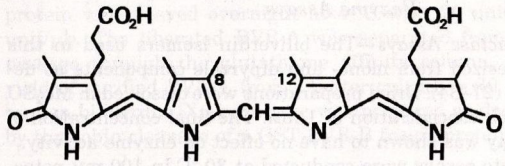

FIG. 3. **Structures of biliverdin isomers 1–16.**

RESULTS

The cloning of human biliverdin-IXβ reductase into the pGEX-KG expression vector to produce a GST-BVR-B fusion protein has been reported previously (37). We have constructed a similar vector for human biliverdin-IXα reductase that allows the production of 40 mg of GST-BVR-A fusion protein/liter of culture. The recombinant protein has been affinity purified on glutathione-Sepharose, and the GST moiety was removed following cleavage with thrombin, yielding a homogenous preparation of BVR-A of the predicted mobility on SDS-PAGE, as shown in Fig. 1. The partial purification of native BVR-A and BVR-B from human erythrocytes was achieved using DEAE-

B

GROUP II BILIVERDINS

9 α,α,α',α'-tetramethyl-Mesobiliverdin-XIIIα

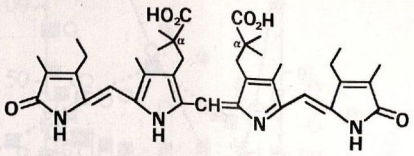

10 α,α'-dimethoxy-Mesobiliverdin-XIIIα

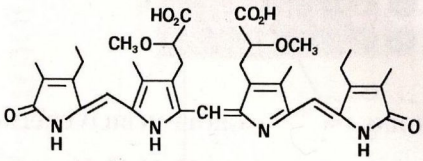

11 (n=3)-Mesobiliverdin-XIIIα

12 (n=5)-Mesobiliverdin-XIIIα

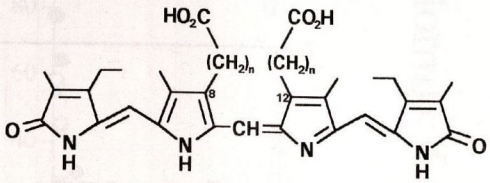

GROUP III BILIVERDINS

13-16 Basic structure: Mesobiliverdin-XIIIα

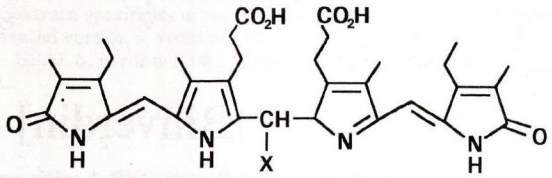

13: x=tertiary butyl

14: x=adamantine

15: x=phenyl

16: x=methyl

FIG. 3—*continued*

cellulose chromatography. The elution profile is shown in Fig. 2*a* and reveals complete separation of the two activities that was subsequently confirmed by immunoblotting (Fig. 2*b*).

Both the native and recombinant form of human BVR-A migrate on SDS-PAGE with an apparent molecular mass of 40 kDa. Mass spectroscopic analysis of recombinant human BVR-A gave a molecular mass of 34,330 Da (data not shown), suggesting that the protein runs anomalously on SDS-PAGE. The molecular mass estimated for BVR-B by SDS-PAGE was confirmed using mass spectroscopy as 22,531 Da.

The structures of the verdins used to assess the substrate specificity of BVR-A and BVR-B are shown in Fig. 3. The

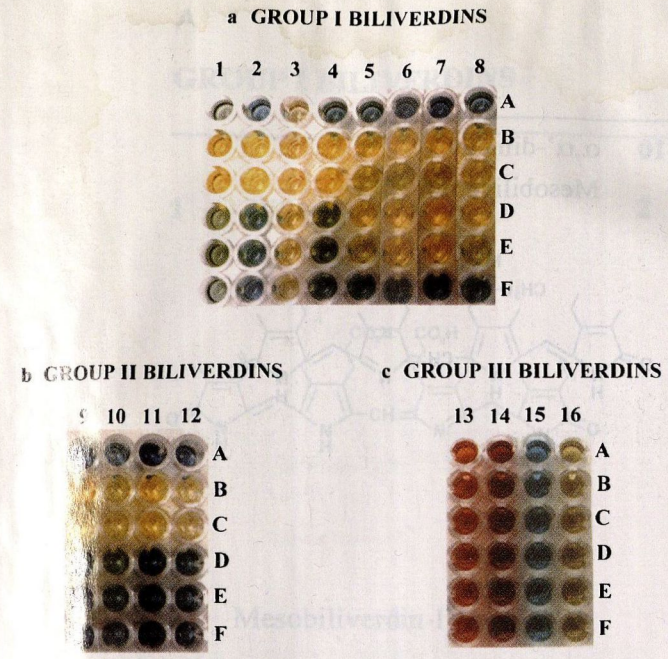

FIG. 4. **A comparison of the substrate specificity of native and recombinant human BVR-A and human BVR-B.** Incubations were carried out in the presence of NADPH (50 μM), BSA (1 mg/ml), and 100 mM potassium phosphate, pH 7.5. *Rows A* and *F* do not contain enzyme. *Rows B* and *C* contain native and recombinant BVR-A, respectively. *Rows D* and *E* contain native and recombinant BVR-B, respectively. Numbers *1–16* represent the various verdin structures illustrated in Fig. 3.

natural IXα isomer (**1**) has vinyl side chains at positions 3 and 18. Fig. 4 shows the result of an overnight incubation of all of the verdin isomers with recombinant human BVR-A (*row C*) and BVR-B (*row E*) and the native forms of human BVR-A (*row B*) and BVR-B (*row D*) isolated from human red blood cells. The incubations were carried out in the presence of NADPH (50 μM), BSA (1 mg/ml), and 100 mM potassium phosphate buffer, pH 7.5. *Rows A* and *F* are control incubations containing no enzyme. It is clear the recombinant enzymes exhibit identical behavior to the native enzymes and that all of the Group I and Group II structures are substrates for BVR-A. In these two groups, those isomers that contained bridging propionates (**1**, **2**, and **4**), modified bridging propionates (**9** and **10**), and extended bridging carboxylate side chains (butyrate, **11**; hexanoate, **12**) were not reduced by BVR-B (either native or recombinant). In our discussion, "bridging propionates" refers to propionate side chains at positions C_8 and C_{12}, effectively bridging the central methene bridge.

The verdins substituted at C_{10} (**13–16**) showed no change in the visible spectrum, which is not surprising because they are not reducible at C_{10}. Unfortunately, none of these compounds are particularly effective inhibitors of BVR-A or BVR-B (which might have been a starting point for anti-hyperbilirubinaemia therapy). The methyl derivative (**16**) was the most potent, exhibiting modest inhibition at 25 μM.

Although the overnight plate incubations allow a crude definition of whether or not the various compounds behave as substrates for the two enzyme forms, it yields little information about the relative rates of reaction. The initial rate kinetics for compounds **1–6**, **8**, and **9** in the presence and absence of BSA (1 mg/ml) with recombinant BVR-A are shown in Fig. 5. It is clear that the addition of BSA has a pronounced effect on the activity with mesobiliverdin-IVα (**3**); however, for biliverdin-IXα (**1**) and 12-ethyl mesobiliverdin-XIIIα (**4**) the effect is mainly on sequestration of substrate. In previous work with ox kidney

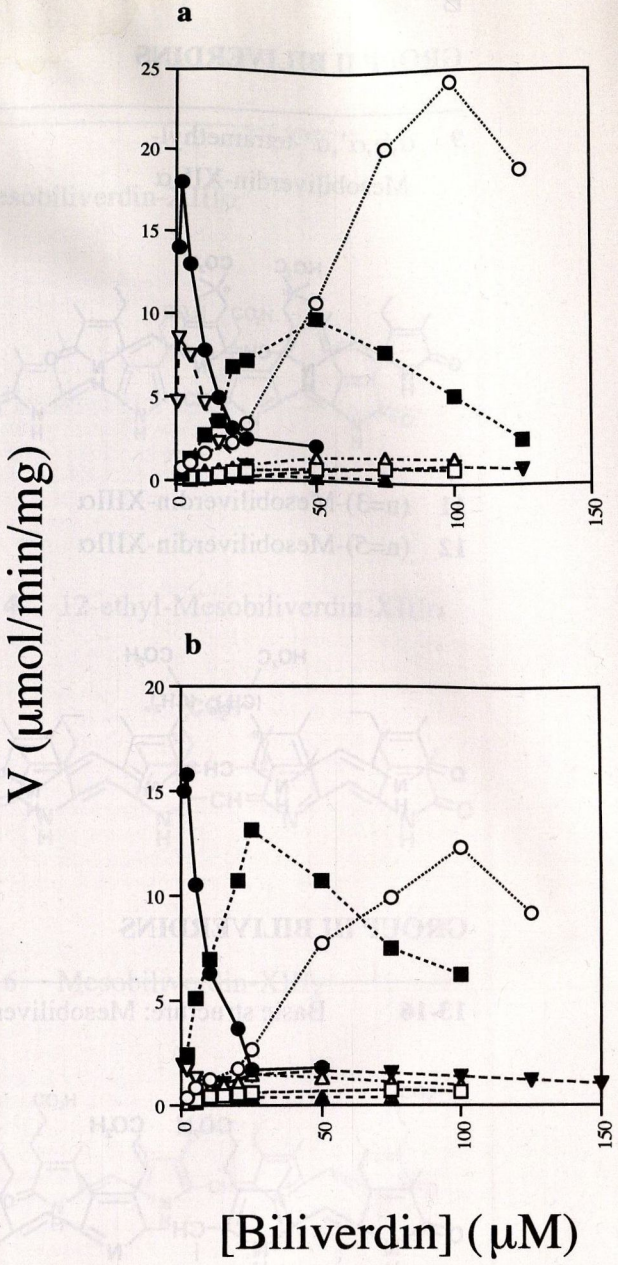

FIG. 5. **Initial rate studies on BVR-A with various isomers of biliverdin.** The substrate specificity of recombinant human BVR-A was examined in the presence (*a*) and the absence (*b*) of BSA. Consumption of verdins 2 (●), 3 (○), 4 (■), 5 (□), 8 (▲), 9 (△), 6 (▼), and 1 (▽) was monitored at 660 nm, and initial rates were calculated using the extinction coefficients given in Table I.

BVR-A (42) and rat kidney BVR-A (43), we have attempted to define the effect of BSA as simple sequestration of the verdin substrate; however, detailed work in our laboratory suggests that this is not the only function (41).[3] The extinction coefficient for bilirubin-IXα at 460 nm is increased on binding to albumin, and the free concentration of biliverdin IXα is also reduced by binding to BSA; however, it is clear that other factor(s) are also operative (44). By monitoring the ΔA_{660}, as opposed to ΔA_{460}, some of these complications are overcome, albeit at the expense of sensitivity.

As the kinetics of BVR-A involve pronounced substrate inhi-

[3] E. M. Rigney, O. Ennis, G. Elliot, and T. J. Mantle, unpublished observations.

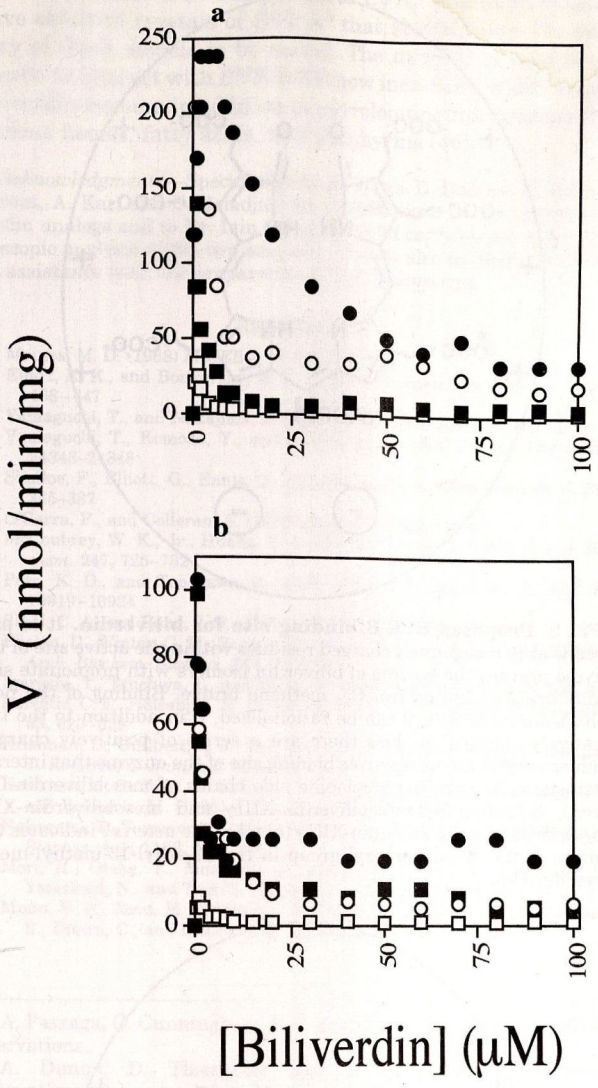

FIG. 6. **Initial rate studies on BVR-B with various isomers of biliverdin.** The substrate specificity of recombinant BVR-B was examined using the indicated verdin. *a*, verdins 7 (●, + BSA; ○, − BSA) and 5 (■, + BSA; □, − BSA). *b*, verdins 8 (●, + BSA; ○, − BSA) and 6 (■, + BSA; □, − BSA).

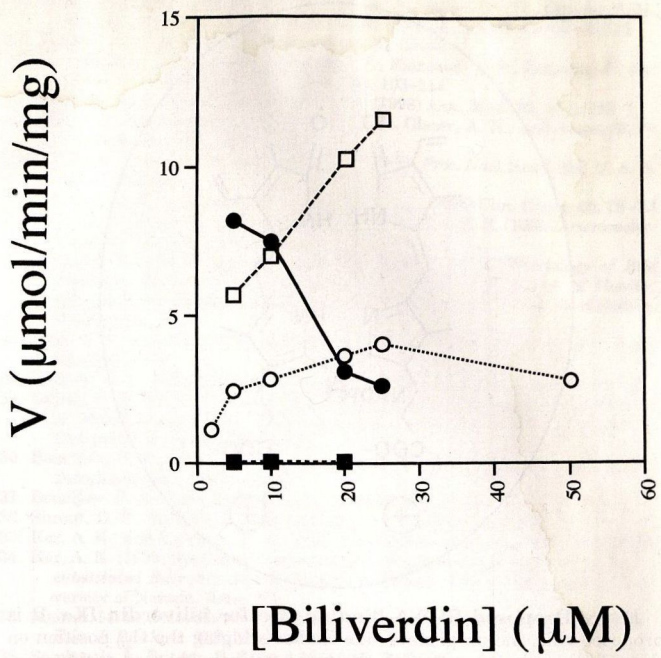

FIG. 7. **Effect of carboxylic acid chain length on human BVR-A activity.** BVR-A activity was measured using mesobiliverdin-XIIIα where the propionate side chains at positions 8 and 12 have been substituted to produce a dimethoxy (□), butyrate (○), and hexanoate (■) derivative (verdins 10, 11, and 12, respectively) as shown in Fig. 3. The reduction of biliverdin IXα is also included in this figure (●).

bition, because the effect of albumin on the initial rate is not clear and, as the present work shows, these effects vary depending on the substrates used, for the present discussion, we define "good" and "poor" substrates for BVR-A in the following way: good substrates are those that, when assayed in the presence of BSA, exhibit an apparent $K_m^{\text{biliverdin}}$ of less than 10 μM and that exhibit a maximal initial rate of greater than 5 μmol/min/mg. We define a poor BVR-A substrate as one with an apparent $K_m^{\text{biliverdin}}$ greater than 20 μM and exhibiting a maximal initial rate no greater that 1 μmol/min/mg. It is clear that the compounds with a bridging propionate are all good substrates (compounds **1**, **2**, and **4**) with two propionates being preferred (*i.e.* biliverdin-IXα (1) and mesobiliverdin-XIIIα (2) exhibit lower apparent K_m values than 12-ethyl-mesobiliverdin-XIIIα (4)). Although all of the other verdins tested were substrates for human BVR-A, the rates were very low compared with those for **1**, **2**, **4**, and **11** (see below).

A quite distinct pattern of substrate specificity is shown by BVR-B. This enzyme cannot tolerate even one bridging propionate side chain in a verdin, so that compounds **1**, **2**, and **4** do not function as substrates (Fig. 6). The plate shown in Fig. 4 has been allowed to go to completion (*i.e.* it was left overnight at room temperature) for compounds **1–16.** Using the spectrophotometric assay, it was not possible to measure BVR-B activity with compounds **1**, **2**, and **4.** In contrast, several of the compounds that are poor substrates for BVR-A are good substrates for BVR-B (Fig. 6). Propionates in any of the nonbridging positions seem to promote activity, with substitutions at positions 3, 5, 6, 7, and 8 being particularly active. It should be noted that the substrate inhibition with BVR-B is far more potent than that observed with BVR-A, having substrate inhibitory K_i values in the submicromolar range. This precluded the determination of any standard kinetic parameters for BVR-B using the spectrophotometric assay.

In a separate experiment, we analyzed the effect of the chain length of the carboxylic acid on activity with both BVR-A and BVR-B by using mesobiliverdin-XIIIα where the propionate side chains at positions 8 and 12 have been substituted by butyrate (**11**) or hexanoate (**12**), respectively. In the case of BVR-B, these behave as bridging substituents, and neither are reduced. However, BVR-A can utilize **11** efficiently, whereas the bulkier hexanoate derivative (**12**) is an extremely poor substrate (Fig. 7).

We have taken advantage of the ability of BVR-B to function as a FR to show that the nonsubstrate mesobiliverdin-XIIIα, (which has bridging propionates), can function as a potent inhibitor of the FR reaction. The inhibition is competitive with respect to FMN and mixed against NADPH, consistent with the hypothesis that the verdin and flavin may compete for a common site (45). Protohemin, which has been reported previously to bind tightly to bovine liver flavin reductase (46), also acts as a potent inhibitor of the human enzyme giving an IC_{50} of 0.8 μM under standard assay conditions. This is also consistent with the hypothesis of a common tetrapyrrole/flavin site. Unfortunately, we have been unable to obtain any evidence to show that lumichrome (an inhibitor of the FR reaction; Ref. 45) behaves as an inhibitor of BVR-B activity. Lumichrome is not a

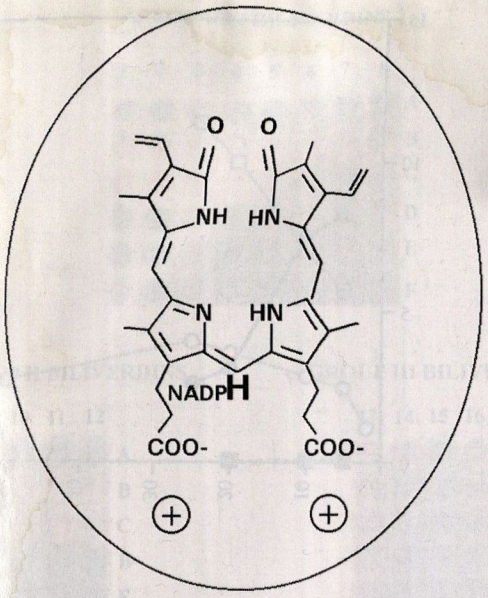

FIG. 8. **Proposed BVR-A binding site for biliverdin IXα.** It is proposed that the propionate side chains bridging the C_{10} position on the tetrapyrrole interact with the two positively charged residues on BVR-A to promote binding and subsequent catalysis. NADPH is included in the figure to indicate the methene bridge, which is reduced by BVR-A.

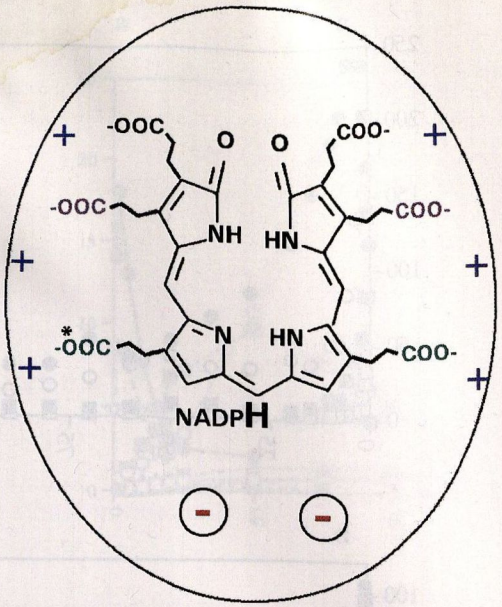

FIG. 9. **Proposed BVR-B binding site for biliverdin.** It is proposed that two negatively charged residues within the active site of the enzyme prevent the binding of biliverdin isomers with propionate side chains bridging the central C_{10} methene bridge. Binding of the non-alpha isomers to BVR-B can be rationalized, if in addition to the two negatively charged residues there are a series of positively charged residues around the tetrapyrrole binding site of the enzyme that interact electrostatically with the propionate side chains of mesobiliverdin-IVα (*green*), 8,12-dimethyl-mesobiliverdin-XIIIγ and mesobiliverdin-XIIγ (*magenta*), and mesobiliverdin-XIIIγ (*black*). The *asterisk* indicates the position of the single carboxyl group in the 12-ethyl-13-methyl-mesobiliverdin-IVα.

particularly potent inhibitor of the FR reaction (K_i 73 μM), and it may be that the marked substrate inhibition seen with BVR-B masks any relatively modest inhibition by lumichrome by shifting the saturation curve to the right. Such an effect may extend the plateau of maximal activity by alleviating substrate inhibition. Intriguingly, protohemin behaves as an activator when BVR-B activity is measured, and this too may reflect an alleviation of substrate inhibition.

DISCUSSION

Both BVR-A and BVR-B exhibit a fairly broad specificity in terms of the tetrapyrrole substrate, with human BVR-A able to reduce all of the structures tested. Early work on partially purified preparations of guinea pig BVR-A (that may have been contaminated with BVR-B) also suggested that, although the IXα isomer was preferred, the β, γ, and δ isomers were also substrates for the enzyme (26), which suggests that significant binding energy may be associated with an interaction between the carboxylate side chains and a residue(s) on the enzyme (presumably lysine or arginine). The observation that those compounds with two bridging propionates (**1** and **2**) have lower apparent $K_m^{\text{biliverdin}}$ values than the monopropionate verdin substrates (12-ethyl-mesobiliverdin XIIIα; **4**) is consistent with the hypothesis that BVR-A may utilize two basic residues to stabilize tetrapyrrole binding (Fig. 8). BVR-B is most distinct in that the bridging propionate rule for BVR-A is the antithesis in this case. This leads us to suggest that, in contrast to BVR-A, there may be a pair of negatively charged residues in BVR-B that do not permit the IXα isomer to bind productively. If we argue that the reduced pyridine nucleotide (H) binds in a similar position (Fig. 9) for both BVR-A and BVR-B, then we suggest that a ring of positively charged residues may surround the tetrapyrrole pocket of BVR-B to facilitate the "non-alpha" isomers in binding productively as substrates. The IX-α isomers (those with bridging propionates) may bind in a nonproductive mode by rotating through 90°, as illustrated (Fig. 10). This would be in agreement with the competitive kinetics observed for mesobiliverdin-XIIIα against FMN. It should be

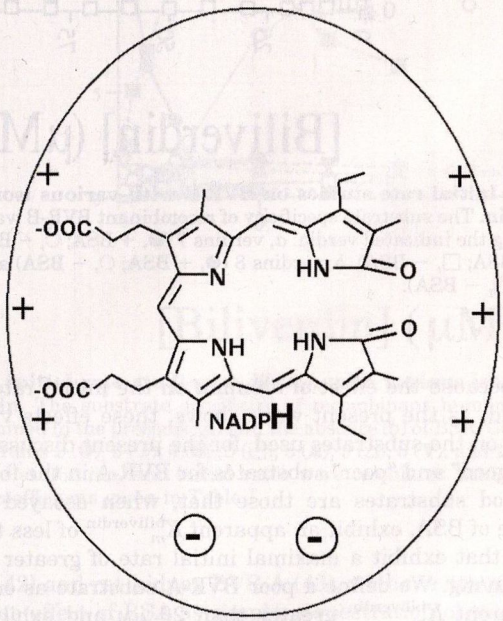

FIG. 10. **Mesobiliverdin-XIIIα inhibition of BVR-B.** Mesobiliverdin-XIIIα is not a substrate for BVR-B; however, it is a potent inhibitor of the flavin reductase activity of the enzyme. This figure illustrates how mesobiliverdin-XIIIα, with its bridging propionate side chains, may orientate itself in the BVR-B tetrapyrrole binding site to overcome the repulsive forces of the two proposed negatively charged amino acids. Its C_{10} carbon is no longer oriented in the correct position for reduction; therefore, the isomer cannot act as a substrate for BVR-B.

noted that open chain tetrapyrroles are forced to adopt a slightly helical structure (47) so that the simple rotation of 90° must be accompanied by some degree of "flexibility." Further work is clearly required to test this hypothesis. We have crys-

tals of human BVR-B that diffract to 1.6 Å,[4] and more recently, have obtained crystals of BVR-A[5] that should allow the accuracy of these models to be tested. The number of compounds known to interact with BVR-B/FR now includes a wide range of biliverdin isomers in addition to pyrroloquinoline quinone (48), various hemes, fatty acids, and porphyrins (46).

Acknowledgments—Special thanks go to Drs. D. Holmes, F. Trull, D. Shrout, A. Kar, and S. Boiadjiev for contributions to the synthesis of verdin analogs and to Dr. Iain Campuzano for carrying out mass spectroscopic analysis of the two enzymes. Thanks also to Gavin McManus for assistance with the preparation of this manuscript.

REFERENCES

1. Maines, M. D. (1988) *FASEB J.* **2,** 2557–2568
2. Elbirt, K. K., and Bonkovsky, H. L. (1999) *Proc. Assoc. Am. Physicians* **111,** 438–447
3. Yamaguchi, T., and Nakajima, H. (1995) *Eur. J. Biochem.* **233,** 467–472
4. Yamaguchi, T., Komoda, Y., and Nakajima, H. (1994) *J. Biol. Chem.* **269,** 24343–24348
5. Shalloe, F., Elliott, G., Ennis, O., and Mantle, T. J. (1996) *Biochem. J.* **316,** 385–387
6. O'Carra, P., and Colleran, E. (1970) *Biochem. J.* **119,** 42–43
7. McCoubrey, W. K., Jr., Huang, T. J., and Maines, M. D. (1997) *Eur. J. Biochem.* **247,** 725–732
8. Poss, K. D., and Tonegawa, S. (1997) *Proc. Natl. Acad. Sci. U. S. A.* **94,** 10919–10924
9. Sinal, C. J., and Bend, J. R. (1997) *Mol. Pharmacol.* **52,** 590–599
10. Phelan, D., Winter, G. M., Rogers, W. J., Lam, J. C., and Denison, M. S. (1998) *Arch. Biochem. Biophys.* **357,** 155–163
11. Igarashi, T., Tsuchiya, T., and Satoh, T. (1991) *J. Biochem. (Tokyo)* **109,** 3–5
12. Sulentic, C. E., Holsapple, M. P., and Kaminski, N. E. (1998) *Mol. Pharmacol.* **53,** 623–629
13. Krishnan, L., Guilbert, L. J., Wegmann, T. G., Belosevic, M., and Mosmann, T. R. (1996) *J. Immunol.* **156,** 653–662
14. Krishnan, L., Guilbert,. L. J., Russell, A. S., Wegmann, T. G., Mosmann, T. R., and Belosevic, M. (1996) *J. Immunol.* **156,** 644–652
15. Nakagami, T., Toyomura, K., Kinoshita, T., and Morisawa, S. (1993) *Biochim. Biophys. Acta* **1158,** 189–193
16. Mori, H., Otake, T., Morimoto, M., Ueba, N., Kunita, N., Nakagami, T., Yamasaki, N., and Tagi, S. (1991) *Jpn. J. Cancer Res.* **82,** 755–757
17. Munn, D. H., Zhou, M., Attwood, J. T., Bondarev, I., Conway, S. J., Marshall, B., Brown, C., and Mellor, A. L. (1998) *Science* **281,** 1191–1193
18. Health-Paglinso, S., Rogers, W. J., Tullis, K., Seidel, S. D., Cenijn, P. H., Brouwer, A., and Denison, M. S. (1998) *Biochemistry* **37,** 11508–11515
19. Walker, P. C. (1987) *Clin. Pharmakinet.* **13,** 26–50
20. Chuniaud, L., Dessante, M., Chantaux, F., Blondeau, J. P., Francon, J., and Trivin, F. (1996) *Clin. Chim. Acta* **256,** 103–114
21. Pitkanen, O. P., and O' Brodovich, H. M. (1998) *Ann. Med.* **30,** 134–142
22. Stoker, R., Yamamoto, Y., McDonagh, A. F., Glazer, A. N., and Ames, B. N. (1987) *Science* **235,** 1043–1046
23. Stoker, R., Glazer, A. N., and Ames, B. N. (1987) *Proc. Natl. Acad. Sci. U. S. A.* **84,** 5918–5922
24. Schwertner, H. A., Jackson, W. G., and Tolan, G. (1994) *Clin. Chem.* **40,** 18–23
25. Hunt, S. C., Wu, L. L., Hopkins, P. N., and Williams, R. R. (1996) *Arterioscler. Thromb. Vasc. Biol.* **16,** 912–917
26. Colleran, E., and O'Carra, P. (1977) in *Chemistry and Physiology of Bile Pigments* (Berk, P. D., and Berlin, N. I., eds) Department of Health, Education and Welfare Publication 77–1100, National Institutes of Health, Washington, D.C.
27. Trull, F. R., Franklin, R. W., and Lightner, D. A. (1987) *J. Heterocyclic Chem.* **24,** 1573–1579
28. Holmes, D. L., and Lightner, D. A. (1995) *J. Heterocycl. Chem.* **32,** 113–121
29. Sabido, P. M. (1997) *Synthesis, Conformational Analysis and Binding Studies of Mesobilirubins-XIIγ, -XIIIγ and Their Verdins.* Ph.D. Dissertation, University of Nevada, Reno, NV
30. Boiadjiev, S. E., Holmes, D. L., Anstine, D. T., and Lightner, D. A. (1995) *Tetrahedron* **51,** 10663–10678
31. Boiadjiev, S. E., and Lightner, D. A. (1998) *J. Org. Chem.* **63,** 6220–6228
32. Shrout, D. P., Puzicha, G., and Lightner, D. A. (1992) *Synthesis,* 328–332
33. Kar, A. K., and Lightner, D. A. (1998) *Tetrahedron: Asymmetry* **9,** 3863–3880
34. Kar, A. K. (1998) *Synthesis, Conformational Analysis and Properties of C(10)-substituted Bilirubin and Biliverdin Analogues.* Ph.D. Dissertation, University of Nevada, Reno, NV
35. Maines, M. D., Polevoda, B. V., Huang, T. J., and McCoubrey, W. K., Jr. (1996) *Eur. J. Biochem.* **235,** 372–381
36. Sambrook, J., Fritsch, E. F., and Maniatis, T. (1989) in *Molecular Cloning: A Laboratory Manual,* 2nd Ed., pp. 1.82–1.84, Cold Spring Harbor Laboratory, Cold Spring Harbor, NY
37. Cunningham, O., and Mantle T. J. (1997) *Biochem. Soc. Trans.* **25,** (Suppl.) 613
38. Rigney, E. M., Phillips, O., and Mantle T. J. (1988) *Biochem. J.* **255,** 431–435
39. Maines, M. D., and Trakshel, G. M. (1993) *Arch. Biochem. Biophys.* **300,** 320–326
40. Yubisui, T., Matsuki, T., Takeshita, M., and Yoneyama, Y. (1979) *J. Biochem. (Tokyo)* **85,** 719–728
41. Phillips, O., and Mantle, T. J. (1981) *Biochem. Soc. Trans.* **9,** 275–278
42. Rigney, E. M., and Mantle, T. J. (1988) *Biochim. Biophys. Acta* **957,** 237–242
43. Ennis, O., Maytum, R., and Mantle, T. J. (1997) *Biochem. J.* **328,** 33–36
44. Phillips, O. (1981) *Studies on Biliverdin Reductase and its Role in Haem Catabolism.* Ph.D. Dissertation, University of Dublin, Trinity College, Ireland
45. Cunningham, O., Gore, M. G., and Mantle, T. J. (2000) *Biochem. J.* **345,** 393–399
46. Xu, F., Quandt, K. S., and Hultquist, D. E. (1992) *Proc. Natl. Acad. Sci. U. S. A.* **89,** 2130–2134
47. Boiadjiev, S. E., Pfeiffer, W. P., and Lightner, D. A. (1997) *Tetrahedron* **53,** 14547–14564
48. Xu, F., Mack, C. P., Quandt, K. S., Shlafer, M., Massey, V., and Hultquist, D. E. (1993) *Biochem. Biophys. Res. Commun.* **193,** 434–439

[4] A. Parraga, O. Cunningham, T. J. Mantle, and M. Coll, unpublished observations.

[5] A. Dunne, D. Thompson, and T. J. Mantle, unpublished observations.